Towards the production of adsorbents from mixed domestic discarded materials using heat pipe pyrolysis

A thesis submitted for the degree of Doctor of Philosophy (PhD)

By:

John Joseph Hoslett

College of Engineering, Design and Physical Sciences, Department of Mechanical and Aerospace Engineering, Brunel University London

March 2021

for Colin William Hoslett

ABSTRACT

Water contamination and municipal waste management are two problems of global significance. The amount of municipal waste generated is expected to increase over the coming century as populations increase and become more urban in nature as developing countries become more developed. Furthermore, water contamination will also become an increasingly significant problem as developing countries become more industrialised. For this reason, solutions are needed to remove contamination from water, and to reduce the amounts of municipal waste being disposed of in unsustainable ways.

The main objective of this thesis was to assess the adsorption ability of biochar produced from mixed municipal discarded material (MMDM) in a novel heat pipe reactor. Another novelty of this thesis is that the use of heat pipes limits the pyrolysis temperature for safety reasons, dependent on the working fluid used. Consequently, biochar produced in the heat pipe reactor contains more oxygen containing functional groups. These interact with aqueous metals in complexation interactions and participate in hydrogen bonding with functional groups present in some organic contaminants.

The biochar adsorbent was characterised using scanning electron microscopy, energy dispersive x-ray analysis, x-ray diffraction crystallography, Fourier transmission infra-red spectroscopy, and Raman spectroscopy.

Following characterisation, batch adsorption experiments were conducted using either copper, methylene blue or tetracycline as the target adsorbate. Batch adsorption experiments were analysed using kinetic, diffusion and isothermal models. This thesis used the non-linear equations of adsorption kinetics and isotherms to remove the transformation errors caused through using the linear kinetic and isothermal models that are commonly used in literature.

This thesis shows that biochar produced using MMDM in a heat pipe reactor can produce an adsorbent that is comparable to other biochar in literature. Copper adsorption reached a maximum of 6.3mg/g, methylene blue adsorption reached a maximum of 7.3mg/g, and tetracycline adsorption reached a maximum of 9.84mg/g. Typically, Elovich and pseudo second order kinetic models were the best fitting adsorption kinetics, with the Langmuir isotherm best describing copper adsorption, and the dual mode isotherm best describing the methylene blue and tetracycline adsorption.

Biochar produced from MMDM is shown to be a promising adsorbent material that could be used in various water treatment applications. Further activation/functionalisation could produce an adsorbent material from discarded materials that could rival current commercial activated carbons. This highlights how this material could be used in a holistic circular economy approach to waste management and water treatment.

DECLARATION

No part of this thesis has been submitted in support of an application for any degree or qualification of Brunel University London or any other University or Institute of Learning.

ACKNOWLEDGEMENT

I would firstly like to express my thanks and gratitude to Professor Hussam Jouhara, who facilitated my research and learning over the past three and a half years. His advice, guidance, mentorship and friendship have been invaluable contributions to my time during my research. I have learned a lot from him, and I look forward to taking his influence on me into the wider world.

I would also like to thank Dr Heba Ghazal, particularly for her contributions, guidance and comments on my published research papers. Without her these publications would not have been possible.

All members of the Heat Pipe Research Group have been instrumental to my time here and my research. Particular thanks go to Navid Khordehgah, Daniel Brough, Nicolas Serey, and Darem Ahmad for their invaluable input on the heat pipe pyrolysis reactor. Without their fabrication and electrical skills, as well as their encouragement, the reactor would not be working as it is now. I would also like to thank Amisha Chauhan for her friendship and conversation over many cups of tea. Valentin Guichet also receives thanks for his friendship and encouragement. Finally, Bertrand Delpech receives my thanks for being a willing participant in philosophical and political debates over lunch breaks, as well as his friendship.

My family and friends outside of Brunel University London have also been very supportive. Special thanks go to my Mum and Dad who have been friends as well as parents during these past few years, listening, picking me up and motivating me when I've most needed it. My parents in law also receive thanks for everything they've done to support me.

I would like to end by expressing my gratitude, thanks and huge love for my wife who has been supportive, patient, honest and loving throughout my research. Without her alongside me I would have found it very difficult to reach the end of my PhD studies.

PUBLICATIONS

1. Hoslett J, Massara TM, Malamis S, Ahmad D, van den Boogaert I, Katsou E, et al. Surface water filtration using granular media and membranes: A review. Science of the Total Environment 2018;639:1268–82. https://doi.org/https://doi.org/10.1016/j.scitotenv.2018.05.247.
2. Hoslett J, Ghazal H, Ahmad D, Jouhara H. Removal of copper ions from aqueous solution using low temperature biochar derived from the pyrolysis of municipal solid waste. Science of the Total Environment 2019;673:777–89. https://doi.org/10.1016/j.scitotenv.2019.04.085.
3. Hoslett J, Ghazal H, Mohamad N, Jouhara H. Removal of methylene blue from aqueous solutions by biochar prepared from the pyrolysis of mixed municipal discarded material. Sci Total Environ 2020;714:136832. https://doi.org/https://doi.org/10.1016/j.scitotenv.2020.136832.
4. Hoslett J, Ghazal H, Katsou E, Jouhara H. The removal of tetracycline from water using biochar produced from agricultural discarded material. Science of the Total Environment 2021;751:141755. https://doi.org/https://doi.org/10.1016/j.scitotenv.2020.141755.

INTERNATIONAL CONFERENCE PAPERS

1. Hoslett J, Ahmad D, van den Boogaert I, Jouhara H. REMOVAL OF COPPER IONS FROM AQUEOUS SOLUTION USING LOW TEMPERATURE BIOCHAR DERIVED FROM THE PYROLYSIS OF MUNICIPAL SOLID WASTE USING HEAT PIPE BASED REACTOR. SEEP 2018 11th Int. Conf. Sustain. Energy Environ. Prot., 2018.
2. Hoslett J, Ghazal H, Jouhara H. Methylene blue sorption to 300oC mixed municipal discarded material derived char. Int. Conf. Adv. Energy Syst. Environ. Eng. 2019-ASEE19, 2019.

1 Table of Contents

LIST OF FIGURES

LIST OF TABLES

NOMENCLATURE

MMDM	Mixed Municipal Discarded Material
PFO	Pseudo first order kinetic model
PSO	Pseudo second order kinetic model
ELO	Elovich kinetic model
K_1	Pseudo first order kinetic rate coefficient
K_2	Pseudo second order kinetic rate coefficient
Q_e	Adsorption at equilibrium conditions
C_i	Initial adsorbate concentration
K_L	Langmuir coefficient
Q_m	Maximum adsorption capacity (Langmuir Model, Dual mode isotherm model, Sips model)
K_F	Freundlich coefficient
n	Freundlich shape coefficient
$K_{DM,nl}$	Dual mode isotherm non-linear coefficient
$K_{DM,l}$	Dual mode isotherm linear coefficient
MSE	Mean squared error
R^2	Coefficient of determination
R_L	Separation factor

1 INTRODUCTION

1.1 Motivation

Two problems of significant note in the world today are water contamination, and waste management. They are often considered as separate areas of research, however increasing focus on sustainability has focused studies on more holistic approaches to engineering problems. The production of materials targeted at water treatment is no exception, where this area has garnered increased research interest over the years with regards to sustainability [1]. Water treatment and waste management can be linked through the production of adsorbents. Indeed, agricultural and environmental residual materials are often researched as feedstock materials for the production of adsorbents through pyrolysis [1,2]. These adsorbent materials are commonly produced at pyrolysis temperatures in excess of 400^{o}C to promote the development of surface area within the adsorbent material. However, these temperatures result in the loss of oxygen and nitrogen containing functional groups which are important for adsorption mechanisms such as inner and outer sphere complexation with aqueous metals, and hydrogen bonding with functional groups in organic contaminants such as pesticides and pharmaceuticals [3]. Furthermore, many studies use specific feedstocks in an effort to maximise the sustainability and/or profits of specific enterprises. These studies therefore focus on industrial discarded materials [4]. However, mixed municipal discarded material (MMDM) originating from domestic sources also contains materials that can be pyrolyzed and possibly produce useful adsorbents. The motivation for this research was therefore to investigate the use of biochar adsorbents produced using a heat pipe reactor, derived from MMDM feedstock.

1.2 General background

1.2.1 Water pollution

Contamination enters water via different pathways largely dependent on the use of the contaminating material. Metals for example can enter surface waters through both natural processes and as a consequence of anthropogenic activities. Acid mine drainage for example is one source of heavy metal contamination, where water passing through disused mines can become contaminated with dissolved heavy metals. When this water exits the mine, surface waters become contaminated with these metals [5]. Industrial production, sewage discharge, and agricultural uses in fertilisers and pesticides are also contributors to heavy metal pollution

in water [6]. Organic compounds are also commonly found contaminants, particularly in areas where pesticides are used in agriculture and gardening practices [7]. Pharmaceutical compounds are another source of water contamination, with many emerging pollutants belonging to this category [8].

The removal of contamination is required in both drinking water and wastewater treatment plants, as such the effluent from these plants must meet standards with regards to drinking water, or wastewater effluent. As such these treatment plants make use of a number of processes including sedimentation, coagulation-flocculation, granular/membrane filtration processes, adsorption and chlorination processes in the case of drinking water treatment plants [9]. Wastewater treatment plants use screens, grit removal, primary settling tanks, aeration tanks, secondary settling tanks, and disinfection to remove contaminants from water, with anaerobic digestion and dewatering used to produce energy from the remaining sludge [10]. Some of these processes are ineffective against some common pollutants such as heavy metals and pesticides, and have recently been shown to be ineffective against emerging pollutants such as pharmaceuticals [11]. Consequently, existing and new processes and materials are required to remove these pollutants from drinking water sources and wastewater effluent. Some of these processes are cheaper than others with adsorbents being amongst the cheaper options when compared to more advanced processes such as ozonation, reverse osmosis and nanofiltration [11].

1.2.2 Waste management

The world bank group has found that 36.6% of waste globally goes to landfill and 33% being placed in open dumps. With 77% of global waste being composed of discarded food, paper/cardboard, wood, plastic, leather and textiles [12]. Municipal waste accounts for 5% of the globes total carbon emissions, primarily due to the release of greenhouse gases from landfill and open dumps. 50% of the carbon emissions from municipal waste are attributed to the discarded food materials in municipal waste. As the global population increases, more municipal waste will be produced resulting in increased carbon emissions from municipal waste if new processes aren't adopted that have lower carbon footprints. Pyrolysis is shown to be a waste management technology that has a smaller carbon footprint than other waste management processes including landfill, and incineration, whilst also being capable to process materials that cannot be processed by composting and anaerobic digestion [13]. Heat

pipes have been implemented in a reactor using domestic waste as a fuel to produce hot water, as well as supplying gases to a household boiler system [14]. It is possible that this same technology could be used to produce adsorbent materials for use in water treatment systems. The temperatures of heat pipe pyrolysis are lower than 400^{o}C, varying depending on the working fluid used in the heat pipes, whereas most biochar produced in literature for use as an adsorbent is produced at temperatures in excess of 400^{o}C.

1.2.3 Low temperature biochar and its properties

Low temperature biochar is an adsorbent material that has not often been investigated as biochar produced at higher temperatures tend to have greater surface areas. This increase in surface area usually results in the increased adsorption of target pollutants as more active sites are available for adsorption processes to take place [3]. However, recent literature has shown that adsorbents produced at lower pyrolysis temperatures are also effective in the removal of aqueous contaminants such as polar organic molecules and heavy metals such as copper [15]. These materials tend to have increased levels of oxygen, and nitrogen which means there is greater potential for inner and outer sphere complexation between aqueous metals [16], as well as increased hydrogen bonding between functional groups present in organic contaminants including some pesticides and pharmaceuticals [17]. However, adsorption studies often use specific feedstocks for pyrolysis, there is consequently a gap in research when it comes to the pyrolysis of mixed feedstocks such as municipal discarded material.

1.3 Aim and objectives of the research

Adsorbents are usually produced using specific feedstocks, with specific industries benefitting from these studies. However, little has been done to produce and research adsorbents both from mixed municipal discarded material (MMDM), at lower pyrolysis temperatures. Furthermore, heat pipe pyrolysis reactors are a new development in the area of waste management and could potentially be used to produce low pyrolysis temperature biochar adsorbents. The objectives of this research are:

- To produce an adsorbent from municipal waste.
- To produce adsorbents using a heat pipe based reactor.

- To characterise the adsorbents produced allowing for comparison with adsorbents produced in literature.
- To assess how well the produced adsorbents remove various contaminants.

The overall objective of this thesis is therefore to show whether MMDM biochar derived from heat pipe pyrolysis can be used as a cheap adsorbent material, and what uses this material may be applicable to. This thesis will achieve these objectives through the following approach:

- Biochar characterisation will be conducted to provide an insight into the material characteristics. This will be done using scanning electron microscopy, energy dispersive X-Ray analysis, Fourier transmission infra-red spectroscopy, X-Ray diffraction crystallography, and Raman spectroscopy.
- Batch experiments will be conducted using three different contaminants, namely copper, methylene blue and tetracycline. These will give an insight into the MMDM biochar ability to remove heavy metals, ionic organic contamination, and pharmaceutical contaminants.
- Kinetic models will be applied to the experimental data to ascertain which kinetic model best describes the adsorption of each contaminant under the experimental conditions used. This will reveal part of the nature of adsorption to MMDM biochar.
- Isothermal models will also be applied to experimental data to determine which model best describes the isothermal behaviour of the MMDM biochar. This will also reveal insights into the adsorption of the three different pollutants to MMDM biochar.
- Diffusion models will also be applied to experimental data to describe the diffusion behaviour of various pollutants into the produced adsorbents.
- Both kinetic models and isothermal models will be fitted to the experimental data using non-linear regression techniques. The majority of literature uses linearised models resulting in transformation errors, and the inaccurate use of statistical analysis to determine the best fitting models. The application of non-linear regression using SAS statistical modelling software is a contribution to existing knowledge where related future research could apply the same technique using the same/similar software to determine the best fitting models without transformation errors from the more easily applied linearised models.

This approach is reflected in the structure of this thesis shown in Figure 1.1.

1.4 Thesis outline

The thesis was structured like this to provide clarity to the reader, as well as to reflect the chronological timeline of the production and use of biochar as an adsorbent. Producing the adsorbent is the first step, followed by characterisation, the final step is the use of the biochar to remove pollutants which can vary. Consequently, chapters 5, 6 and 7 are regarded as the same stage prior to the conclusion of the research.

Chapter 1. This chapter is the introductory chapter to the thesis, outlining the motivation, objectives and methodology used throughout the thesis. This chapter also provides an overview of all of the chapters in the thesis.

Chapter 2. This chapter presents a state of the art of the main technologies used in water treatment processes including membrane and granular media processes, the main benefits of using pyrolysis compared with other waste management procedures, and the processes by which adsorption to biochar materials can occur with respect to the pyrolysis conditions used to produce them.

Chapter 3. This chapter outlines the materials, methodologies and model equations used to determine the behaviour of the biochar adsorbents.

Chapter 4. This chapter presents a characterisation of the produced biochar based on data collected using X-ray diffraction crystallography, Fourier Transmission Infra-Red spectroscopy, Scanning electron Microscopy, Energy Dispersive X-Ray Analysis, and Raman spectroscopy characterisation techniques.

Chapter 5. This chapter analyses the adsorption of copper to the produced biochar using kinetic, isotherm and diffusion models as well as a discussion comparing the copper adsorption to MMDM biochar to data collected from similar studies. This chapter ends by suggesting applications for MMDM biochar with regards to copper removal, as well as suggesting methods of improving the copper adsorption performance of the MMDM biochar.

Chapter 6. This chapter analyses the adsorption of methylene blue to the produced biochar using kinetic, isotherm and diffusion models as well as a discussion comparing methylene blue removal by MMDM biochar to data collected from similar studies. This chapter ends by suggesting applications for MMDM biochar with regards to the removal of methylene blue and other persistent organic contaminants such as pesticides.

Methods of improving the adsorption of methylene blue and other similar contaminants to the MMDM biochar are also suggested.

Chapter 7. This chapter analyses the adsorption of Tetracycline to MMDM biochar using kinetic, isotherm and diffusion models as well as a discussion comparing tetracycline removal by MMDM biochar to data collected from similar studies. This chapter ends by suggesting applications for MMDM biochar with regards to the removal of tetracycline and other biologically significant contaminants including antibiotics. Methods of improving the adsorption of tetracycline and other similar contaminants to the MMDM biochar are also suggested.

Chapter 8. This chapter lays out the conclusions of this thesis and suggests ways in which research into MMDM biochar produced using heat pipe reactors can be further researched.

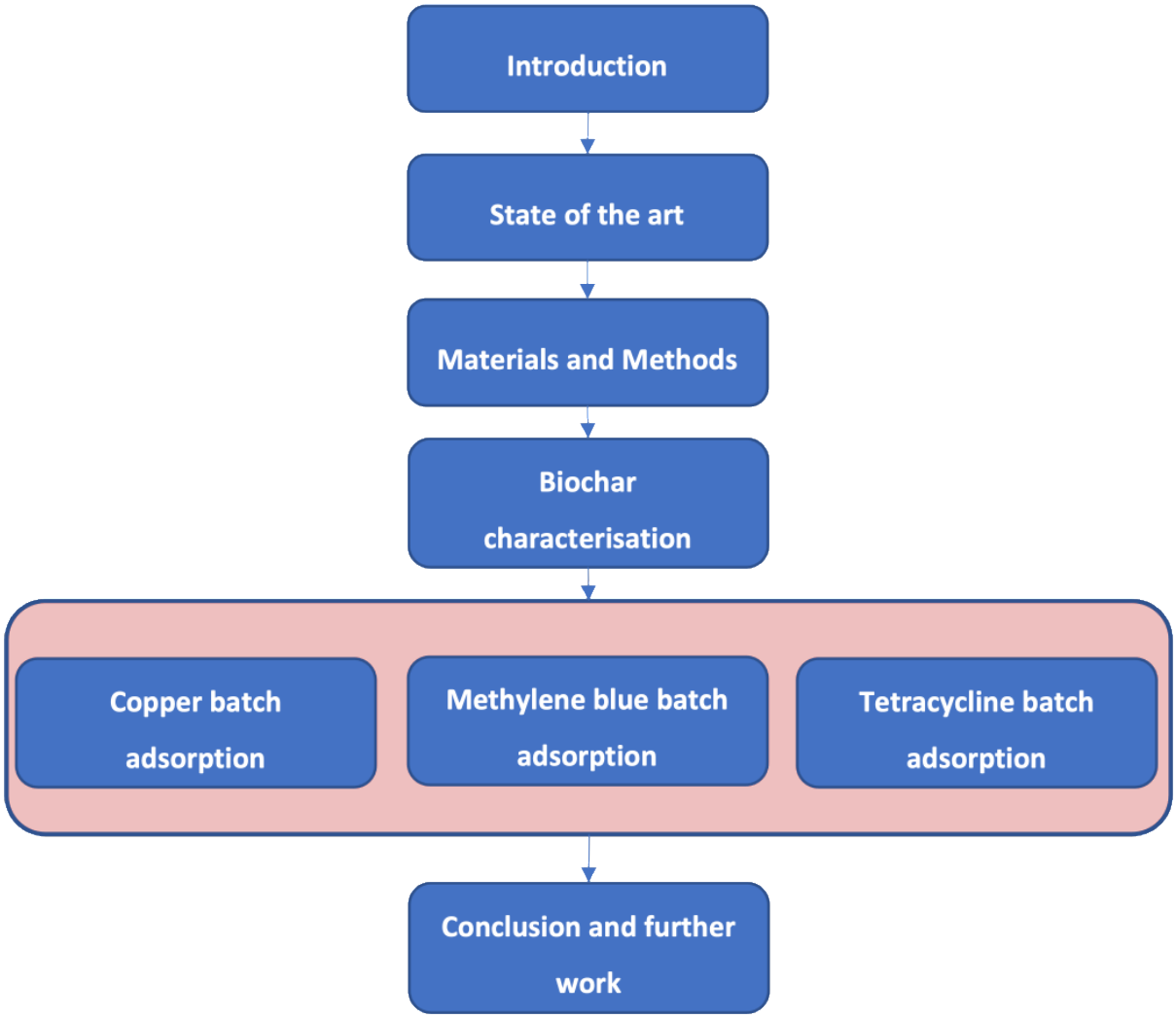

Figure 1.1 – Thesis outline

2 STATE OF THE ART ON WATER TREATMENT METHODS

The Earth's surface is around 71% water that is mostly saline. Water is also present in the ground, air and within living organisms [18]. Climate change, population growth and increased urbanization pose huge challenges to water supply systems and place an ever-increasing demand on the finite freshwater resources. The World Health Organisation (WHO) estimates that 844 million people worldwide lack a safe drinking-water service, including 159 million people who are dependent on surface water. The United Nations (UN) Sustainable Development Goal Six calls for countries to ensure universal and equitable access to safe and affordable drinking water by 2030 [19]. Investing in efficient and cost-effective treatment technologies is essential to mitigate against the effect of water scarcity especially in low and low-middle income countries. This chapter will explore factors affecting the supply of potable water and will introduce the water quality standards required for water to be considered potable, as well as the water treatment processes currently used in household water treatment applications.

2.1 Socio-economic effects on drinking water coverage throughout the world

It is important to understand the economic and social factors affecting the consumption of a basic water supply. The Joint Monitoring Programme (JMP) defines a basic water supply as one that provides acceptable quality water, within a 30-minute round trip of the consumer [20]. Figure 2.1 and Figure 2.2 show the basic water supply for urban and rural communities, respectively. Five relative income levels are shown from poorest to richest. The most notable observation from Figure 2.1 and Figure 2.2 is that the basic supply coverage increases with population percentage towards a point where the relative income levels account for equal proportions of the population percentage. This concentration of data values indicates that a Lorenz curve showing cumulative wealth (%) plotted against cumulative population (%) would be close to the equality line, for a society with almost 100% access to an at least basic supply [21]. This shows that wealth distribution potentially has a significant impact on basic water supply coverage or vice versa. This is more pronounced in urban areas than in rural areas. Wealth distribution could also be indicative of other factors that also affect basic water supply coverage. The lower R^2 values in rural areas suggest that other factors have a more significant impact on variation in basic supply coverage than is the case in urban areas. Another notable observation is that urban areas show a much lower data range for both population percentage

in different income levels, and basic supply coverage compared to rural areas. The inequality between higher and lower relative incomes is visible in both urban and rural areas where poorer income levels typically tend to have lower basic supply coverage. The inequality between urban and rural areas is also observable where the range of basic supply coverage in urban areas is 40-100% compared to 15-100% in rural areas. This may be explained due to rural areas having lower population densities, and thus increased distance between user and water source [22].

Figure 2.1 – Figure showing Basic Supply Coverage Against Percentage of Population in a Given Relative Income Level in the Urban Population

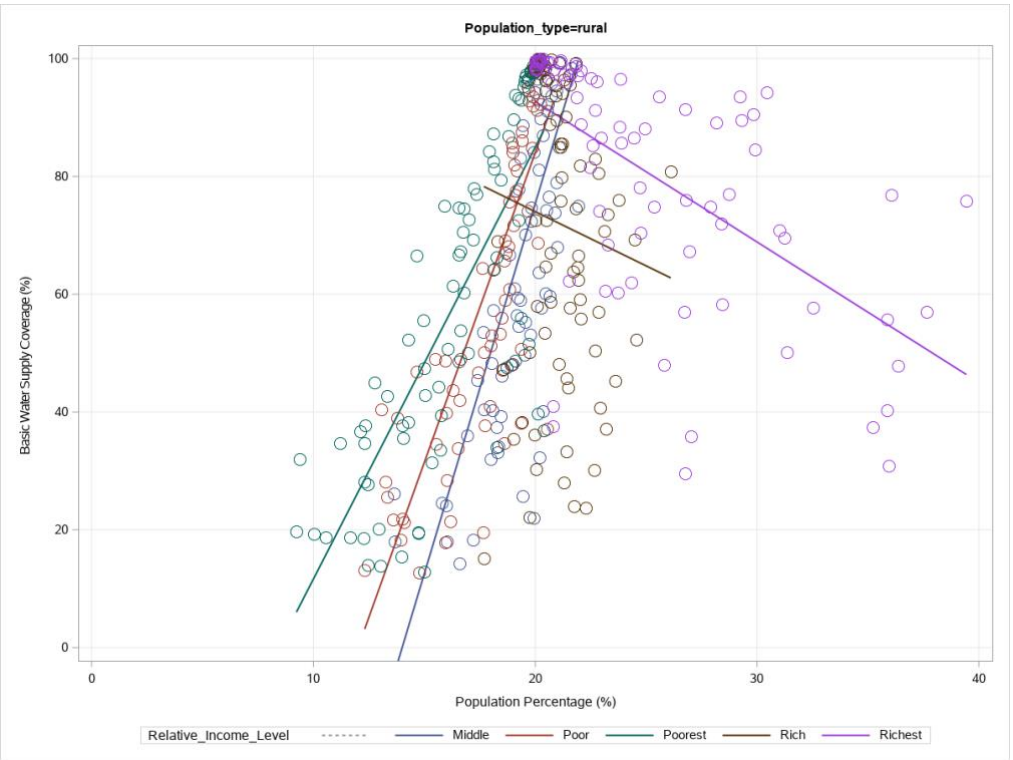

Figure 2.2 – Figure showing Basic Supply Coverage Against Percentage of Population in a Given Relative Income Level in the Urban Population

Table 2.1 – Table showing linear regression analysis for **Error! Reference source not found.**

and

Figure 2.2 – Figure showing Basic Supply Coverage Against Percentage of Population in a Given Relative Income Level in the Urban Population

Relative Income Level	Population Type	Coefficient	R^2	p-value	Statistically significant?
Poorest	Urban	7.339	0.9311	<0.05	Yes
Poor	Urban	11.473	0.6973	<0.05	Yes
Middle	Urban	-1.643	0.0106	0.357	No
Rich	Urban	-2.745	0.2215	<0.05	Yes
Richest	Urban	4.545	0.1694	<0.05	Yes
Poorest	Rural	7.333	0.6240	<0.05	Yes
Poor	Rural	10.521	0.6800	<0.05	Yes
Middle	Rural	12.568	0.5298	<0.05	Yes

Rich	Rural	-1.841	0.0107	0.354	No
Richest	Rural	-2.385	0.3543	<0.05	Yes

Figure 2.3 shows a scatter chart in which the joint monitoring programme's data on different types of water supply coverage are plotted against GDP per capita data from the world bank group. What is shown is that as GDP per capita decreases, the reliance on surface water, limited services, and unimproved sources increases. This is probably not a direct link, however, using GDP per capita as an indicator of a country's development it is clear that less developed countries still use less than basic water supplies.

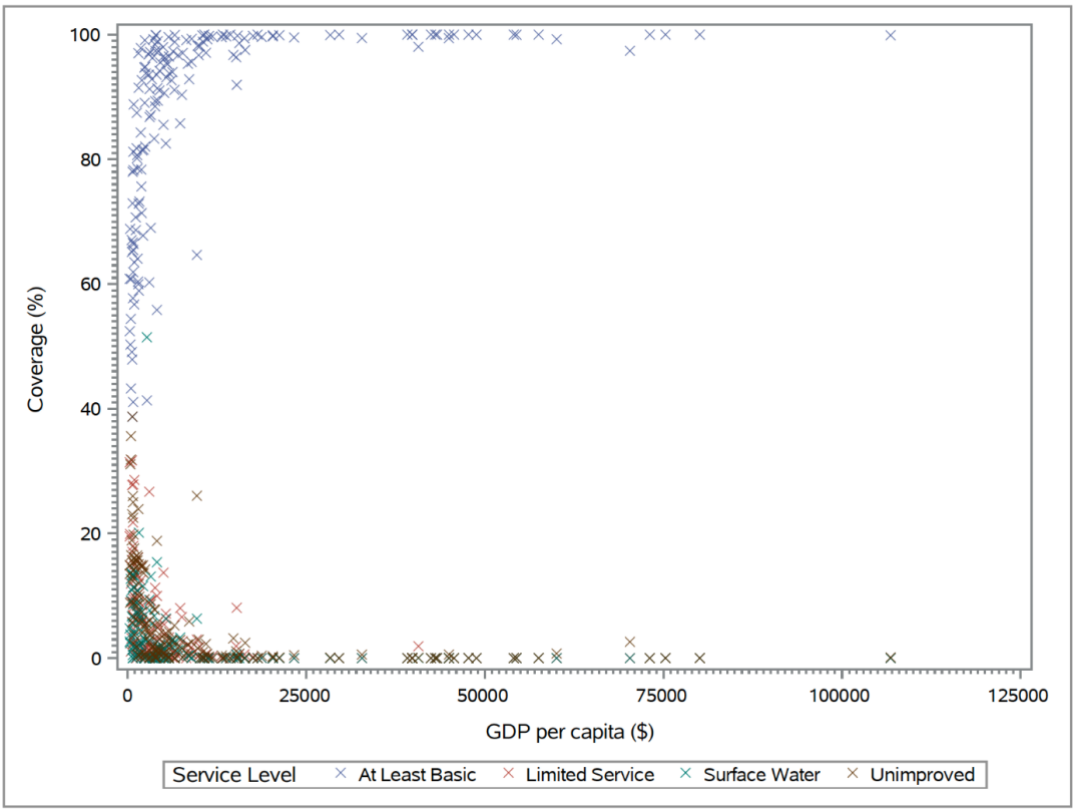

Figure 2.3 – Bubble plot showing Service level coverage against GDP per capita, with bubbles weighted by population supplied

Figure 2.4 shows the coverage of "At least basic" water supply in terms of population percentage plotted against GDP per capita, with rural population % shown as a colour response. The figure clearly shows that at least basic supply coverage in low-income rural countries is lower than in higher income, more urban countries.

It is easier to provide a basic supply to an urban population than a more rural one since urban populations have greater population densities. Despite this fact, urban slum areas can be deprived of a basic water supply as is evidenced in Figure 2.1[23]. Rural communities also become more isolated as countries develop with populations becoming more urban. This makes providing a centralised water supply to rural communities problematic for several reasons. Pumping suitable potable water would represent a significant expense with 25-50% energy consumption of the water industry being in pumping [24]. Pumped water systems also require expert knowledge, a well-designed distribution network and regular maintenance [25]. Money and expertise are not abundant in developing nations, therefore finding ways to reduce the cost of water treatment is of paramount importance for such nations, as well as finding methods to improve the sustainability of water treatment in more developed nations.

It can be seen in Figure 2.3 that in low-income countries, as much as 40% of the water supply can be from less than basic water supplies which include surface water and unimproved sources such as contaminated groundwater. A water treatment method that can produce potable water from such water sources could therefore have a dramatic effect on the number of people without access to an “at least basic” supply.

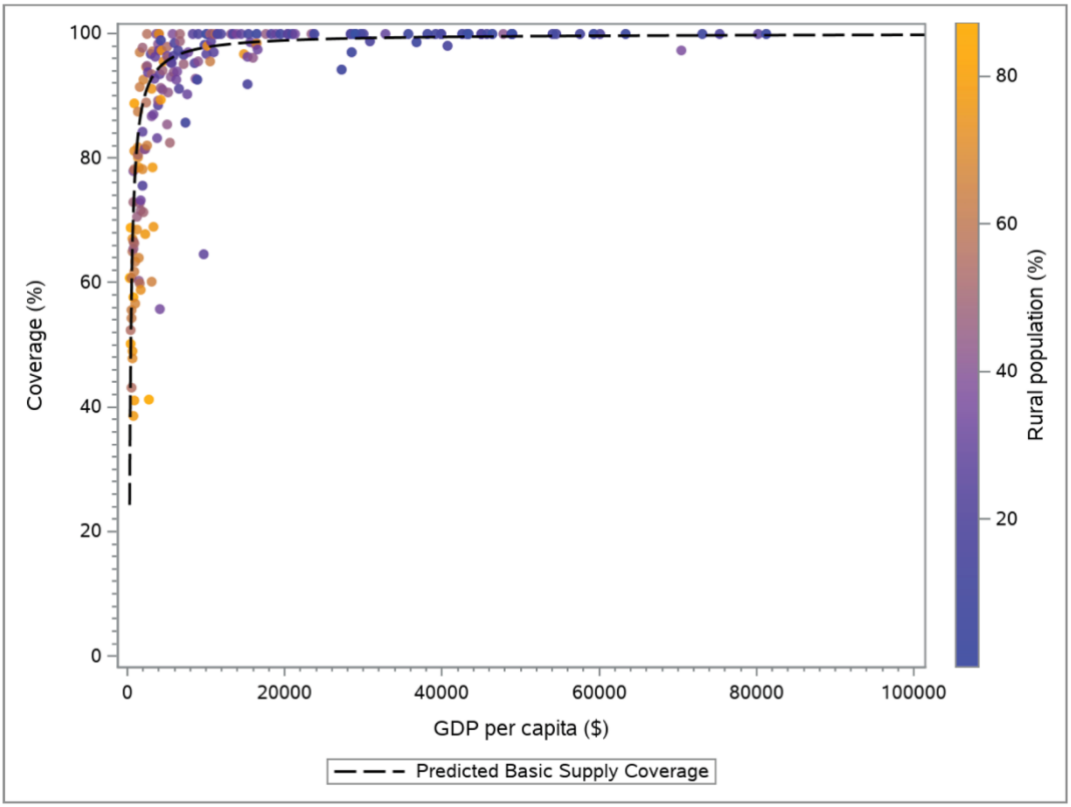

Figure 2.4 – Figure showing Basic Coverage plotted against GDP per capita

2.2 Natural and Anthropogenic Effects on Surface Water

Due to the variability in geological strata and other factors such as soil type, altitude, ecology supported by a certain water body, etc., surface water quality can vary for different areas. For instance, more natural/background organic content is expected in humic waters than in non-humic ones. Hence, the dissolved organic carbon (DOC) concentrations in surface waters vary depending on the type of water environment [26]. Evidently this means water treatment which uses surface water as a source needs to be versatile in order to produce drinking water that is within the drinking water standards set out by the world health organisation (WHO) [27].

Anthropogenic activity also plays a large role in the quality of surface water globally. Specific industries can lead to the contamination of waters with a wide range of different pollutants which must be removed from water to make it potable. This is an issue of particular significance in developing nations where industrial standards are enforced less stringently [28]. Consequently, surface water in a developing nation can potentially be more highly polluted than surface water found in more developed nations, where industrial standards are more stringent. Industrial activity varies geospatially, being highly dependent on the location

of raw materials, population, and market access [29–31]. Therefore, industrial pollution of surface water also varies geospatially. In addition to industry, domestic and agricultural environments also have an impact on surface water quality. Run-off water in urban areas can for example wash elevated levels of nutrients, heavy metals, organic compounds and particulate matter into surface water systems during precipitation events [32,33]. Agricultural activities such as fertilisation can also result in the increase of nutrients and organic compounds in surface waters [34]. Additionally, the use of pesticides in such activities pollutes surface water with both pesticides and their degradation products [35]. The sources of water pollution are important to note as a water treatment system must be able to reduce/remove all contamination to an acceptable level if water is to be made potable.

2.2.1 Typical Problems in Surface Water

2.2.1.1 Nitrogen (N)

Nitrogen (N) is present in water mainly in three forms: i.e. ammonium (NH_4^+), nitrite (NO_2^-), and nitrate (NO_3^-). These are parts of the "nitrification chain" with NH_4^+ as the first link and NO_3^- as the last one before its conversion into nitrogen gas (N_2). Nitrogenous pollutants are significant as they are particularly harmful when ingested; NO_3^-, specifically, is linked to the "blue baby syndrome" that is potentially fatal [36]. Nitrogen is removed in conventional water treatment processes through the use of biological processes. These include aerobic conditions and anaerobic/anoxic conditions. Aerobic bacteria are responsible for the production of nitrates from ammonium, the nitrates are then metabolised in anaerobic/anoxic conditions where other bacteria are forced to metabolise oxygen found in nitrates due to the lack of dissolved oxygen, releasing nitrogen gas [37].

2.2.1.2 Eutrophication

Another problem in surface waters is eutrophication. When an excess of nutrients enters a water body, an algal bloom occurs inducing increased consumption of the dissolved oxygen in the water. This is particularly an issue in still waters such as ponds and lakes. Eutrophication issues are difficult to predict and result from the application of chemical fertilisers, as well as from nutrient leaching and wastewater discharge to surface water [38,39].

Another issue related to eutrophication is the appearance of cyano-bacteria in surface water. These micro-organisms can produce cyano-toxins that are harmful to many higher organisms

such as fish, cattle and humans [40]. Thus, it is not only important to treat wastewater discharged to surface water for nutrients, but also to disinfect the water to inactivate bacteria [41]. A common source of municipal, agricultural and industrial water are lakes and reservoirs. These are susceptible to environmental changes as they have low flow velocity; the latter is translated into a decreased natural ability to replenish dissolved oxygen. Eutrophication can thus cause significant issues [42]. Nutrients and natural organic matter can be removed by processes such as activated sludge and sand filtration, and the microorganisms produced due to the nutrient enrichment can be removed by microfiltration and ultrafiltration [43–45].

2.2.1.3 Heavy Metals

Heavy metal concentrations that generate short-term contamination events in surface water principally originate from anthropogenic activities (e.g. coal burning, mining, pesticide use, battery production and disposal, welding, etc.). Over time, ecosystems usually adapt to cope with elevated heavy metal levels of natural origin [46]. Heavy metals and metalloids, especially cadmium (Cd), zinc (Zn), lead (Pb) and Arsenic (As), are of particular concern; once an organism absorbs them, there is no easy excretion. Hence, they are bio-accumulated in food chains [47–50]. Surface water is also heavily affected by industrial effluents. For instance, a case study in Bangladesh found that surface water near industrial areas is likely to be contaminated with a variety of pollutants including NO_3^-, phosphates (PO_4^{3-}), heavy metals, As, etc [51]. Specifically, surface water near a coal fired power station was found with PO_4^{3-}, Cd and iron (Fe) concentrations exceeding the World Health Organization (WHO) guidelines. Similarly, another case study concluded that heavy metal concentrations are expected to be higher in urban rather than rural areas [42].

Heavy metals and metalloids are commonly removed from wastewater and surface water using granular activated carbon. However, this can require process optimization to achieve higher/complete removal [52]. Forward osmosis and reverse osmosis can alternatively be used. A “draw solution” that requires the addition of solute including ammonium bicarbonate (NH_4HCO_3) is used in forward osmosis. However, these chemicals need to be removed from the treated water to be considered safe for reuse. Hydraulic pressure is applied in reverse osmosis, thus causing it to have a higher power consumption than forward osmosis [53]. According to more recent advances, ultra- and nanofiltration can also remove some heavy metals and metalloids [54,55].

2.3 Principles of Water Treatment

The WHO issues guidelines in contaminant parameters that must be met for water to be considered safe and drinkable. It also sets guidelines for the performance of specific parts of a water treatment system. This involves different guidelines for centralised and decentralised systems. Some components of centralised systems are beyond what is achievable in decentralised systems, thus other methods are adopted in decentralised solutions to remove pollution to similar standards [56].

Water treatment aims at producing water which respects the quality standards that depend on its use after treatment [57]. In developed countries, surface water is processed in wastewater treatment plants and drinking water treatment plants which apply various treatment steps including coarse and fine screening, sedimentation, coagulation/flocculation, various filtration methods, AS, primary and residual disinfection, etc. [58].

Each method usually targets specific pollutant groups. For example, activated sludge processes remove natural organic matter, NO_3^- and PO_4^{3-} from wastewater [44,59–61]. Coagulation and flocculation remove ionic/colloidal material such as clay particles and dissolved metals. Filtration and disinfection are required for the remaining material such as bacteria, viruses and other dissolved metals [62–71].

The focus from herein will be on filtration (microfiltration, ultrafiltration, nanofiltration, reverse osmosis, and sand filtration) and granular activated carbons that target specific pollutants such as heavy metals and metalloids (e.g. Cd, Pb, As, copper (Cu)), and indicator parameters (e.g. total organic carbon, E. Coli, oil emulsions, etc.). The methods assessed will be compared as such with the WHO guidelines [WHO, 2017a, b]. In recent years, each of these methods has been the focus of research. Hence, this literature review presents an overview of the microfiltration, ultrafiltration, nanofiltration, reverse osmosis, sand filtration and granular activated carbon systems in terms of efficiency, and cost aspects.

2.4 Comparison of water filtration methods

2.4.1 Membrane Filtration Methods

Membrane filtration consists of a single layer of material (i.e. membrane) allowing water and potentially a part of the dissolved or suspended material to pass. Specifically, microfiltration, ultrafiltration, and nanofiltration can filter out 0.5 - 5, 0.005 - 0.5 and 0.0007

- 0.005 micron particles, respectively. Reverse osmosis can remove almost all contaminants larger than a water molecule [72]. Membranes are usually made of woven fibres [43], ceramics [73], polymeric or metallic materials [74]. They can also be modified to improve their performance; for example, decrease fouling [75], or increase the removal of specific pollutants (e.g. As) [76].

2.4.2 Micro and Ultrafiltration

Microfiltration does not remove the smaller particles that ultrafiltration and nanofiltration can remove. However, it is effective in eliminating bacteria [43]. Microfiltration can be used in domestic water recycling systems [77]. Moreover, it can constitute a pre-treatment stage before ultrafiltration, nanofiltration, and reverse osmosis [78], thus reducing the possibility of fouling these processes since it removes potential foulants (i.e. bacteria) [79]. If the microfiltration flux is to be kept constant, then transmembrane pressure is to be augmented as the resistance of the fouling cake across the filter becomes increasingly influential with time. Therefore, it is necessary to backwash or clean the filters when they become overly fouled [78]. *Table 2.2* presents the main findings of several studies investigating the performance of microfiltration/ultrafiltration systems applied for the removal of organic pollutants such as oil and algae.

Table 2.2. Overview of studies on the performance of microfiltration/ultrafiltration systems implemented for the removal of specific pollutants.

Filter Material	Filter Production	Pollutant	Trans Membrane Pressure	Filtration Configuration	Main Findings & Observations	Source
Ceramic	Clay powders mixed with polyvinyl alcohol; membrane modified with TiO_2 nanoparticles	200 mg L^{-1} crude oil	69-207kPa	Cross-flow *microfiltration*	93-100% rejection of oil emulsion: ceramic support 99-100% rejection of oil emulsion: ceramic support modified with TiO_2 TiO_2 increased hydrophilicity & flux across the membrane High oil retention: effective removal of total organic carbon No assessment of biological parameters or other (inorganic) contaminants	[80] [80]
Anodisc	Anodised alumina	10-30% oil emulsion	25-100kPa	Dead-end filtration *microfiltration*	Complete retention: effective total organic carbon removal no assessment of biological parameters or other (inorganic) contaminants	[81] [81]
Polycarbonate (PCTE)	PCTE membrane modified with polyvinylpyrrolidone to enhance hydrophilicity	10-30% oil emulsion	25-100kPa	Dead-end filtration *microfiltration*	Partial total organic carbon removal Larger oil particles broken into smaller particles No assessment of biological parameters or other (inorganic) contaminants	[81] [81]
Cellulose acetate	Sartorius AG cellulose acetate membrane	10-30% oil emulsion	25-100kPa	Dead-end filtration *microfiltration*	No retention but oil particle size reduced Filter not satisfying WHO guidelines on organic/ inorganic contaminants	[81] [81]

***Table 2.2**. Continued*

Hydrophilic mixed cellulose ester membrane	Corning cellulose ester filter membrane	10 mg L^{-1} Chlorella sp. (algae); polymethylmethacrylate 10-40 mg L^{-1}	20, 40, 60 kPa	Cross-flow *microfiltration*	Presence of Polymethyl methacrylate (PMMA) particles increased algal cake porosity & reduced its compressibility Lesser final flux possibly due to algal cake compression by drag forces No assessment of organic/inorganic contaminants	[82] [82]
Ceramic	80 wt% fly ash	50-200 mg L^{-1} oil emulsion	69-345kPa	Dead-end *microfiltration*	80-85% rejection for 50 mg L^{-1} oil emulsion (decreasing with increasing pressure) 92-99.94% rejection for 200 mg L^{-1} oil emulsion (decreasing with increasing pressure) No assessment of inorganic contaminants	[83] [83]
Ceramic	70 wt% fly ash	50-200 mg L^{-1} oil emulsion	69-345kPa	Dead-end *microfiltration*	68-82% rejection for 50 mg L^{-1} oil emulsion (decreasing with increasing pressure) 87-96% rejection for 200 mg L^{-1} oil emulsion (decreasing with increasing pressure) No assessment of organic/inorganic contaminants	[83] [83]
Ceramic	14.5 wt% Kaolin; 17.6wt% clay	50-200 mg L^{-1} oil emulsion	69-35kPa	Dead-end *microfiltration/ultrafiltration*	93-96% rejection for 50 mg L^{-1} oil emulsion (decreasing with increasing pressure) 71-86.5% rejection for 200 mg L^{-1} oil emulsion (decreasing with increasing pressure) No assessment of organic/inorganic contaminants	[84] [84]
Ceramic	14.5 wt% Kaolin; 17.6% clay; modified with TiO_2	50-200 mg L^{-1} oil emulsion	69-35kPa	Dead-end *microfiltration/ultrafiltration*	97-99% rejection for 50 mg L^{-1} oil emulsion (decreasing with increasing pressure) 84-92% rejection for 200 mg L^{-1} oil emulsion (decreasing with increasing pressure) No assessment of organic/inorganic contaminants	[84] [84]

Table *2.2* is indicative of the major research that has been conducted regarding microfiltration/ultrafiltration and the pollutants they can remove from water (natural organic matter is the principal one); impressive if not complete retention results have been noted [e.g. [80,83,84]].

2.4.3 Nanofiltration and Reverse Osmosis

Nanofiltration is used to remove larger solutes than reverse osmosis. In terms of size of removed contaminant, it lies between ultrafiltration and reverse osmosis; nanofiltration is effective at removing particles between 100-1,000 Daltons in size [85,86]. Nevertheless, nanofiltration membranes can foul quickly due to their small pore sizes unless sufficient pre-treatment steps (e.g. coagulation, microfiltration) are undertaken [87]. Compared to reverse osmosis, nanofiltration is less effective at filtering ions from water, but more cost-effective as lower transmembrane pressures are required to produce the same permeate flow of water [88]. For certain contaminants (e.g. pharmaceutically active compounds), nanofiltration generally shows greater removal capability than ultrafiltration [89]. ultrafiltration, nanofiltration, and reverse osmosis can all be chemically adjusted to improve the removal of specific contaminants. For instance, it was found that increasing the solution pH from 4 to 10 increased the removal of arsenates (AsO_4^{3-} or As(V)), arsenites (AsO_3^{3-} or As(III)), chromates (CrO_4^{2-}), and perchlorates (ClO_4^-). On the contrary, increasing the solution conductivity produced the opposite phenomena [90].

Reverse osmosis is a membrane process that removes ions from water by providing hydraulic pressure to overcome the osmotic pressure, thus reversing the natural flow of water towards the more concentrated solution. Therefore, this process requires energy to generate the pressure required to overcome osmotic pressure. Furthermore, pre-treatment of the feed water through other processes (e.g. microfiltration, nanofiltration) is needed to remove bacteria, viruses and larger ions that are likely to generate reverse osmosis fouling problems [91,92].

Recent advances in the reverse osmosis treatment include the introduction of forward osmosis as an added improvement. Being a natural process, it does not require any energy input. Hence, it can greatly decrease the amount of applied pressure required in the reverse osmosis step to overcome the osmotic pressure difference [93]. The forward osmosis

membrane can be partially self-cleaning with the fouling material being simply sheared off by flow. Even in this case, however, fouling gradually occurs and membrane replacement/remediation is still required. For this reason, combatting forward osmosis fouling by operating at a higher cross flow velocity has been suggested [94]. Especially for desalination purposes, forward osmosis membranes can be applied with wastewater as the feed solution and seawater as the draw solution; this results in diluting the seawater, as well as in water recovery from wastewater [95]. Research is also needed particularly with regard to draw solutes; inorganic draw solutes are amongst the least researched in this field [96].

The reverse osmosis performance is influenced by various parameters. For example, membrane permeability depends on temperature and the difference between hydraulic and osmotic pressure. During desalination, initial salt concentrations along with temperature significantly impact on the final salt rejection, thus affecting the quality of produced reverse osmosis effluent [97,98]. Furthermore, greater pressure is connected with higher water recovery [99]. However, if pre-treatment and membrane coatings are used, poor reverse osmosis membrane performance due to fouling can be prevented [100,101]. **Table 2.3** shows the removal of ionic material by reverse osmosis and nanofiltration.

Table 2.3. *Overview of studies presenting the efficiency of reverse osmosis and nanofiltration for the removal of ionic material.*

Filter Material	Filter Production	Pollutant	TMP	Filtration Configuration	Pollutant Removal	Source
Polyamide	Filter TW30-4040 (DOW corporation)	As(III): 100 µg L^{-1} As(V): 100 µg L^{-1}	1.5MPa	Cross-flow reverse osmosis	As(V): ≈100% As(III): 77-81% after 1st filtration; 95% after 2nd filtration Almost respecting WHO guideline after 1st filtration; <WHO benchmark after 2nd filtration	[102] [102]
Polyamide	SG1812C-28D reverse osmosis spiral membrane	Firefighting water; fluorinated surfactant: 20 mg L^{-1}	2MPa	Cross-flow reverse osmosis	Fluorinated surfactant: 99.9% fluoride concentration<WHO benchmark	[103] [103]
Polyamide	XLE Filmtec	Swimming pool water; haloacetic acid: 100 µg L^{-1}	0.69MPa	Cross-flow reverse osmosis	Haloacetic acid: 80-100%	[58] [58]
Cellulose Acetate	SB50 TriSep	Swimming pool water; haloacetic acid: 100 µg L^{-1}	0.69MPa	Cross-flow reverse osmosis	Haloacetic acid: 50-100%	[58] [58]
Polyamide	XLE Filmtec	Domestic grey water; NaCl: 50 mg L^{-1}	0.69MPa	Cross-flow reverse osmosis	NaCl:77-85%	[104] [104]
Amine-functionalized thin-film	Interfacial polymerisation (modified with multiwalled carbon nanotube)	NaCl: 2,000 mg L^{-1}	1.5MPa	Cross-flow reverse osmosis	NaCl: 95-97.2%	[105] [105]
RO thin-film	Espa 2 (Hydranautics)	NO_3: 15.5 mg L^{-1} NH_4: 9.53 mg L^{-1}	1.5MPa	Cross-flow reverse osmosis	NO_3: 97.4% NH_4: 90.8%	[106] [106]
Polyamide	BW30 (Filmtec)	Ca: 451.2 mg L^{-1} Cl: 81.6 mg L^{-1} SO_4: 1,101.7 mg L^{-1}	0.5-2.5MPa	Cross-flow reverse osmosis	Ca: 99% Cl: 96-99% SO_4: 98-100%	[107] [107]
Polyamide	SS-NF1-2540: RisingSun Membrane	NaCl: 100 mg L^{-1} $MgSO_4$: 100 mg L^{-1}	0.414-0.828MPa	Cross-flow nanofiltration	Up to 60%	[108] [108]

Table 2.3 *Continued.*

Polyamide	JCM-1812-50N by JCM	Na: 14,864 mg L^{-1} Ba: 209 mg L^{-1} Ni: 6.2 mg L^{-1} TDS: 61,500 mg L^{-1} Cr: 5.3 mg L^{-1}	0.758MPa	Cross-flow nanofiltration	Na: 79.6% Ba: 85.3%; >WHO benchmark; additional treatment needed Ni: 77.4%; >WHO benchmark; additional treatment needed TDS: 56.3% Cr: 58.5%; >WHO benchmark; additional treatment needed	[109] [109]

According to the data reported in **Table 2.3**, reverse osmosis/nanofiltration can remove ionic material to an impressive extent [e.g. [102,105,110]]. It can also be noted that most of the implemented membranes are made of polyamide (i.e. non-woven polyester fabric membranes coated in monomers) [e.g. [102–104]]. These membranes are thin and fragile, produced through interfacial polymerisation. Given that they can be damaged after contact with free chlorine radicals, using them after disinfection is ill advised [111,112]. Another observation resulting from **Table 2.3** is that reverse osmosis is not an impenetrable barrier to ionic material. Even though greater than 95% retention rates are attained [e.g. [105,107]], complete retention of target pollutants is hard to achieve [e.g. [108,109]]. Moreover, it can be seen that As(V) is more easily removed than As(III), probably due to physical changes in As(III). This could be the case for other elements such as iron (Fe(II) and Fe(III)) at different oxidation states in reverse osmosis [102].

Reverse osmosis/nanofiltration membranes require certain technical chemical knowledge and involve complicated production processes. In addition, training and expertise is important to run the reverse osmosis /nanofiltration processes due to their sensitivity to environmental factors such as temperature, pollutant concentration, etc. As previously discussed, reverse osmosis can be used in conjunction with forward osmosis to recover water from wastewater streams. Nevertheless, the latter is not a priority in developing countries that mainly focus on the production of safe drinking water. microfiltration, ultrafiltration and other granular filter media remove larger contaminants (e.g. microbes and extracellular polymeric substances and can produce water of acceptable quality for drinking [80–82,113].

As far as the WHO guidelines are concerned, it is seen in **Table 2.3** that nanofiltration/reverse osmosis can remove most forms of pollution to a good degree (e.g. [102,103]). In some cases, though, the produced effluent failed to meet the WHO guidelines for water quality (e.g. [109]). However, such cases typically deal with highly polluted industrial water, the concentrations of which are unlikely in most natural environments.

Finally, it was previously analysed that pre-treatment (e.g. microfiltration) is usually an indispensable step before reverse osmosis to decrease the possibility of fouling. In this concept, reverse osmosis is often a needless and costly addition to properly designed DWTPs for countries under development. reverse osmosis applicability is generally high in areas that

need high-quality water for industrial processes, or in places where sea water is the main source of drinking and sanitation water [114].

2.4.4 Production process of water filtration membranes

Water filtration membranes can be a highly effective method of water filtration as already discussed. They also typically require less space than granular filters for the same output of water [115]. This makes them popular products for use in water treatment [115].

2.4.4.1 Production of microfiltration membranes

Micro-filtration modules are perhaps the easiest of the four membrane filtration types discussed to produce. This is because materials used for the microfiltration membranes include ceramics, metals and woven fabrics that can be modified with different materials (e.g. titanium dioxide (TiO_2) nanoparticles or polyvinylpyrrolidone) to increase characteristics such as hydrophilicity and disinfection [81,116]. As shown in Table *2.2*, recent research has indeed pushed in the direction of *microfiltration/ultrafiltration* membranes impregnated with materials to enhance their performance [e.g. [80,81,84]]. These chemically altered membranes are possible to produce in developing nations as is demonstrated by several projects that produce such filters in small-medium enterprises. This is commonly achieved through the use of ceramics impregnated with disinfecting nanoparticles derived from materials such as silver [117,118]. However, in a setting where raw materials such as clay minerals and disinfectants such as silver are not in abundance, modified membrane filtration methods may not be suitable.

Additionally most of the membrane materials involve relatively intensive procedures for the membrane production (e.g. [80,83,84]). For instance, ceramics require several heating processes, with high temperatures (i.e. ≥600^{o}C), as well as compaction. Woven membrane production requires the use of machinery and/or skilled labour. Moreover, it is possible that chemical additives are needed to improve the filtration characteristics. These factors are no issue in more developed nations where electrical supply, skilled labour and chemical deliveries are more accessible, but this is not always the case in less developed countries [119]. Membranes, particularly of woven fibre, can be fragile and expensive. This means that a microfiltration process is highly dependent on the proper training of personnel, and a well

organised infrastructure for continued successful operation. This makes microfiltration membranes more easily applicable in centralised systems.

In terms of compliance with the WHO standards, it can be concluded that *microfiltration/ultrafiltration* can effectively remove organic material from wastewater (e.g. [80,81]). However, partial removal or even the reduction of the size of organic particulates was also reported in some cases (e.g. [81,83]). More importantly, most of the cited studies do not assess the *microfiltration/ultrafiltration* capability to remove inorganic pollutants such as heavy metals/metalloids (e.g. [82–84]). This suggests that such membranes do not adequately remove these pollutants without modification or further treatment processes.

2.4.4.2 Production of reverse osmosis membranes

Reverse osmosis membranes are the most technically complicated membranes to synthesise. Their production often involves the immersion of a polysulfone support material in a solution of different organic compounds, followed by tightly controlled drying and rinsing procedures [120]. This process is known as interfacial polymerisation [121]. Interfacial polymerisation involves the formation of a membrane at the boundary between two media. These often consist of two different solvents, containing the monomers required to produce the membrane at the boundary. It is evident from literature that many factors affect the performance of a reverse osmosis membrane. These include the solvents used [122], as well as the support material [123].

These materials require careful handling as they are known to be either fragile or dangerous. Some organic solvents used for example are flammable at low temperatures, in addition to being health hazards. Furthermore, the produced membranes are highly influenced by the conditions of the fluid they are designed to filter. They require specific, controlled conditions in order to function optimally, these include temperature, pH, organic content of solute, etc. [124]. As well as the technical requirements for production, reverse osmosis processes require power where pressure is provided to overcome the osmotic pressure difference between the feed solution and the effluent solution. For these reasons, reverse osmosis is often only applied for drinking water treatment when absolutely necessary, for example in water poor regions where brackish and saline water are used as feed water for a drinking water treatment plant.

2.4.5 Granular Media

2.4.5.1 Rapid Sand Filtration

Rapid sand filtration is a physical filtration process. Unlike slow sand filtration, rapid sand filtration produces no significant biological layer. Hence, it requires prior and post treatment stages to remove pathogenic substances and prevent fouling. It constitutes a common treatment process for the SS removal in urban areas where land use needs to be optimised and continuous electrical supply is accessible [125]. The typical design of a water treatment plant involves several rapid sand filters to allow for one or more to be "offline" for backwashing purposes. Consequently, some filters must deal with a higher flow during backwashing compared to the flow when no backwashing is occurring. This "flow surge" can then lead to increased particle concentrations in the effluent [126]. Additionally, the quality of sand in a rapid sand filter deteriorates over the course of years due to the adsorption of organics and inorganics on the surface of sand granules [127].

The removal of inorganics (e.g. such as Fe, manganese (Mn)) in rapid sand filters is achieved through homogenous, heterogeneous and biological oxidation. Heterogeneous and biological oxidation mainly occur on the surfaces of granular material since contaminants either adsorb to filter media or are oxidised by microbes attached to the granular matter. Homogenous oxidation occurs in the supernatant and water phase in the filter [128]. *Table 2.4* shows sand filters in addition to modifying agents that have been applied to enhance their ability to remove trace contaminants (e.g. As). These contaminants can exist in several different oxidation states (in aqueous state), some of which are more easily removed than others (e.g. As(V) and thallous cation (Tl(I)) when compared to As(III) and thallic cation (Tl(III)), respectively) [129,130].

Rapid sand filters are operated at higher flow rates than slow sand filters. Consequently, they often require pumping systems to maintain the high flow rate, in addition, pumping systems are required for the backwashing of the filters during cleaning [131,132]. Rapid sand filters typically remove physical pollutants as discussed, consequently removing dissolved pollutants is achieved through using rapid sand filters in conjunction other techniques that are capable of removing aqueous pollutants.

2.4.5.2 Slow Sand Filtration

Slow sand filtration has been used for around 150 years as a relatively simple and easy-to-operate process that allows raw water to pass through a sand medium. As the water passes through the sand, solids, microorganisms and heavy metals (e.g. Cu and chromium (Cr)) are removed. A bacterial community gradually forms a layer (called 'Schmutzdecke') and preys upon bacteria present in the water [45,133,134]. However, slow sand filtration requires large areas per unit volume of water treated. Thus, it is either undesirable or even ruled out in densely populated areas or areas where land is expensive [135]. The latter makes slow sand filtration an option mostly suited to rural communities rather than large towns or cities. Other major issues with filters used for slow sand filtration include low flow rate as well as their requirement for a maturation period before they are available for use (up to 40 days). Unlike other filters that can be restored to use quickly after cleaning, slow sand filtration filters need time for the Schmutzdecke to regrow [136].

A range of different factors can affect the performance of slow sand filtration. For instance, caffeine, oestrogens and other PhACs contained in the influent can negatively impact on the ability of the Schmutzdecke to remove bacteria [137]. Influent salinity can also display an inverse relationship with organic content removal [138]. Excessive suspended solids (SS) can also clog the filters, thus reducing their ability to convey water. Heavy metal removal, specifically, is expected to be improved under conditions of higher total organic content in the influent, greater depth of sand and lower flow velocity [134].

Table *2.4* shows that sand filtration can be improved in terms of heavy metal removal by means of additives such as Fe or Mn oxides, or polyaniline (PAn) [e.g. [130,139,140]]. Virgin sand shows some ability to remove trace metals that can be toxic or carcinogenic [e.g. [141]]. However, this ability can be significantly improved for even small concentrations of trace heavy metals by the coating of sand with Fe or Mn oxides. These metal-based additives increase the surface area and adsorption capabilities of sand media [142]. The results in Table *2.4* show that modifying the sand filters to reduce harmful heavy metals such as Pb and Cr can be achieved in a simple manner. Nevertheless, it shall be noted that sand filtration shows mixed results with regards to the WHO guidelines on drinking water. In few cases, the remaining contaminant concentration meets the WHO guidelines (e.g. [141]); these typically involve additives such as Fe or Mn. The mixed results suggest that sand filtration should be

used in conjunction with another treatment method to ensure the removal of heavy metals/metalloids.

Slow sand filter technology has been adapted in recent years into decentralised devices known as “Biosand filters”. These devices are smaller than municipal slow sand filters, and in addition are typically operated at the point of use, rather than in centralised systems [143]. These filters don’t necessarily require a constant supply of water where a slow sand filtration does require a constant flow to maintain the output. This means that they can be operated by a family or small community, where the water supply is typically topped up daily. In addition to this, these biosand filters are very easy to construct, operate, and maintain, as only basic skills, equipment, and materials are required. No moving parts are necessary, and no external energy is usually needed for their operation [144].

Slow sand filters can remove pollutants of emerging concern such as pesticides and heavy metals. However, this is usually achieved with modification to the design of the filter system as already mentioned. This may involve the addition of layers containing Iron (III) [145,146], activated carbon [147,148], or the installation of additional filtration processes such as membranes or ceramic filter modules [149]. In previous sections of this chapter, it was noted that membrane and ceramic filters may not be achievable in all settings. Their addition to a biosand filter to remove emergent pollutants such as heavy metals and pesticides is thus not sustainable under all conditions. Additionally, iron (III) layers require a source of iron, a material which may not be available to all users, since its availability is dependent on available minerals as well as transport infrastructure [150]. An over dependence on iron in a rural water treatment process could lead to its failure should the required infrastructure function poorly [151]. A study in Table *2.4* from China found that using a layer of oxidised, disused iron nails removed Arsenic significantly [140]. However, this is also dependent on the user having access to a supply of oxidised iron nails. Activated carbon can remove both heavy metals and pesticides and can be operated in gravity fed columns [152]. This makes the operation of a biosand filter with an additional activated carbon filter plausible in a developing rural setting. However, production of the filter material is again an issue. The use and production of carbon-based adsorbents is discussed in the following section of this chapter.

Table 2.4. Overview of studies presenting the removal of trace inorganics using sand media. Additives were implemented to improve removal.

Target Pollutant	Additive to Sand Media	Operating Conditions (flow rate, temperature, concentration, etc.)	Main Findings	Importance	Source
As	Sand preloaded with drinking water/ As(III) & drinking water/ NH_4^+ & drinking water/ Mn(II) & drinking water/ As(III) & groundwater	Flow rate: 1m h^{-1} Column diameter: 90mm Height: 1m Filter: 0.5m quartz sand (0.4-0.8mm) Supernatant: 10cm (drinking water); 2cm increasing to 15cm due to clogging before backwashing (aerated groundwater)	Preloaded NH_4^+ column: almost complete removal of NH_4^+ indicating conversion to NO_3^- No significant differences seen in influent & filtrate of Mn and As(III) preloading As (III) preloaded sand beds immediately oxidised As(III) to As(V); virgin sand beds took 22 days for total oxidation of As(V)	As(V) more negatively charged than As(III) at neutral pH; thus, more easily removed by adsorption processes	[129] [129]
As	Fe	Bucket capacity: 80L Gravel (5-13mm) depth: 7cm Finer gravel (3-5m) depth: 3cm Washed sand (2mm) depth: 30cm Unwashed sand (<2mm) depth: 5cm 2cm Fe nails added in various configurations: beneath unwashed sand & above sand in diffuser basin	Biosand filters effectively removed As; 81% removal decreasing to 50% after 5 months; As concentration only once below 50µg L^{-1}, this >> WHO benchmark (10 µg L^{-1}) Fe addition to sand filter; As removal: 86-95% (As concentration consistently<50µg L^{-1}); however; hovering just above the WHO benchmark; additional treatment needed	As can be removed very simply after the Fe addition to the sand filters; despite not meeting the WHO benchmark, method significantly reducing As concentration in contaminated areas	[140] [140]
Trace Tl(I) & Tl(III)	Dosing of MnO_2 colloids at the same time as Tl input	Flow rate: 3.18m^3 m^{-2} h^{-1} Diameter: 18mm Height: 300mm Quartz sand: d=3mm Temperature: 25°C Initial concentration of Tl(I) & Tl(III): 0.5µg L^{-1}	The higher the MnO_2 concentrations, the higher the removal of both Tl(I) & Tl(III) Tl(I) removal more effective; Tl(III) more stable forming complexes in water Quartz sand alone unable to remove Tl	Tl is highly toxic even at low concentrations; thus, TI removal via the addition of MnO_2 to sand filtration can be useful during the WWTP operation	[130] [130]
Pb(II)	Fe	Flow rate: 0.764m^3 m^{-2} h^{-1} Diameter: 20mm Height: 250mm Quartz sand: 0.15mm (average) Temperature: room temperature Initial Pb(II) concentration: 38.14mg L^{-1}	80% removal at pH=4; remaining concentration: 7.62mg L^{-1}>>WHO benchmark 99% removal at pH=11; remaining concentration: 0.39mg L^{-1}>WHO benchmark; additional removal required Fe coating improved Pb(II) removal Bed depth also increased Pb(II) removal	Pb water pollution is an issue in areas with old piping; hence, especially in countries under development	[139] [139]

Table 2.4. *Continued*

Pb(II)	PAn composites	Flow rate: 0.764m^3 m^{-2} h^{-1} Diameter: 20mm Height: 250mm Quartz sand: 0.15mm (average) Temperature: room temperature Initial Pb(II) concentration: 38.14mg L^{-1}	57% removal at pH=4; >WHO benchmark; additional removal required 68.8% removal at pH=11; >WHO benchmark; additional removal required PAn coating improved Pb(II) removal Bed depth also increased Pb(II) removal	See above	[139] [139]
Cr(VI)	MnO_2	Diameter: 0.106-0.125mm Temperature: 25°C pH: 6 Cr(VI) concentration: 500µg L^{-1}	95.12% adsorption of Cr(VI) after 60 minutes with a MnO_2 dose of 8.9mg L^{-1}; remaining Cr(VI) concentration: 24.4µg L^{-1}<WHO benchmark	Cr(VI) is a carcinogen found in naturally contaminated groundwater, as well as in anthropogenically polluted surface water	[141] [141]
As & Cu	Activated bauxsol coating (produced as in [153]) Activated bauxsol coating (produced as in [153])	Particle size: 0.5mm Temperature: 22°C pH: 6.5	Almost complete As & Cu removal	Significant As & Cu water contamination due to acid mine drainage & industrial activities	[154] [154]

2.4.5.3 Granular Activated Carbon (GAC)

Activated Carbons currently used in water treatment are made of a variety of materials (e.g. nutshells, wood, coal and petroleum) [155]. Moreover, they differ in terms of characteristics (e.g. number of micro and macro-pores, surface area, functional groups, etc.) [156]. GAC is commonly used as a filtration or post filtration method to adsorb organic/taste/odour compounds, synthetic organic chemicals and PhACs with results that depend on the carbon quality, pollutant type and concentration. When used for post filtration, GAC receives high-quality water to adsorb organic compounds that were not filtered out in previous stages. If applied as filters, GACs often replace or are combined with rapid sand filters, thus reducing the need for further filtration. GAC filters can operate at higher loading rates than slow sand filtration. Therefore, they are popular in treatment plants where space is a limiting factor [157,158]. Furthermore, GAC can be added to the anaerobic digestion process to improve methane production. It can also enhance the sludge digestion process by increasing the removal of SS (including volatile SS) [159–161].

When the lifecycle of a GAC filter is discussed, it is uncertain how long it will take before it becomes saturated with target pollutants. Some target pollutants will saturate the GAC filter more rapidly than others [162]. Biological activity is observed in GAC; this has beneficial effects such as further removal of NOM. However, this can also generate problems such as clogging, anaerobic/dead zones and detachment of microbes from the GAC. In the initial stages, GAC removes NOM through adsorption. As the process progresses, a biofilm grows, and NOM is removed by combined adsorption and biodegradation [158].

Table 2.5. Overview of studies presenting the removal capability of GAC implemented for specific pollutants.

Target Pollutant	GAC Material	Operating Conditions (flow rate, temperature, concentration, etc.)	Main Findings	Importance	Source
Turbidity, DOC, UV_{254nm}	Bituminous coal	GAC bed height: 0.95m Bed diameter: 0.08m Media volume: 4.8L Empty bed contact time: 13-20mins Average linear velocity: 3-4.5 m h^{-1} Bed porosity: 0.4	Turbidity removal>88% DOC removal>72% UV_{254nm} removal>64% Uncertain whether this material can completely satisfy the WHO guidelines	GAC was used in this study to mitigate reverse osmosis membranes biofouling	[163] [163]
NO_3^-	Coconut shell char modified with NaOH	GAC bed height: 0.2m Bed diameter: 0.01m Bed volume: 0.019L Empty bed contact time: 9.5mins Flow rate: 2mL min^{-1} Average linear velocity: 1.53m h^{-1} Temperature: 25°C Initial NO_3^- concentration: 10mg L^{-1}	80% removal Initial NO_3^- concentration already<WHO guidelines; however, high removal indicative of material's potential to meet WHO guidelines regarding NO_3^-	NO_3^- are significant pollutants in surface water due to agricultural, industrial & domestic activities	[164] [164]
Cu(II)	GAC produced from bituminous Calgon MRX-POX, modified with 20% HNO_3 & impregnated with carboxybenzotriazole	Bed diameter: 4.86mm Bed depth: 120mm Average linear velocity: 0.873m h^{-1} Empty bed contact time: 8.24mins Initial Cu Concentration 31.8mg L^{-1}	105mg Cu adsorbed g^{-1} of adsorbent No detectable Cu concentration in effluent for up to 400BV Cu WHO benchmark: 2mg L^{-1} Data suggesting that material highly effective at Cu removal and during useful life	Cu(II) more easily recovered by GAC & modified GAC than traditional methods (e.g. flocculation/coagulation)	[165] [165]
Cr(VI)	GAC produced from apple peel & impregnated with H_3PO_4	Batch experiment Stirring speed: 400rpm Contact time: 2h Temperature: 28°C Initial Cr(VI) concentration: 10-50 mg L^{-1} in 10 mg L^{-1}steps	18.78mg Cr(VI) adsorbed g^{-1} of adsorbent Results suggesting that WHO can be met under provision of correct dosage	Cr(VI) is a carcinogen present in groundwater, but also in surface water due to anthropogenic activity	[166] [166]

Table 2.5. *Continued*

Cr(VI)	GAC produced from calcinated egg shell & modified with wheat bran	Batch experiment Stirring speed: 180rpm Contact time: 5h Temperature: 35^{o}C Initial Cr concentration: 10mg L^{-1}	96.96% removal; remaining Cr concentration: 0.304 mg L^{-1}>WHO benchmark: 0.05mg L^{-1} Note: very high initial Cr concentration, rarely seen in the environment	See above	[167] [167]
Pb(II)	GAC produced from phragmites australis reed & impregnated with K_2SiO_3, H_3PO_4 & humic acid	Batch experiment Stirring speed: 120rpm Contact time: 12h Temperature: 30^{o}C	160mg of Pb(II) g^{-1} of adsorbent after 30mins	Pb(II) a significant issue in areas with old water pipe networks, or where poor industrial waste management practices occur	[168] [168]
PhACs including: Codeine, Diclofenac, Tramadol, etc.	GAC: Aquasorb 5000/Jacobi	Bed diameter: 150 mm Bed depth: 1000mm Empty bed contact time: 60 mins Supernatant: 400-500mm Average linear velocity: 6.2m h^{-1}	Overall PhAC removal>99%.	PhACs are a significant issue in modern societies where drugs can be potentially bio-accumulated if not removed from wastewater streams	[169] [169]
Atenolol (ATL)	GAC oxidised by Ammonium Persulphate (APS) & sulfuric acid	Batch experiment Adsorption time: 12h APS concentration increased from 0.5mol L^{-1} to 2.5 mol L^{-1} Shaking speed: 250 rpm Temperature: 25^{o}C	ATL adsorption capacity increased from 40mg g^{-1} to >90mg g^{-1} of adsorbent for APS concentration from 0.5 to 2mol L^{-1} ATL adsorption capacity dropped for a higher APS concentration of 2.5mol L^{-1} After 2h: ATL adsorption capacity stabilized at 85mg g^{-1} of adsorbent for 2mol L^{-1} of APS	See above	[170] [170]

Table 2.5. *Continued*

Ibuprofen (IBU), Triclosan (TCS), Naproxen (NPX), Bisphenol-A (BPA), Ketoprofen (KFN)	GAC: Filtracarb CC60	Bed width: 50mm Bed depth: 40mm Initial IBU concentration: 2µg L^{-1} Average linear velocity: 3.1 m h^{-1} Number of columns in series: 4 Removal percentages measured after 5th day of operation	Removal percentage after: 1st column: BPA>50%; TCS: 60%; IBU:30%; NPX>35%; KFN:40% 2nd Column: BPA: 75%; TCS: 85%; IBU>55%; NPX: 65%; KFN: 60% 3rd Column: BPA: 95%; TCS>95%; IBU>85%; NPX: 90%; KFN> 90% 4th Column: BPA: 100%; TCS: 100%; IBU: 95%; NPX> 95%; KFN> 95%	See above	[171] [171]

According to the results reported in *Table 2.5*, granular activated carbon is a rather versatile filtration material that can reduce various forms of pollution. It can generally be used and produced in relatively simple ways to remove remaining organics such as viruses and pesticides (e.g. after a gravity sand filter) [168,169,172]. The major queries with these materials is their ease of production and replication, as well as their ability to meet WHO guidelines (e.g.[163–165]). As seen in *Table 2.5* [e.g. [165,166]], a common modification of AC to improve heavy metal removal is impregnation with acids, typically nitric (HNO_3) or orthophosphoric acid (H_3PO_4) [165,168]. As discussed before, chemical modification in this way is achievable in places where chemicals can be synthesised, transported, and stored easily. However, the latter can add cost to the activated carbon material[172]. Whilst the more complex ACs can remove heavy metals and other contaminants [e.g. see *Table 2.5*: [169,171]], these ACs usually require modification, often to increase the chemical characteristics that favour metal adsorption. ACs implemented in less developed nations can be used in conjunction with other methods (e.g. microfiltration and slow sand filtration) to face pollution that results from the outdated water network [e.g. see *Table 2.5*: [168]] and, finally, produce water that is of acceptable drinking quality.

2.5 Adsorption of pollutants to biochar and activated carbons

Adsorption mechanisms can be grouped into two categories: Physisorption and Chemisorption. Physisorption encompasses all mechanisms where the rate of their transfer from solution to the solid adsorbate is limited by a physical process, whereas chemisorption includes all processes where the transfer rate is determined by a chemical reaction.

Carbon adsorbents are used to remove a wide range of different pollutants, from inorganics such as heavy metals [173–175], minerals and nutrients such as nitrates to a limited extent [176] and phosphates [177], to organics including pesticides [178], pharmaceutically active compounds (PhACs) [179], and biological contaminants including E.Coli [180]. Recent literature has focused on carbon adsorbents produced from more sustainable feedstocks including discarded organic materials such as fruit stones, bark, rice husks, and nut shells, to produce biochar adsorbent [181]. These pyrolysed feedstocks can be enhanced by activation procedures such as high temperature, steam, or chemical activation. This thesis focuses on the use of low temperature biochars as adsorbents. For this reason, the adsorption to biochar produced in this study will be analysed using methylene blue, and copper as model organic

and inorganic pollutants respectively. Tetracycline hydrochloride is also analysed as an example of pharmaceutical contamination. It is important to understand how a low temperature biochar will interact with such pollutants.

Adsorption is affected by many different factors, these include feedstock [182], pyrolysis temperature [183], activation procedure [184], different pollutants [185]. Conditions such as these are modified to produce biochars with different characteristics. Biochar properties are very important when it comes to their ability to adsorb specific pollutants. Some pollutants are more readily adsorbed by a biochar produced from a different process, when compared to another biochar. Furthermore, different pollutants have different adsorption affinities for the same biochar [186]. This underlines the complexity of using biochar as an adsorbent in a real-world application where water quality is a much more complicated matrix than in laboratory scenarios.

The causes of the variation in adsorption between different pollutants and biochars are the various adsorption mechanisms that occur in biochar. More specifically some of these adsorption mechanisms can be more responsible for the adsorption of one pollutant over another [187]. Heavy metals are for example typically found to be adsorbed in greater amounts by biochars containing higher O/C ratios [173].

Chemical and physical characteristics of biochar are majorly affected by pyrolysis temperature. The scatter plot in Figure 2.5 shows H/C plotted against O/C values collected from 23 different articles published between 2015-2020 [182,183,188–208]; this is also known as a Van Krevelen diagram. A cluster analysis was conducted using H/C and O/C ratios as the input data. The cluster analysis conducted made use of Ward's method which groups data into clusters based on the sum of squares index calculated between data points in a cluster and that cluster's respective mean. The ellipses were produced using an alpha value of 0.32 in order to display one standard deviation from the mean of each cluster. Other variables were then used to produce box and whisker plots, including the pyrolysis temperature used to produce biochar, and the surface area and pH of each biochar. Several box and whisker plots were produced using the cluster from the previous cluster analysis to categorise the data.

A box plot of pyrolysis temperatures is shown in Figure 2.6, using the pyrolysis temperature as the analysis variable and categorising by cluster. What the scatter plot and the box plot

show is that typically, as pyrolysis temperature increases, both the O/C and H/C ratios decrease. Other effects on the O/C and H/C ratios are also clearly displayed in Figure 2.5 and Figure 2.6. Notably cluster 6 has a similar pyrolysis temperature range to clusters 2 and 3, but data points in cluster 6 have higher O:C ratios than clusters 2 and 3. This suggests that a significantly different feedstock or pyrolysis process was used to create the majority of biochars found in cluster 5 compared with other biochars. In addition to the variation seen between clusters 2, 3 and 6 at temperatures greater than 500^{o}C, clusters 4 and 5 show larger standard deviations than clusters 1, 2 and 3. This suggests that at lower pyrolysis temperatures factors such as feedstock, activation procedure, and differences between pyrolysis processes play a more significant role in the amount of Oxygen and Hydrogen in the biochar after pyrolysis. At higher pyrolysis temperatures it can be seen that O/C and H/C ratios are significantly smaller when compared with biochars produced at lower pyrolysis temperature. This can be explained due to hydrogen and oxygen containing compounds being driven off at higher pyrolysis temperatures, leaving behind a matrix richer in carbon. The evaporated material leaves behind void spaces, meaning biochars produced at greater temperatures generally have higher surface areas. However, what the figure also shows is that as pyrolysis temperature is increased past 700 ^{o}C, surface area begins to decrease as void spaces in the biochar begin to collapse due to calcining occurring at these temperatures. Indeed, Figure 2.8 shows that surface areas start to decrease in cluster 1 which has the highest average temperature of all the clusters.

Surface area in Figure 2.8 shows very little variation in clusters 4 5 and 6, however it shows wide variation in clusters 1, 2 and 3. This indicates that as well as pyrolysis temperatures being higher in these clusters, other factors are responsible for the development of surface areas in biochars, where high pyrolysis temperature doesn't guarantee a large surface area.

Figure 2.7 shows the pH of biochars in these other studies, this is typically measured by a 20:1 dilution of deionised water with powdered biochar which is then left for up to 24h, the pH is then measured. In this regard, what is actually measured is how the biochar affects the pH of the solution it is in. If the solution becomes more acidic, it means that the biochar is releasing hydrogen ions from its surface as in equation 2.1. If the pH of the solution becomes greater, this means the biochar is capturing hydrogen from the water as in equation 2.2. What Figure 2.7 shows therefore is that as the pyrolysis temperature is increased, more hydrogen is driven

off, thus resulting in a biochar that as a higher pH under the 20:1 pH test, with the opposite being true for lower pyrolysis temperatures.

$$R - O - H + H_2O \rightleftharpoons R - O^- + H_3O^+ \qquad (2.1)$$

$$R - O^- + H_2O \rightleftharpoons R - O - H + OH^- \qquad (2.2)$$

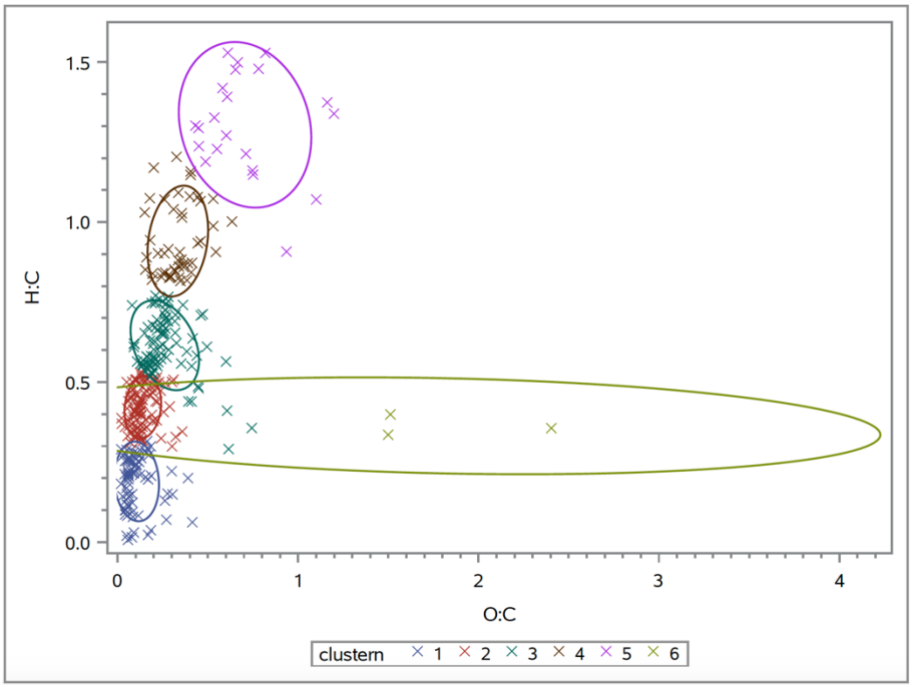

Figure 2.5 – Scatter plot showing the effect of pyrolysis temperature on O/C and H/C ratios, with ellipses sizes determined by surface area, data from various literature sources [182,183,188–208]

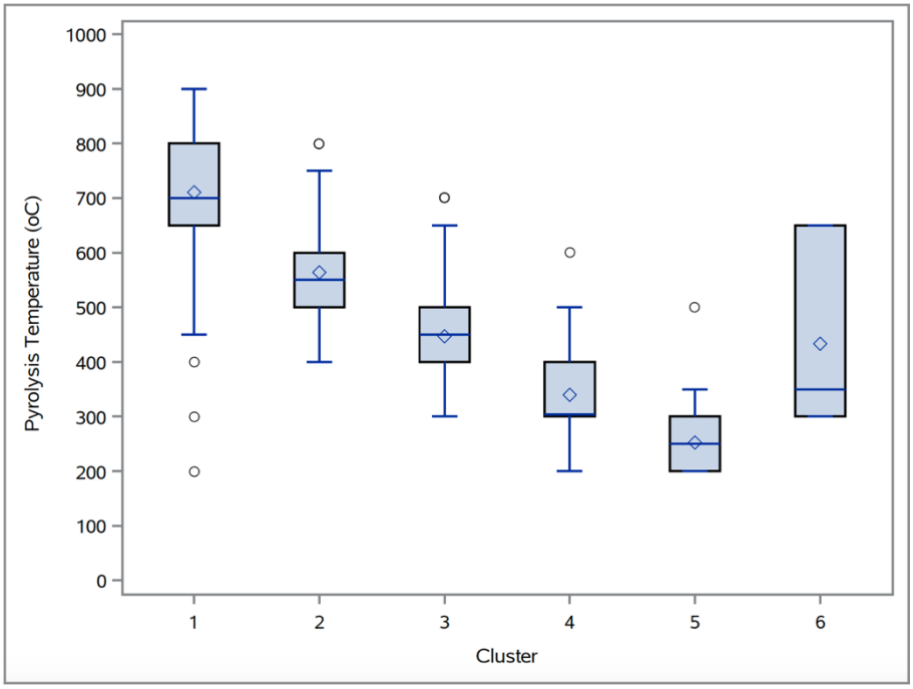

Figure 2.6 – Box plot of temperature ranges within clusters, data from various literature sources [182,183,188–208]

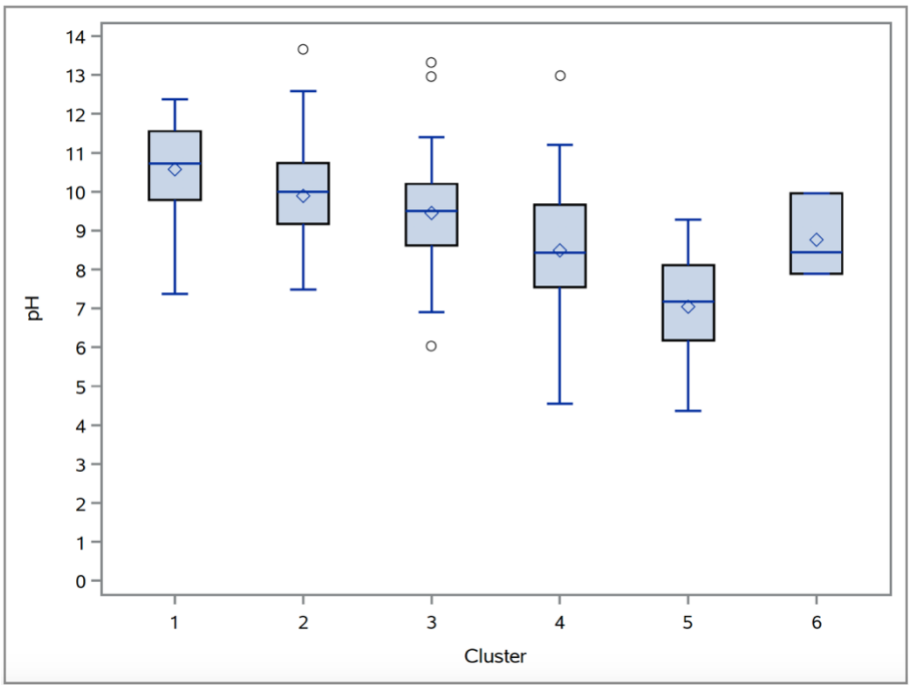

Figure 2.7 – Box plot of pH ranges within clusters, data from various literature sources [182,183,188–208]

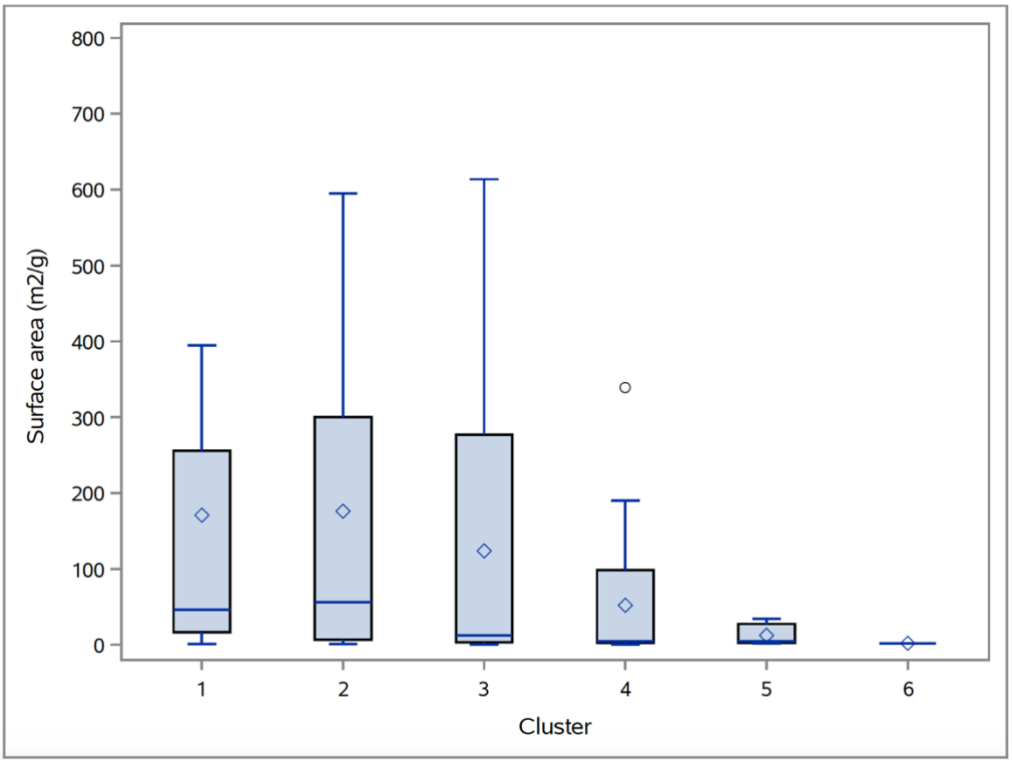

Figure 2.8 – Box plot of surface area within clusters, data from various literature sources [182,183,188–208]

2.5.1 Functional groups and their importance for adsorption

Surface chemistry of a biochar determines a wide range of interactions between the biochar, water and any suspended pollutants. As shown in the previous section, the low

temperature biochar used in this work will likely contain greater amounts of oxygen and hydrogen containing functional groups than biochars produced at higher temperatures. Some of these such as hydroxy and phenol groups interact with water in an amphoteric manner meaning they can hold positive, neutral or negative charge depending on the conditions in the water [209].

Figure 2.9 shows the surface of a biochar with hydroxy and/or phenol groups on the surface. The lone-pair electrons in these functional groups can interact with some pollutants via several different mechanisms that are explained later.

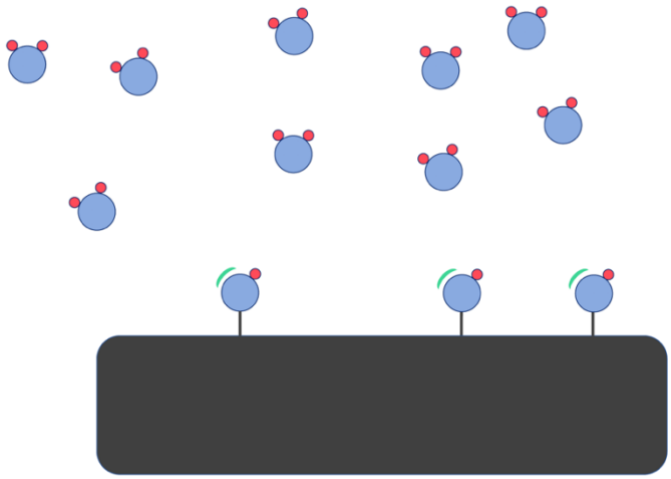

Figure 2.9 – Biochar with oxygen containing functional groups exposed to an aqueous solution

Figure 2.10 shows how a biochar adsorbent containing OH groups interact with a low pH solution, with the hydronium ions protonating the amphoteric OH groups on the surface leading to the development of a positive surface functional group. This shows that hydronium ions occupy the active sites that could otherwise occupied by dissolved pollutants. Additionally, the hydronium ions that do interact these active sites can cause the charge of the active site to become positive, causing the repulsion of positively charged contaminants, or having the opposite effect on negatively charged pollutants [210,211].

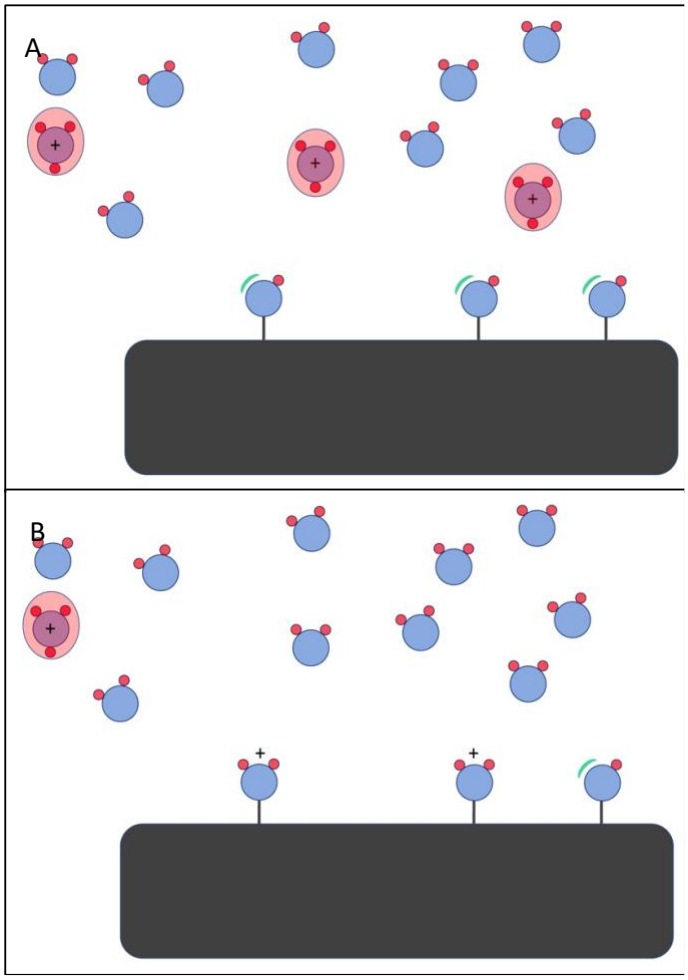

Figure 2.10 – Interaction of OH groups with hydronium ions

Figure 2.11 summarises how OH groups on the surface of a biochar particle interact with hydroxide ions in high pH solutions. The hydroxide ions withdraw protons from the surface of the biochar, transferring the negative charge to the surface of the biochar in the process. This process is known as deprotonation. Similarly, to low pH conditions, high pH conditions can also promote or inhibit the adsorption of aqueous pollutants. Negatively charged aqueous contaminants will consequently be repelled from the surface of a biochar which is coated in negatively charged active sites as a result of deprotonation, with the opposite being true for positively charged contaminants [212].

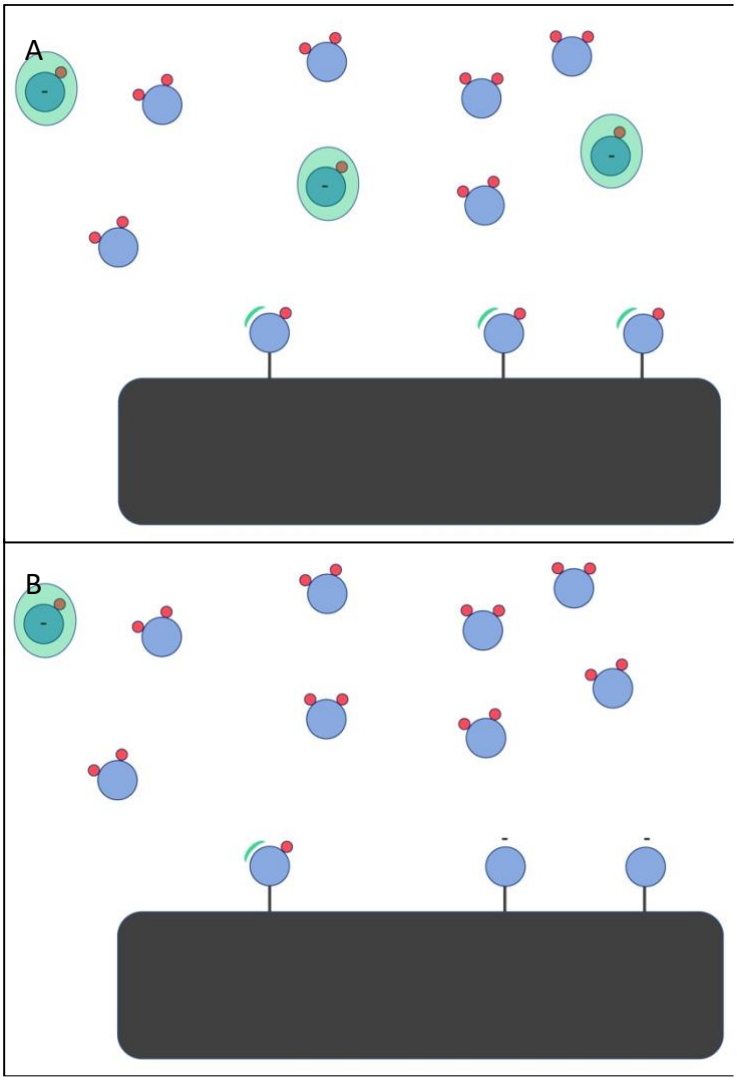

Figure 2.11 – Interaction of surface OH groups with hydroxide ions

2.5.2 Complexation interactions

With the large number of oxygen-containing functional groups expected in low temperature biochar, complexation interactions are expected to play a large role. There are two ways in which these interactions can occur, these two complexation interactions are known as inner and outer sphere complexation.

Figure 2.12 A shows an inner-sphere complex formed on an oxygen containing functional group on the surface of a biochar. This is an example of a chemical bond and is thus an example of chemisorption. On the contrary, Figure 2.12 B shows an example of an outer sphere complex formed between an aqueous metal complex and an oxygen containing functional group on the surface of the biochar. This is an example of a hydrogen bond between the $\delta+$ end of the water molecules surrounding the metal ion, and the $\delta-$ of the

oxygen on the surface of the biochar. These hydrogen bonds are dipole-dipole interactions and are thus examples of physical interactions, consequently the outer sphere complex is a physisorption process that takes place on the biochar surface.

It can be seen from Figure 2.10, Figure 2.11, and Figure 2.12 that the formation of both inner and outer sphere complexes, is pH dependent. When pH is low, the lone pair electrons are used during the protonation of the biochar surface at low pH. Therefore the “active sites” are occupied at low pH by H^+. On the other hand, at high pH, the biochar surface functional groups become deprotonated, leading to the development of negative charge on the biochar surface. In this instance the adsorption of metals to the biochar surface is changed, resulting in ionic and electrostatic interactions between the biochar adsorbent and adsorbate as well as complexation reactions.

The outer sphere type complex is also possible between OH groups in organic molecules and the OH groups present on the surface of the biochar, only in this instance these bonds are known as hydrogen bonds rather than outer sphere complexes. Again, these are examples of a physisorption process.

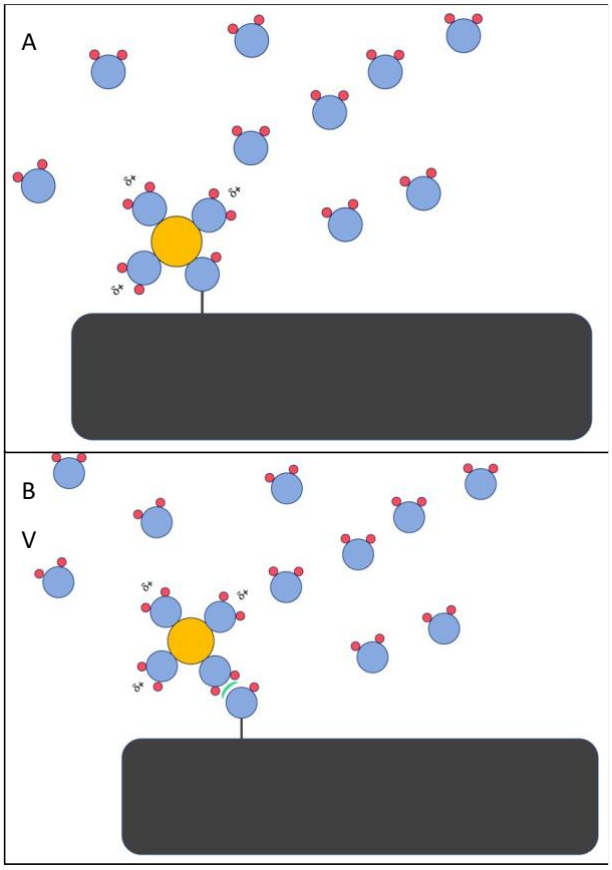

Figure 2.12 – A) Inner sphere metal complex, B) Outer sphere metal complex

2.5.3 Metal oxide inclusions

Metal oxide inclusions in the biochar can also interact with pollutants. These may be present due to the oxidation of some mineral inclusions in the initial stages of the pyrolysis process, when oxygen gas has not yet been expelled from the pyrolysis chamber or used up oxidising the pyrolysis feedstock. This is potentially possible in some pyrolysis systems that do not involve nitrogen/inert gas purging systems prior to a pyrolysis step. Therefore, oxygen will be available towards the beginning of the process to oxidise both the feedstock as well as any mineral inclusions in the feedstock.

Mineral oxide adsorbents are known to develop OH surface groups when interacting with water. Figure 2.13 A – D shows how these OH groups develop when the metal oxide is exposed to water. These OH groups present on the surface of the metal oxide also possess lone pair electrons. Therefore, the formation of outer and inner sphere complexes between these oxygen surface groups and dissolved metal contamination, is also possible on the surface of metal oxide inclusions in the biochar as is seen earlier in Figure 2.12.

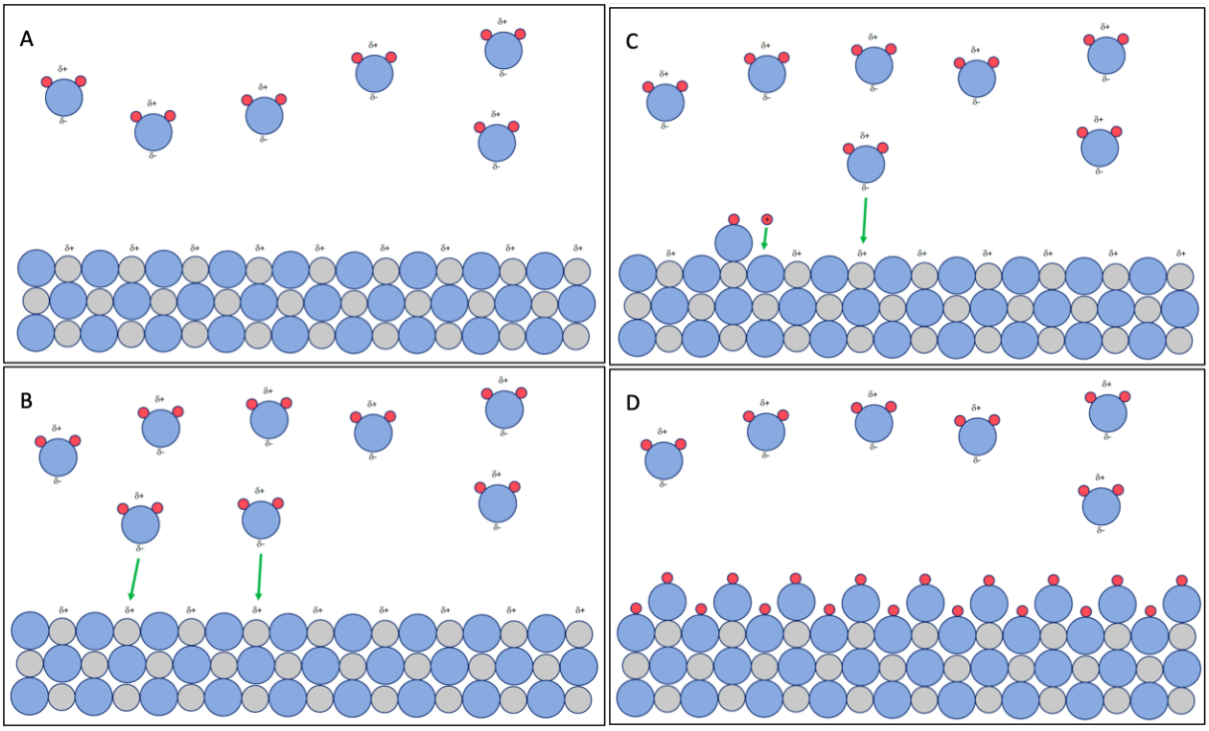

Figure 2.13 – Development of OH groups on the surface of mineral adsorbents

Figure 2.14 shows how an acidic solution interacts with the surface of a metal oxide solution. The amphoteric OH groups on the surface of the metal oxide adsorbent under conditions of

low pH become protonated, resulting in a positively charged -OH_2^+ site, and a reduction in hydronium concentration in solution.

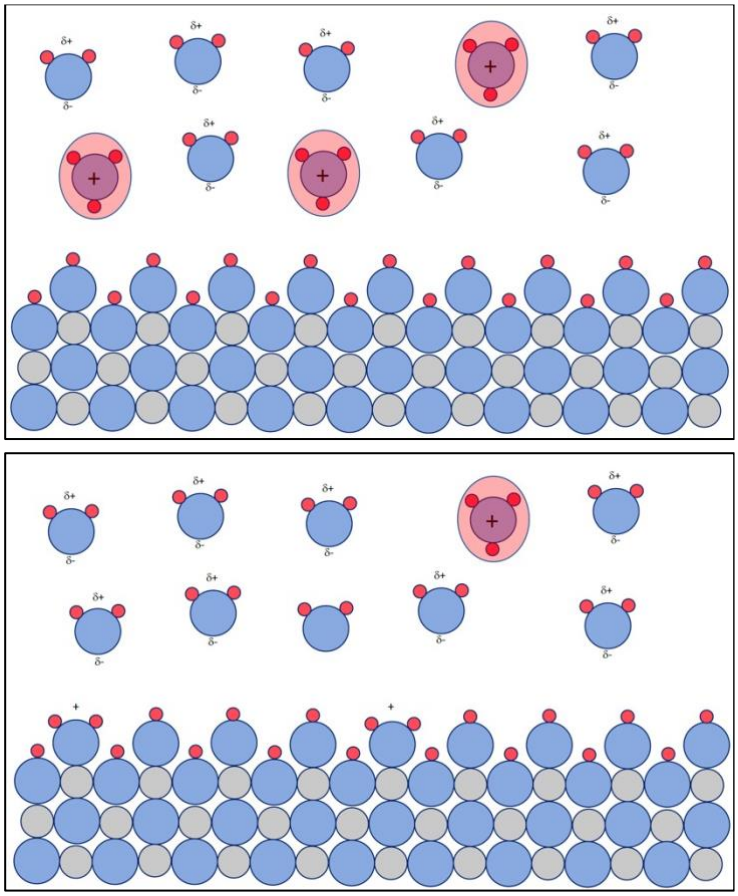

Figure 2.14 – Mineral adsorbent in low pH solution

Figure 2.15 shows how an alkaline solution interacts with the surface of a metal oxide adsorbent. The hydroxide ion withdraws a proton from the surface of the metal oxide adsorbent resulting in a more negatively charged surface.

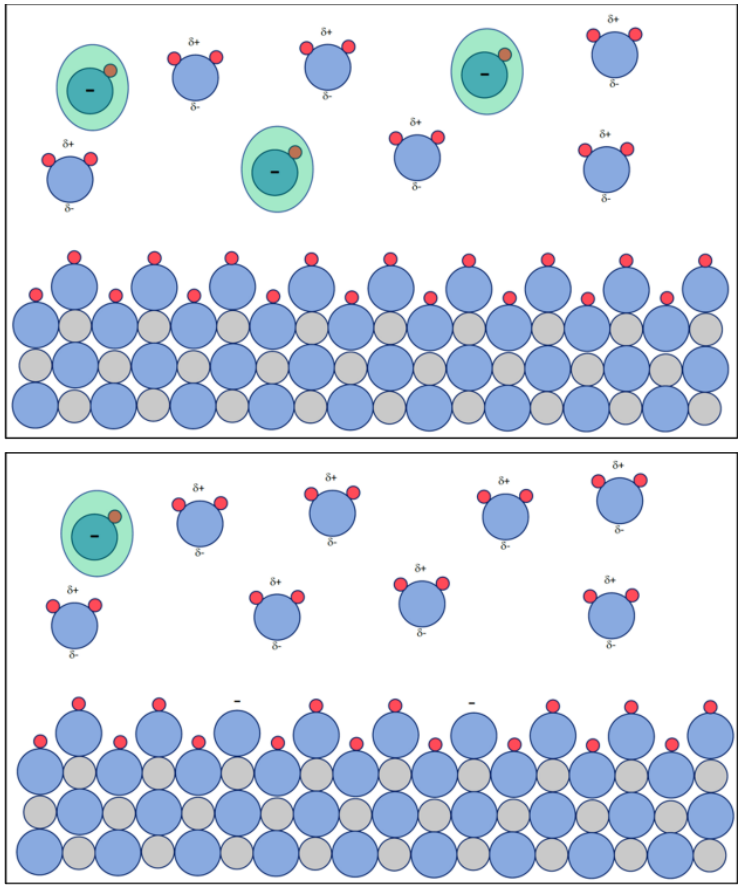

Figure 2.15 – Mineral adsorbent in high pH solution

2.5.4 Ion exchange interactions

Minerals bonded to the biochar surface can also result in ion exchange interactions with ions in solution. These form bonds with surface oxygen that are more ionic in nature than the bond that exists between oxygen and hydrogen in hydroxyl groups on the surface of biochar. This ionic nature enables anions bonded with oxygen on the biochar surface to exchange into solution, depending on their electronegativity and the electronegativity of anions in solution.

Figure 2.16 shows an aromatic carbon structure, with two sodium atoms ionically bonded to two oxygen atoms. The electron density surface with electronegativity colour response in Figure 2.16 B, shows the dissociation of the sodium electrons which are donated to the oxygen in an ionic bond.

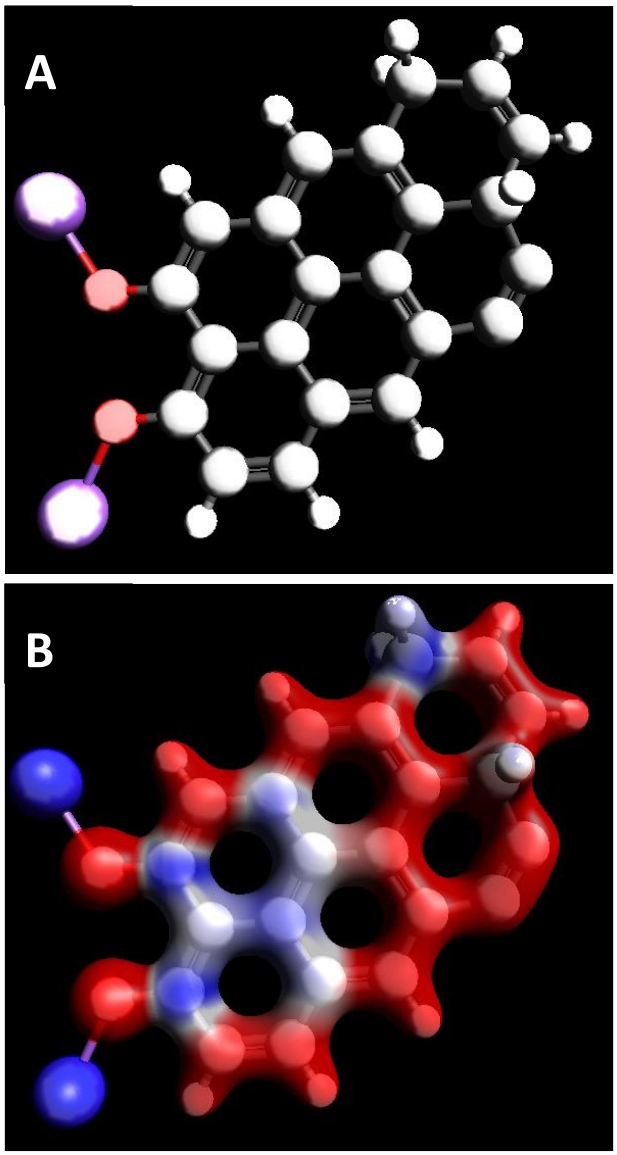

Figure 2.16 – A shows a delocalised carbon structure containing two sodium atoms bonded to two separate oxygen atoms on the left hand side, B shows the electron density surfaces as calculated by Density Functional Theory (DFT) by orca molecular orbital modelling software, with electronegativity shown on these surfaces as a colour response where blue represents positive charge and red represents negative charge

2.5.5 Pi Interactions

These interactions occur because of the nature of the C-C double bond. This bond type consists of one σ bond and one π bond [213]. The electron density in a σ bond is concentrated between the two bonding atoms, whereas a π bond is formed by the overlap of two p orbitals, meaning the electron density is concentrated above and below the bonding plane [214]. Interactions involving π bonds are therefore possible, where the electron orbitals in a π bond can be influenced by electron orbitals of adjacent compounds. No chemical bond is formed

during these types of interaction, consequently these π interactions are examples of physisorption.

One example of such an interaction is the π-π stacking interaction. These interactions occur where the π orbital of the adsorbate interacts with the π orbital in the adsorbent. This mechanism of adsorption is also known as π stacking interaction.

These bonds are common between aromatic groups at the biochar surface, and an aromatic pollutant such as methylene blue, with this type of bonding being particularly important in waters with a pH below that of the pH of zero charge [215]. The pH of the adsorbate solution influences the adsorption process as the chemical and physical properties of a biochar surface are altered by the presence of hydronium ions. Specifically negatively charged sites on the surface of the biochar may be bonded with H^+ ions thus removing the electrostatic attraction of the "active site" causing a reduction in physical, as well as chemical adsorption processes [185]. This explains why the π-π interaction typically becomes a more significant overall adsorption mechanism as solution pH decreases, where π orbitals are not significantly affected by acidic solutions.

π electrons are needed to allow π-π interactions between an adsorbent and adsorbate, it thus follows that the more aromatic a biochar adsorbent, the more π interactions between adsorbent and adsorbate are possible. Indeed, Zhendong et al. show that biochar produced at higher pyrolysis temperatures have lower H/C ratios and have higher double bond equivalent ratios [216]. This is particularly important for the adsorption of non-polar contaminants, where a biochar with greater amounts of -OH groups and lesser aromaticity would not adsorb these contaminants as readily as more polar contaminants. For this reason, higher pyrolysis temperatures are required to produce an adsorbent targeted at non-polar contaminants.

2.5.5.1 Complexation and Hydrogen Bonding

Complexation is a mode of adsorption that typically involves oxygen containing functional groups such as alcohols, carboxylic acids, ketones and aldehydes [217–219]. Hydrogen bonding would also typically be promoted by biochars with greater amounts of oxygen containing functional groups [220]. Typically, the biochars with the greatest amounts of oxygen are produced at lower pyrolysis temperatures as is evidenced in the earlier van-

Krevelen diagram and cluster analysis. Complexation is a method of adsorption that involves a metal ion and OH groups on the surface of the biochar. There are two types of complexation that occur at the surface of an adsorbent, known as inner and outer sphere complexation. Mineral adsorbents have been shown to interact with water molecules when immersed in water, producing a surface covered in OH groups. These groups on the surface of the mineral adsorbents are amphoteric, this means that they can gain or shed an H^+ ion creating either an $-OH_2^+$ or an $-O^-$ surface group. OH groups act in much the same way on the surface of biochar or activated carbon adsorbents where they also have an amphoteric nature.

Biochars produced at lower temperatures tend to have lower specific surface areas, as is evidenced by the box plots produced from the cluster analysis earlier in Figure 2.8. Despite the greater amounts of oxygen in these biochars produced at lower pyrolysis temperatures, the reduced surface area of the biochar may result in restricted access of aqueous pollutants to oxygen containing functional groups in the biochar. The difference between mineral adsorbents and biochar/activated carbon adsorbents is that the -OH groups are already present in the biochar, whereas in mineral adsorbents, these groups develop from the interaction of water with the surface of the adsorbent. This means that if a biochar is being designed to target aqueous metallic pollution, then the surface -OH groups must either be added after pyrolysis processes or maintained in a way utilising either chemicals or low temperature pyrolysis.

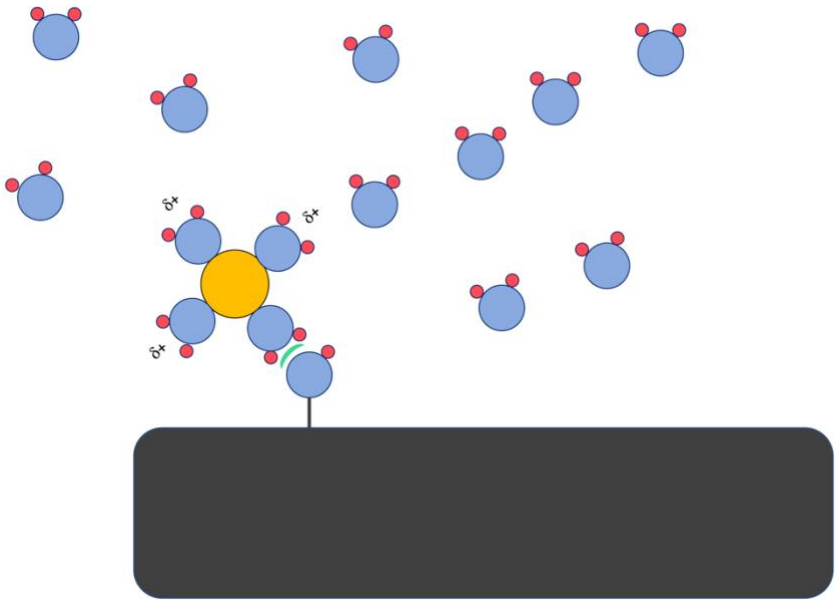

Figure 2.17 – Outer sphere complexation of aqueous metal ions with oxygen containing functional groups on the biochar surface

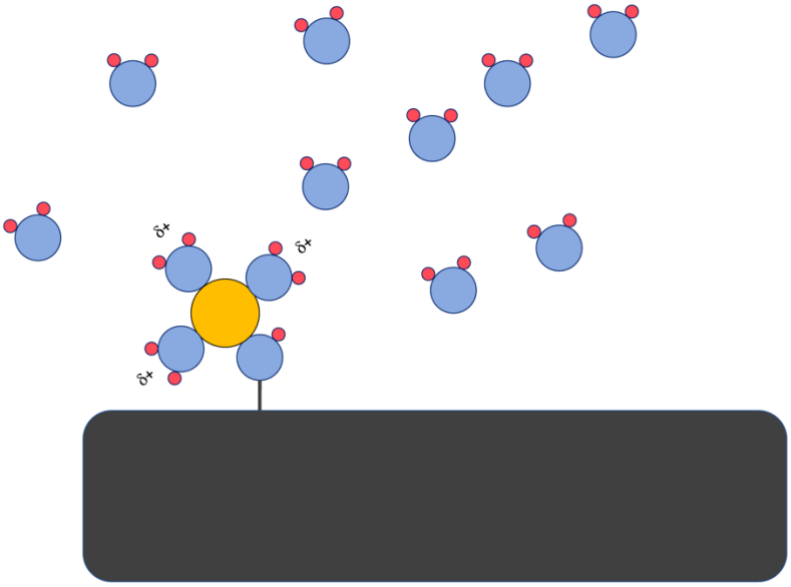

Figure 2.18 – Inner Sphere complexation of aqueous metal ions with oxygen containing functional groups on the surface of biochar

2.5.5.2 Electrostatic Interaction

Electrostatic interactions between biochar and an aqueous pollutant are generally due to biochar possessing a negative surface charge. The electrostatic potential of biochars are also found as is the case with complexation and hydrogen bonding to be enhanced with increased amounts of oxygen containing functional groups [221]. However, the effect of pH can be favourable as well as detrimental to adsorption, depending on the chemistry of the adsorbate. Congo-red for example is an anionic dye and with increased adsorption at lower pHs where an H+ ion binds with a repulsive negatively charged site; this has the opposite effect on the adsorption of a cationic dye such as malachite green [222].

2.5.6 Centralized and decentralised systems

With the focus on rural, remote areas of middle/low-income countries where the provision of drinkable quality is a major issue, two scenarios are mainly suggested, and their applicability compared. The first includes a decentralised water treatment system using slow sand filtration (Biosand) filtration techniques followed by GAC/biochar filters. The second scenario is a more conventional, centralised DWTP, which applies multiple treatment stages (screening, sedimentation, chemical coagulation/flocculation, filtration, disinfection).

A decentralised system is generally operated by the user and as such a configuration to treat raw surface water must be easy to operate and maintain with little training required.

Several current projects are based on this concept, for instance, the PureMadi project where silver ceramic pot filters are used to remove pathogens and viruses from water [117]. The Aqsolutions biochar filter system is another example where gravel, sand and biochar filters are used to remove SS, pathogens, viruses and harmful chemicals [172]. The capital costs of ceramic filters used in decentralised systems range from $2 to $40, with the majority of them typically costing between $2 and $5 [223]. The average yearly cost of running a ceramic and biochar water filtration system is estimated at $0.74 per m^{-3} of treated wastewater [224–227].

Typically, centralised systems are considered as more cost-effective. They are usually developed in areas of higher population density where the distance between treatment plants and consumers is limited. However, such systems are not always economical in more isolated rural areas, since pumping water over long distances is difficult and expensive [223]. Furthermore, it shall be noted that the predominant energy-consuming process in drinking water treatment is the distribution/conveyance step. It has been reported that domestic water distribution can reach up to 50% of the total energy expended during the whole water treatment process [228]. Moreover, installing various smaller conventional DWTPs in remote agricultural communities is likely to be an unsustainable option due to lack of transportation and energy infrastructure that can ensure the continuous DWTP supply. In addition, smaller facilities tend to produce water with a higher cost per unit of treated water compared to larger treatment plants [229].

A gravity-fed sand/biochar filter system can be constructed to serve a remote community. Such a system could constitute a viable “semi-centralised” alternative for a rural community. It can combine the benefit of a centralised system (i.e. reduced cost per unit of treated water) with the advantage of decentralised systems where pumping is not required for the water distribution. More importantly, the suggested sand/biochar filter system is cheap and simple; it can be constructed using local materials and operated with gravity. However, it cannot account for areas where desalination is required; reverse osmosis is needed in such cases.

The calculation of the energy used for water treatment is a highly complex issue, with the average energy requirements of conventional DWTPs reported to range between 0.29-1.3 kWh m^{-3} [228,230]. If sophisticated treatment is needed (e.g. desalination via reverse

osmosis), the average energy consumption of a plant can increase up to 3 kWh m^{-3} [231]. The range of energy requirements mentioned previously is quite wide mainly due to the local, global and temporal differences in the prices of drinking water production and transportation [229]. Therefore, it is difficult to construct a single effective universal benchmark relating energy requirements and cost regarding drinking water production. Hence, case studies on different environments and settlement types are suggested as necessary further work. This is outside the scope of this thesis which is targeted at the water quality that can be achieved using filtration technologies with regards to the WHO guidelines. More specific information on the operational costs of filtration and granular media technologies follows.

2.5.7 Operational Costs for the microfiltration/ultrafiltration, nanofiltration/reverse osmosis, Sand Filters and GAC Systems

Table *2.6* provides indicative information on the operational costs of the *microfiltration/ultrafiltration*, nanofiltration/reverse osmosis, slow sand filtration, rapid sand filtration and GAC technologies. The direct comparison among the different cited studies is not straightforward due to the variability of a number of factors including plant capacities, experimental assumptions and the scale of each study. Nevertheless, general conclusions can be drawn. Table *2.6* shows that in areas where viruses and dissolved contamination are not the primary treatment target, a system employing *microfiltration/ultrafiltration* can provide effluents of acceptable quality by being more cost-effective than one employing both *microfiltration/ultrafiltration* and nanofiltration/reverse osmosis. It is also worth noting that there are alternative (and cheaper) methods for the removal of ionic contamination from water, typically coagulation/flocculation. These are reported to remove high amounts of most heavy metals with aluminium (Al), iron or biopolymer coagulants considered the best for removal. According to recent technological advances, electro-coagulation using scrap metals is an effective treatment option [66,67,69,70]. *microfiltration/ultrafiltration* and coagulation/flocculation present lower operational costs compared to reverse osmosis. However, reverse osmosis remains a necessity in areas where seawater is the water source.

Table 2.6. Operational cost for the microfiltration/ultrafiltration, nanofiltration/reverse osmosis, *sand filters and GAC systems.*

Filtration Method/Membrane	**Operational Cost (£)**	**Contaminants removed**	**Source**
microfiltration/ultrafiltration	0.02 \$ m^{-3} for a plant capacity of 20,000 m^3 day^{-1}	SS, dissolved solids, bacteria (including pathogens), viruses, organic material	Dore et al. [232] Dore et al. [232]
	0.1-0.15 \$ m^{-3} for a plant capacity of 20,000 m^3 day^{-1} (after running the optimization model)		Bick et al. [233] Bick et al. [233]
nanofiltration/reverse osmosis	0.68 \$ m^{-3} for a plant capacity of 30,000 m^3 day^{-1}	SS, dissolved solids, bacteria (including pathogens), viruses, organic material, ions	Banat [234] Banat [234]
	0.5 \$ m^{-3} by using modern desalination techniques		Energy and Capital [235] Energy and Capital [235]
slow sand filtration	0.001 \$ m^{-3} assuming filtering 0.04 m^3 day^{-1} for 10 years	SS, dissolved solids, bacteria (including pathogens), viruses, organic material, some metallic material (after modification)	Centre for Disease Control and Prevention [236] Centre for Disease Control and Prevention [236]
	slow sand filtration followed by chlorination for rainwater treatment in airports: total monthly cost=1.05 \$ m^{-3}; 60%<price paid to water supply company		Moreira et al. 2012 [237] Moreira et al. 2012 [237]
rapid sand filtration	0.05 \$ m^{-3} for a 15-year operation	SS, dissolved solids, bacteria	Sanchez et al. [238] Sanchez et al. [238]
	0.02 \$ m^{-3} for a pilot-scale rapid sand filtration performing tertiary treatment of municipal wastewater		Heinonen-Tanski et al. 2003 [239] Heinonen-Tanski et al. 2003 [239]
GAC	0.31 \$ m^{-3} for a plant of 300,000 population equivalents	SS, dissolved solids, bacteria (including pathogens), viruses, organic material, some metallic material (with modification)	Mulder [240] Mulder [240]
	0.13 \$ m^{-3} for a pre-industrial scale system enabling the reuse of industrial laundry effluents with a feed of 360 m^3 d^{-1}		Ciabattia et al. 2009 [241] Ciabattia et al. 2009 [241]

Granular media can be used and modified with adsorbents. These can be applied for the removal of harmful ions in water before or after a *microfiltration/ultrafiltration* phase.

slow sand filtration can remove a vast amount of pollution in one step when compared to other methods such as *microfiltration/ultrafiltration*, nanofiltration/reverse osmosis and rapid sand filtration. Nevertheless, it does have the drawback of relatively high capital cost and land requirements [236]. Despite the latter, cheap and simple operation mean that slow sand filtration remains an interesting and valuable water treatment option. Rapid sand filtration can be used to treat water, however backwashing is required to keep the filter media clean adding an additional design requirement, with pumps being required as well as multiple filters being needed to backwash the sand and maintain the water output respectively. Finally, GAC filters are a more sophisticated filtering method that can remove most groups of pollutants, possibly after some modification. The challenge is to produce GAC from discarded materials that will be of adequate quality for water filtration, thus decreasing the cost of the GAC implementation, and also potentially making biochar/activated carbon used for water treatment more sustainable.

2.6 Waste Management and Treatment

Another issue that is of paramount importance around the world is waste management. The improper management of municipal waste can lead to many harmful outcomes including the pollution of water, proliferation of pests, and consequently the spread of disease [242]. Many different methods can be implemented in order to better manage and treat waste. However, these different waste management and treatment processes can lead to pollution through the emission or improper management and disposal of by-products. Typical waste management processes include biogas production, incineration, composting, and pyrolysis. What follows is a qualitative assessment of each of these processes.

2.6.1 Biogas production

Biogas production is often achieved through the use of anaerobic digestion. Heterotrophic bacteria in this process break down organic matter and produce methane which can be burnt as a fuel [243]. The feedstock for biogas production often involves manures, and other organic matter such as food waste. However, some feedstocks such as lignin containing feedstocks cannot be broken down by anaerobic digestion [244]. Furthermore, biogas production is dependent on certain conditions in order for the heterotrophs to flourish, these involve fairly precise margins of both pH and temperature [245,246]. Furthermore, biogas production does not result in products with the diverse range

of uses seen in pyrolysis products, therefore storage of biogas is required if production exceeds demand. This can be difficult, and if the gases are not stored properly, they represent fire and health risks due to their flammability, and associated health hazards.

2.6.2 Composting

Composting is a process that involves the biological decomposition of waste organic materials. The product is compost, which can be applied to in agriculture and horticulture to improve soil quality [247,248]. This process occurs at low temperatures compared with pyrolysis and incineration and can be achieved relatively simply [249].

However, as is the case with biogas production, the biological components on which composting relies are sensitive to both pH and temperature margins, as well as other factors such as heavy metal contamination of the compost feedstock [247,250]. As is the case with biogas production, it is also true that composting cannot process all feedstocks that pyrolysis can. For example meats and other products sourced from animals can result in unwanted types of bacteria entering the compost, causing it to release a foul odour, and can also result in the compost containing elevated levels of E.Coli [251].

2.6.3 Incineration

Incineration is the combustion of waste at very high temperatures, typically around 1000^{o}C [252]. The energy produced by incineration is collected and used for electricity production or heating purposes [253]. The use of incineration is often a centralised process where it can be more easily monitored to reduce the production of harmful by-products [254]. Compared with pyrolysis, this process does not represent as significant a carbon buffer, where carbonaceous waste is simply combusted, the carbon being immediately reintroduced to the atmosphere. If operated irresponsibly, incineration can also result in the dissemination of polycyclic aromatic hydrocarbons (PAHs), dioxins and other toxic/harmful gases into the atmosphere [255]. Some of these toxins are capable of bioaccumulating, building up to harmful levels in the environment.

2.6.4 Pyrolysis

Pyrolysis as a waste management process is capable of producing valuable products from discarded material. These products include syngas, bio-oils, and biochar [256]. Biochar particularly has a diverse range of uses where it can be used as an adsorbent as already explored, it can also be used as a fuel when dried, or a soil additive to enhance nutrient and

water retention in soils [257,258]. A pyrolysis system can produce biochar for a range of uses including water treatment, as well as providing a source of energy in the combustion of pyrolysis gases and liquids.

Pyrolysis unlike biogas production is not impacted strongly by outside factors such as pH and ambient temperature. All that is required is an atmosphere mostly or completely deprived of oxygen, heat and a carbonaceous feedstock. The feedstock influences the pyrolysis products as is seen earlier. The point being made here is that, unlike biogas production, pyrolysis can occur regardless of the nature of the carbonaceous feedstock used. Other processes such as biogas production, incineration, and composting are either impacted more heavily by process conditions and/or can result in the production of secondary pollutants that require removal. Mixed carbonaceous waste streams can be pyrolysed together, with less sorting required than is the case for biogas production and composting, and the production of dioxins is reduced compared to dioxin production in incineration. Despite this, PAHs can still be produced by a pyrolysis process. To mitigate this, lower temperatures can be used to reduce the production of PAHs [259], however this is often avoided in literature regarding the production of adsorbents, where characteristics such as high surface areas and surface pH are more frequently achieved at higher pyrolysis temperatures as seen in Figure 2.7 and Figure 2.8.

2.7 Implications

This review chapter reveals that water treatment as a process is dependent on different factors. The use of membrane filtration technologies such as nanofiltration and reverse osmosis is questionable in sustainability terms since membrane filters require specialist knowledge and materials to maintain, they are costly to produce and maintain; furthermore, the resulting water from nanofiltration and reverse osmosis requires the addition of minerals to make it suitable for potable use. Granular media are more attractive in this regard, particularly carbon adsorbents as these can be produced from by-products of other industries such as waste materials from agricultural, food, and forestry industries. Slow sand filtration techniques can be operated without additional power input, this has led to the modification of slow sand filters into point of use “biosand filters” in the past 30 years. Despite their ability to remove a range of different pollutants, slow sand filters aren’t completely effective against pollutants such as some heavy metals, pesticides and pharmaceutically active products. Rapid

sand filters are another example of sand filtration that can treat water for potable use. These require lower amounts of sand and have a lower footprint than slow sand filters. Despite this, rapid sand filters do not remove biological contamination such as viruses and bacteria, dissolved pollutants such as heavy metals, pesticides and pharmaceuticals are also not removed by rapid sand filters. Both microfiltration and ultrafiltration membranes are similar to rapid sand filtration in the regard that they require regular maintenance such as back washing to maintain flow rate. An additional similarity with rapid sand filtration is that microfiltration struggles to remove both bacteria, viruses and dissolved contaminants, whilst ultrafiltration struggles to remove viruses and aqueous pollutants. Therefore, an additional treatment process is required to further improve water quality to remove the pollution not removed these filtration techniques.

Drinking water treatment plants often involve a combination of different water treatment techniques. Some example diagrams of such systems can be seen in Figure 2.19. Biochar could be used as a replacement in the filtration stage for anthracite material, this would reduce the requirement of fossil materials in the water treatment process, reducing the environmental impact of water treatment. Additionally, powdered activated carbon has been used to enhance removal of aromatic pollutants and dissolved organic carbon in the coagulation flocculation process [260,261]. An economical approach more circular in nature can be promoted through the pyrolysis of appropriate domestic discarded materials such as food scraps and discarded paper with the aim of producing cheaper adsorbent materials.

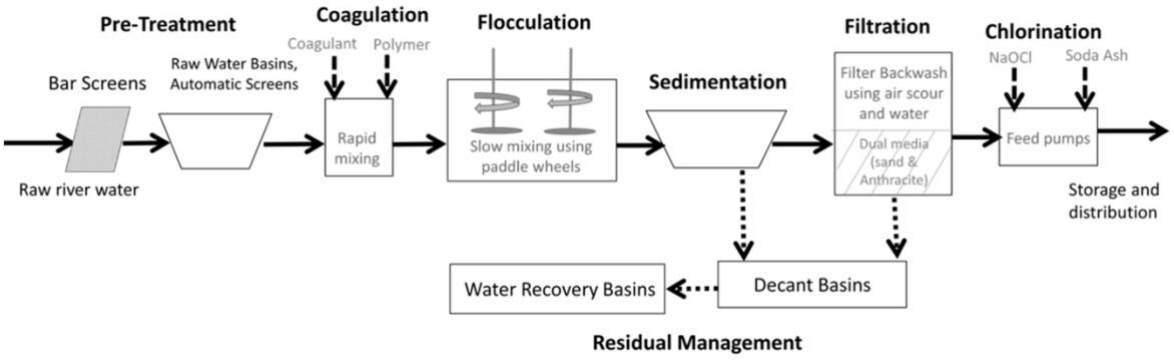

Figure 2.19 – Drinking water treatment plant process diagram [262]

Waste management processes are similar to water treatment processes in that their applicability can change based on the pressures they have to contend with. Anaerobic digestion has been implemented for biogas production across the world, it is however

dependent on conditions of temperature, pH, electrical conductivity, etc. Composting is also a technique that has been implemented to produce a valuable product from waste. Both anaerobic digestion and composting are unable to process certain feedstocks particularly those containing lignin. Furthermore, anaerobic digestion introduces the need for gas storage which is an additional expense and hazard. Incineration is a process that is not as dependent on factors such as feedstock, temperature or pH when compared with anaerobic digestion and composting. However, incineration can produce harmful gases containing PAHs and dioxins. Incineration also results in the direct reinjection of carbon into the atmosphere, with any carbon sequestered in the feedstock combusted and released back to the atmosphere as CO_2 and other combustion by-products. Pyrolysis is more attractive in this regard. Pyrolysis decomposes organic feedstocks, driving off non-carbon elements such as nitrogen, oxygen and hydrogen, resulting in biochar, bio-oil and syngas. Biochar is a highly carbonaceous material making it a potential carbon buffer. With increased surface area and other characteristics that make it a good adsorbent material, biochar produced from discarded municipal material could potentially be incorporated in water treatment processes to improve the quality of effluent water through processes of adsorption onto the biochar. This represents a circular economy approach that would produce a valuable resource from an otherwise worthless one. However, the production of PAHs is increased at higher pyrolysis temperatures, with lower temperatures being avoided in favour of producing adsorbents with higher surface areas. Despite this, some recent studies have found that biochar produced at lower temperatures can still be used in adsorbent applications. These biochars contain more oxygen, suggesting greater amounts of functional groups that are beneficial for complexation and hydrogen bonding interactions between aqueous transition metals and organic pollutants capable of forming hydrogen bonds.

There is a demonstrable gap in research into the use of adsorbents produced at low temperatures, with most studies into the use of these adsorbents making use of adsorbents produced at temperatures generally greater than 400 ^{o}C. This is typically due to the biochar at these higher temperatures having a greater specific surface area due to the evaporation of more volatile materials present in the feedstock which typically contain oxygen, hydrogen and nitrogen. Whilst the increased surface area is beneficial to adsorption and pollutant removal, the loss of oxygen, nitrogen and hydrogen results in a reduction in the ability of the biochar

to remove of aqueous contaminants through hydrogen bonding and complexation mechanisms. Furthermore, the production of biochar as an adsorbent is often conducted in literature using specific feedstocks. Municipal discarded material however is not often explored as a feedstock for the production of biochar adsorbents. This is a diverse group of materials with varying characteristics, which is why it is often avoided as a feedstock in literature. However, most non-industrial waste is mixed, and sorting it can be both economically and energy intensive due to the processes and personnel required to sort the waste. This indicates the importance of exploring mixed feedstocks as a source of material for adsorbent production, where sorting procedures prior to production could potentially be minimised. There are two gaps in research and knowledge identified and populated by this thesis:

1) The use of biochar produced at temperatures below 300 ^{o}C as an adsorbent of aqueous pollutants.
2) The use of biochar adsorbents produced from a mixture of feedstocks as opposed to specific feedstocks.

Consequently, the aim of this thesis is to assess the applicability of biochar produced in a novel low temperature pyrolysis reactor for use as an adsorbent.

3 MATERIALS AND METHODS

3.1 Biochar production

3.1.1 Pyrolysis

A novel heat pipe pyrolysis reactor was utilised for the production of biochar. A schematic diagram of this reactor can be seen in Figure 3.1, a top view of the heat pipe pyrolysis reactor can be seen in Figure 3.3, and an image of the data collection control box, heat pipe control box, display and thermocouple inputs can be seen in Figure 3.2.

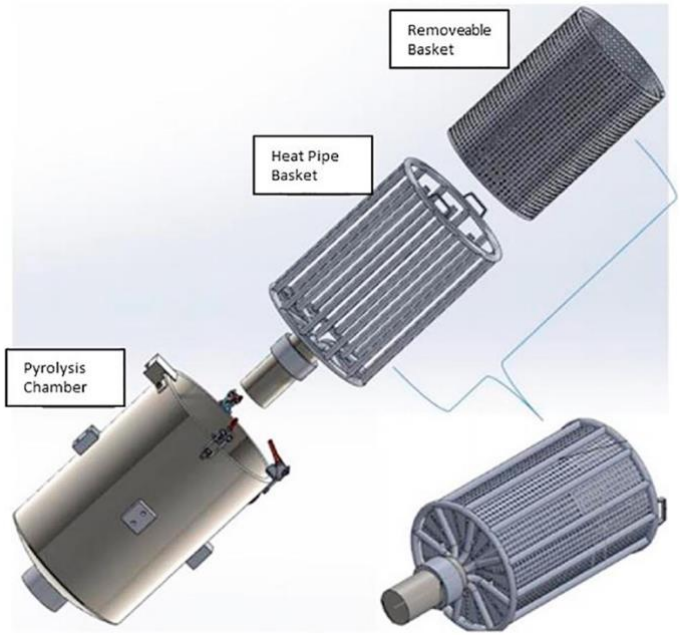

Figure 3.1 – Schematic diagram of heat pipe pyrolysis reactor

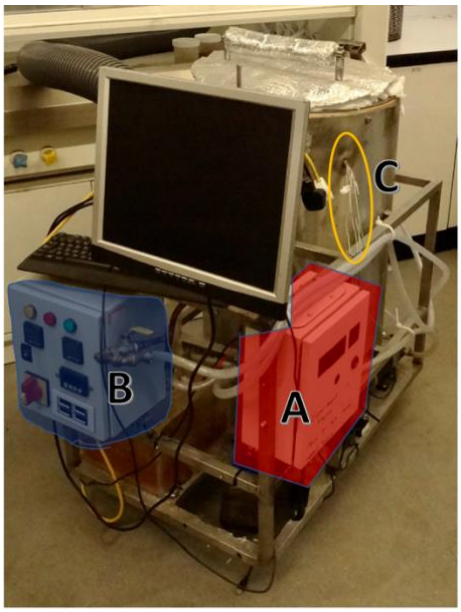

Figure 3.2 - Pyrolysis reactor showing data logging control box (A), Heat pipe and heater control box (B), and the thermocouple wiring for the data logging thermocouples (C)

Figure 3.3 – Internal image of heat pipe reactor, with small mesh baskets for pyrolysis of fine material

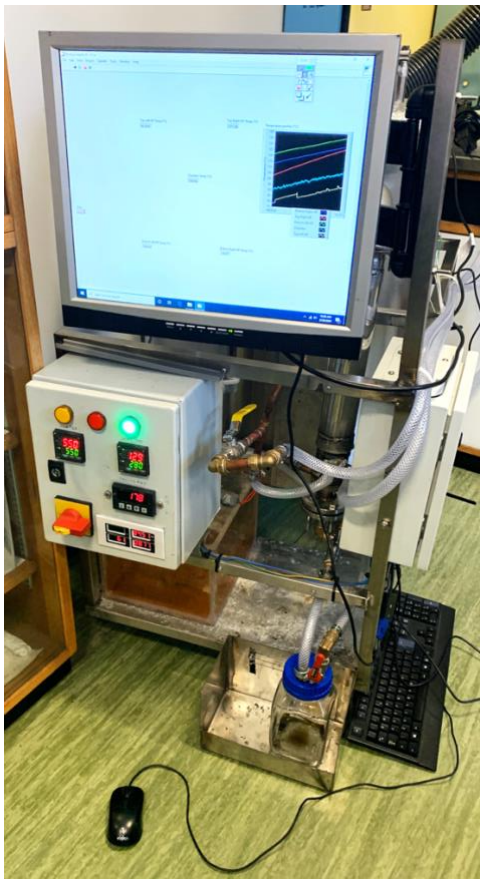

Figure 3.4 – Heat pipe pyrolysis reactor during operation

The pyrolysis process was conducted so that the maximum temperature is held for 4 hours after it has been reached. After holding the temperature at its set point for 4 hours the heater was turned off and the reactor was allowed to cool naturally until it was around 50^{o}C. After the chamber had reached 50 ^{o}C the lid was opened, and the biochar was removed. The biochar was then placed in airtight containers and allowed to cool further to room temperature before further preparation and use.

3.1.2 Sieving

Once the biochar had cooled, it was sieved using sieves such as those shown in Figure 3.5. This ensured that all material passed through a 1mm sieve and no material used for adsorption experiments passed through a 0.15mm sieve. Once these smaller pieces had been sieved, the larger pieces retained on the 1mm sieve were ground and subjected to the same sieving process so that all material used for adsorption experiments passed through the 1mm sieve and was retained on a 0.15mm sieve. Once the biochar was sieved, it was stored in an airtight container until use.

Figure 3.5 – Sieves used to ensure biochar particle sizes ranged between 1mm and 0.15mm

3.2 Biochar characterisation

Biochar characterisation was conducted using several different techniques, including scanning electron microscopy (SEM), Energy Dispersive X-Ray analysis (EDAX), Raman

spectroscopy, and Fourier Transmission Infra-Red Spectroscopy (FTIR). These were all available at the Experimental Techniques Centre at Brunel University London.

3.2.1 Scanning Electron Microscopy

A Zeiss Supra scanning electron microscope was used to collect images of the biochar surface. Prior to analysis, biochar was gold coated for 180 seconds in a sputter coater. The gold coating was used to prevent charging of the highly carbonaceous surface of the biochar in the scanning electron microscope. Charging of the biochar in the SEM makes it difficult to capture high quality images, the gold coating reduces/prevents this phenomenon allowing for better quality imaging of the biochar surface.

The electron gun energy was set to 10kV, and the working distance of the detector set to 14mm.

3.2.2 Energy Dispersive X-Ray analysis

Energy dispersive X-ray analysis was used to collect data regarding the elemental composition of the biochar. This is achieved through the analysis of the energy of X-rays produced by the biochar surface, whilst it is being bombarded by electrons in the SEM. The bombarding electrons can knock electrons out of atoms in the biochar, creating “holes” in the electron orbitals. Holes can be filled by electrons from higher energy level orbitals, as these electrons pass from the higher energy orbital into the created hole, they release an X-ray with a specific energy equal to the difference in energy between the energy levels they have transferred between. The differences in energy between electron orbitals in different elements are unique to each element.

Figure 3.6 – X-Ray detector attached to SEM apparatus used for EDAX

The main issue with the EDAX technique is that the user has to have a good idea of what elements they expect to find in their sample. Biochar produced from mixed municipal discarded material will contain large amounts of carbon and oxygen due to the presence of discarded food materials, plastics and paper, with these discarded materials also containing nitrogen, and minerals such as potassium, calcium, magnesium, phosphorous, and sulphur. The other element expected to display a large peak in the EDAX analysis is gold due to the gold coating of biochars prior to SEM analysis. This element is assumed to be absent from pre-coated biochar samples, percentage elemental composition of the biochar is consequently calculated using Equation 3.1. Where x_{exp} is the percentage elemental amount of a specific element x from the area of biochar analysed, Au is the percentage elemental amount of gold from the area of biochar analysed, and x_{actual} is the percentage elemental amount of x in the biochar omitting the gold elemental percentage.

$$\frac{x_{exp}}{100-Au} \times 100 = x_{actual} \quad (3.1)$$

3.2.3 Fourier Transmission Infra-Red

FTIR analysis was conducted to determine the functional groups present on the surface of the biochar. These functional groups, as explored in the state-of-the-art chapter, are particularly important for adsorption to low temperature biochar. FTIR scans were conducted using the Perkin Elmer FTIR spectrometer shown in Figure 3.7, these spectra were collected between wave numbers of 400-4000cm^{-1}.

Figure 3.7 – Perkin Elmer FTIR

3.2.4 Raman spectroscopy

Raman spectroscopy was conducted to determine the carbon structures present in the biochar. This was conducted using a Renishaw Raman microscope shown in Figure 3.8, with laser wavelength of 514nm. Spectra were collected at wavenumbers between 0 and 2800cm^{-1}.

Figure 3.8 – Renishaw Raman Apparatus

3.2.5 X-Ray diffraction crystallography

X-Ray Diffraction was used to determine the presence of any crystalline structures present in the mixed municipal discarded material biochar derived from heat pipe pyrolysis. Samples were prepared by grinding the granular biochar in a pestle and mortar until a fine powder was produced. This was then placed into a sample holder and mounted into the XRD apparatus shown in Figure 3.9.

Figure 3.9 – X-Ray Diffraction apparatus

3.3 Copper batch adsorption

3.3.1 Copper batch adsorption experiments

Batch adsorption experiments to assess the removal of copper from bulk solution by biochar produced from mixed municipal discarded material were conducted. Firstly a stock solution of aqueous copper(II) was prepared through the dissolution of 12.49g copper sulphate pentahydrate (Sigma Aldrich) in 500ml of deionised water produced by a vision 250 deioniser (RS solutions). This solution was used as the source of copper ions for adsorption experiments. 100ml solutions of 0, 50, 100, 150, 200, and 250mg/l copper were produced through the addition of amounts of stock solution indicated in Table 3.1. These amounts were measured precisely using Eppendorf pipettes.

Table 3.1 – Amount of stock solution required to produce required experimental concentrations

Concentration (mg/l)	**Amount of stock solution required (ml)**
0	0
50	0.787
100	1.574
150	2.36
200	3.147
250	3.934

The pH of solutions was adjusted through the dropwise addition of Titripur 0.5 M sulphuric acid, and Titripur 0.5M sodium hydroxide. For kinetic and isothermal experiments, the pH of the solutions was adjusted to 5. For experiments assessing the effect of pH on copper adsorption to biochar, the copper concentration was 150mg/l and the pH was adjusted to values of 3, 3.5, 4, 4.5, 5, 5.5 and 6. Once the pH has settled at the desired level, the solution was poured from the beaker into a 500ml borosilicate conical flask. The neck of the conical flask was filled with a bung to prevent water loss to evaporation. The conical flask was then placed on a VELP Scientific Arex magnetic stirrer hotplate, and a thermocouple connected to a port at the rear of the stirrer was inserted through the bung. The thermocouple was inserted so that the tip of the thermocouple was submerged approximately halfway through the height of the solution. When the thermocouple was in place, the stirring rotation was set at 360rpm

and the temperature dial was increased slowly until the temperature of the solution reached 30 °C. The temperature was increased slowly to avoid overshooting the temperature of 30°C. Once the solution reached 30 °C, 0.5g of biochar was added to the solution. A timer was started as soon as the biochar was added to solution. Stirring experiments for determining kinetic models were conducted under these conditions for 1, 5, 10, 30, 120 and 1440 mins.

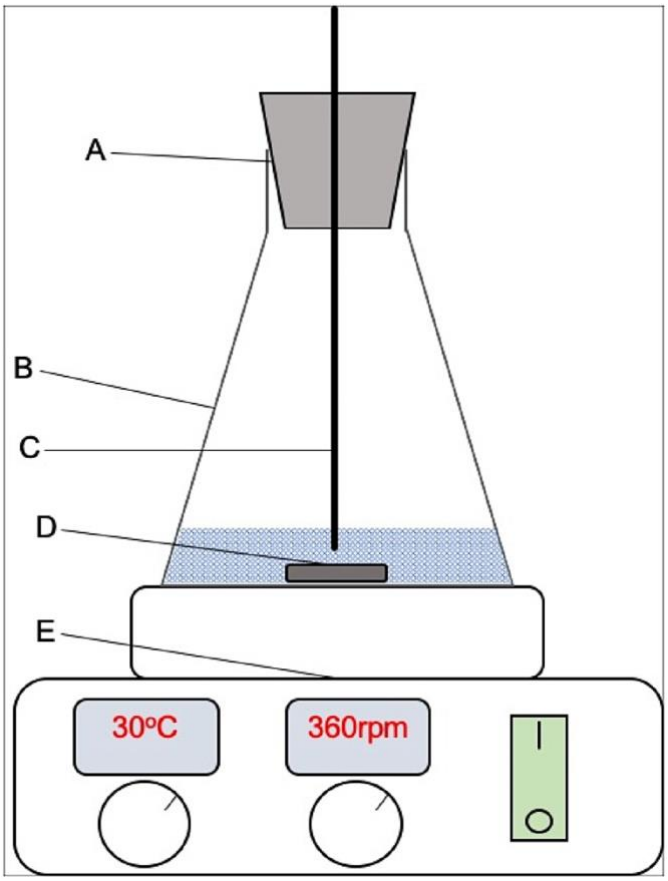

Figure 3.10 - Experimental set up for MB Kinetic and Isothermal experiments (A) shows the rubber bung in the neck of the conical flask (B), with the temperature control probe (C) inserted through a small hole in the bung, (D) shows the magnetic stirring pill and (E) shows the magnetic stirring plate itself

3.3.1.1 Sampling procedure for initial solution pH 5.5 and 6

Samples were collected by drawing the solution into a 25ml syringe. A 0.45 µm Nalgene syringe filter (Thermofisher) was then attached to the syringe, and the sample was then stored in a 15ml centrifuge tube prior to analysis. For solutions of initial pH values of 5.5 and 6, the samples were passed through a syringe filter into centrifuge tubes and centrifuged at 6000rpm for 5 minutes. This was conducted using the fisherbrand microcentrifuge shown in Figure 3.11.

Figure 3.11 – Fisherbrand minicentrifuge used to separate suspended precipitate from solution

The supernatant present in the centrifuge tubes was then stored in a 15ml centrifuge prior to analysis. The centrifuging process removes the solid $Cu(OH)_2(H_2O)_4$ precipitate from the solution. A second sample was drawn from solutions with an initial pH of 5.5 and 6 and only passed through the 0.45 µm nalgene syringe filters into the 15ml storage vessels prior to analysis. This enabled the determination of the effect of copper hydroxide precipitation on copper adsorption to biochar at these higher pHs.

3.3.2 Copper concentration determination

Copper (II) sulphate pentahydrate (99.995% trace metals basis) was purchased from Sigma-Aldrich. A stock solution of aqueous copper(II) was prepared through the dissolution of 12.49g copper sulphate pentahydrate in 500ml of deionised water produced by a vision 250 deioniser (RS solutions). This solution was used to prepare the standard solutions for the calibration

curve of flame atomic absorption spectroscopy (F-AAS), and also for dosing copper into solution for batch experiments described later in 3.3.1.

Copper concentration in solution was determined using F-AAS. Firstly, standard solutions of copper were produced, these were used to produce a calibration curve using F-AAS. Solutions prepared for F-AAS were acidified using 3.571ml of 70% Nitric Acid, to produce 50ml samples acidified to 5%. The calibration concentrations used for copper determination were 0, 1, 2, 3, 4 and 5 mg/l. These solutions were produced using 0, 0.00787, 0.01574, 0.02360, 0.03147, and 0.03934ml of the prepared stock solution. At these concentrations, the absorption of electromagnetic radiation at a wavelength of 324.8nm follow a linear relationship that is proportional to the concentration of copper in solution. This wavelength was selected as the absorption of electromagnetic radiation is greatest for copper at this wavelength.

Absorption is a dimensionless parameter, calculated by (3.2) where I_A is the intensity of light at a given wavelength after passing through the ionised sample, and I_i is the initial intensity of the light beam prior to passing through an ionised sample.

$$A = \frac{log\ (I_A)}{log\ (I_i)} \qquad (3.2)$$

The linear relationship between absorption and concentration can be described numerically by Beer's law seen in Eqaution 3.3. A is the absorption of light a given wavelength as calculated by Equation 3.2, ε is the absorption coefficient of the sample at the given wavelength (l mg^{-1} cm^{-1}), b is the path length of the light through the ionised sample (cm), and c is the concentration of the ionised sample (mg l^{-1}).

$$A = \varepsilon bc \qquad (3.3)$$

The calibration curve used to determine copper concentration in solution using F-AAS can be seen in Figure 3.12.

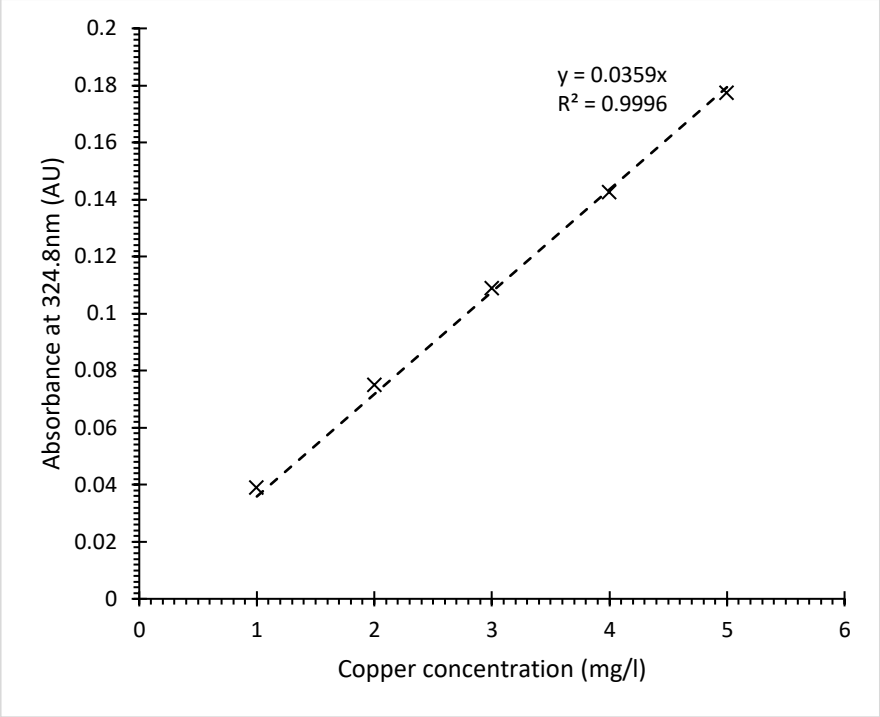

Figure 3.12 – Calibration curve for copper determination using F-AAS

3.3.3 Determination of copper concentration in collected samples

The calibration curve produced was used to determine the concentration of copper in solutions. The initial concentrations used to conduct batch experiments are all greater than the standard solutions used to calculate the calibration curve. Consequently, samples were diluted to determine their concentrations using the calibration curve. Subsequently, dilution factors were required to determine actual concentration, these were determined using Equation 3.4. Where D is the dilution factor, C_s is the sample concentration before dilution (mg/l), and C_d is the concentration of a sample of c_s after dilution (mg/l). The dilution factor can also be expressed by Equation 3.5 where V_d is the volume of solvent used to dilute a sample (l), and V_s is the volume of sample diluted (l). Equation 3.4 and Equation 3.5 can be rearranged so that the concentration of the original sample C_s can be determined using Equation 3.6.

$$D = \frac{C_s}{C_d} \tag{3.4}$$

$$D = \frac{V_d}{V_s} \tag{3.5}$$

$$C_d \frac{V_d}{V_s} = C_s \tag{3.6}$$

3.3.4 Amount of copper adsorbed to biochar

Equation 3.7 determines the amount of copper adsorbed to the biochar where q_t is the amount of copper adsorbed to the biochar at time (t, mins) in a solution of a given volume V (l), c_i is the initial copper concentration (mg/l), c_t is the copper concentration at the sampling time (mg/l), m is the biochar dosage (g). Equation 3.8 is used to calculate the adsorption at equilibrium conditions, where q_e is the amount of copper adsorbed to the biochar at equilibrium (mg/g), c_i is the initial copper concentration of the solution (mg/l), c_e is the copper concentration of the solution at equilibrium, V is the volume of the solution (l), and m is the mass of biochar added (g).

$$q_t = \frac{(C_i - C_t) \cdot V}{m} \quad (3.7)$$

$$q_e = \frac{(C_i - C_e) \cdot V}{m} \quad (3.8)$$

3.4 Methylene blue batch adsorption

3.4.1 Methylene blue batch experiments

Methylene blue batch experiments were conducted using the same experimental set up as the copper batch experiments in 3.3.1. Firstly, a 1000mg/l stock solution of methylene blue was produced through the dissolution of 1.125g methylthioninium chloride (Sigma Aldrich) in deionised water collected from a Milli-Q water purification system to produce a volume of 1l of stock solution. This was stored in a sealed glass bottle and stored in the dark until needed for use. 500ml solutions of varying concentration were produced in order to assess the isothermal and kinetic behaviour of methylene blue adsorption to biochar. These concentrations and the amounts of the stock solution needed to produce these can be seen in Table 3.2.

Table 3.2 – Amount of 1000mg/l methylene blue stock solution required to produce initial experimental concentrations

Concentration (mg/l)	Amount of stock solution required (ml)
0	0
10	5
25	12.5
50	25
75	37.5
100	50

The pH of these 500ml solutions was then adjusted to 7 through the dropwise addition of Titripur 0.5 M sulphuric acid, and Titripur 0.5M sodium hydroxide. The solutions were then poured into the borosilicate conical flask, the bung inserted in the neck and placed on the VELP Arex magnetic stirrer hotplate. The thermocouple was then submerged to roughly halfway into the solution through the bung. The temperature was then gradually increased up to 30^{o}C, and the rotation rate set to 360rpm. 2.5g of biochar was then added to the solution and a timer started.

3.4.2 Difference between methylene blue and copper batch adsorption

Methylene blue experiments were carried out differently to copper experiments to improve the biochar experiments. Firstly, biochar was produced without using plastic as a feedstock, where previous literature has shown that this feedstock produces elevated levels of PAHs and dioxins in the gaseous emissions, even at the lower pyrolysis temperatures used in this thesis [263–265]. Secondly, it was realised that the use of mixed feedstock means that it is not possible to know exactly the feedstock composition of the biochar material inside the batch adsorption experiment. This may not be of much consequence in future larger scale industrial applications, where the make-up of domestic discarded material is fairly consistent in a given economic level [266]. The larger amounts of mixed feedstock adsorbent used in industrial scale water treatment applications could minimise the effect feedstock variation has. However, in the small-scale experiments conducted for this thesis, variation in the biochar

could have a larger effect on the adsorption of a contaminant to the biochar surface. The batch adsorption process was therefore altered for later experiments.

The altered batch adsorption experiments involved a number of assumptions:

1. The concentration of a contaminant in the batch adsorber at any given time is unchanged by withdrawing a sample.
2. The amount of water lost to evaporation due to opening the batch adsorber to collect a sample is negligible.
3. The biochar concentration in a sample is the same as the biochar concentration in the batch adsorber.

The added benefit of this altered method is that it means batch adsorption experiments using heated magnetic stirrers can be conducted much more efficiently, provided the stirring rate is high enough to prevent the biochar settling in the solution. This procedure can be visualised in Figure 3.13, where with each sampling procedure, an amount of biochar and aqueous solution are removed from the batch adsorber, reducing the total volume and biochar present in the batch adsorber.

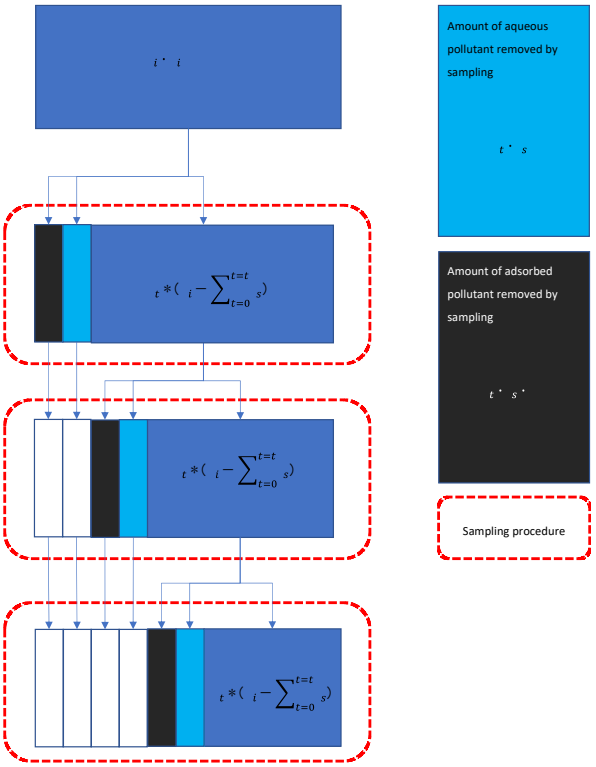

Figure 3.13 – Visualisation of mass balance for modified batch adsorption experiments for methylene blue and tetracycline adsorption

The visualisation is ultimately described by Equation 3.9, where $q_{t,c}$ is the adsorption of a contaminant at the time of sampling (mg/g), c_i is the initial concentration of the solution (mg/l), V_i is the volume of contaminated water at the start of the experiment (l), c_t is the concentration of the solution at time t (mg/l), V_s is the volume of a sample (ml), t,p is the time referring to the previous sampling procedure, D is the biochar dosage (g/l), and $q_{t,p}$ is the amount of pollutant adsorbed to the biochar in the previous sampling procedure (mg/g).

$$q_{t,c} = \frac{C_i V_i - C_t\left(V_i - \sum_{t=0}^{t=t,p} V_s\right) - \sum_{t=0}^{t=t,p} C_t V_s}{D\left(V_i - \sum_{t=0}^{t=t,p} V_s\right)} - q_{t,p} V_s D \qquad (3.9)$$

The first term ($C_i V_i$) of Equation 3.9 refers to the total mass of pollutant initially in the solution before adsorption. The second term refers to the total mass of pollutant in the solution at time t ($C_t(V_i - \sum_{t=0}^{t=t} V_s)$). The third term refers to the total mass of the pollutant in solution removed by previous sampling procedures ($\sum_{t=0}^{t=t,p} C_t V_s$). The denominator refers to the total mass of adsorbent present in the batch adsorber at time t ($D(V_i - \sum_{t=0}^{t=t,p} V_s)$). Finally, the last term refers to the mass of adsorbent present in the biochar removed in sampling ($q_{t,p} V_s D$).

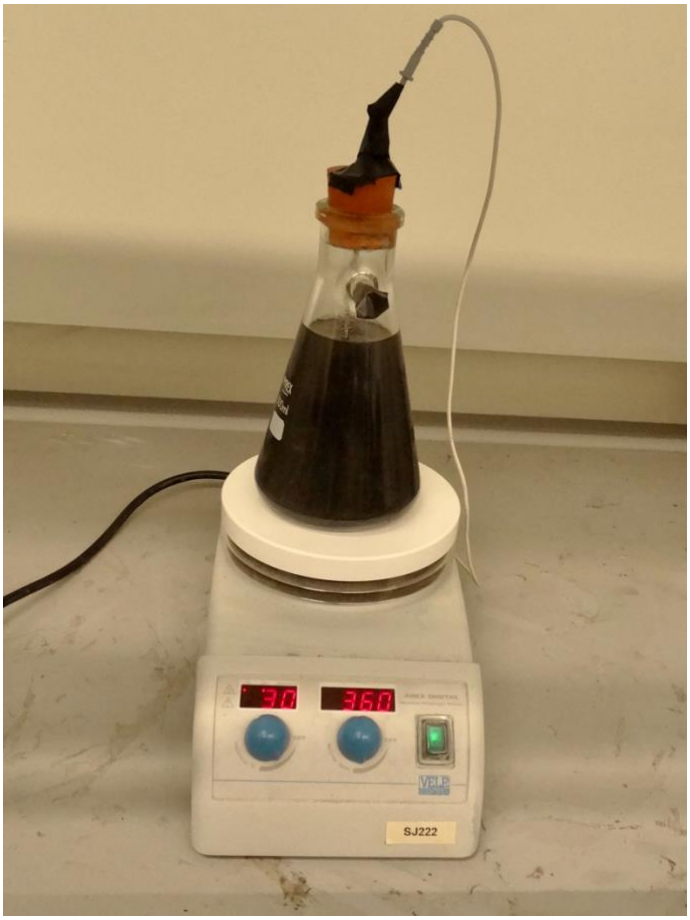

Figure 3.14 – Altered experimental set-up for methylene blue and later tetracycline experiments

3.4.3 Methylene blue concentration determination

Methylene blue concentration was determined using a Perkin Elmer UV-Vis spectrophotometer with a path length of 1cm. The apparatus used to determine the methylene blue concentration can be seen in Figure 3.15.

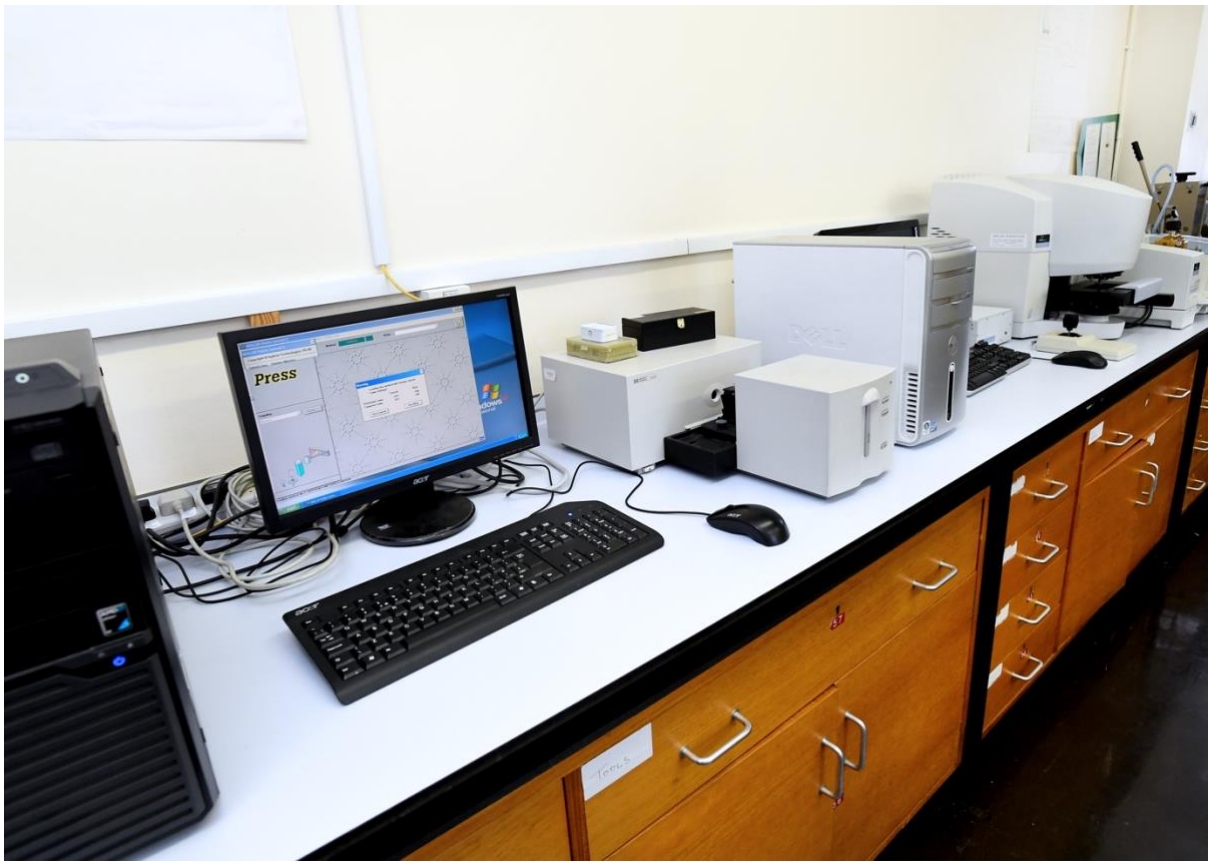

Figure 3.15 – Hewlett Packard UV-Vis spectrophotometer used to determine methylene blue and tetracycline concentration in solution

Standard solutions of methylene blue were produced between concentrations of 0, 0.5, 1, 1.5, 2, 2.5 and 3 mg/l as the absorption of electromagnetic radiation at a wavelength of 664nm between these concentrations obey Beer's law shown in Equation 3.3. These standard solutions were produced through the addition of 0, 0.05, 0.10, 0.15, 0.2, 0.25, and 0.3ml of stock solution to 100ml of deionised water. The calibration curve produced can be seen in Figure 3.16.

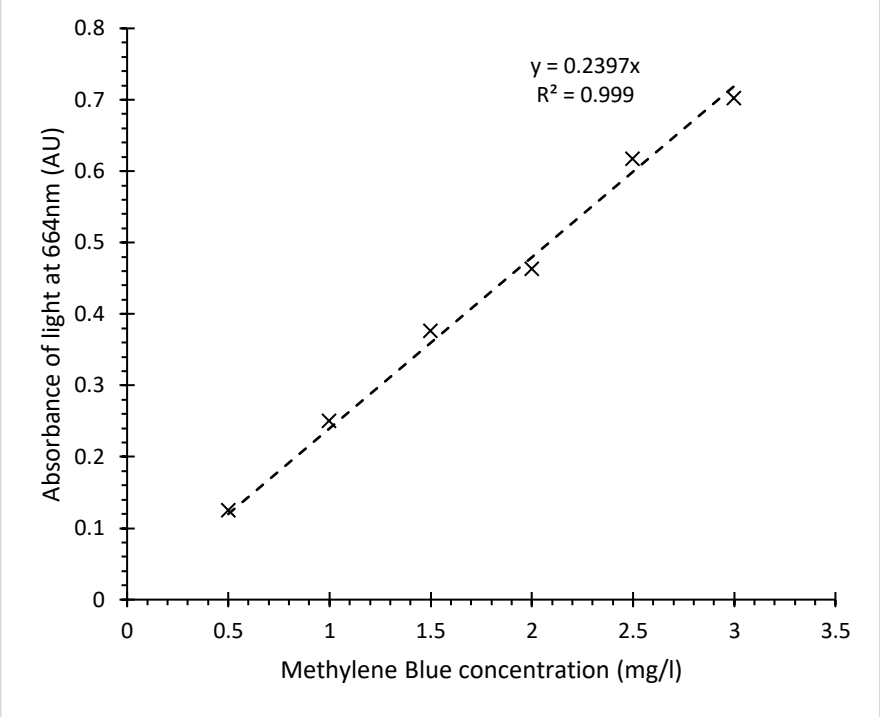

Figure 3.16 – Calibration curve for Methylene Blue determination

All initial concentrations of methylene blue used during adsorption experiments being greater than concentrations used for the calibration curve. Consequently, the dilution procedure outlined in 3.3.3 was followed to determine concentrations of samples collected after adsorption experiments using the calibration curve.

3.5 Tetracycline batch adsorption

Tetracycline hydrochloride (≥95% (European Pharmacopoeia HPLC assay) was purchased from Sigma-Aldrich. A 1000mg/l stock solution was produced through the dissolution of 1.082g of tetracycline hydrochloride into a volume of 1l of deionised water obtained from a Milli-Q water purification system. This was stored in a sealed glass bottle in the dark until use. 500ml solutions of varying concentration were produced in order to assess the isothermal and kinetic behaviour of tetracycline adsorption to biochar. These concentrations and the amounts of the stock solution needed to produce these can be seen in Table 3.3.

Table 3.3 – Amount of 1000mg/l Tetracycline stock solution required to produce initial experimental concentrations

Concentration (mg/l)	Amount of stock solution required (ml)
0	0
20	10
40	20
60	30
80	40
100	50

Tetracycline batch experiments were conducted using the same procedure as outlined in 3.4.2, using a mass balance procedure.

3.5.1 Tetracycline concentration determination

Tetracycline concentration was determined using a Perkin Elmer UV-Vis spectrophotometer shown in Figure 3.15, with a path length of 1cm. The maximum absorption wavelength used for tetracycline concentration determination was 359nm. Standard solutions between 0 – 50mg/l were produced using the stock solution. A calibration curve of tetracycline concentration at a maximum wavelength of 359nm was derived from solutions in this concentration range. The relationship of absorbance to tetracycline concentration in this range again follows Beer's law as shown in Equation 3.3. The calibration curve can be seen in Figure 3.17.

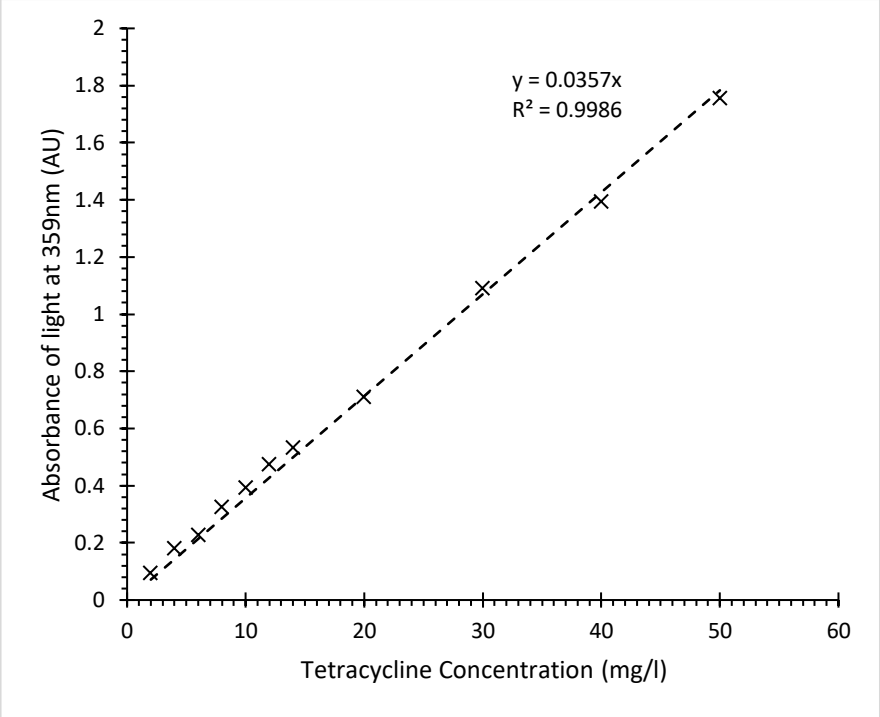

Figure 3.17 – Calibration curve for tetracycline determination

The actual tetracycline concentration of the undiluted sample can also be determined using Equation 3.6 as in 3.3.3.

3.6 Batch adsorption kinetics

Kinetic models make assumptions about the chemistry of the biochar. The parameters in these models are then analysed using non-linear regression techniques. The coefficient of determination then shows which model best describes the removal of a pollutant from aqueous solution, and thus the likely mechanisms of sorption to a sorbent.

3.6.1 Pseudo first order model

The pseudo first order model was defined by Sten Lagergren in 1898 it is displayed in its original form in Equation 3.10.

$$\frac{dx}{dt} = k(X - x) \tag{3.10}$$

In this work the notation used is different and is displayed in Equation 3.11.

$$\frac{dq_t}{dt} = k_1(q_e - q_t) \tag{3.11}$$

The above equation can be integrated to the equation shown in Equation 3.12.

$$k_1 t = ln(q_e) - ln(q_e - q_t) \tag{3.12}$$

This can then be rearranged to the non-linear equation shown in Equation 3.13 where t is the time of sampling (mins), qt is the adsorption of a pollutant to biochar at time t (mg/g), qe is the adsorption of a pollutant to biochar at equilibrium (mg/g), and k1 is the pseudo first order adsorption coefficient (min-1).

$$q_t = q_e(1 - e^{-k_1 t}) \quad (3.13)$$

The pseudo first order model is generally considered to describe physisorption processes. Therefore, if this model is found to more strongly describe the adsorption of a pollutant to biochar than other kinetic models, then the removal of a contaminant can be almost entirely attributed to physisorption processes [267].

3.6.2 Pseudo second order model

The pseudo second order model was defined by Ho et al this can be seen in Equation 3.14.

$$\frac{dq_t}{dt} = k_2(q_e - q_t)^2 \quad (3.14)$$

This can be integrated to Equation 3.15

$$k_2 t = \frac{1}{q_e - q_t} - \frac{1}{q_e} \quad (3.15)$$

This in turn can be rearranged to the non-linear form in Equation 3.16.

$$q_t = \frac{k_2 {q_e}^2 t}{1 + k_2 q_e t} \quad (3.16)$$

If this kinetic model better describes the adsorption of a contaminant to the biochar, then multiple mechanisms can be attributed to the adsorption of this contaminant. Additionally, a stronger fit of this model indicates that chemisorption is the rate limiting step of adsorption rather than physisorption [268].

3.6.3 Elovich model

The Elovich model was proposed in the 1930s. It is represented by the differential equation shown in Equation 3.17.

$$\frac{dq_t}{dt} = a * e^{-\beta * q_t} \quad (3.17)$$

This can be integrated to the form shown in Equation 3.18

$$\frac{e^{\beta * q_t}}{\beta} = a * t \quad (3.18)$$

This can be rearranged to the form shown in Equation 3.19

$$q_t = \frac{1}{\beta} ln(a * \beta) + \frac{1}{\beta} ln\,(t) \quad (3.19)$$

3.7 Diffusion Models

3.7.1 Intraparticle diffusion model

This model describes the diffusion of an adsorbate into a biochar particle once it has passed through the liquid film surrounding the biochar particle. If Intraparticle diffusion processes occur, then the plot of adsorption against the square root of the time will produce either a single, or multiple straight lines. If intraparticle diffusion is the sole rate limiting step, then one of the straight lines should pass through the origin [269]. The equation describing intraparticle diffusion is displayed in Equation 3.20. Where qt is the adsorption at time t (mg/g), ki is the intraparticle diffusion coefficient (mg/g/min1/2), t is the time of sampling (mins), and C is a constant that is proportional to the thickness of the boundary layer [270].

$$q_t = k_i t^{1/2} + C \quad (3.20)$$

Intraparticle diffusion however is likely not the only interaction that limits the rate of adsorption to biochar, with liquid film diffusion and other processes such as chemisorption also limiting the rate of adsorption to the biochar.

3.7.2 Liquid film diffusion model

The liquid film diffusion model describes the movement of an adsorbate across the film that exists between the bulk solution and the surface of the biochar [271]. The equation used to model the liquid film diffusion in biochar can be seen in Equation 3.21 [270].

$$ln\left(1 - \frac{q_t}{q_e}\right) = -k_{l,f} \cdot t \quad (3.21)$$

This can be rearranged to a non-linear form as seen in Equation 3.22. Where qt is the adsorption of a contaminant to the biochar at a given time (mg/g), qe is the adsorption of an adsorbate to biochar at equilibrium (mg/g), kf is the liquid film diffusion coefficient (min-1), and t is time (mins). It can be seen that this equation is identical to the pseudo first order adsorption model. Consequently, it can be stated that the liquid film diffusion model and the pseudo first order adsorption model describe the same phenomenon.

$$q_t = q_e(1 - e^{-k_f t}) \quad (3.22)$$

3.8 Batch Adsorption Isotherms

Isotherms are used to determine how the adsorption characteristics change with changing equilibrium concentrations.

3.8.1.1 Langmuir Isotherm

The Langmuir isotherm assumes a monolayer of coverage of sorbate over a sorbent. Therefore, a strong fit with this isotherm over others suggests that adsorption takes place across the entire surface of the sorbent in a monolayer fashion. This means that the Langmuir isotherm makes the assumption that the adsorption of a pollutant to an adsorbent will reach a maximum, and the sorption will no longer increase with an increase in equilibrium concentration after this point has been reached. Therefore, this isotherm typically describes chemisorption processes where only a finite number of "sorption sites" are available and can therefore be exhausted. This means that the Langmuir adsorption process can be represented as a chemical equation. The derivation of the Langmuir isotherm can be seen below.

$$A_s + A_l \rightleftharpoons A_a \tag{3.23}$$

Where A_s is the number of empty sorption sites on the surface of the adsorbent, A_l is the amount of sorbate in the bulk solution, and Aa is the amount of sorbate present in the sorbent. The equilibrium constant of such a system can be defined as shown in Equation 3.24.

$$K = \frac{[A_a]}{[A_s][A_L]} \tag{3.24}$$

$$A_s \propto q_m - q_e \tag{3.25}$$

Where q_m is the maximum possible adsorption (mg/g), and q_e is the adsorption at the equilibrium conditions (mg/g).

$$A_l \propto C_e \tag{3.26}$$

Where C_e is the equilibrium concentration of an adsorbate in solution (mg/l).

$$A_a \propto q_e \tag{3.27}$$

With these proportionalities assumed, the equilibrium constant can be calculated using Equation 3.28.

$$k_L = \frac{q_e}{C_e(q_m - q_e)} \tag{3.28}$$

This can be rearranged and reciprocated to the equation shown in Equation 3.29.

$$\frac{1}{k_L C_e} = \frac{q_m}{q_e} - 1 \quad (3.29)$$

This can in turn be rearranged and reciprocated, finally solving for q_e gives the equation shown in Equation 3.30. (3.30

$$q_e = \frac{k_L C_e q_m}{1 + k_L C_e} \quad (3.30)$$

3.8.1.2 Freundlich isotherm

The Freundlich isotherm was developed from Langmuir's isotherm. Freundlich made the assumption that adsorption occurs in a heterogenous, multilayer fashion across the surface of the adsorbent. The derivation of this isotherm can be seen below.

$$-\frac{dC}{dt} = k_1(S_0 - S)C^{n_1} - k_2 S \quad (3.31)$$

Assuming that S<<S0 Equation 3.31 becomes Equation 3.32:

$$-\frac{dC}{dt} = k_1 S_0 C^{n_1} - k_2 S \quad (3.32)$$

When the concentration of an adsorbate in bulk solution and in the adsorbent reaches equilibrium, then the change in concentration with respect to time is considered to be 0. Consequently Equation 3.33 describes the adsorption as described by the Freundlich model at equilibrium.

$$k_2 S = k_1 S_0 C^{n_1} \quad (3.33)$$

This can be rearranged resulting in the equation below

$$S = \left(\frac{k_1}{k_2}\right) S_0 C^{n_1} \quad (3.34) \; [272]$$

This equation can then be simplified to Equation 3.34 which is the version of the Freundlich model used in this thesis as well as being commonly used in literature either in linear or non-linear form to describe the isothermal behaviour of adsorption to biochar.

$$q_e = k_f {C_e}^{1/n} \quad (3.35)$$

Where q_e is the adsorption at equilibrium (mg/g), k_f is the Freundlich constant (l/g), and n is the curvature constant.

3.8.2 Use of kinetic equations in literature

In literature both linear and non-linear models have been used to determine the kinetic models of adsorption for biochar in batch adsorption experiments. The benefits of using the linearised models are that the computation of the model is simpler, with the unknown parameters of adsorption at equilibrium (q_e) and n^{th} order rate constant (k_n) derived from the gradient and intercept of the linear graph. However, on inspection of the pseudo first order, and pseudo second order linear equations, there is a clear issue with using linearised equations for describing batch adsorption kinetics. This is that as q_t approaches equilibrium, the experimental value of $\ln(q_e - q_t)$ becomes increasingly influenced by uncertainties in the q_t value. This means that small variations in the value of q_t that are close to the value of q_e can have a significant impact on the fit of the linear pseudo first order model to the experimental data. Whereas, in the linear pseudo second order model, the experimental value of 1/qt is less influenced by small uncertainties in the value of q_t, where small variations in the value of q_t result in only a small deviation from the linear pseudo second order model.

Research has commonly used R^2 values calculated from linearised kinetic models to determine the kinetic behaviour of batch adsorption. This approach is flawed seeing as the R^2 values are calculated on different scales for different linearised models. This means that R^2 values calculated on linearised plots may correspond to different R^2 values for these models in non-linear plots of adsorption (q) against time (t). With modern computers, the use of non-linear regression is now a reality rather than a possibility. This means that non-linear kinetic models no longer need to be linearised to enable timely calculations, where iterative non-linear regression can be carried out using computer software. This enables direct comparison of different kinetic models on the same scale, allowing for a more accurate determination of adsorption kinetics. Consequently, the models for batch adsorption in this thesis are calculated using SAS 9.2 statistical modelling software, using the non-linear regression tools available in this software package.

3.8.3 Kinetic and Isothermal model fitting using Non-linear regression

Non-linear regression was used to fit kinetic and isothermal model equations to the collected data. This was conducted using the Gauss-Newton method available for use in the SAS university edition software. This is an iterative process that minimises an objective function. The objective function for minimisation in the case of this thesis is the sum of square residuals

(RSS). The calculation for RSS can be seen in Equation 3.35, where RSS is the residual sum of squares, qexp is the adsorption determined experimentally, and qpred is the adsorption predicted by a given kinetic or isothermal model.

$$RSS = \sum_{i=1}^{i=n}(q_{exp} - q_{pred})^2 \quad (3.36)$$

3.8.4 Statistical analysis of batch adsorption models

Statistical analysis of batch adsorption kinetic models was carried out to determine which kinetic equations best describe the adsorption of a contaminant to a biochar produced from mixed municipal discarded material in a heat pipe reactor. Typically, in literature, the coefficient of determination is used to determine how well a kinetic model describes adsorption to an adsorbent. The equation to calculate the coefficient of determination can be seen in Equation 3.36, where qexp is the amount of pollutant adsorbed to the biochar (mg/g) as calculated using Equation 3.7, qpred is the adsorption predicted by a given kinetic or isothermal model (mg/l). Mean squared error was also used in this thesis to describe how well the kinetic and isothermal models described the adsorption of pollutants to biochar, this can be seen in Equation 3.37. Where n is the number of samples, qexp is the experimentally determined adsorption (mg/g), and qpred is the adsorption predicted by a kinetic or isothermal model (mg/g).

$$R^2 = \left(\frac{n(\sum q_{exp}q_{pred}) - (\sum q_{exp})(\sum q_{pred})}{\sqrt{[n\sum {q_{exp}}^2 - (\sum q_{exp})^2][n\sum {q_{pred}}^2 - (\sum q_{pred})^2]}} \right)^2 \quad (3.37)$$

$$MSE = \frac{1}{n}\sum_{i=1}^{n}\left(q_{exp} - q_{pred}\right)^2 \quad (3.38)$$

Models with a better combination of R^2 and MSE values will be considered to be the best fitting models that describe the adsorption of pollutants to biochar derived from municipal mixed discarded material in a heat pipe reactor [273].

4 BIOCHAR CHARACTERISATION RESULTS AND DISCUSSION

Biochar was characterised using several different techniques in order to explore its physical and chemical properties, and to describe how the biochar may interact with aqueous pollutants. As outlined in the materials and methods section, characterisation was carried out using scanning electron microscopy, energy dispersive x-ray analysis, Fourier transmission infra-red, Raman microscopy, and X-Ray Diffraction crystallography.

4.1 Temperature of biochar production

The pyrolysis process to produce the biochar derived from mixed municipal discarded material is shown in Figure 4.1 and Figure 4.2. Once the maximum temperature of 250 ^{o}C was reached, a timer was started, and the pyrolysis reactor was held at this temperature for 3 hours before turning off the heater. Figure 4.1 shows temperature measured by K type thermocouples at the bottom and top of the heat pipe basket inside the pyrolysis reactor. The temperature of both the bottom left and bottom right-hand side of the heat pipe basket are shown to increase in temperature first, with the temperatures of both the top right and top left heat pipe remaining at around the starting temperature of 30 ^{o}C for a time before also increasing. This is due to the nature of heat pipes, where the working fluid inside the heat pipe needs to evaporate for the heat pipe basket to transfer thermal energy from the evaporator at the bottom to the condenser section inside the pyrolysis reactor. After 20 minutes of operation, the heat pipe basket had received enough thermal energy for the lower part of the condenser section inside the pyrolysis chamber to begin heating up the chamber. Further time elapsed before the temperature of the top left and top right parts of the heat pipe basket started to increase as well. This is also due to the nature of wickless heat pipes, where at the beginning of heating, more working fluid condenses before it can reach the top of the heat pipe basket inside the pyrolysis reactor. This results in a difference in latent heat transfer between the bottom and top of the heat pipe basket where lesser amounts of working fluid are condensing in the higher portions of the heat pipe basket. This causes the temperature of bottom of the heat pipe basket to increase more rapidly than the top at the beginning of the heating process. As the heating process progresses, the condenser section of the heat pipe basket begins to transfer energy more uniformly once steady state conditions are reached, with the temperatures at the top of the heat pipe basket approaching and eventually equalling those at the bottom of the heat pipe basket [274].

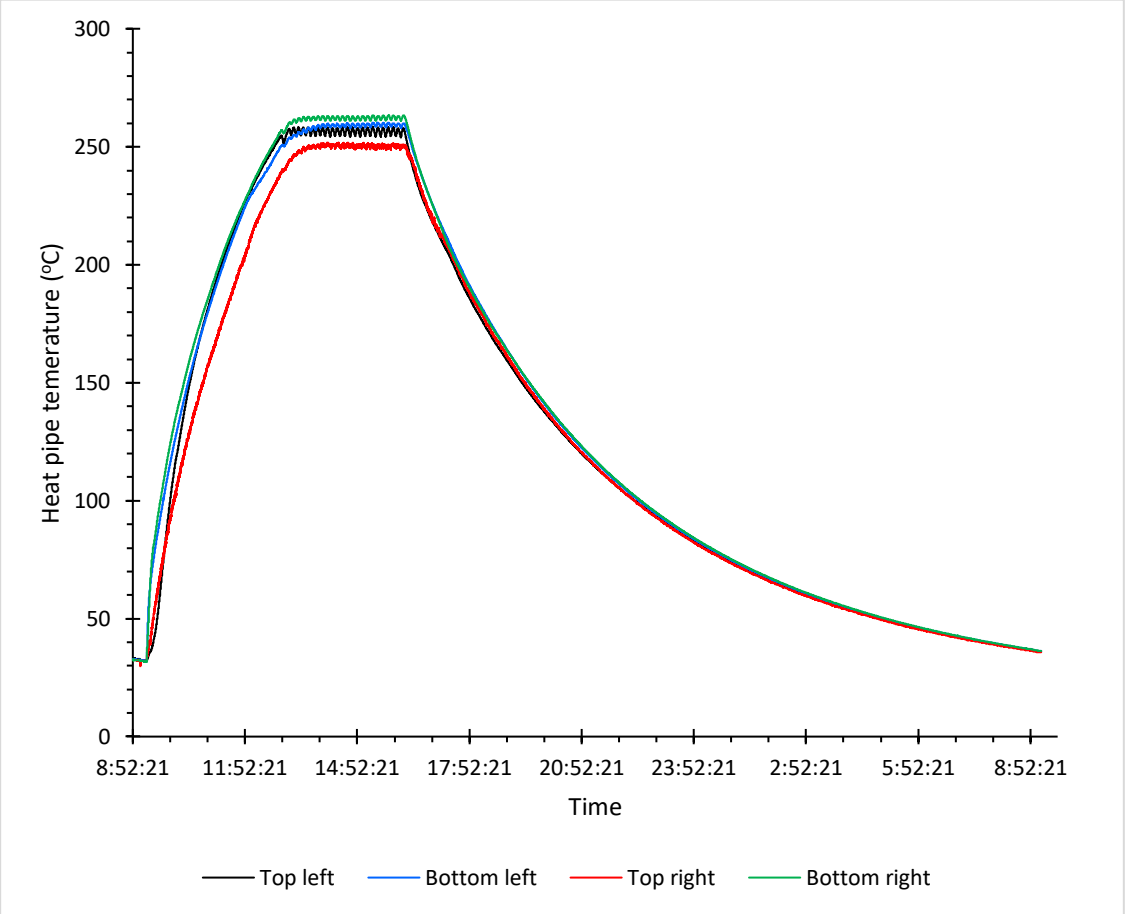

Figure 4.1 – Graph showing the temperatures of different points on the heat pipe basket throughout the course of the biochar production

Figure 4.2 also shows the point at which hemicellulose begins to thermally decompose [275]. At any point above the red line in Figure 4.2 hemicellulose present in the mixed municipal discarded feedstock undergoes pyrolysis This is particularly important where vegetable scraps are present in mixed municipal discarded material, as the fibres of such materials are largely made up of hemicellulose, cellulose, and lignin respectively [276]. The figure shows that the temperature was above that at which hemicellulose decomposes for 5 hours. Furthermore, discarded animal waste in the form of meats has been shown to begin thermally decomposing at 200 °C [277].

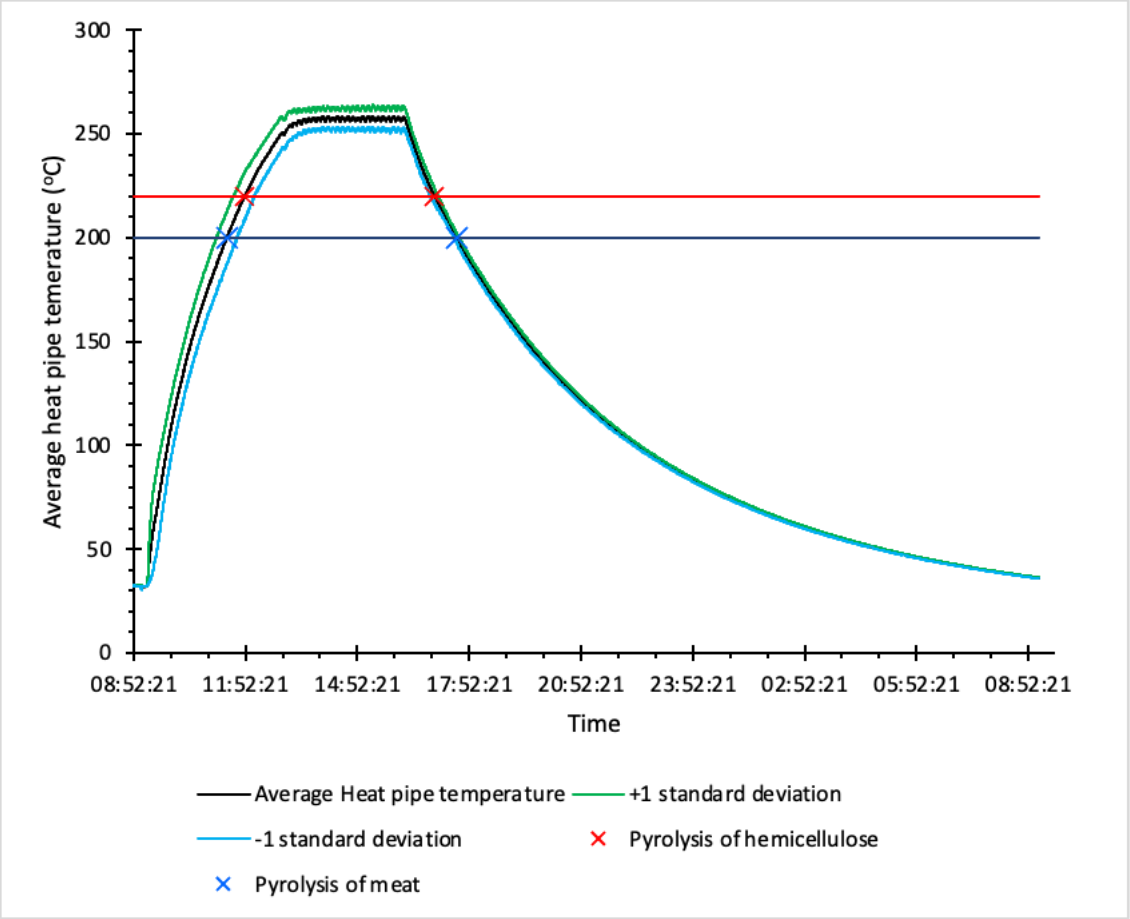

Figure 4.2 – Graph showing the average temperature of the heat pipe reactor during the pyrolysis process from start to finish

4.2 Scanning electron microscopy

Figure 4.3 shows an SEM image of char material derived from discarded plastics produced in the heat pipe reactor. The image shows that almost no pores have developed in the solid. This is indicative of a low surface area for biochar derived from the plastic fractions of mixed municipal discarded material. Another notable feature of this char is the presence of small particulates that appear to have crystalline features. This could be indicative of mineral oxides present on the surface of the biochar derived from plastic. As explored in the state of the art, mineral oxide inclusions can act as adsorbents in the biochar derived from mixed municipal waste.

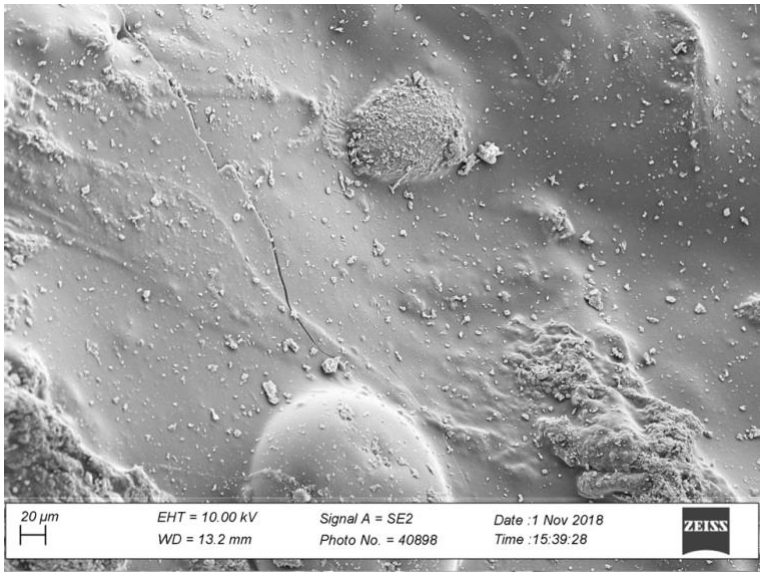

Figure 4.3 – Scanning Electron Microscope image of biochar derived from plastic waste

Figure 4.4 shows an SEM image of char material derived from discarded food materials in the mixed municipal discarded material pyrolyzed in the heat pipe reactor. This SEM shows a large number of pores present in the biochar. The image also shows that these pores have varying sizes, indicative of micro, meso and macropores present in biochar derived from discarded food materials in the heat pipe reactor. This shows that this biochar has a larger surface area than the biochar derived from discarded plastics shown in Figure 4.3.

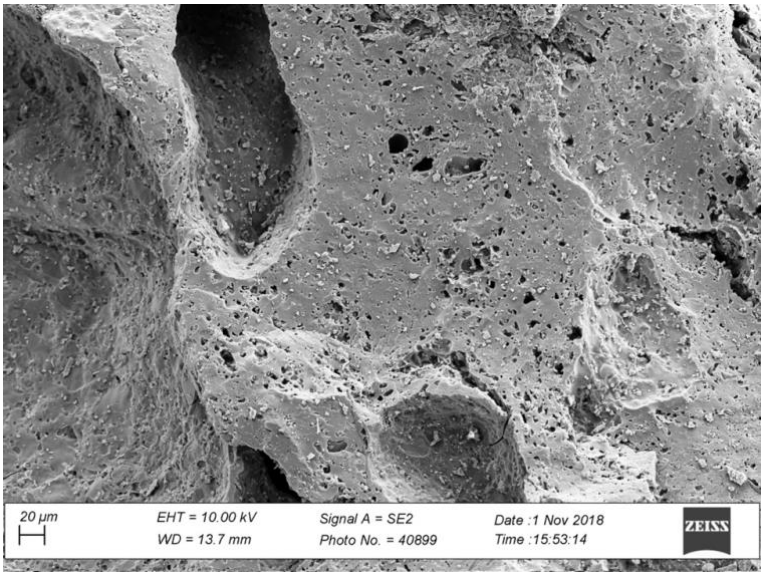

Figure 4.4 – Scanning Electron Microscope image of biochar derived from discarded food materials

Figure 4.5 shows an SEM image of biochar derived from discarded paper/cardboard. Paper and cardboard are produced through the flattening and drying of cellulose fibres in a wet environment. This SEM image shows that discarded paper/cardboard when pyrolyzed retains

its fibrous nature. Additionally, it can be seen that compared with discarded food in Figure 4.4, fewer pores have developed on the surface of the biochar material produced from discarded paper and cardboard.

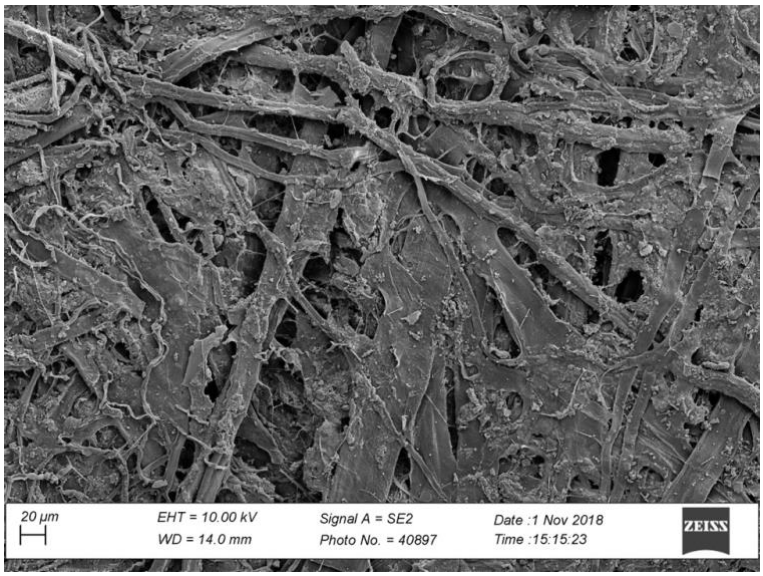

Figure 4.5 - Scanning Electron Microscope image of biochar derived from discarded paper and cardboard

4.3 Energy Dispersive X-Ray Analysis

Energy Dispersive X-Ray analysis shows biochar produced from different feedstocks found in mixed municipal discarded material has different elemental compositions as well as different physical characteristics as demonstrated by scanning electron microscopy in Section 4.2. Figure 4.6 shows biochar derived from discarded plastic in a heat pipe reactor. The most common element found in this biochar is shown to be carbon with the EDAX scan of the whole area (Area 6) of the related SEM image showing 75% of the atomic mass present in the scan can be attributed to carbon atoms. Area 1 in Figure 4.6 shows the EDAX scan of a small particulate on the surface of the plastic biochar. This scan returned a much smaller carbon signal than was present in the other EDAX scans of other areas of the plastic biochar. The same scan also returned a much larger calcium and oxygen signal. This is probably due to the presence of calcium carbonate in the plastic feedstock where calcium carbonate is used as a filler material in the manufacture of certain plastics, giving these plastics more attractive bright surfaces, as well as increasing the hardness of the plastic [278].

Nitrogen was also shown to be present in all of the scans representing between 2-8% of the total weight of the analysed areas. This kind of material is to be expected where food packaging, particularly of meat and dairy produce, can be composed of polyamides [279].

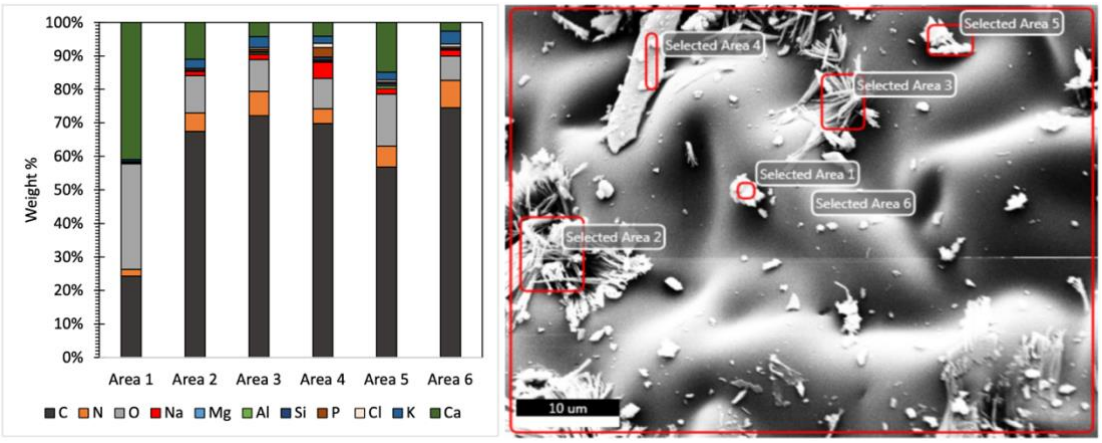

Figure 4.6 – Energy Dispersive X-Ray analysis of Biochar derived from discarded plastics in a heat pipe reactor

EDAX analysis of biochar derived from discarded paper in a heat pipe reactor is shown in Figure 4.7. Again, the most common element found in the biochar derived from discarded paper is carbon with the whole area scanned returning a signal showing 50% of the mass of the entire scanned area (Area 5) is comprised of carbon atoms, with the other 50% being made up of other elements including calcium (20%), oxygen (15%), aluminium (4%), silicon (5%), zinc (3%), sulphur (2%), phosphorus (1%), magnesium (1%) and chlorine (<1%). Variation is seen throughout the paper biochar as well, with areas containing fragmented particulate matter (Areas 1 and 3) containing higher amounts of minerals and oxygen and lesser amounts of carbon, than areas without particulates. Calcium and oxygen is probably present in high amounts due to the use of calcium carbonate in the paper industry as a brightening agent [280]. Aluminium and silicon are present in char derived from discarded paper due to the use of kaolin as a filler material, which improves the strength and visual properties of paper [281].

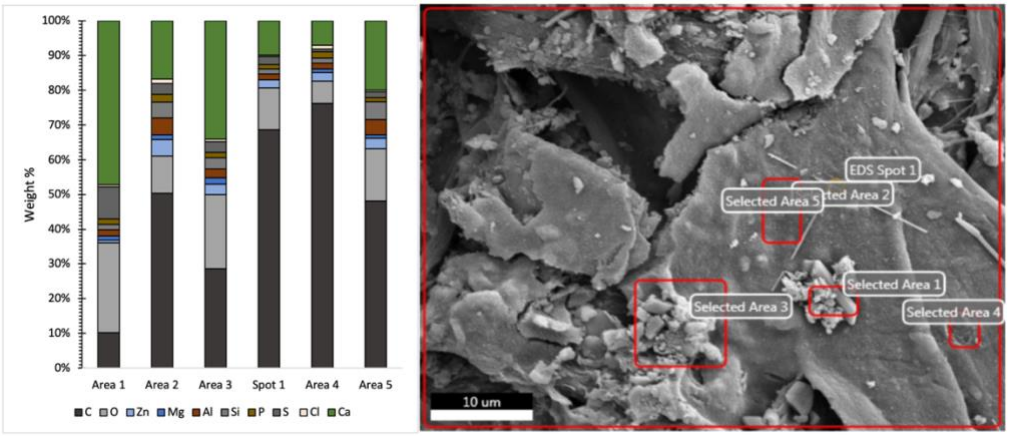

Figure 4.7 – Energy Dispersive X-Ray analysis of Biochar derived from discarded paper in a heat pipe reactor

Figure 4.8 shows energy dispersive x-ray analysis of biochar derived from discarded food material in a heat pipe reactor. The biochar shown in Figure 4.8 contains carbon (76 wt%), chlorine (9 wt%), potassium (5 wt %), sodium (4 wt%), phosphorus (2 wt%), Nitrogen (1 wt%), silicon (<1 wt%), magnesium (<1 wt%). As is the case in biochar derived from both discarded paper and discarded plastic, the elemental composition of the biochar derived from discarded food was also shown to be heterogenous. The particulate matter present on the surface of the discarded food biochar contains large amounts of potassium, sodium and chlorine. This shows that in terms of elemental composition, biochar derived from discarded food contains more sodium, potassium and chlorine, and less calcium and oxygen, than biochar derived from discarded paper and plastic. Potassium, sodium and chlorine are probably present in the discarded food biochar due to the presence of chloride salts in the feedstock prior to pyrolysis [282].

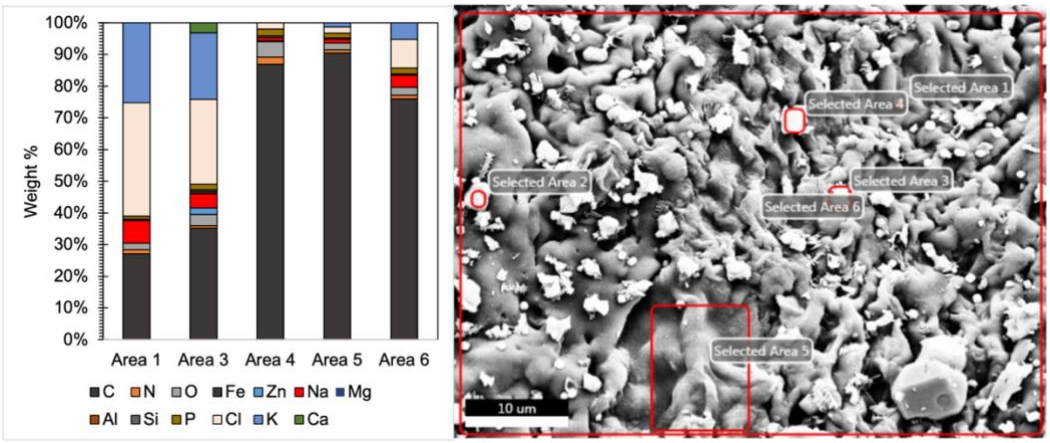

Figure 4.8 – Energy Dispersive X-Ray analysis of Biochar derived from discarded food material in a heat pipe reactor

4.4 Fourier Transmission Infra-Red Spectroscopy

The FTIR spectra in Figure 4.9, Figure 4.10 and Figure 4.11 show biochar derived in a heat pipe reactor under the same conditions from food, paper and plastic feedstock, respectively. Both food and paper feedstocks are shown to produce biochar with similar characteristics as determined by FTIR spectra. The large peak at 1423cm^{-1} in both discarded paper and food biochar show the presence of C=O and O-H groups in the biochar, but can also be attributed to C-O stretching [283]. The peak at 1030cm^{-1} shows C-H stretching in ordered graphitic units, and is also representative of primary alcohol C-O groups, as well as the stretching of non-conjugated C=O groups [284]. The peak at 873cm^{-1} is also indicative of the vibration of aromatic C-H bonds, further confirming that the biochar contains C-H as well as aromatic C=C groups [285]. Calcite is shown to be present in these biochar samples also, where the peak at 713cm^{-1} is indicative of CO_3^{2-} in the biochar, with the additional peak for this material present at 876cm^{-1}; this peak is potentially masked by the vibration of aromatic C-H bonds at 873cm^{-1} [286].

Figure 4.11 shows the FTIR spectra of biochar derived in a heat pipe pyrolysis reactor from discarded plastic material. Peaks at 873cm^{-1} and 713cm^{-1} are also present in the plastic biochar. This again shows that, as in the case with discarded paper and discarded food biochar, biochar derived from discarded plastic also contains aromatic C-H groups, and CO_3^{2-} due to the presence of calcite. These peaks are however less intense than the same peaks present in the previous discarded paper and discarded food biochar. This could show that the pyrolysis of discarded plastic is not as complete as in the case of discarded paper and discarded food biochar, where C=C groups are not created by the degradation of R-C-H. Alternatively, it could be the case that the discarded plastic used for the pyrolysis experiments was already lacking in hydrogen, therefore the presence of aliphatic and aromatic C=C groups may not be indicated by their corresponding C-H groups.

C=O groups are shown to exist in the biochar derived from discarded plastic, with a peak at 1576cm^{-1} indicating this [287]. This peak is also indicative of N-H in plane bending and C-N stretching in amides. A peak at 1241cm^{-1} is caused by C-O-C groups present in the biochar [288,289].

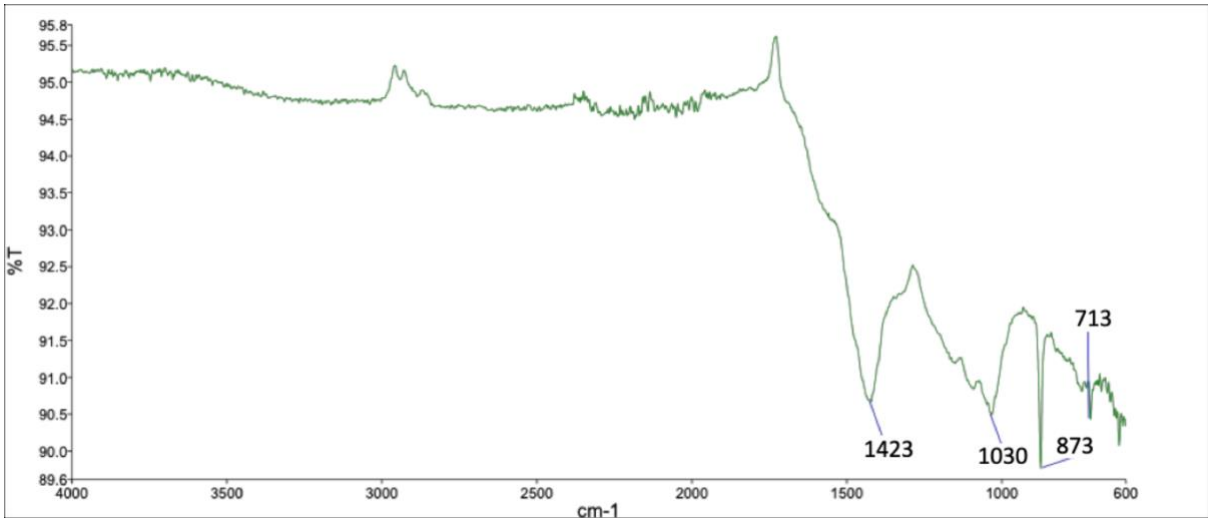

Figure 4.9 – Fourier Transmission Infra-Red spectra of discarded food feedstock biochar derived in a heat pipe reactor

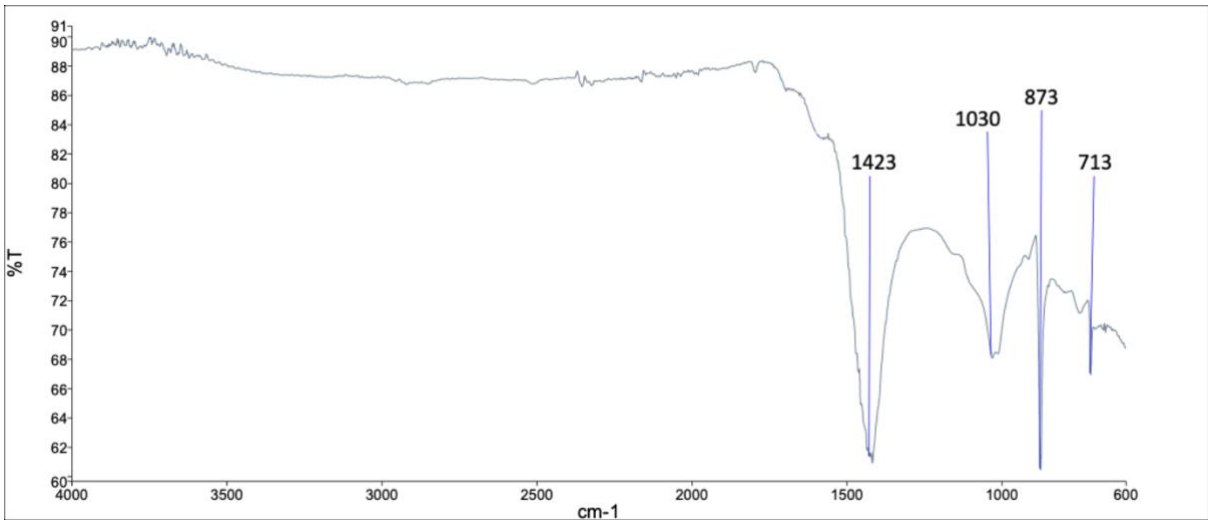

Figure 4.10 – Fourier Transmission Infra-Red spectra of discarded paper feedstock biochar derived in a heat pipe reactor

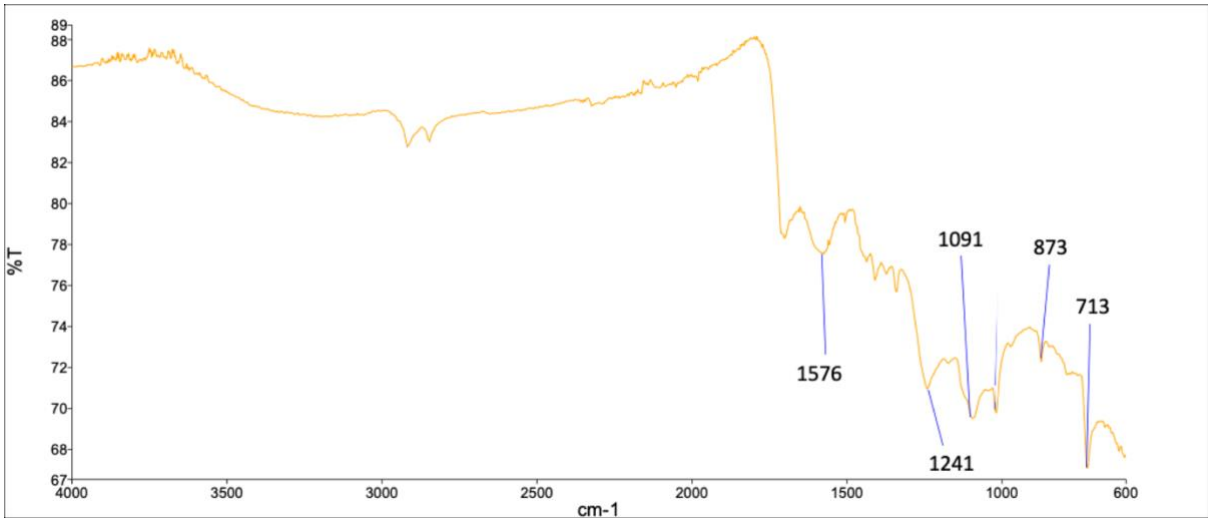

Figure 4.11 – Fourier Transmission Infra-Red spectra of discarded plastic feedstock biochar derived in a heat pipe reactor

4.5 X-Ray Diffraction Crystallography

Figure 4.12 shows the XRD spectra collected for mixed feedstock biochar. The largest peak in terms of intensity is shown at a 2θ value of 29.3887°. This large peak along with the smaller peaks present at 23.064°, 35.9892°, 40.558°, and 43.1596° are indicative of a form of calcium carbonate known as calcite [290,291]. This material was also shown to exist in Raman spectra.

Other smaller peaks at 31.7145°, 47.517°, 48.5099°, 57.4269°, indicate the presence of sodium chloride crystalline structures in the biochar.

The peak at 40.558° shows the potential presence of potassium chloride in the biochar.

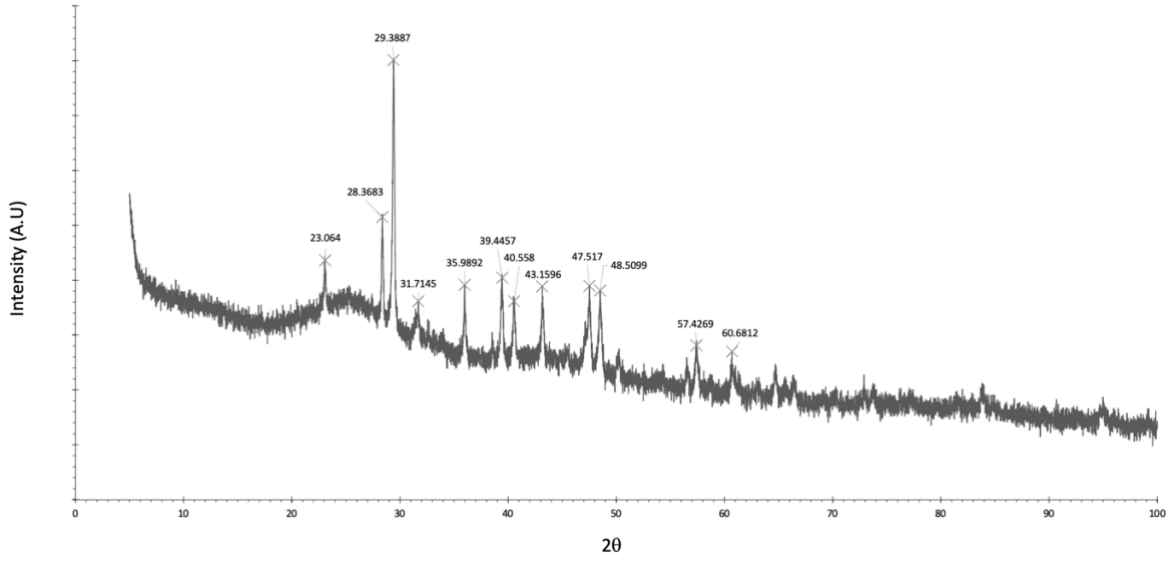

Figure 4.12 – X-ray Diffraction Crystallography spectra of mixed biochar material

4.6 Raman Spectroscopy

The Raman spectra presented in Figure 4.13 shows peaks at 1086cm^{-1}, 1370cm^{-1} and 1601cm^{-1}. The sharp peak present at 1086cm^{-1} is indicative of the presence of calcite in biochar derived from mixed municipal discarded material pyrolyzed in a heat pipe reactor. This further confirms what has been shown by peaks at 713cm^{-1} and 873cm^{-1} in FTIR spectra shown in Figure 4.9, Figure 4.10 and Figure 4.11, which indicate the presence of CO_3^{2-} ions in the biochar.

The D band is identified at 1370cm^{-1}, this peak is indicative of disordered aromatic carbon in the biochar such as condensed benzene rings in amorphous carbon materials in the biochar. The G band is identified at 1601cm^{-1} with this peak being indicative of graphitic structures within the biochar [292].

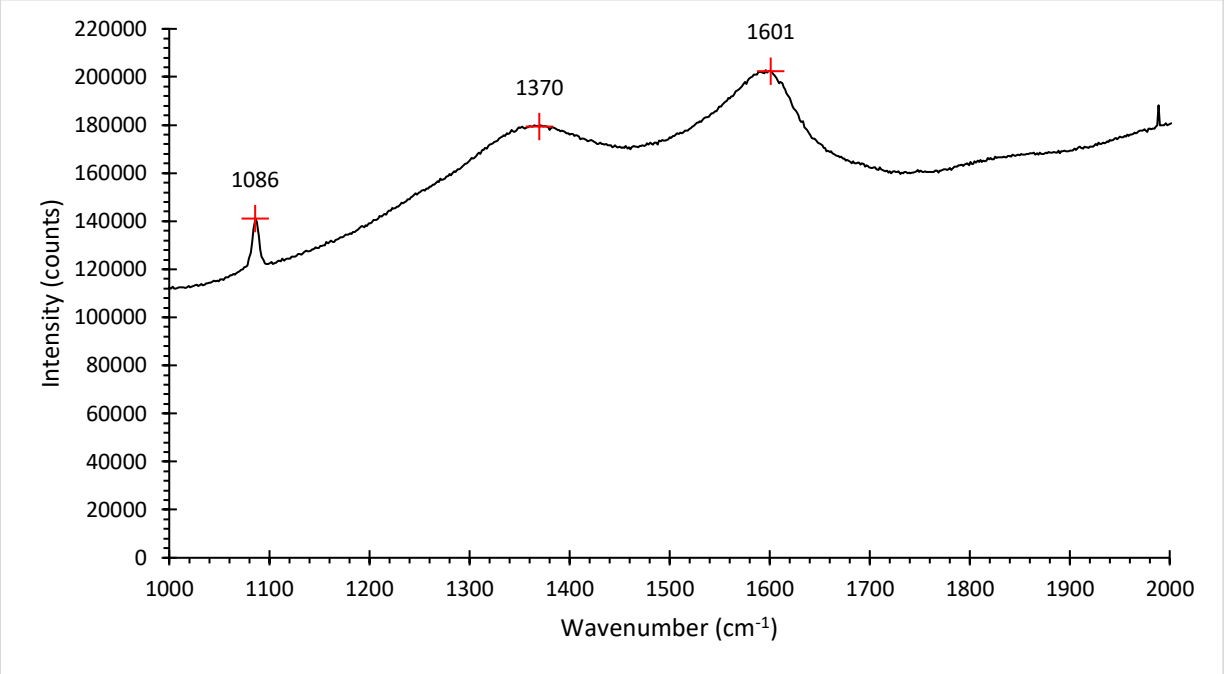

Figure 4.13 – Raman spectra data of biochar derived from mixed municipal discarded material in a heat pipe reactor

4.7 How biochar characteristics Affect adsorption

As shown in the previous sections, biochar produced through the pyrolysis of mixed municipal discarded material in a heat pipe reactor is a variable material, with physical and chemical characteristics revealed using SEM, EDAX and FTIR analyses changing depending on the feedstock. Furthermore, XRD crystallography shows the presence of calcite and chloride salts, as was suspected from the EDAX analysis. Raman Spectroscopy showed that the carbon matrix of the biochar is varied with both disordered and graphitic structures present in the

material. All of these characteristics revealed by the various characterisation techniques used have an impact on how biochar derived from mixed municipal discarded material in a heat pipe reactor will interact with different aqueous pollutants.

4.7.1 Copper Adsorption

Transition metals, including copper are adsorbed to biochar adsorbents by different mechanisms. The presence of oxygen containing functional groups in the biochar shown in FTIR analyses of biochar derived from discarded paper and food shows that outer sphere and inner sphere complexation of aqueous copper is possible in these materials. These functional groups are absent from biochar produced in higher temperature pyrolysis experiments in other studies, where the FTIR peaks are notably absent. In these other studies physical adsorption processes were suggested as the major adsorption mechanism for copper, due to the increased surface area and reduced functional groups of the biochar adsorbents used [293,294]. The opposite is true for the biochar adsorbents produced at lower pyrolysis temperatures from mixed municipal discarded material, where functional groups are shown to be fairly abundant in both discarded paper and food chars. This suggests that a mixture of chemical and physical adsorption processes will be responsible for the adsorption of copper to these biochar materials. As a result, SEM-EDAX analysis of the biochar after copper adsorption for both discarded paper and food derived biochar is expected to return a fairly uniform distribution of copper across the scanned surface area. As a result, regression analyses of copper against positive ions, negative ions and oxygen detected by EDAX should return low R^2 values, and p values should exceed 0.05. This is because the copper should not be strongly associated with areas containing increased amounts of such elements if a more uniform distribution of copper across the biochar surface has occurred. In such cases, the coefficient of determination will return a value significantly lower than 1 indicating a weak relationship between copper and positive ions, negative ions and oxygen. The p values calculated will be greater than 0.05 showing that the relationship between copper and positive ions, negative ions and oxygen is not statistically significant.

However, the absence of such groups in the plastic biochar shows that adsorption to this material is unlikely to be attributed to inner and outer sphere complexation, with other mechanisms likely to have a greater relative impact on adsorption. Other such mechanisms include precipitation, and ion exchange, as well as adsorption to clay minerals and calcite on

the biochar surface [295]. These interactions may still occur in the biochar derived from discarded food and paper chars, however, these mechanisms for copper adsorption will probably be much more obvious in plastic biochar, where adsorption of copper to functional groups distributed more evenly across the biochar surface is significantly reduced in plastic char due to the reduced amounts of functional groups. Plastic biochar was shown in SEM images in section 4.2, and EDAX analysis in section 4.3, to have a flat surface with calcite and other mineral deposits distributed in small particulates across the surface. If these small particulates are significantly responsible for copper removal in biochar, copper will be concentrated on areas with greater amounts of mineral elements such as potassium, sodium and calcium [296]. As a result, SEM-EDAX analysis of plastic biochar after adsorption experiments will show greater concentrations of copper around minerals and negative ions on the biochar surface if precipitation and/or ion exchange have been significantly responsible for copper adsorption to plastic char. The opposite will be true of the areas in plastic char that have fewer amounts of these calcite and mineral particulates with copper concentration being reduced in these areas. If copper is closely associated with calcite and other mineral deposits in the plastic char, a regression analysis should return R^2 values closer to 1 than 0, and p values calculated at a 95% confidence limit will be lower than 0.05. This would indicate a strong and statistically significant relationship between copper and positive ions, negative ions or oxygen.

4.7.2 Methylene Blue

Methylene blue is organic in nature, meaning that it can interact with the biochar produced in the heat pipe reactor in different ways to copper. Figure 4.14 shows methylene blue dissolved in water. This image reveals several parts of the methylene blue molecule that are capable of interacting with the biochar produced in this thesis. The positive charge shown on the left-hand amine group is capable of interacting with negative sites present on the biochar. The amine shown on the right-hand side of the methylene blue molecule can take part in hydrogen bonding interactions with surface functional groups in the biochar shown to exist through the FTIR analysis of biochar.

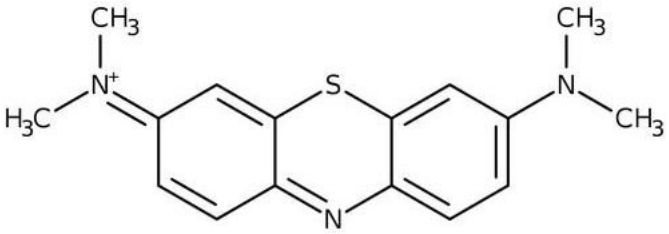

Figure 4.14 – Methylene blue chloride in aqueous solution [297]

The double bonded carbon atoms, particularly those located in the benzene ring towards the right of the molecule displayed in Figure 4.14 can participate in π electron interactions with the aromatic surfaces of the biochar shown to exist by Raman spectroscopy. Making use of Avogadro molecular modelling software and orca molecular orbital software allows the orbitals of the methylene blue molecule to be calculated and displayed using density functional theory. The highest occupied molecular orbitals calculated using the outlined software can be seen in Figure 4.15 with a "birds eye view" of the methylene blue molecular orbital shown in Figure 4.15 A and a "side view" shown in Figure 4.15 B. Both of these views show that the electron orbitals exist above and below the bonding plane. This shows that π interactions between methylene blue in solution and the mixed municipal discarded material biochar can occur where the Raman analysis proves the existence of aromatic structures in the produced biochar, these also contain π electrons. At the lower pyrolysis temperature used to produce the biochar in the heat pipe reactor, the aromatic fractions in the produced biochar act as π electron acceptors [298]. π interactions are identified as the dominant adsorption mechanism in methylene blue adsorption to biochar produced at higher pyrolysis temperatures (>700^{o}C) [299]. However, FTIR analysis of biochar produced from mixed municipal discarded material at low pyrolysis temperatures (<300 ^{o}C) showed functional groups capable of participating in adsorption interactions with methylene blue.

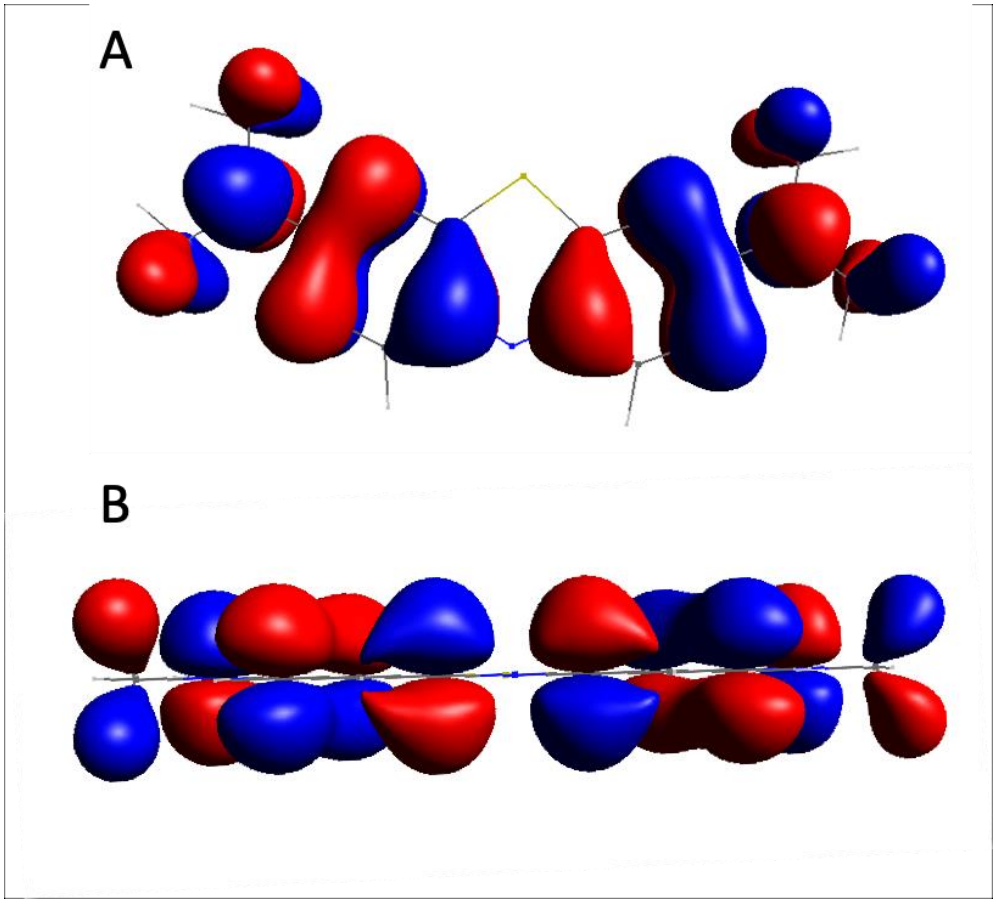

Figure 4.15 – Molecular orbital modelling of methylene blue in aqueous solution

The charge of methylene blue molecules dissolved in an aqueous solution is dependent on the pH of the solution in which they are dissolved. In acidic conditions, in which pH values are low, methylene blue can be protonated to form a more positive ion; conversely as pH increases, methylene blue remains a singly charged ionic species methylene blue [300], with mixed municipal discarded material containing oxygen functional groups such as alcohols and carboxylic groups that can act in an amphoteric manner in aqueous solution. Low pH conditions cause these functional groups to be protonated leading to positively charged active sites whereas high pH conditions resulting in these functional groups being deprotonated and negatively charged active sites [301]. Methylene blue is consequently more readily adsorbed by biochar produced at lower pyrolysis temperatures at higher pHs where the negative active sites in the biochar material attract the positively charged methylene blue molecule to them [15,299].

4.7.3 Tetracycline

Figure 4.16 shows tetracycline dissolved in water. As is the case with methylene blue dissolved in water, amine groups present in tetracycline can interact with functional groups in the biochar to form hydrogen bonds. Furthermore, a benzene ring is also present in tetracycline, indicating that π electron interactions with the aromatic fractions of the biochar are possible, with the biochar again acting as a π electron acceptor. Tetracycline also contains five hydroxyl functional groups which are capable of forming hydrogen bonds with biochar. These hydroxyl groups can also interact with water to form $-O^-$, or $-OH_2^+$ groups, depending on the pH of the solution tetracycline is adsorbed in.

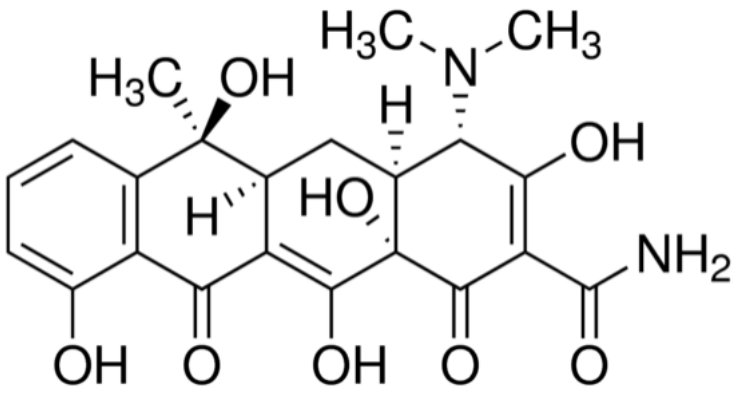

Figure 4.16 – Tetracycline dissolved in aqueous solution [302]

Indeed, tetracycline does speciate depending upon the pH of the solution in which it is dissolved. In a strong acidic solution (pH lower than 3.3), the majority tetracycline species is the singly positive H_4TC^+ species. At neutral pH (pH between 4 and 7.2) the majority tetracycline species is the neutral H_3TC species, with minor amounts of H_4TC^+ and H_2TC^- species in weak acidic and weak basic conditions respectively. In moderate basic conditions (pH between 8 and 9.7) the majority tetracycline species was H_2TC^-, with minor amounts of H_3TC and HTC^{2-} under weaker basic and stronger basic conditions respectively. Finally in strong basic conditions, the majority tetracycline species is HTC^{2-} [303,304]. It is important to note the varying speciation of tetracycline in aqueous solutions. These species can clearly interact with an adsorbent in different ways. This interaction is also however dependent on the characteristics of the adsorbent. FTIR spectra, as well as SEM-EDAX analysis, of biochar produced from mixed municipal discarded material in the heat pipe reactor show that significant amounts of oxygen containing functional groups exist in the biochar. Specifically, the hydroxyl groups present in alcohols and carboxylic groups on the surface of the biochar

are capable of interacting with aqueous solutions in the same way, releasing hydrogen from these groups in basic conditions, and withdrawing hydrogen from aqueous solutions in acidic conditions. This leads to the development of negative charge on the surface of the biochar adsorbent derived from mixed municipal discarded material in basic conditions, with positive charge developing at the sites where these functional groups exist in acidic conditions [305]. In the case of mixed municipal discarded material produced at lower pyrolysis temperatures, tetracycline will be more poorly adsorbed in both acidic and basic conditions. This is because the charges present on the "active sites" of the biochar and the dissolved tetracycline molecules are the same, causing repulsion between such sites and tetracycline molecules in these conditions. Consequently, the optimum conditions in terms of pH for tetracycline adsorption are in the neutral pH range, where the dominant tetracycline species is neutral H_3TC [306].

4.8 Summary

In summary, biochar derived from the heat pipe pyrolysis of mixed municipal discarded material displays a heterogenous structure, comprising different physical and chemical characteristics. These characteristics are also found to vary depending on the type of discarded material used as a feedstock. The adsorption of copper is therefore expected to fit Elovich, and pseudo second order kinetic models, more closely than the pseudo first order kinetic model. This is due to the presence of functional groups in the biochar, giving this adsorbent the ability to interact with copper via chemisorption mechanisms such as inner sphere complexation. Precipitation and ion exchange interactions will probably also occur between the biochar and aqueous copper, particularly at sites where calcite is present; calcite has been used as an adsorbent of copper in other literature [307,308]. Methylene blue is expected to be removed from solution via hydrogen bonding mechanisms. π-π interactions between the aromatic moieties of both the methylene blue molecule itself and the biochar are also expected. Electrostatic interactions between the positively charged methylene blue and negatively charged sites in the biochar will also play a role in adsorption. Methylene blue adsorption is consequently expected to produce a stronger fit with Elovich, and pseudo second order kinetic models, compared with the pseudo first order kinetic model. Finally, Tetracycline is expected to interact with the biochar in a similar manner to methylene blue, with the benzene ring participating in π-π interactions with the aromatic moieties in the

biochar. The abundant hydroxyl groups and single amine group in the dissolved tetracycline will interact with the functional groups in the biochar to form hydrogen bonds.

5 COPPER ADSORPTION TO BIOCHAR DERIVED FROM MIXED MUNICIPAL DISCARDED MATERIAL IN A HEAT PIPE REACTOR

5.1 Copper in the environment

Copper is a vital mineral involved in the production of blood cells [309]. It is also involved in biological processes in plants [310]. It is therefore highly important for the health of all living organisms. However, copper is also a toxin known to impact both humans and the environment. In humans, copper is stored in the liver, brain, bones, muscles and kidneys. The exposure to copper at toxic levels can cause complications involving the liver, kidneys, and heart failure, brain damage, and loss of red blood cells. Furthermore, congenital disorders as well as other diseases can reduce the human bodies capability to remove copper. Wilson's disease is a congenital disorder that causes the body to store excessive amounts of copper [311]. This can lead to copper levels increasing to dangerous levels in the human body. It is therefore important to remove copper from drinking water to reduce the prevalence of such health complications, as well as improving the life of those with diseases that cause the dangerous storage of copper in bodily tissues.

Copper can enter the environment in numerous ways. These may be either natural or anthropogenic in nature. Natural sources of copper mainly involve the dissolution of copper containing rock or soils. Anthropogenic sources of copper are much more varied than natural sources. Acid mine drainage is a combined natural-anthropogenic copper source, caused by the dissolution of copper containing minerals by acidic ground, surface or rainwater [312]. Copper has also been used as an anti-fungal in agricultural industries such as in coffee growing and other similar applications [313–315].

The recommended concentration of copper in drinking water is stated by the world health organisation as 2mg/L [316], with standards in the United Kingdom also set at 2mg/L at the consumer's faucet by the drinking water inspectorate [317]. Environmental surface water standards are also in place around the world, with bioavailable copper limited to 1μg/L in the European union and the United Kingdom [318]. As a result, pressure is placed upon industries who pollute to reduce their pollution or be made economically responsible for the treatment of pollution [319]. It is therefore in the interest of industries that result in environmental copper pollution to find ways to reduce this. One such way to remove copper from the water is through adsorbents. These as identified in the state of the art can be expensive and possibly hard to produce. Another problem identified due to domestic waste being sent to landfill or

incineration, is the emission of carbon-based greenhouse gases; composting and anaerobic digestion which are both processes sensitive to the composition of carbonaceous materials used. The pyrolysis of mixed municipal discarded materials (MMDM) could therefore result in the production of a cheap adsorbent, potentially capable of reducing copper concentrations in both the environment and in drinking water treatment processes. This chapter subsequently investigates the adsorption of copper to biochar produced from discarded domestic materials.

5.2 Adsorption kinetics

5.2.1 Introduction

Adsorption kinetics are used to determine the kinetic behaviour of the removal of an adsorbate by an adsorbent. It is generally agreed that the adsorption of an aqueous contaminant follows four main stages. These being bulk diffusion of an adsorbate to the film surrounding adsorbent particles, film diffusion across the liquid film present between the adsorbent and bulk solution, pore diffusion of an adsorbate into an adsorbent, and adsorption processes at the active sites on the surface of an adsorbent [320]. The three kinetic models used in this thesis as stated in the materials and methodology section are the pseudo first order, pseudo second order and Elovich models. Each of these kinetic models are derived using a separate set of assumptions about an adsorbent surface. The pseudo first order model assumes that the rate of change of adsorption is directly proportional to the difference in concentration between the adsorption under conditions of equilibrium between the adsorbent and bulk solution, and the adsorption at any given time. This model is particularly applicable where the removal of an adsorbate is governed by diffusion processes into an adsorbent. The pseudo second order model assumes that adsorption is limited by chemisorption processes. In this regard the pseudo second order assumes that the rate of adsorption is dependent on the adsorption capacity of an adsorbent and not the concentration of an adsorbate. Finally, the Elovich model assumes that adsorption is limited by chemisorption processes that occur in a heterogenous fashion across the surface of an adsorbent due to energetic differences over the surface of an adsorbent [321]. It was expected that adsorption of contaminants to heat pipe derived MMDM biochar will more closely fit the Elovich model over the other two kinetic models, where SEM-EDAX analysis displayed heterogeneity in the biochar.

5.2.2 Copper adsorption to MMDM biochar

As discussed in the materials and methods section, the adsorption kinetics describe the nature of the adsorption of copper to the biochar surface over time. The statistical analyses in Table 5.1 of the models displayed in Figure 5.1, Figure 5.2 and Figure 5.3 show that R^2 values follow the order of Elovich > pseudo first order > pseudo second order, with both MSE and 95% confidence intervals following the order pseudo first order > pseudo second order > Elovich. This suggests that the adsorption to MMDM derived biochar from solution containing 50mg/L copper, at initial pH of 5 is limited by chemisorption processes with the biochar surface in a heterogenous manner. The stronger fit of the Elovich model is known to denote the tight binding of an adsorbate to an adsorbent surface, this indicates that this biochar material is capable of immobilising the copper it adsorbs from solution [322].

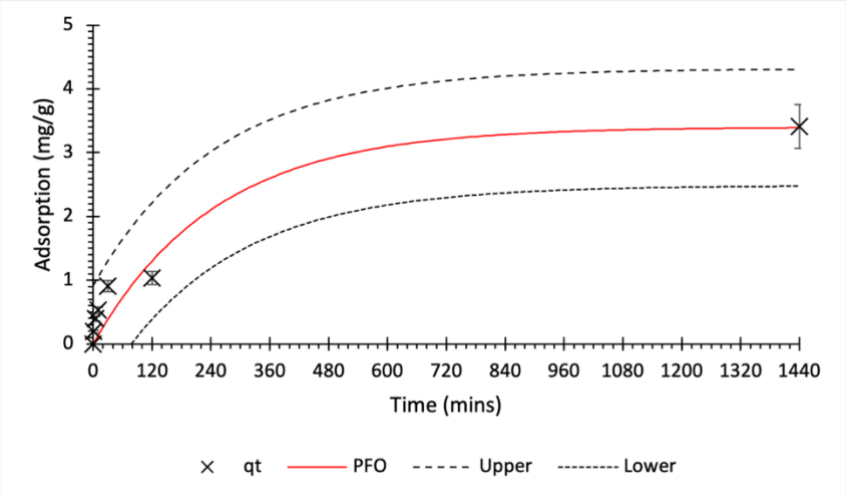

Figure 5.1 – Pseudo First Order model of copper adsorption, with upper and lower 95% confidence intervals displayed (initial concentration 50mg/L, initial pH 5)

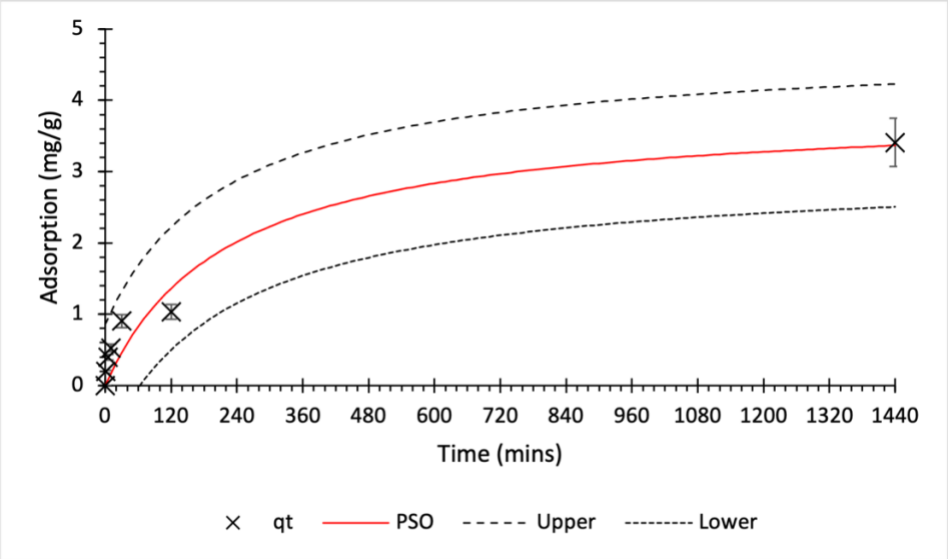

Figure 5.2 – Pseudo Second Order model of copper adsorption, with upper and lower 95% confidence intervals displayed (initial concentration 50mg/L, initial pH 5)

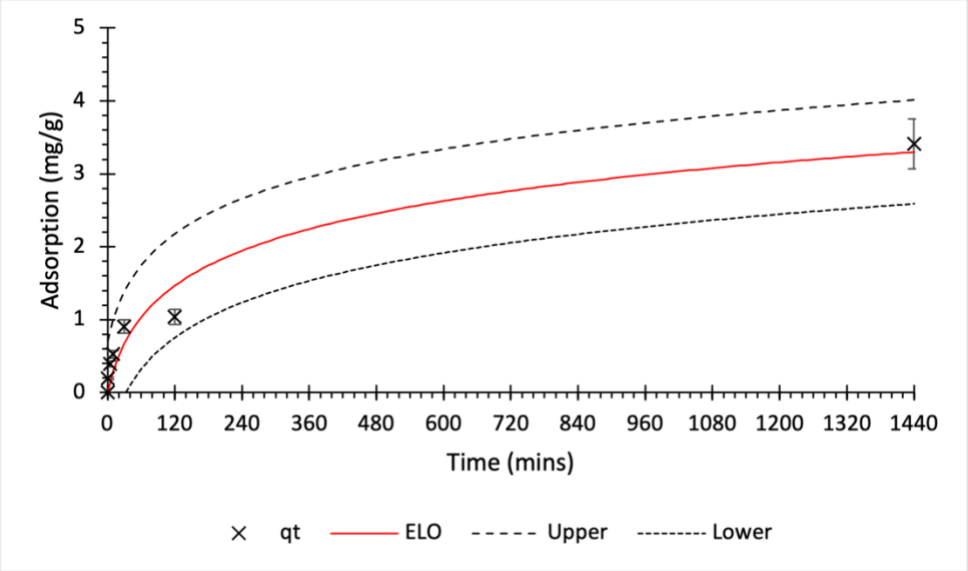

Figure 5.3 – Elovich model of copper adsorption, with upper and lower 95% confidence intervals displayed (initial concentration 50mg/L, initial pH 5)

Table 5.1 – Table showing statistical analysis of different kinetic modelling data for experiments with an initial copper concentration of 50 mg/L and initial pH of 5

Kinetic model		
Pseudo first order	**K_1**	0.004
	q_e	3.402
	R^2	0.9562
	MSE	0.0860
	95% Confidence interval	0.9161
Pseudo second order	**K_2**	0.001
	q_e	3.891
	R^2	0.9534
	MSE	0.0758
	95% Confidence interval	0.8666
Elovich	**A**	0.036
	B	1.271
	R^2	0.9603
	MSE	0.0548
	95% Confidence interval	0.712

Table 5.2 shows the statistical analyses of the experimental data against the kinetic models displayed in Figure 5.4, Figure 5.5, and Figure 5.6 for the stated conditions. The models fit to the data as measured by R^2 in the order of Pseudo second order > Elovich > Pseudo first order. The values of mean squared error are in the order of pseudo first order > pseudo second order > Elovich. The 95% confidence interval values are in the order of pseudo first order > pseudo second order > Elovich. This suggests that the adsorption of copper to biochar with initial copper concentrations of 100mg/L and initial solution pH of 5, with a 5g/L dose of biochar is limited by chemical interactions with the surface of the biochar. This occurs in a heterogenous fashion across the biochar surface, with some areas of the biochar showing more affinity than other areas for copper adsorption.

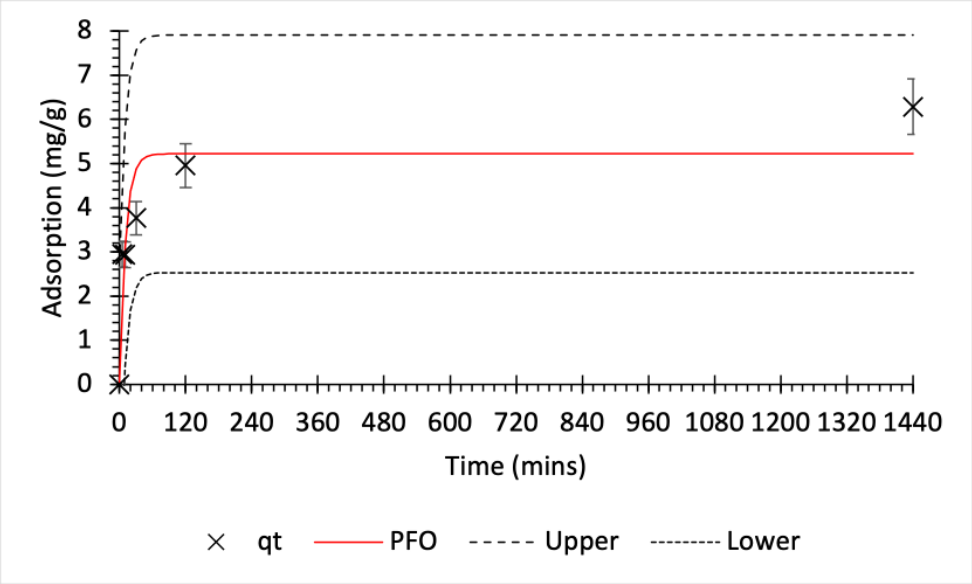

Figure 5.4 – Pseudo First Order model of copper adsorption, with upper and lower 95% confidence intervals displayed (initial concentration 100mg/L, initial pH 5)

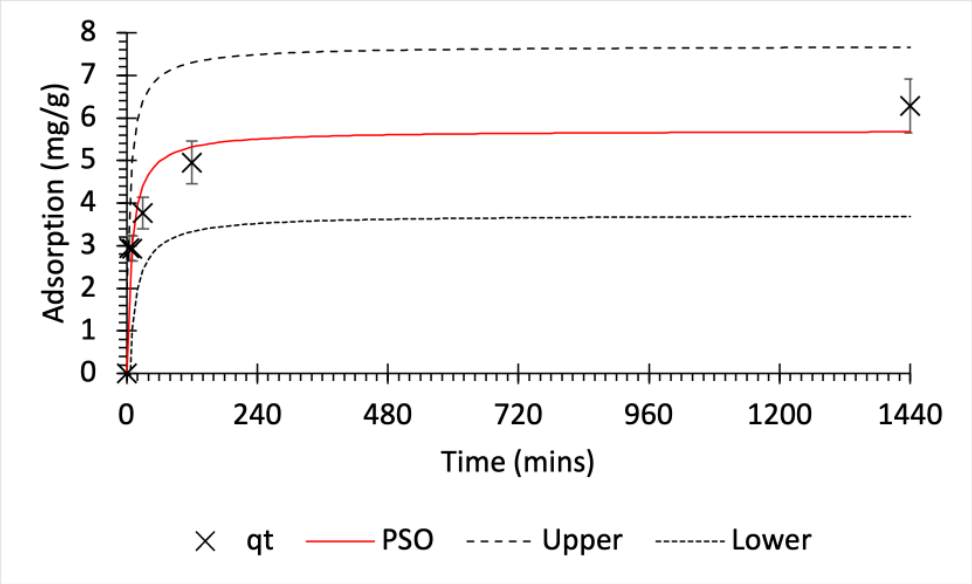

Figure 5.5 – Pseudo Second Order model of copper adsorption, with upper and lower 95% confidence intervals displayed (initial concentration 100mg/L, initial pH 5)

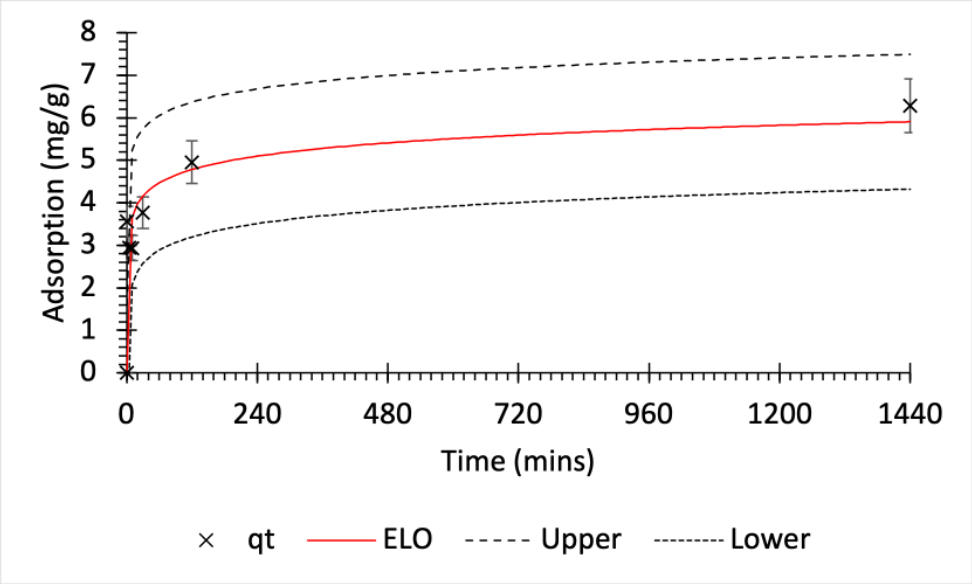

Figure 5.6 – Elovich model of copper adsorption, with upper and lower 95% confidence intervals displayed (initial concentration 100mg/L, initial pH 5)

Table 5.2 – Table showing statistical analysis of different kinetic modelling data for experiments with an initial copper concentration of 100 mg/L and initial pH of 5

Kinetic model		
Pseudo first order	**K_1**	0.0975
	q_e	5.1765
	R^2	0.8499
	MSE	0.5390
	95% Confidence interval	2.612
Pseudo second order	**K_2**	0.0224
	q_e	5.6330
	R^2	0.9278
	MSE	0.2798
	95% Confidence interval	1.799
Elovich	**A**	145.3
	B	2.209
	R^2	0.9167
	MSE	0.2715
	95% Confidence interval	1.5848

Table 5.3 shows the statistical analyses of the collected experimental data against the different kinetic models displayed in Figure 5.7, Figure 5.8, and Figure 5.9. The calculated R^2 values follow the order of Elovich > pseudo second order > pseudo first order, with the MSE values following the order pseudo first order > pseudo second order > Elovich. 95% confidence intervals follow the order pseudo first order > pseudo second order > Elovich. Again, this suggests that under these conditions copper adsorption is limited by chemical

interactions with the biochar surface [321]. The adsorption occurs in a heterogenous fashion under these conditions.

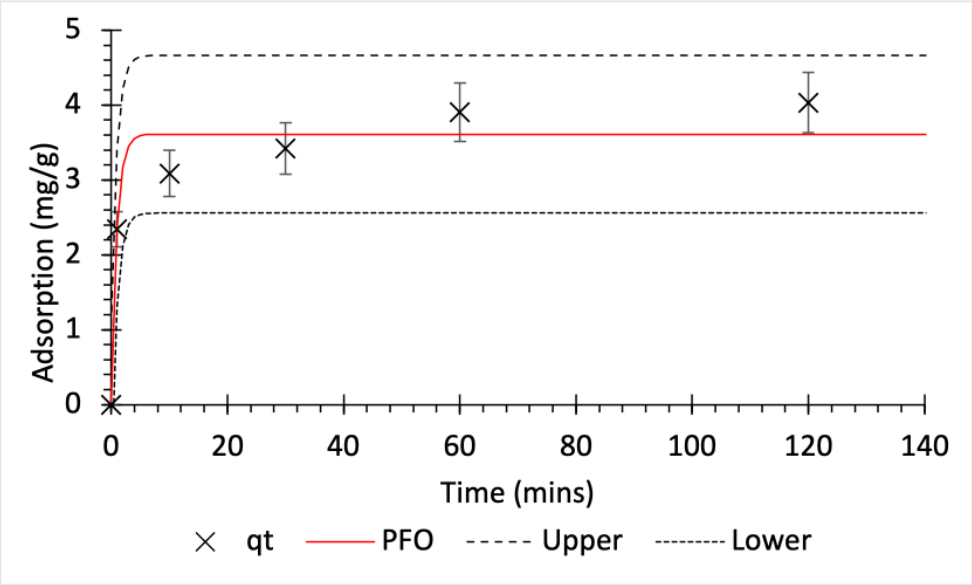

Figure 5.7 – Pseudo First Order model of copper adsorption, with upper and lower 95% confidence intervals displayed (initial concentration 150mg/L, initial pH 6)

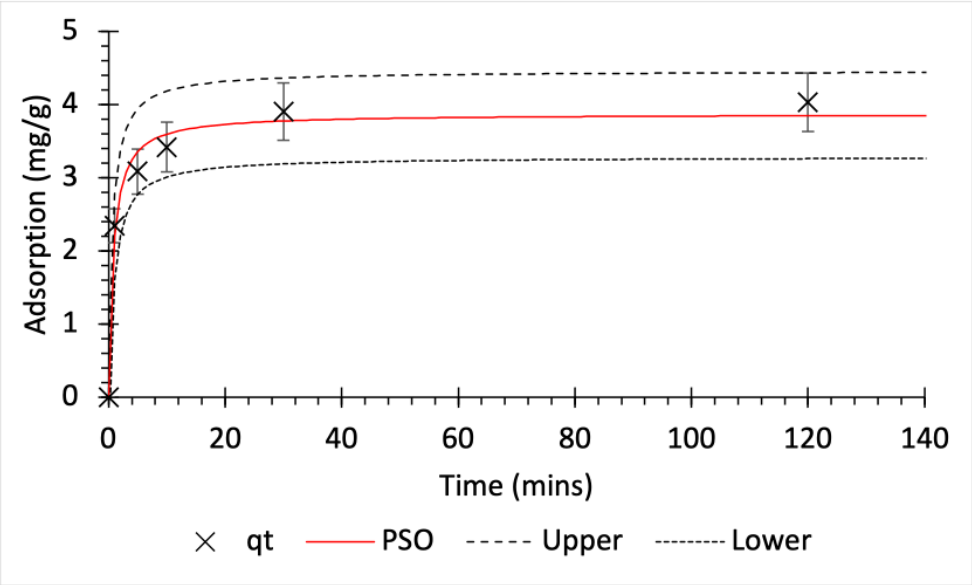

Figure 5.8 – Pseudo Second Order model of copper adsorption, with upper and lower 95% confidence intervals displayed (initial concentration 150mg/L, initial pH 6)

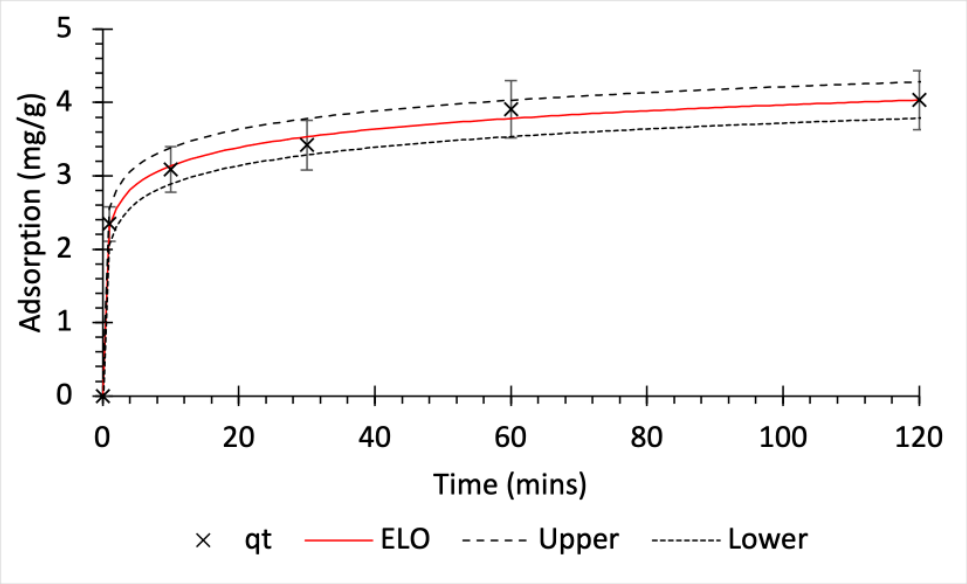

Figure 5.9 - Elovich model of copper adsorption, with upper and lower 95% confidence intervals displayed (initial concentration 150mg/L, initial pH 6)

Table 5.3 – Table showing statistical analysis of different kinetic modelling data for experiments with an initial copper concentration of 150 mg/L and initial pH of 6

Kinetic model		
Pseudo first order	**K_1**	1.0483
	q_e	3.6109
	R^2	0.9489
	MSE	0.0958
	95% Confidence interval	1.053
Pseudo second order	**K_2**	0.4066
	q_e	3.7255
	R^2	0.9660
	MSE	0.0298
	95% Confidence interval	0.587
Elovich	**A**	213.5
	B	2.7697
	R^2	0.9972
	MSE	0.0053
	95% Confidence interval	0.247

Table 5.4 shows the statistical analyses of these models against the experimental data displayed in Figure 5.10, Figure 5.11 and Figure 5.12. R^2 values are shown to follow the order pseudo first order > pseudo second order > Elovich. MSE values follow the order Elovich > pseudo second order > pseudo first order. Finally, the 95% confidence interval values follow the order Elovich > pseudo second order > pseudo first order. This suggests that for conditions of initial copper concentration of 150mg/L and initial solution pH of 5, the adsorption of

copper to the biochar surface is limited to a greater extent by physical adsorption processes compared with conditions of lower initial concentration and higher initial pH [321].

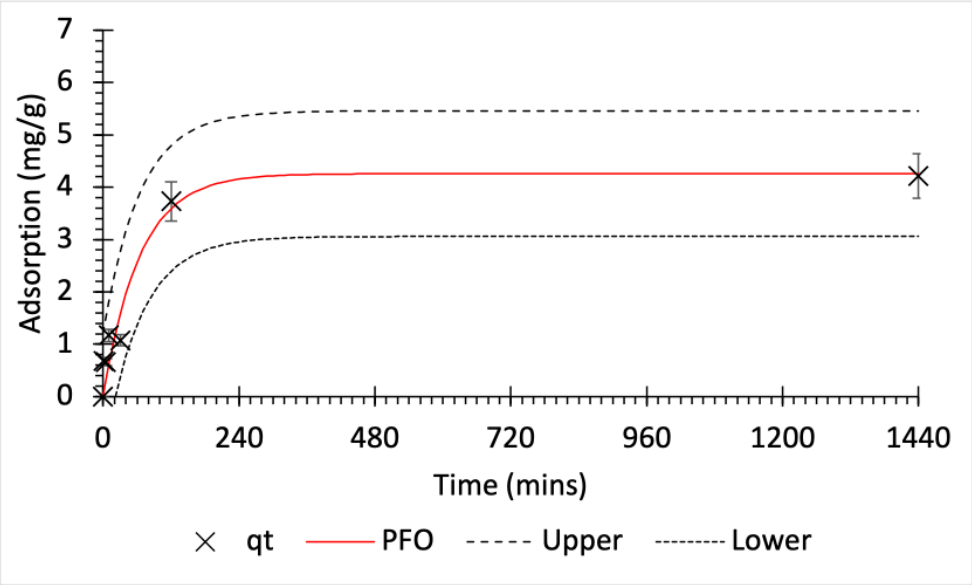

Figure 5.10 – Pseudo First Order model of copper adsorption, with upper and lower 95% confidence intervals displayed (initial concentration 150mg/L, initial pH 5)

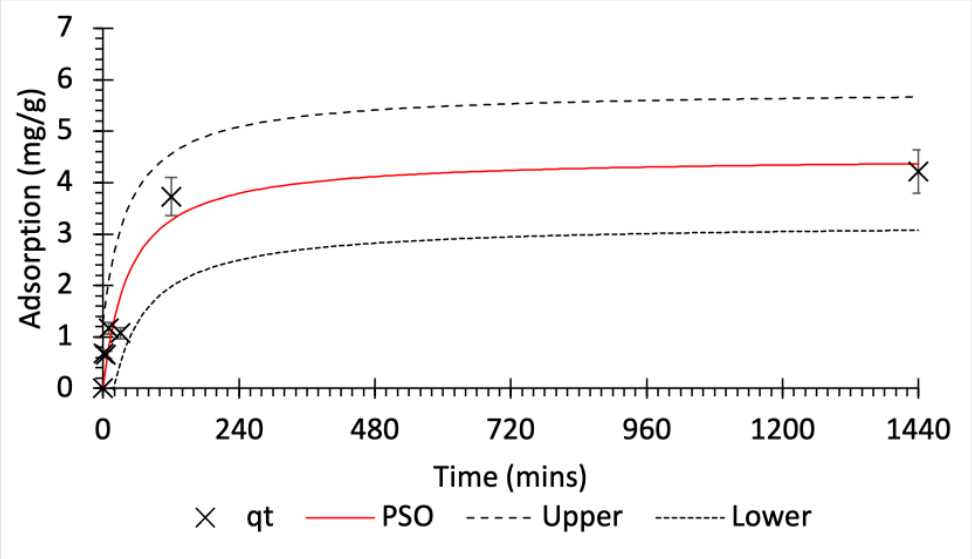

Figure 5.11 - Pseudo Second Order model of copper adsorption, with upper and lower 95% confidence intervals displayed (initial concentration 150mg/L, initial pH 5)

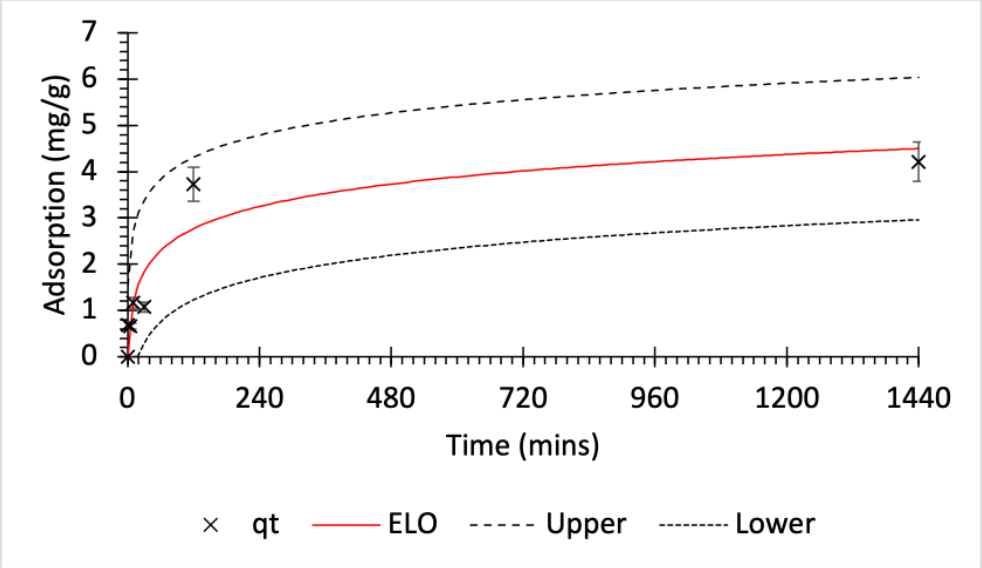

Figure 5.12 - Elovich model of copper adsorption, with upper and lower 95% confidence intervals displayed (initial concentration 150mg/L, initial pH 5)

Table 5.4 – Table showing statistical analysis of different kinetic modelling data for experiments with an initial copper concentration of 150 mg/L and initial pH of 5

Kinetic model		
Pseudo first order	**K_1**	0.0155
	q_e	4.2580
	R^2	0.9524
	MSE	0.1556
	95% Confidence interval	1.120
Pseudo second order	**K_2**	0.0049
	q_e	4.506
	R^2	0.9311
	MSE	0.1809
	95% Confidence interval	1.294
Elovich	**A**	0.2960
	B	1.4247
	R^2	0.8897
	MSE	0.2561
	95% Confidence interval	1.539

Table 5.5 shows the statistical analyses of these models against the experimental data displayed in Figure 5.13, Figure 5.14 and Figure 5.15. R^2 values follow the order of pseudo second order > pseudo first order > Elovich. MSE values follow the order of pseudo second order > pseudo first order > Elovich. Finally, the 95% confidence intervals follow the order of pseudo second order > pseudo first order > Elovich. This suggests that the adsorption of copper to biochar derived from MMDM in a heat pipe reactor is limited by a mixture of chemical and physical processes at conditions of high initial concentration and pH of 5. This

in combination with the results regarding initial copper concentrations of 150mg/L and pH 5 as well as the lower 95% confidence limits for Elovich models compared with other models shows that copper adsorption to the biochar is a heterogenous process comprising of both physical and chemical interactions with the biochar surface.

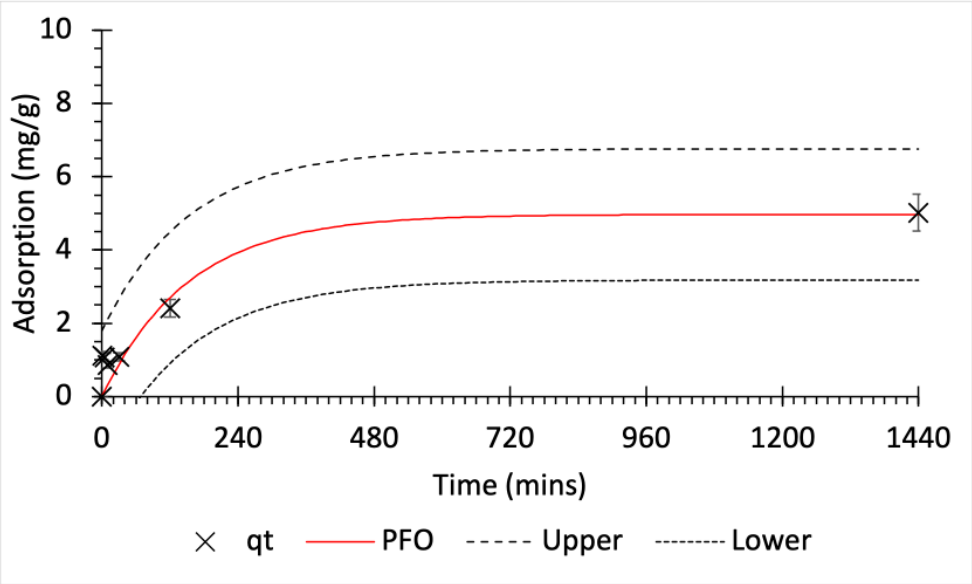

Figure 5.13 – Pseudo First Order model of copper adsorption, with upper and lower 95% confidence intervals displayed (initial concentration 250mg/L, initial pH 5)

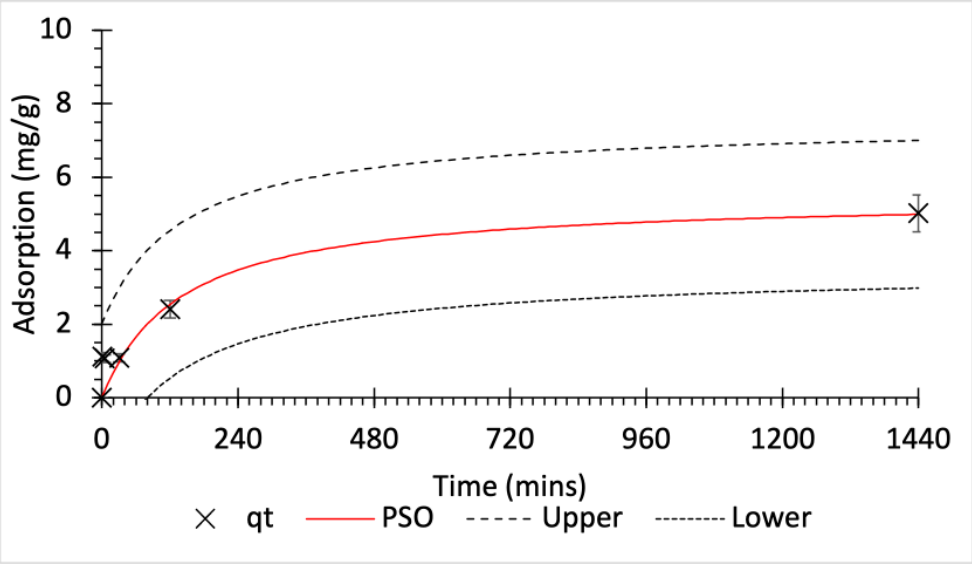

Figure 5.14 – Pseudo Second Order model of copper adsorption, with upper and lower 95% confidence intervals displayed (initial concentration 250mg/L, initial pH 5)

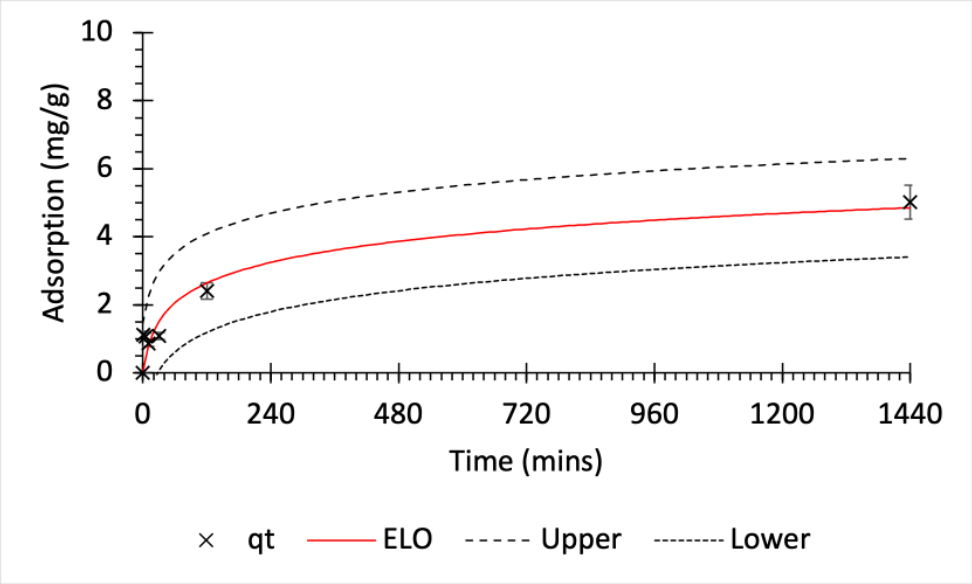

Figure 5.15 – Elovich model of copper adsorption, with upper and lower 95% confidence intervals displayed (initial concentration 250mg/L, initial pH 5)

Table 5.5 – Table showing statistical analysis of different kinetic modelling data for experiments with an initial copper concentration of 250 mg/L and initial pH of 5

Kinetic model		
Pseudo first order	**K_1**	0.00619089
	q_e	4.98892925
	R^2	0.9381
	MSE	0.3526
	95% Confidence interval	1.792
Pseudo second order	**K_2**	0.00132623
	q_e	5.46677142
	R^2	0.9395
	MSE	0.3490
	95% Confidence interval	2.009
Elovich	**A**	0.13035822
	B	1.09888006
	R^2	0.9231
	MSE	0.2269
	95% Confidence interval	1.449

5.2.3 Summary of Kinetic models

The kinetic models show that in general chemisorption processes best describe the adsorption of copper to biochar derived from MMDM pyrolyzed in a heat pipe reactor. The available functional groups are consequently very important for adsorption. Precipitation and ion exchange may also occur at sites on the biochar where calcite and kaolin minerals are present.

Initial pH clearly influences the kinetics of adsorption to biochar produced from MMDM at low pyrolysis temperatures. The adsorption kinetic models produced with initial pH of 6 and initial concentration of 150mg/L clearly reached equilibrium in a much shorter time frame than adsorption experiments with the same initial concentration and initial pH of 5.

The kinetic models also show that the use of mixed feedstock can lead to variability in adsorption characteristics. Additionally, the wide 95% confidence intervals, particularly at higher concentrations show that physical adsorption processes become more prominent than chemical adsorption processes. Chemisorption processes are therefore more prominent at lower concentrations and/or higher initial solution pH.

5.3 Diffusion Models

5.3.1 Intraparticle diffusion model

The intraparticle diffusion model describes the diffusion of an adsorbent into the pores of an adsorbent. Weber Morris plots will produce a line of best fit that passes through the origin if the intraparticle diffusion model is the only process describing the movement of an adsorbate into an adsorbent. Figure 5.16, Figure 5.17, Figure 5.18 and Figure 5.19 show Weber-Morris plots for the different conditions identified in the captions. All of these plots show a rapid initial linear phase. This is representative of the diffusion of aqueous copper across the film between the biochar particles and the bulk solution.

A second linear phase then follows, with the linearity of this suggesting that intraparticle diffusion does indeed describe the movement of copper into the biochar. However, it can also be seen that the intercept for this second linear phase does not pass through the origin. This confirms that as well as the intraparticle diffusion process, other processes also limit the movement of copper into the biochar [323]. Liquid film diffusion occurs rapidly in the first linear phase. Results in section 5.2 also suggest that a range of physical and chemical adsorption processes also occur. Figure 5.16 shows that at conditions of initial copper concentrations of 150mg/L and initial pH of 6, a third line can be derived which is almost flat. This indicates that within the time limit of 120 minutes, the net movement of copper into the biochar reached equilibrium.

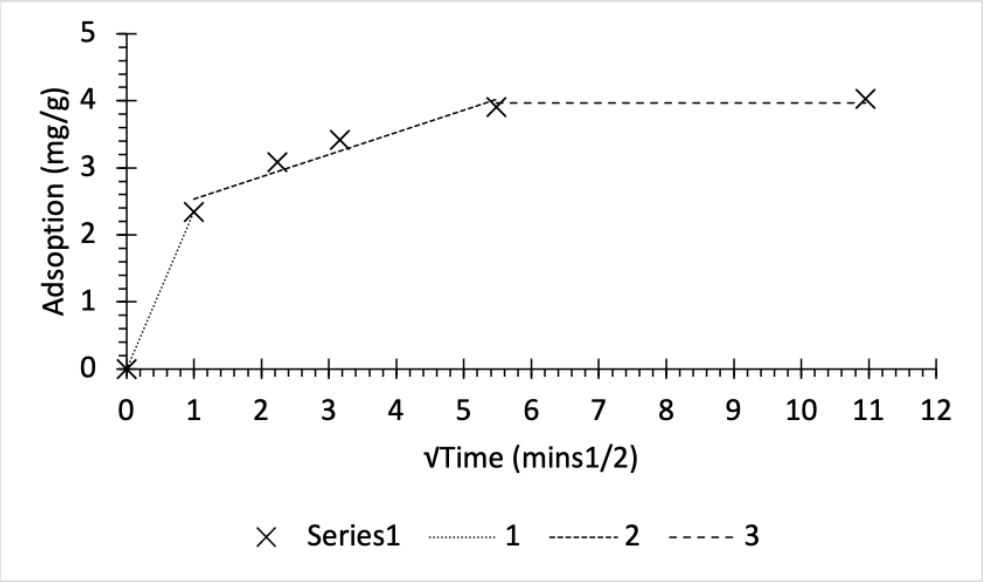

Figure 5.16 – Intraparticle plot for copper adsorption at pH 6 and initial copper concentration of 150mg/L to biochar derived from heat pipe pyrolysis of MMDM

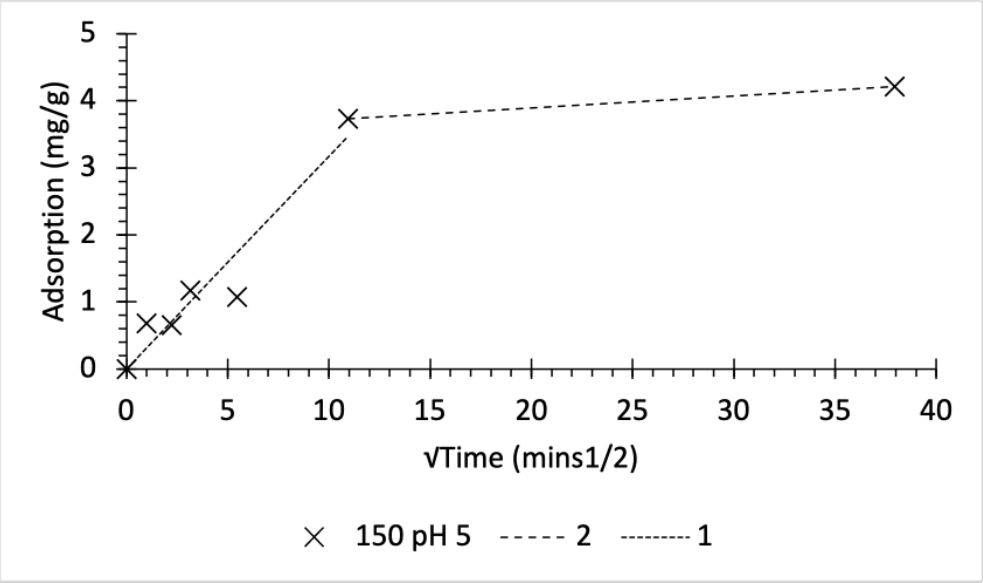

Figure 5.17 – Intraparticle plot for copper adsorption at pH 5 and initial copper concentration of 150mg/L to biochar derived from heat pipe pyrolysis of MMDM

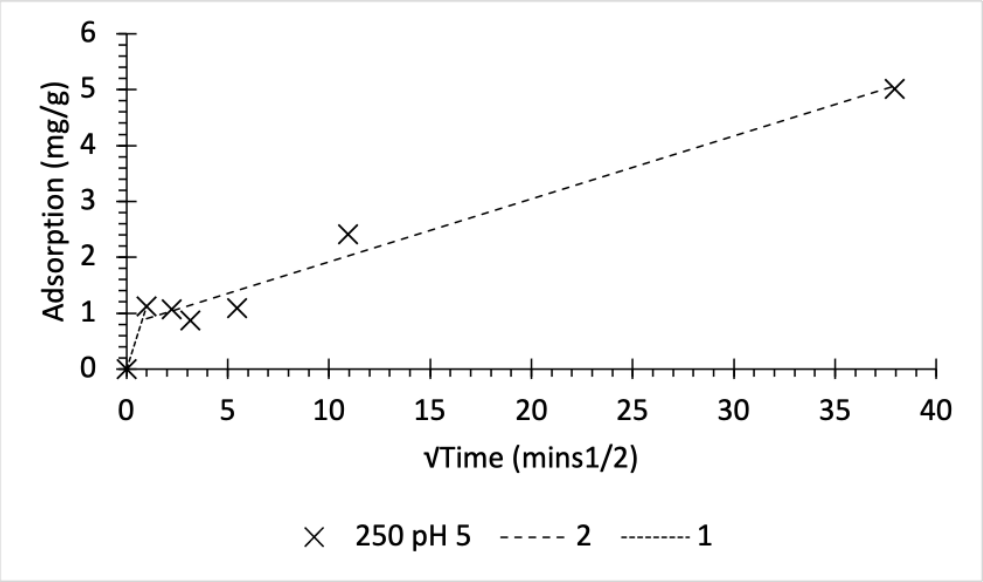

Figure 5.18 – Intraparticle plot for copper adsorption at pH 5 and initial copper concentration of 250mg/L to biochar derived from heat pipe pyrolysis of MMDM

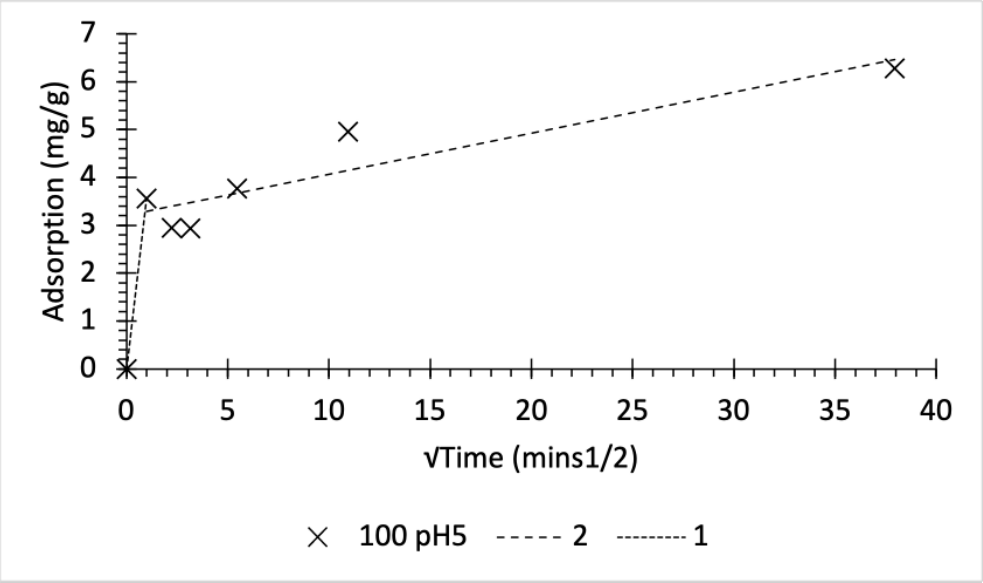

Figure 5.19 – Intraparticle plot for copper adsorption at pH 5 and initial copper concentration of 100mg/L to biochar derived from heat pipe pyrolysis of MMDM

5.3.2 Liquid film diffusion model

Boyd plots show the likelihood that liquid film diffusion is the rate limiting step of copper movement into the biochar adsorbent. Figure 5.20, Figure 5.21, Figure 5.22 and Figure 5.23 are Boyd plots for the different conditions denoted in the captions. Table 5.6 shows the statistical analysis of the data presented in the Boyd plots. The p-value was calculated using a two-tail t test assuming unequal variance between the sample time and the B_t value. All of the p-values were greater than 0.05, indicating that the regression line passes through the

origin of the Boyd plot. This indicates that the liquid film diffusion process is not as significant as other processes with regards to the limiting of copper diffusion and adsorption to biochar produced from MMDM in a heat pipe reactor.

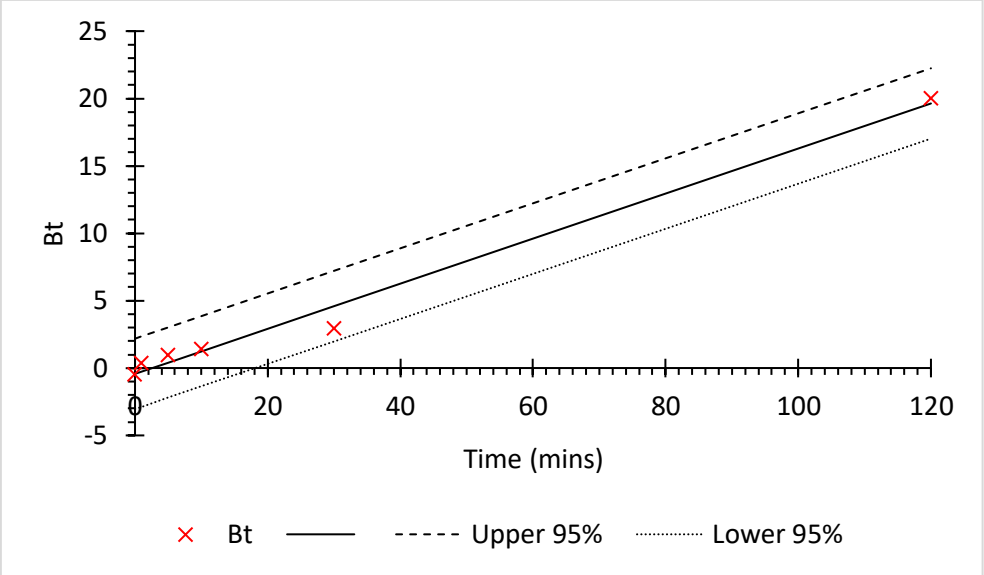

Figure 5.20 – Boyd plot of copper adsorption to biochar derived from MMDM in a heat pipe reactor at initial pH 6 and initial copper concentration of 150mg/L, with upper and lower 95% confidence intervals displayed

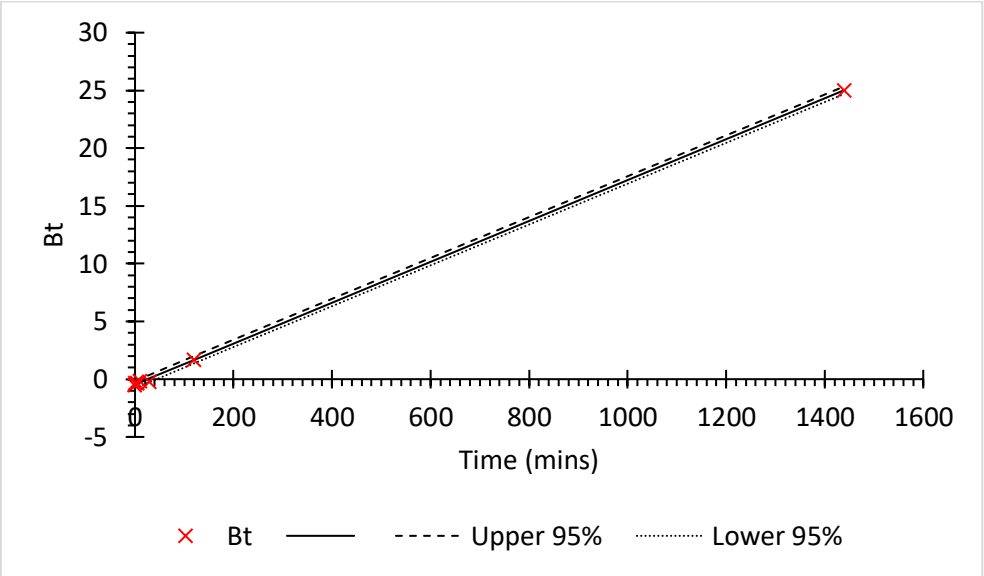

Figure 5.21 – Boyd plot of copper adsorption to biochar derived from MMDM in a heat pipe reactor at initial pH 5 and initial copper concentration of 150mg/L, with upper and lower 95% confidence intervals displayed

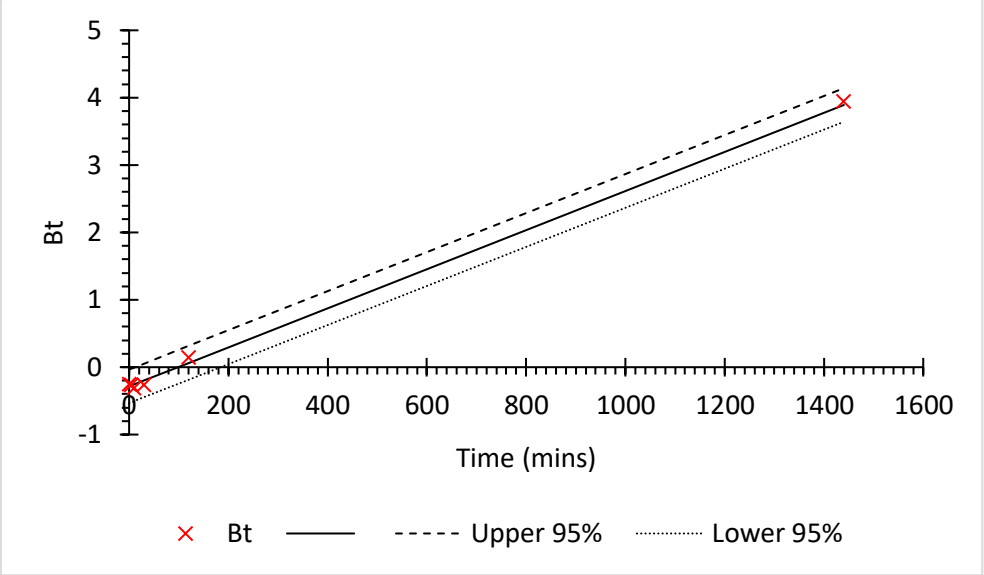

Figure 5.22 – Boyd plot of copper adsorption to biochar derived from MMDM in a heat pipe reactor at initial pH 5 and initial copper concentration of 250mg/L, with upper and lower 95% confidence intervals displayed

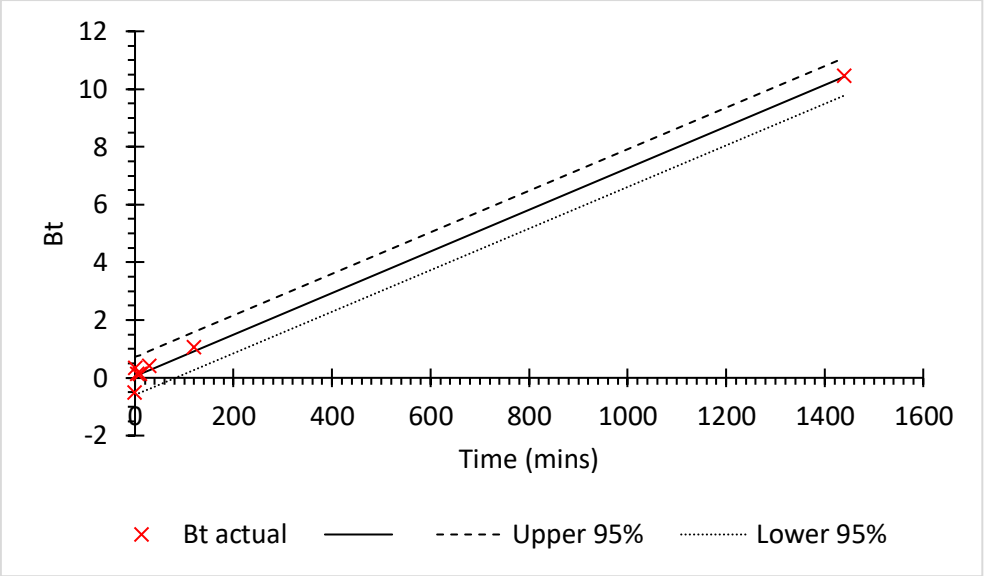

Figure 5.23 - Boyd plot of copper adsorption to biochar derived from MMDM in a heat pipe reactor at initial pH 5 and initial copper concentration of 100mg/L, with upper and lower 95% confidence intervals displayed

Table 5.6 – Table showing statistical analysis for the Boyd plots in Figure 5.20, Figure 5.21, Figure 5.22 and Figure 5.23

	R^2	MSE	p-value
150mg/L, pH 5	0.9998	0.0151	0.154
150mg/L, pH 6	0.9885	0.5043	0.137
250mg/L, pH5	0.9966	0.0107	0.150
100mg/L, pH 5	0.9953	0.0608	0.152

5.4 Adsorption isotherms

As discussed in the materials and methods section, isotherms describe the behaviour of an adsorbent with respect to the equilibrium concentration. Figure 5.24, Figure 5.25, Figure 5.26 and Figure 5.27 show plots of the calculated Freundlich, Langmuir, Dual mode Langmuir, and Sips isothermal models respectively. Table 5.7 shows the statistical analyses of the different isothermal models against the collected experimental data. It is immediately recognisable from Table 5.7 that the dual mode model could not find a better solution than the original Langmuir model that it is based upon. This shows that partitioning of copper into biochar material is not a significant effect, as the linear term in the dual mode isotherm is zero. The Sips model also could not find a better solution than the Langmuir model, where the value of n was equal to 1, leading the Sips model to be identical to the Langmuir model of adsorption.

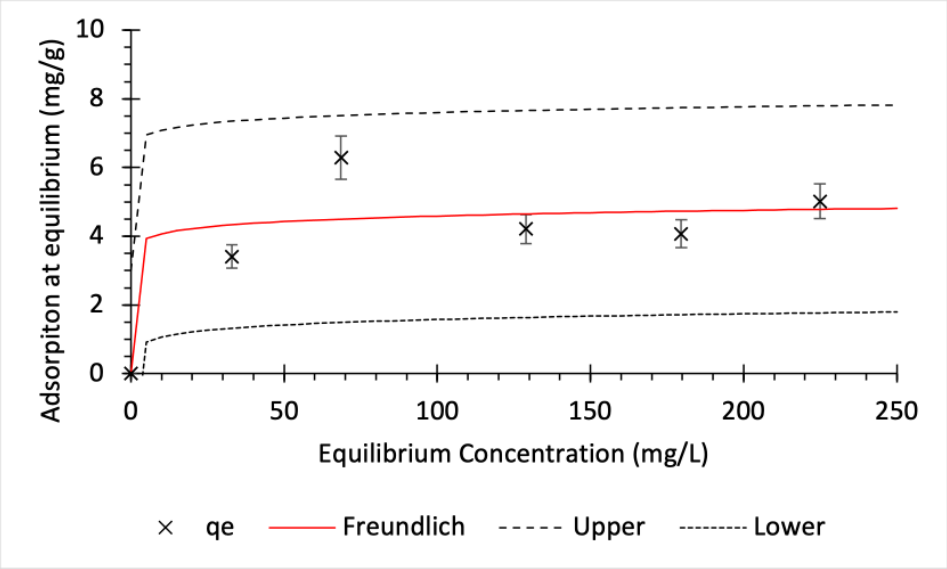

Figure 5.24 – Freundlich model of copper adsorption (pH = 5), with upper and lower 95% confidence intervals displayed

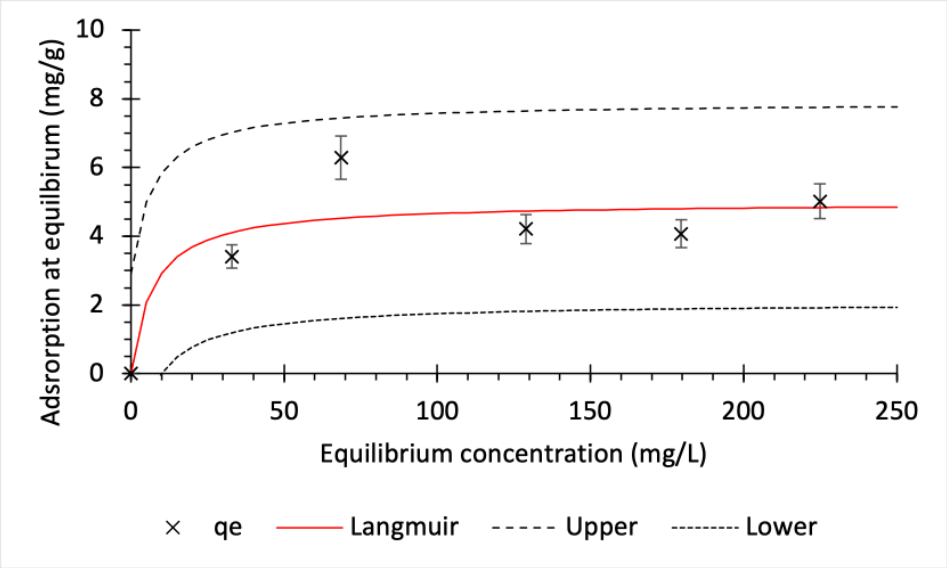

Figure 5.25 – Langmuir model of copper adsorption (pH = 5), with upper and lower 95% confidence intervals displayed

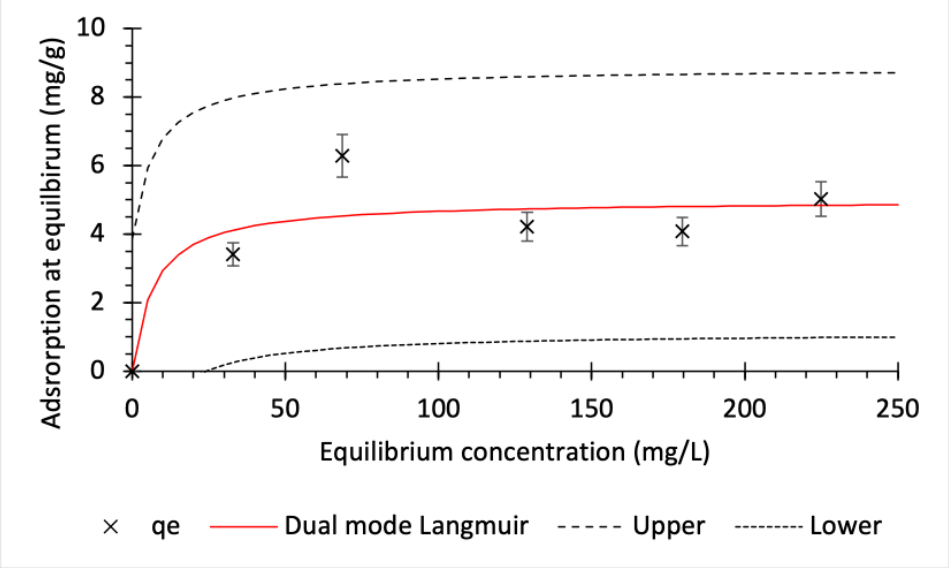

Figure 5.26 – Dual mode model of copper adsorption (pH = 5), with upper and lower 95% confidence intervals displayed

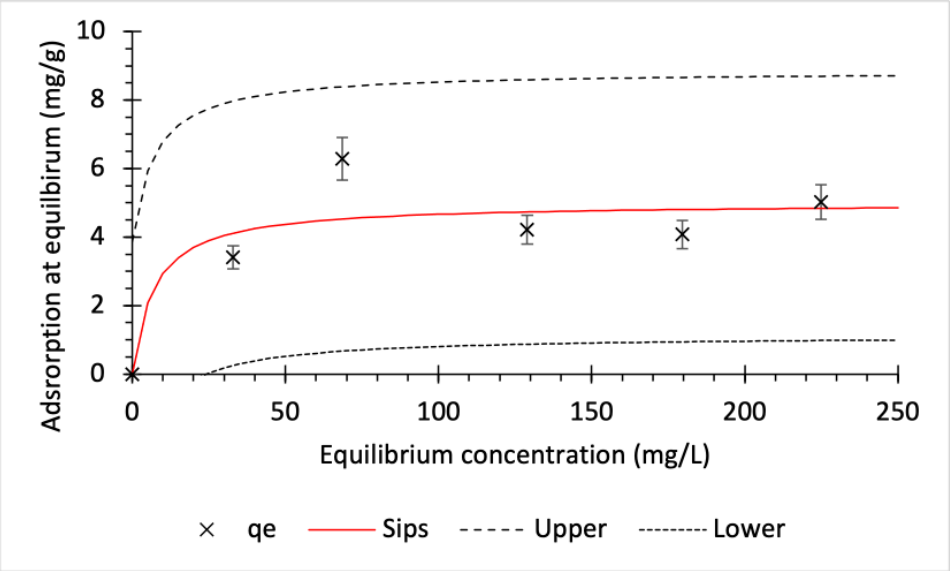

Figure 5.27 – Sips model of copper adsorption (pH = 5), with upper and lower 95% confidence intervals displayed

Table 5.7 – Statistical analyses of isothermal models

Kinetic model	R^2	MSE	95% Confidence interval
Langmuir	0.8037	0.7357	2.917
Freundlich	0.7906	0.7846	3.012
Sips	0.8037	0.7357	3.860
Dual mode	0.8037	0.7357	3.860

5.5 Effect of initial solution pH

The adsorption of copper to biochar is generally affected by the solution of the pH in which the copper is adsorbed. Indeed Figure 5.28 shows that as the initial pH is increased from 3 to 6, in general the adsorption capacity of the biochar also increases. At initial solution pH of 6, precipitation of copper is shown to be significant, with over 20mg/g of the apparent adsorption being attributed to the precipitation of copper hydroxide out of solution. This means that at initial pH of 6 and above, copper is predominantly present in the form of $Cu(OH)_2(H_2O)_4$ [324]. As a result, the amount of copper in the aqueous form is decreased for the experiments conducted at pH 6. This means that the proportion of aqueous copper removed from solution is greater in solutions of initial pH 6 compared with initial pH of 5.5 and below [296]. This suggests that at higher pH, the efficiency of adsorption of aqueous copper from solution to biochar derived from MMDM at pyrolysis temperatures of below 300^{o}C is increased at higher pH. This can be seen in Figure 5.29 where the adsorption of aqueous copper to biochar accounts for a higher percentage of the aqueous copper in

solution. The amount of copper removed by precipitation was determined as is stated in the materials and methodology section through passing two samples through 0.45μm syringe filters. One of these samples was then acidified prior to AAS, dissolving the copper hydroxide precipitate, the other sample was centrifuged with the supernatant then being withdrawn and centrifuged prior to AAS. The difference in copper concentration between the two samples was therefore used to calculate the copper removal due to precipitation.

The increase of adsorption efficiency of copper with pH can be explained by a number of different effects. Firstly, the functional groups on the biochar surface interact with water molecules in an amphoteric manner as discussed in the state-of-the-art. At low pH, hydronium ions compete with aqueous copper ions for the “active sites” that are functional groups exposed to the solution. Furthermore, once these active sites have been protonated, some of these functional groups become positively charged leading to the repulsion of aqueous copper ions [325]. At low pH copper is also less likely to precipitate onto the biochar surface at sites where calcite is present where copper hydroxide and other copper precipitates are less likely to form at low pH [296].

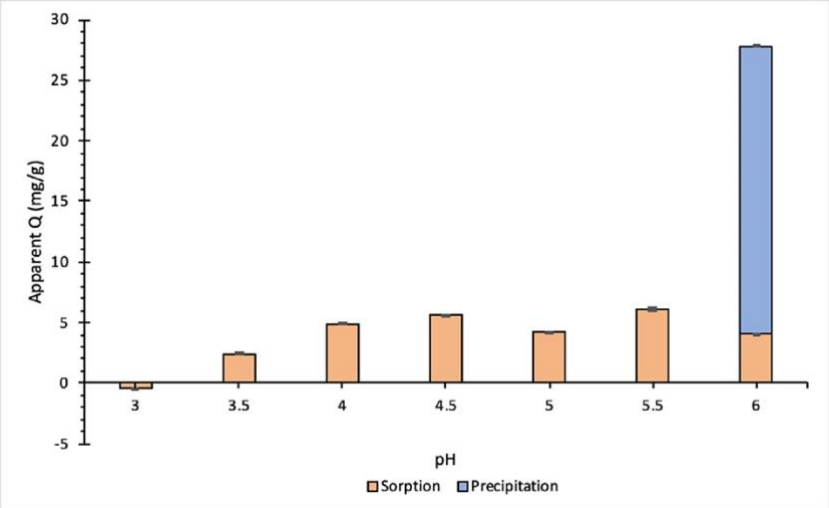

Figure 5.28 – Chart of measured adsorption against initial solution pH

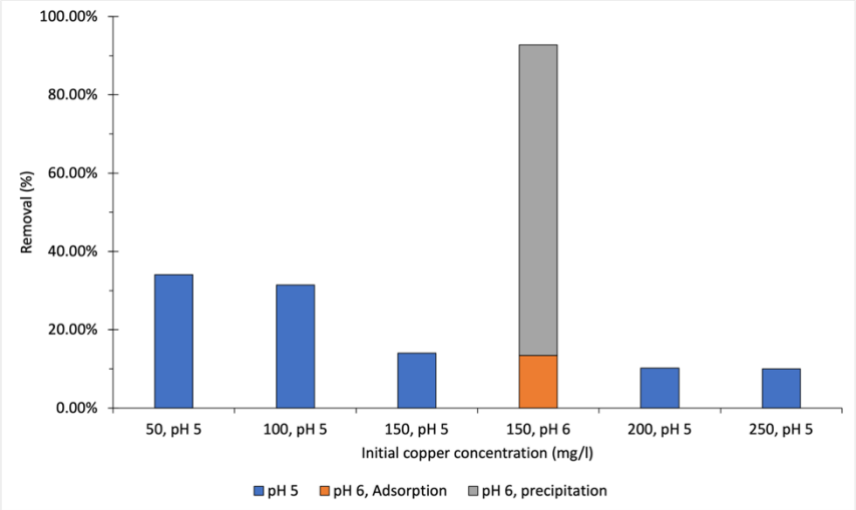

Figure 5.29 – Bar chart showing percentage removal of aqueous copper from solution by biochar at varying conditions of initial concentration and pH, with data labels showing amount of aqueous copper in solution (mg/L)

5.6 EDAX analysis after adsorption

Biochar was analysed using SEM-EDAX after adsorption experiments. The results of which can be seen in Figure 5.30. Regression analyses of copper with different elemental inclusions of biochar are shown in Table 5.8. It can be seen from Table 5.8 that the distribution of copper throughout the biochar is more variable in plastic biochar than in discarded paper and food biochar. With statistical analyses showing that in plastic biochar, copper is highly associated with positive ions, negative ions and oxygen with p-values for these regression analyses being below 0.05. This indicates that in plastic biochar, copper adsorption occurs in a heterogenous fashion across the surface, with the highest amounts of adsorption occurring around mineral inclusions such as calcite and kaolin containing inclusions of the plastic biochar. As discussed in the state of the art and in the previous section on biochar characterisation, these minerals can be used for copper adsorption on their own [326]. The SEM images of plastic biochar in the biochar characterisation section also show a biochar lacking in porosity, indicating that plastic biochar has a low surface area. FTIR spectra for the plastic biochar also showed lower intensity peaks at 1423cm^{-1} and 1030cm^{-1} than in the paper and discarded food biochar. This suggests that for plastic biochar the adsorption of copper to surface functional groups is reduced compared to the other two biochar samples in Figure 5.30. The reduces surface area, porosity and reduced presence of functional groups in plastic biochar produced in a heat pipe reactor supports the conclusion from the EDAX analysis that copper adsorption in plastic biochar can be highly attributed to the mineral fractions in the plastic biochar.

For discarded paper and food biochar, the regression analyses for copper against oxygen, positive ions and negative ions produces p-values greater than 0.05. This suggests that copper adsorption for these biochar samples is less heterogenous than is the case in plastic biochar. This points towards copper adsorption occurring across the surface of the biochar, and not being limited to mineral inclusions. Indeed, SEM images from biochar characterisation show that both biochar materials derived from discarded paper and discarded food have more varied physical surfaces, with visible porous structures indicating a larger surface area than is the case for plastic biochar. Additionally, FTIR spectra of both discarded paper and food biochar showed intense peaks at 1430cm^{-1} and 1030cm^{-1} indicating the presence of carboxylic groups, and primary alcohols. Additionally, calcite detected in these biochar materials with FTIR peaks at 873cm^{-1} and 713cm^{-1} can also act as an adsorbent surface for copper as is the case in discarded plastic biochar. The increased surface area, and presence of functional groups in both discarded food and discarded paper biochar explains why the regression analyses displayed in Table 5.8 do not produce a statistically significant correlation between copper and oxygen, positive ions or negative ions. This is due to copper being adsorbed at sites where functional groups are present, with these being distributed more ubiquitously across the surface of the biochar.

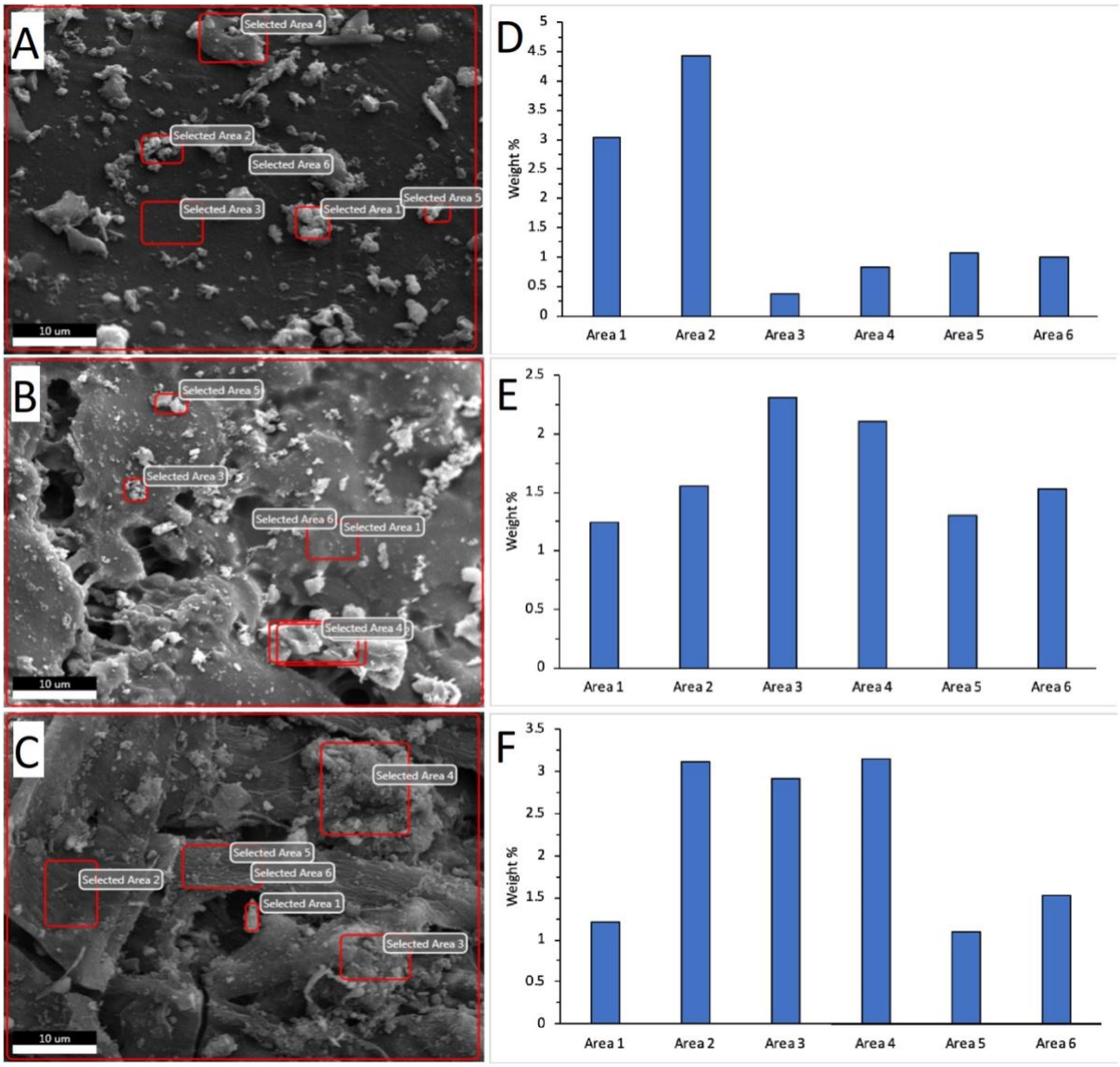

Figure 5.30 – Figure showing SEM-EDAX results of copper in biochar samples after adsorption experiments with A, B and C showing SEM images of plastic, discarded food, and paper biochar respectively where D, E and F are the respective amounts of copper detected in SEM-EDAX images of adjacent SEM micrographs

Table 5.8 – Table showing regression analysis of copper with either oxygen, positive ions or negative ions detected in EDAX analysis of different biochar samples

	Plastic	Paper	Organic
	Oxygen: copper		
Oxygen content range	6.14–25.12%	5.94–30.44%	6.96–10.86%
R^2	0.9681	0.41	0.1955
Coefficient	0.029	0.0152	0.1239
Intercept	−0.0772	0.3452	0.6409
p-Value	0.0024	0.1708	0.2562
	Positive ions: copper		
Positive ions content range	0.92–13.06%	6.21–29.22%	4.94–9.29%
R^2	0.9855	0.2024	0.0094
Coefficient	0.047	0.014	0.0246
Intercept	0.0464	0.3279	1.5028
p-Value	0.0007	0.3707	0.7884
	Negative ions: copper		
Negative ions content range	0.44–1.55%	0.88–2.71%	1.20–2.51%
R^2	0.8834	0.0904	0.1126
Coefficient	0.4983	0.1115	0.095
Intercept	−0.1349	0.3927	0.3426
p-Value	0.0175	0.5625	0.5155

5.7 Potential production and application of biochar produced from municipal discarded material using heat pipe reactors

Copper adsorption to biochar derived from MMDM in a heat pipe reactor is shown to exhibit adsorption capacities up to 6.3 mg/g under the conditions studied in this chapter. Compared with other studies, this seems to be a fairly low adsorption capacity. However, as is stated in the state of the art, these studies make use of specific feedstocks, and often employ pyrolysis temperatures in excess of 500 ^{o}C to produce the biochar [182,183,188–208]. Furthermore, many such studies make use of chemical modifying agents to improve the characteristics of their biochar adsorbent [327,328]. What is shown in this chapter is that whilst unmodified biochar produced in a heat pipe reactor using discarded domestic material as a feedstock is not as highly performing as other commercial and experimental adsorbents, it is nonetheless

capable of removing aqueous copper from solution in noticeable amounts. Furthermore, the heat pipe pyrolysis reactor is operated using mains electricity, showing that a home or small business could manufacture this adsorbent from the municipal waste they produce. This would represent a reduction in the waste footprint, as well as a potential increase in the profitability and sustainability of a business or household.

In section 5.5 the varying of pH showed that the produced biochar was capable of removing aqueous copper from solution after the precipitation of the majority of copper in the form of copper hydroxide. Water treatment plants employ precipitation and other processes such as ion exchange, adsorption and electrochemical treatment are also used. The adsorption of copper to the produced biochar after precipitation at pH 6 shows that this adsorbent can be used as a pre-treatment step to these later processes. This use could optimise chemical precipitation processes by reducing the amount of precipitant required to remove heavy metals such as copper to the required drinking water standards [329–331]. This pre-treatment could also extend the life of subsequent ion exchange materials, adsorbents and electrochemical processes, where the concentrations of copper and other heavy metals reaching these stages have already been reduced.

Drinking water treatment plants make use of screens to remove debris and other smaller detritus from water prior to further treatment to protect pipework and other components of the treatment plant from physical damage. The screening process generates waste containing leaves, algae, and plankton as well as other organic and inorganic materials present in the influent water , this is similar in nature to MMDM which contains cellulose, hemicellulose and other biological carbonaceous materials [332]. Biochar material similar to that produced in this thesis could therefore be produced from some waste materials produced by drinking water treatment plants. Indeed, coagulation-flocculation sludge has been studied as a potential feedstock for pyrolysis based adsorbents with promising results [333]. Using heat pipe pyrolysis from materials captured on various sizes of mesh screens at the inlet to the plant as well as the sludge generated by coagulation-flocculation procedures could therefore

produce a cheap adsorbent material for further pre-treatment processes from materials that would otherwise be disposed of [334].

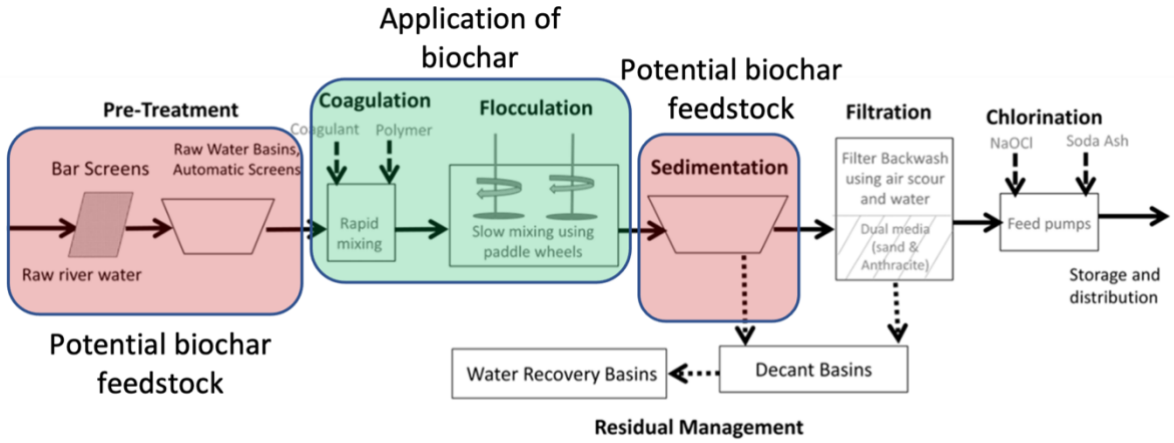

Figure 5.31 – Drinking water treatment plant process diagram identifying processes producing potential biochar feedstock (red box), and processes that could benefit from biochar addition (green box) [262]

An alternative use for biochar produced from MMDM using heat pipe pyrolysis could also be in soft engineering applications such as sustainable urban drainage systems where it could remove environmental heavy metal pollution [335–337]. Furthermore, this material could also be employed in land remediation or as a soil additive where it could reduce the bioavailability of heavy metals [336,338]. Indeed the extra oxygen containing functional groups in the biochar produced using the heat pipe reactor are known to be beneficial for the adsorption of copper to soils in sustainable urban drainage systems [339]. An added benefit of using this biochar as a soil additive or as a drainage material in sustainable drainage systems is that it represents a carbon sink, where incineration and landfill lead to the release of carbon from plastics, food and paper waste as carbon dioxide, and methane respectively which are both known greenhouse gases [340].

5.8 Comparison with literature

Table 5.9 shows the copper adsorption from the experiments conducted for this thesis and copper adsorption from other studies. What can be seen is that most biochar produced in other studies appears to have better adsorption capacities than the biochar produced from discarded domestic material at low temperatures. On inspecting the experimental parameters used, it can be seen that whilst most adsorbents do indeed outperform the biochar investigated in this chapter, the adsorption of copper to biochar produced in the heat

pipe reactor from is nonetheless comparable. This supports the claim in 5.7 that biochar could be produced on site at a water treatment plant and used for the removal of copper and potentially other heavy metals from influent water.

Another notable observation from the literature displayed in Table 5.9 is the use of feedstock. Literature as stated already in the state-of-the-art makes use of specific feedstock materials to produce adsorbents. Biochar material produced from MMDM is more holistic since MMDM is available almost everywhere on the planet, with its composition varying depending mainly on income level rather than on the availability of the feedstock [12]. These other adsorbent materials can only be sustainably produced in localities where the utilised feedstocks are available.

Whilst the biochar produced using MMDM may not be preferential for high copper concentration applications, it may be effective in applications where copper and other heavy metals are expected in lower concentrations, such as in sustainable drainage systems or in the initial stages of a drinking water treatment plant. Furthermore, converting this material to biochar for a further use would produce a valuable product from a material without worth. It is also stated by several studies that the pyrolysis of materials with the aim of producing biochar, results in lower environmental impact than sending this feedstock to landfill or incineration [341–343]. Furthermore, the carbon footprint of biochar can be reduced through using MMDM as a feedstock. Using a mixture as a feedstock results in a lower carbon footprint as pyrolysis does not require as much sorting as other recycling processes [344].

Table 5.9 – Comparison of collected copper adsorption data and a selection of adsorption data from literature

Feedstock	Adsorbent production	Biochar dosage (g/L)	Initial solution conc. (mg/L)	Initial solution pH	Adsorption (mg/g)	Source
Discarded Domestic Material	<300°C pyrolysis	5	50	5	3.41	This chapter
Discarded Domestic Material	<300°C pyrolysis	5	100	5	6.28	This chapter
Discarded Domestic Material	<300°C pyrolysis	5	150	5	4.22	This chapter
Discarded Domestic Material	<300°C pyrolysis	5	200	5	4.07	This chapter
Discarded Domestic Material	<300°C pyrolysis	5	250	5	5.02	This chapter
Discarded Domestic Material	<300°C pyrolysis	5	150	6	4.03	This chapter
Brown Seaweed	300°C pyrolysis	0.005	300	5	105	[345]
Brown Seaweed	500°C pyrolysis	0.005	300	5	130	[345]
Brown Seaweed	700°C pyrolysis	0.005	300	5	220	[345]
Ginko leaf	800°C pyrolysis	1	50	5	16.23	[346]
Peanut shell	800°C pyrolysis	1	50	5	4.7	[346]
Metasequoia leaf	800°C pyrolysis	1	50	5	3.94	[346]
Lobster shell	300°C pyrolysis, demineralised in HCl	2	100	5	52.7	[347]
Lobster shell	600°C pyrolysis, demineralised in HCl	2	100	5	54.6	[347]
Rice straw	300°C pyrolysis	2	100	5	15	[348]
Rice straw	400°C pyrolysis	2	100	5	23.5	[348]
Rice straw	500°C pyrolysis	2	100	5	29.5	[348]
Bidens pilosa L.	500°C pyrolysis	1	20	7	20.01	[349]
Praxelis clematidea	500°C pyrolysis	1	20	7	17.61	[349]
Ipomoea cairica	500°C pyrolysis	1	20	7	19.10	[349]
Mikania micrantha	500°C pyrolysis	1	20	7	20.10	[349]
Lantana camara L.	500°C pyrolysis	1	20	7	16.51	[349]

5.9 Summary

In summary, copper adsorption appears to occur on heat pipe derived biochar in a heterogenous fashion limited by chemical adsorption. However, as initial copper concentration increased physical adsorption processes may become more significant, as is shown by the increasing fit of the pseudo first order kinetic model with increasing concentration. Increased pH is also shown to impact on the adsorption kinetics, with adsorption occurring much more rapidly at higher pH.

EDAX analysis confirms that copper is distributed fairly evenly across the surface of biochar derived from discarded food, and paper. This suggests that copper is removed by functional groups present in these materials as well as ion exchange and/or precipitation processes around calcite or other mineral inclusions. Biochar derived from discarded plastic however showed a much lower distribution of copper across the biochar surface, with concentrations particularly concentrated around sites containing positive and negative ions. This suggests that the adsorption of copper is predominantly due to precipitation and/or ion exchange processes in biochar derived from discarded plastics.

Intraparticle diffusion models reveal that whilst intraparticle diffusion does occur, it is not the only diffusion process limiting the removal of copper from bulk solution. An initial and rapid diffusion process is shown to occur in the Weber-Morris plots. This step is likely the liquid film diffusion process which is shown to occur by the strong fit of the Boyd plots. The Boyd plots also reveal that the rapid liquid film diffusion process is not the rate limiting step where the regression line passes through the origin. This suggests that intraparticle diffusion processes into pores in the biochar material are more limiting than the diffusion of copper across the liquid film between the bulk solution and the biochar.

The Langmuir model was shown to describe the isothermal behaviour of copper adsorption to the biochar best. This means that copper adsorption is best described by a monolayer of adsorbent distributed evenly across the biochar surface. The Dual mode model also could not provide a better fit than the Langmuir model. This indicates that partitioning is not a major process in the removal of copper from bulk solution by this biochar.

Overall copper could be removed from solution by MMDM biochar with greater removal percentages at lower initial concentrations. This suggests that this material could be used in applications where copper concentrations are expected to be elevated but not excessive, with

initial copper concentrations below 50mg/L. This would result in a carbon sink/buffer where MMDM that would be directly burnt as fuel in incinerators or landfilled is converted into a useful product. This product could also extend the service life and/or demand on more specialist materials such as higher quality activated carbons and ion exchange resins.

6 METHYLENE BLUE ADSORPTION TO BIOCHAR DERIVED FROM MIXED MUNICIPAL DISCARDED MATERIAL IN A HEAT PIPE REACTOR

6.1 Methylene Blue

Methylene blue is a dye that is widely used in the textile industry as well as other industries [350]. The use of methylene blue in these industries leads to the contamination of wastewater with methylene blue dye. This dye has been found to reduce the growth of certain aquatic micro-algae, due to a number of effects including its inhibitory effect on photosynthesis [351]. It is therefore highly important to remove methylene blue, as well as other dyes from the wastewater of such processes to reduce their impact on the environment.

Aqueous methylene blue contamination can be reduced through a number of different processes outlined in the state of the art. These include: nanofiltration, reverse osmosis, forward osmosis and adsorption, as well as additional processes such as ozonation, and photocatalysis. In recent years, much research has been conducted on the use of photocatalysis to remove dyes from water. This technology however has not reached the industrial scale in a meaningful way as of yet [352]. The other technologies listed can be expensive and/or technically complicated to operate. Indeed, nanofiltration and reverse osmosis membranes as explored in the state of the art are produced using interfacial polymerisation and require carefully monitored operating conditions to improve their efficiency as well as to protect the membranes from fouling and damage [353]. Furthermore, these processes do not remove methylene blue from the waste stream, they simply recover water from the contaminated source [354]. Forward osmosis makes use of a draw solution that contains a known salt, this is often used to recover water from wastewater. As is the case with nanofiltration and reverse osmosis, a concentrated retentate solution remains therefore methylene blue is not removed from the waste stream, rather water is recovered from it. Ozonation is capable of removing methylene blue from solution as it causes the oxidation methylene blue. This predominantly occurs due to the presence of different reactive oxygen species in water when ozone is introduced, these include the more selective ozone and the less selective hydroxyl radical [355,356]. The hydroxyl radical is only produced in noticeable amounts under specific conditions of pH, this means that as well as having an on-site ozone generator, a water treatment system must also consume reagents that alter the pH of solution in order to optimise the ozonation process. This makes an ozonation system costly to run, especially if it is not necessarily required.

Adsorption is often employed as a method of reducing aqueous pollution where it can be operated fairly easily. Mineral adsorbents have been investigated for the removal of organic dyes from solution and have shown a strong ability for the removal of methylene blue from aqueous solution [357,358]. Activated carbon is also a widely used material for the removal of organic dyes from aqueous solution [359,360]. These are produced from materials including clay minerals including bentonite, with anthracite, coal and biogenic carbon being used for the production of activated carbon. This means that mineral adsorbents and some activated carbons are produced from non-renewable sources of material. For this reason, in recent years the production of biochar and activated carbon from renewable sources of biogenic carbon has become an area of increased research interest. Many studies as stated in previous chapters typically involve the high temperature pyrolysis of a specific feedstock with either steam or chemical activation. There is however growing interest in carbonaceous adsorbents that are produced at lower temperatures for organic dye removal. This is due to these materials containing greater amounts of oxygen containing functional groups capable of interacting with some organic dyes including methylene blue in hydrogen bonding interactions and cation exchange [15,361,362]. The purpose of this chapter is therefore to determine the efficacy of methylene blue adsorption to biochar produced using a heat pipe pyrolysis reactor with MMDM as a feedstock.

6.2 Adsorption kinetics

Figure 6.1, Figure 6.2 and Figure 6.3 show the pseudo first order, pseudo second order and Elovich kinetic models respectively. The R^2 values show that the kinetic data follows the order Elovich>pseudo second order>pseudo first order. With MSE values following the order pseudo first order>pseudo second order>Elovich. Finally, 95% confidence intervals follow the order pseudo first order>pseudo second order>Elovich. This indicates that at initial concentrations of 10mg/l and initial pH of 7 chemisorption processes of methylene blue are the rate limiting steps of adsorption to biochar produced by the pyrolysis of mixed municipal discarded material under the experimental conditions. These chemisorption processes occur in a heterogenous fashion across the surface of the biochar with the Elovich model fitting the experimental data best.

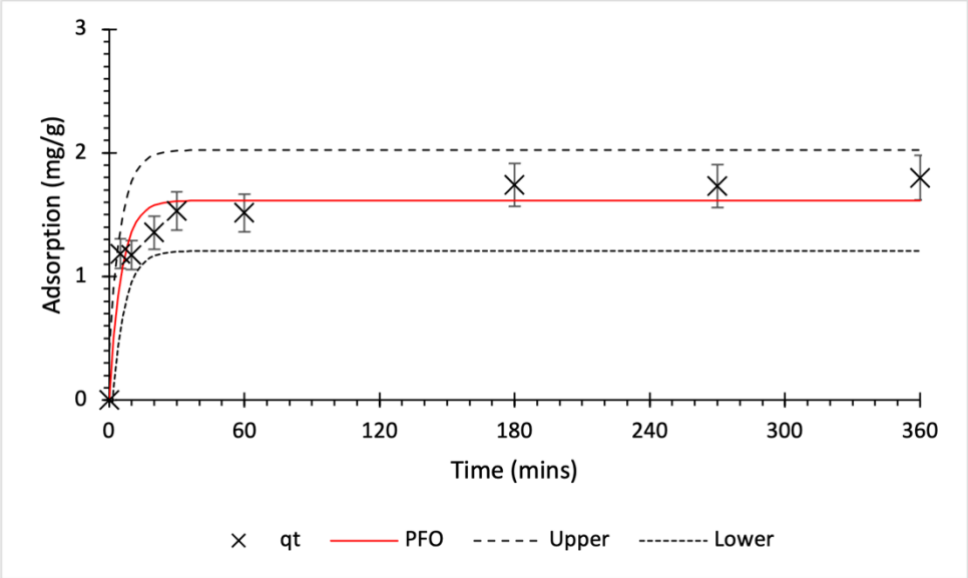

Figure 6.1 – Pseudo first order model of methylene blue adsorption (C_i=10mg/l, pH=7) to biochar derived from mixed municipal discarded material pyrolyzed in a heat pipe reactor

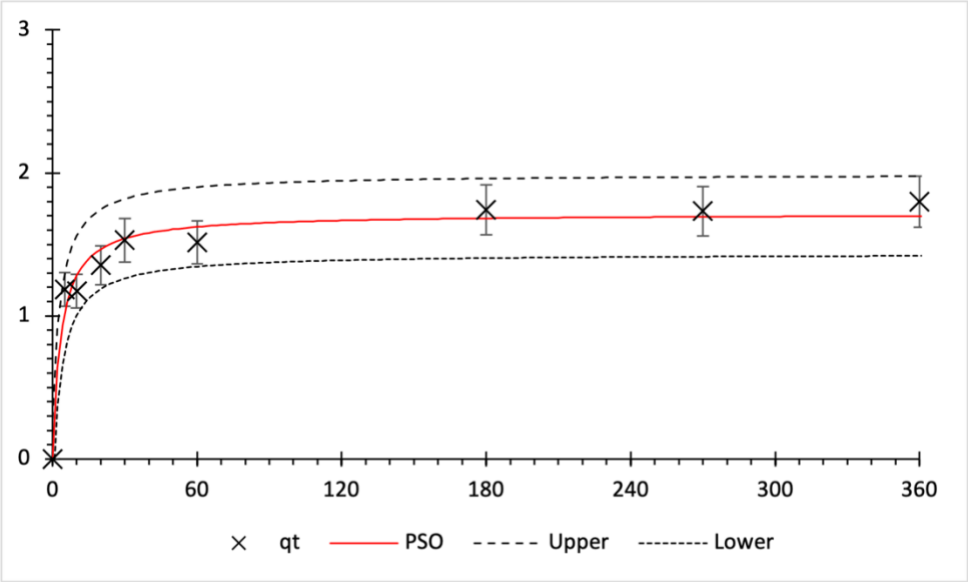

Figure 6.2 – Pseudo second order model of methylene blue adsorption (C_i=10mg/l, pH=7) to biochar derived from mixed municipal discarded material pyrolyzed in a heat pipe reactor

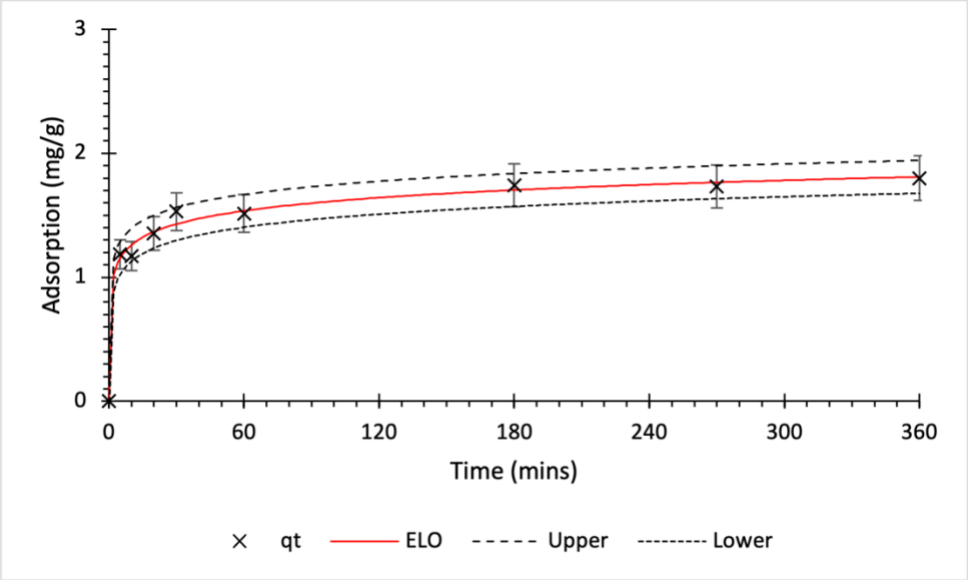

Figure 6.3 – Elovich model of methylene blue adsorption (C_i=10mg/l, pH=7) to biochar derived from mixed municipal discarded material pyrolyzed in a heat pipe reactor

Table 6.1 – Statistical analyses of kinetic models and experimental data for initial concentration of 10mg/l and initial pH of 7

Kinetic model		
Pseudo first order	**K_1**	0.1854
	q_e	1.615
	R^2	0.9154
	MSE	0.0231
	95% Confidence interval	0.408
Pseudo second order	**K_2**	0.1733
	q_e	1.714
	R^2	0.9683
	MSE	0.0086
	95% Confidence interval	0.249
Elovich	**A**	57.91
	B	6.531
	R^2	0.9910
	MSE	0.0025
	95% Confidence interval	0.133

Figure 6.4, Figure 6.5 and Figure 6.6 show the pseudo first order, pseudo second order and Elovich kinetic models plotted with experimental data collected for initial methylene blue concentration of 25mg/l and initial pH of 7 respectively. Table 6.2 shows the statistical analyses for the respective models. The statistical analysis returns R^2 values in the order of

Elovich>pseudo second order>pseudo first order, MSE values in the order of pseudo first order>pseudo second order>Elovich, and 95% confidence intervals in the same order as MSE values. These statistical analyses reveal again that for the indicated experimental conditions, the adsorption of methylene blue to the produced biochar is limited by chemisorption processes that occur in a heterogenous manner across the biochar surface.

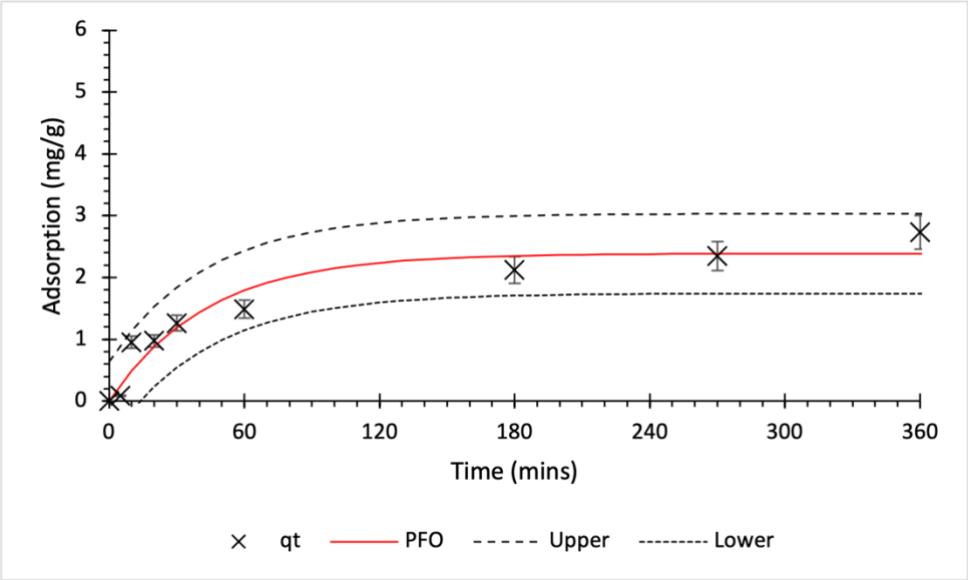

Figure 6.4 – Pseudo first order model of methylene blue adsorption (C_i=25mg/l, pH=7) to biochar derived from mixed municipal discarded material pyrolyzed in a heat pipe reactor

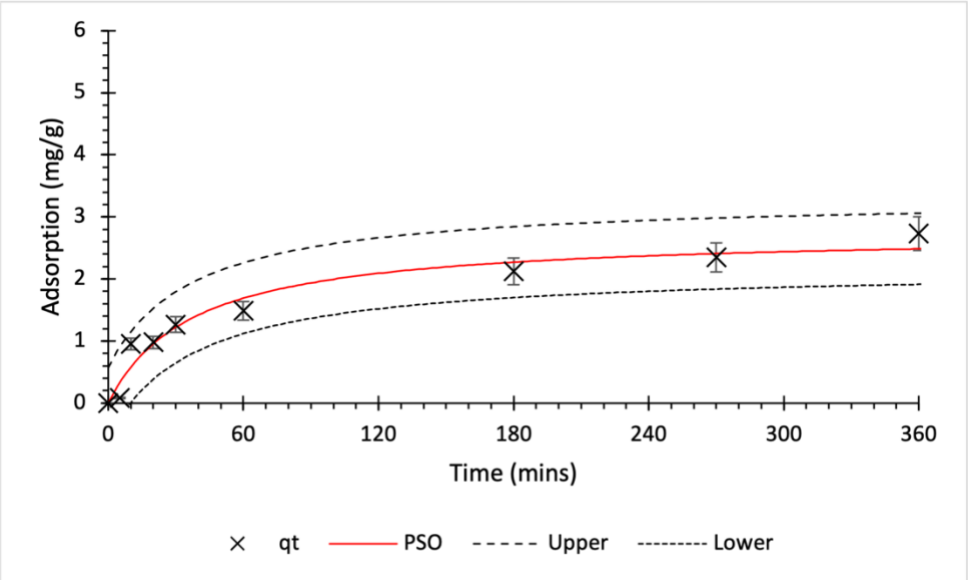

Figure 6.5 – Pseudo second order model of methylene blue adsorption (C_i=25mg/l, pH=7) to biochar derived from mixed municipal discarded material pyrolyzed in a heat pipe reactor

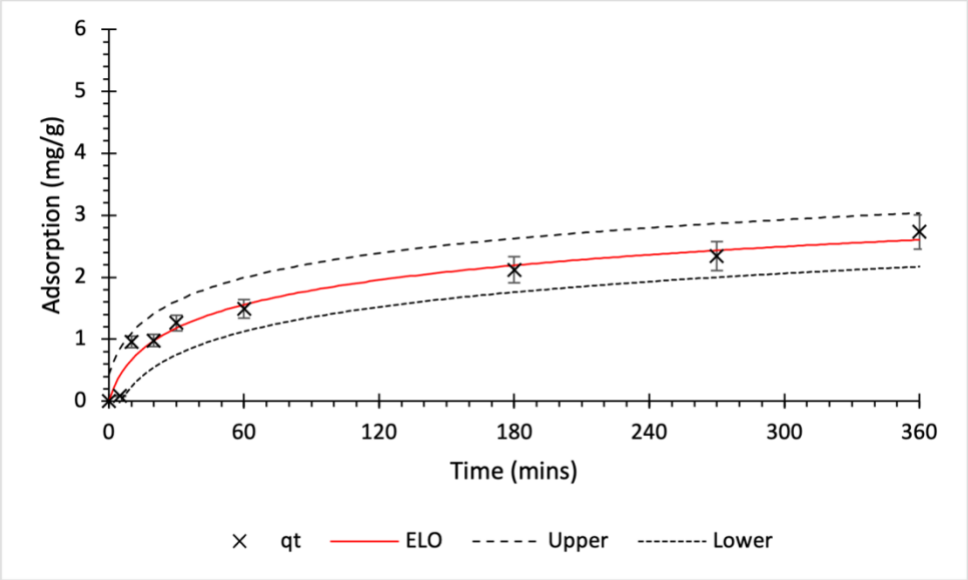

Figure 6.6 – Elovich model of methylene blue adsorption (C_i=25mg/l, pH=7) to biochar derived from mixed municipal discarded material pyrolyzed in a heat pipe reactor

Table 6.2 – Statistical analyses of kinetic models and experimental data for initial concentration of 25mg/l and initial pH of 7

Kinetic model		
Pseudo first order	**K_1**	0.0231
	q_e	2.389
	R^2	0.9304
	MSE	0.0579
	95% Confidence interval	0.645
Pseudo second order	**K_2**	0.0097
	q_e	2.744
	R^2	0.9547
	MSE	0.0364
	95% Confidence interval	0.572
Elovich	**A**	0.122
	B	1.648
	R^2	0.9677
	MSE	0.0261
	95% Confidence interval	0.433

Figure 6.7, Figure 6.8 and Figure 6.9 show the pseudo first order, pseudo second order, and Elovich kinetic models for methylene blue adsorption to biochar produced from mixed municipal discarded material respectively with initial bulk solution concentration of 50mg/l and initial pH of 7. Table 6.3 shows the statistical analyses for these models. The R^2 values follow the order of Elovich>pseudo second order>pseudo first order, with MSE following the

order pseudo first order>pseudo second order>Elovich with the 95% confidence interval again following the same order as MSE. Therefore, for initial concentrations of 50mg/l and initial solution pH of 7, the adsorption of methylene blue is limited by chemisorption processes that occur in a heterogenous fashion.

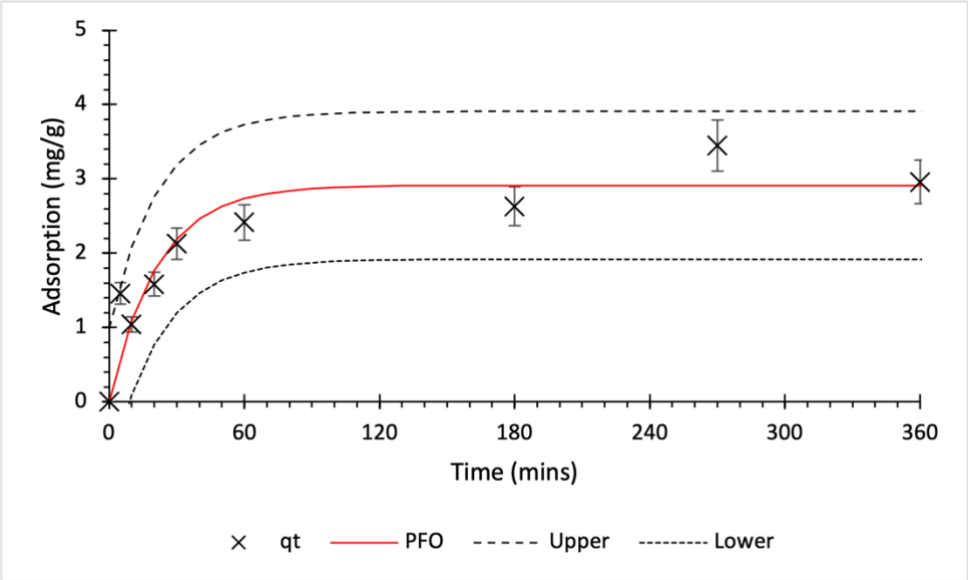

Figure 6.7 – Pseudo first order model of methylene blue adsorption (C_i=50mg/l, pH=7) to biochar derived from mixed municipal discarded material pyrolyzed in a heat pipe reactor

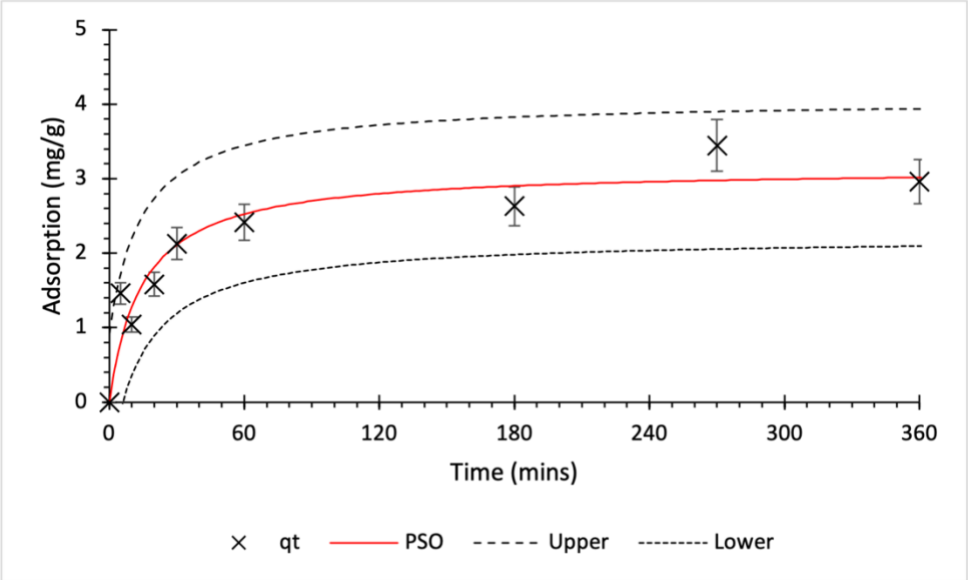

Figure 6.8 – Pseudo second order model of methylene blue adsorption (C_i=50mg/l, pH=7) to biochar derived from mixed municipal discarded material pyrolyzed in a heat pipe reactor

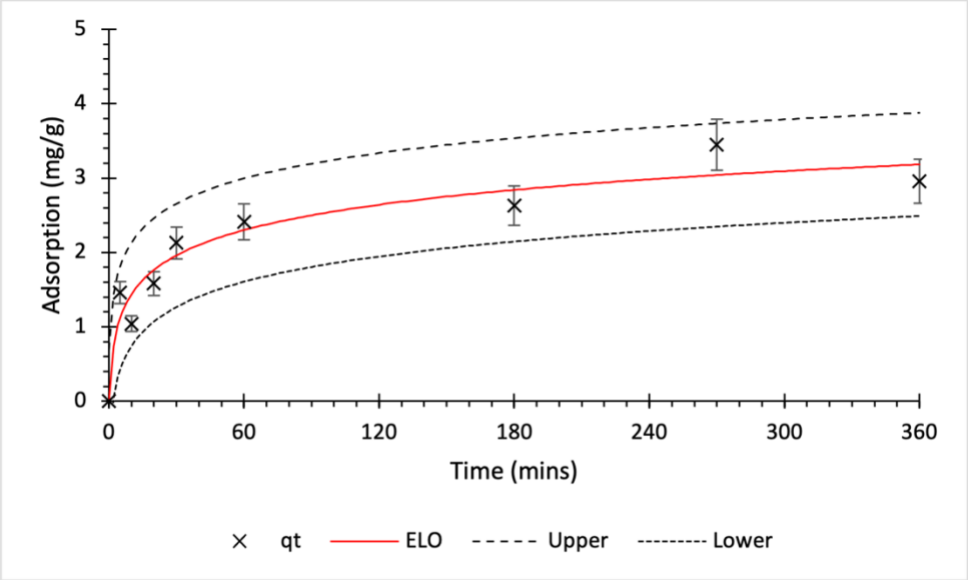

Figure 6.9 – Elovich model of methylene blue adsorption (C_i=50mg/l, pH=7) to biochar derived from mixed municipal discarded material pyrolyzed in a heat pipe reactor

Table 6.3 – Statistical analyses of kinetic models and experimental data for initial concentration of 50mg/l and initial pH of 7

Kinetic model		
Pseudo first order	**K_1**	0.0466
	q_e	2.913
	R^2	0.8776
	MSE	0.1377
	95% Confidence interval	0.995
Pseudo second order	**K_2**	0.0218
	q_e	3.139
	R^2	0.9083
	MSE	0.0974
	95% Confidence interval	0.922
Elovich	**A**	0.853
	B	2.020
	R^2	0.9327
	MSE	0.0671
	95% Confidence interval	0.695

Figure 6.10, Figure 6.11 and Figure 6.12 show the pseudo first order, pseudo second order and Elovich kinetic models for methylene blue adsorption to biochar produced from mixed municipal discarded material with initial solution concentration of 75mg/l and initial solution pH of 7. Table 6.4 shows the statistical analyses for these models. R^2 values follow the order of pseudo second order>Elovich>pseudo first order, with both MSE and 95% confidence interval values following the order of pseudo first order>Elovich>pseudo second order. This suggests that under these initial condition's adsorption of methylene blue to the produced

biochar is limited by chemisorption processes, however the heterogeneity of these adsorption processes is reduced under these conditions compared with the previous conditions with lower initial methylene blue concentrations.

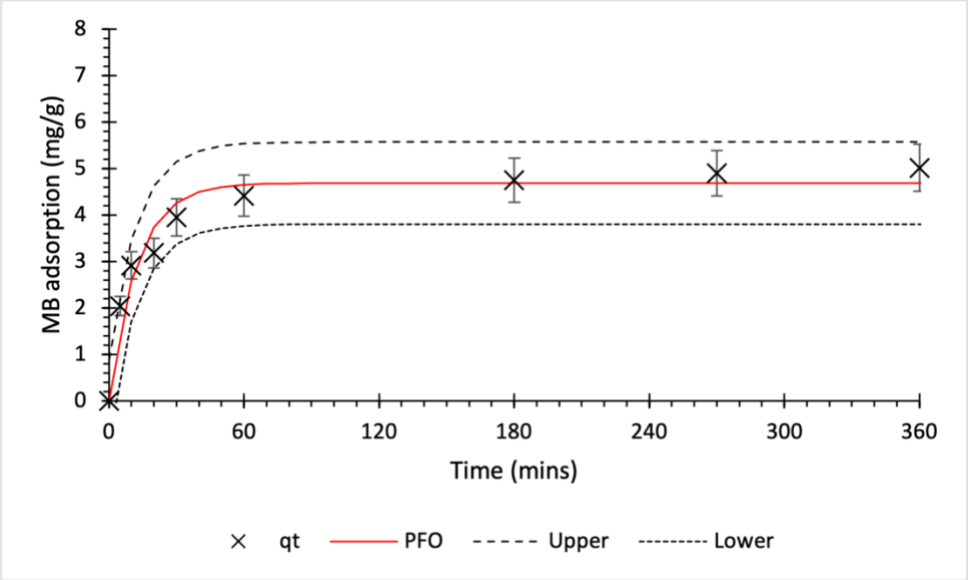

Figure 6.10 – Pseudo first order model of methylene blue adsorption (C_i=75mg/l, pH=7) to biochar derived from mixed municipal discarded material pyrolyzed in a heat pipe reactor

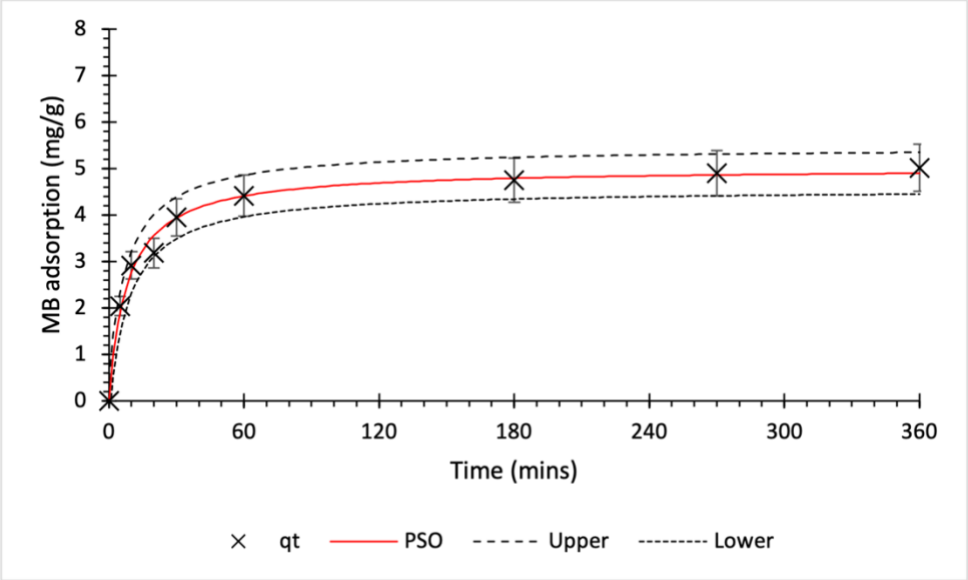

Figure 6.11 – Pseudo second order model of methylene blue adsorption (C_i=75mg/l, pH=7) to biochar derived from mixed municipal discarded material pyrolyzed in a heat pipe reactor

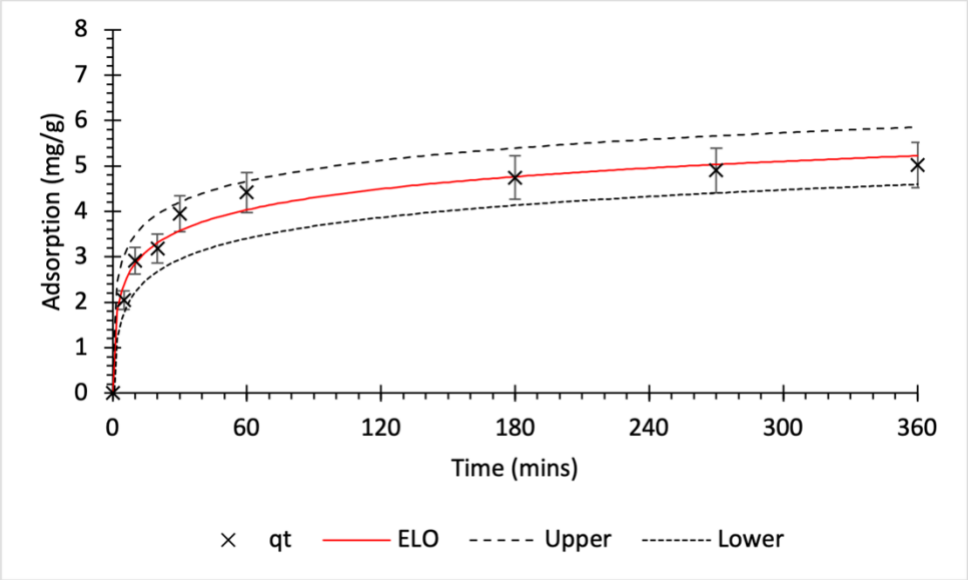

Figure 6.12 – Elovich model of methylene blue adsorption (C_i=75mg/l, pH=7) to biochar derived from mixed municipal discarded material pyrolyzed in a heat pipe reactor

Table 6.4 – Statistical analyses of kinetic models and experimental data for initial concentration of 75mg/l and initial pH of 7

Kinetic model		
Pseudo first order	**K_1**	0.0062
	q_e	4.989
	R^2	0.9583
	MSE	0.1086
	95% Confidence interval	0.883
Pseudo second order	**K_2**	0.0245
	q_e	5.010
	R^2	0.9908
	MSE	0.0224
	95% Confidence interval	0.449
Elovich	**A**	4.773
	B	1.504
	R^2	0.9771
	MSE	0.0550
	95% Confidence interval	0.629

Figure 6.13, Figure 6.14 and Figure 6.15 show the pseudo first order, pseudo second order and Elovich models plotted against experimental adsorption data for initial methylene blue concentrations of 100mg/l and initial solution pH of 7. Table 6.5 shows the statistical analyses for these experiments. R^2 and 95% confidence interval values follow the order Elovich>pseudo second order>pseudo first order, with MSE values following the order pseudo second

order>Elovich>pseudo first order. The values for R^2, MSE and 95% confidence intervals are very similar to one another, this reveals that as the initial methylene blue concentration is increased from 75 to 100 mg/l. This shows that the processes limiting the adsorption of methylene blue to the biochar produced from mixed municipal discarded material become more physical rather than chemical in nature [363].

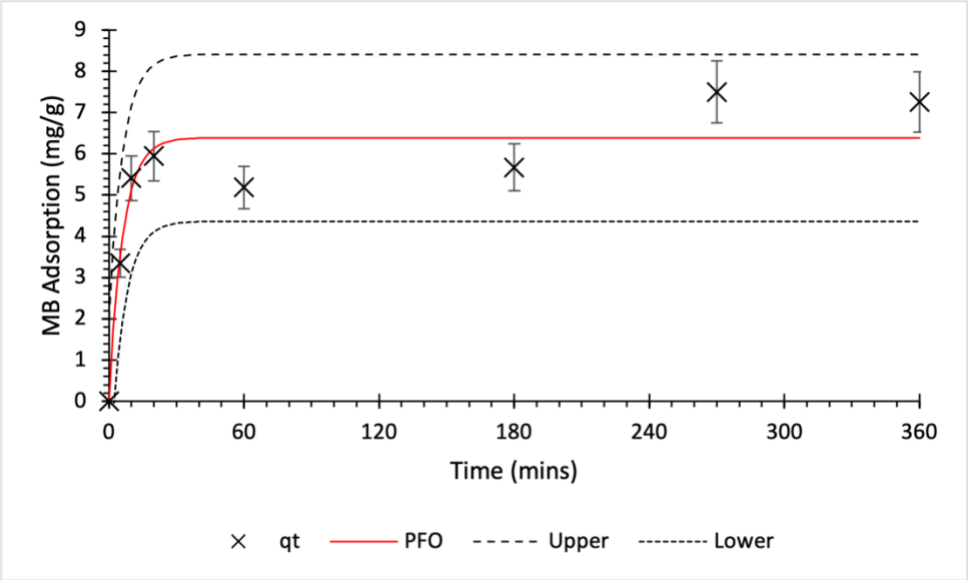

Figure 6.13 – Pseudo first order model of methylene blue adsorption (C_i=100mg/l, pH=7) to biochar derived from mixed municipal discarded material pyrolyzed in a heat pipe reactor

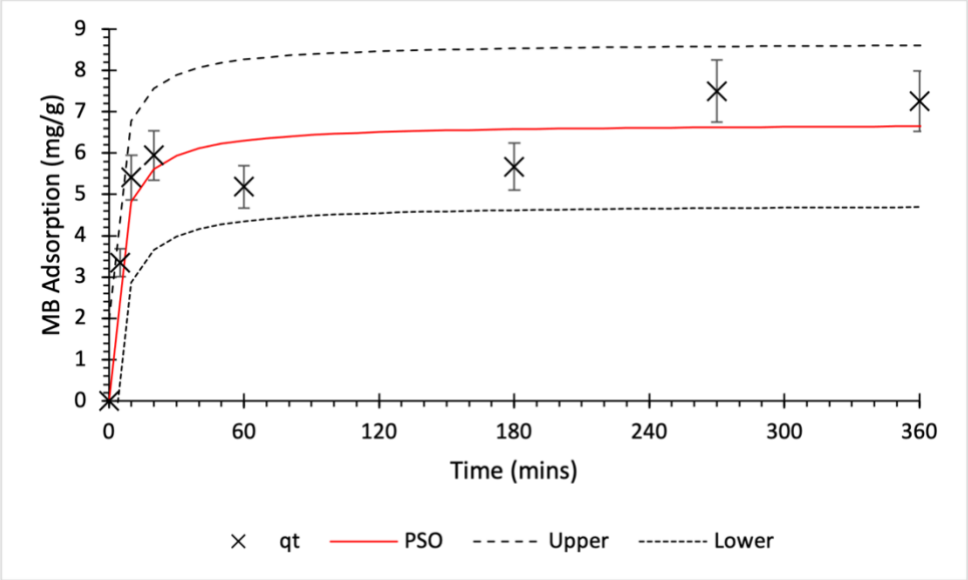

Figure 6.14 – Pseudo second order model of methylene blue adsorption (C_i=100mg/l, pH=7) to biochar derived from mixed municipal discarded material pyrolyzed in a heat pipe reactor

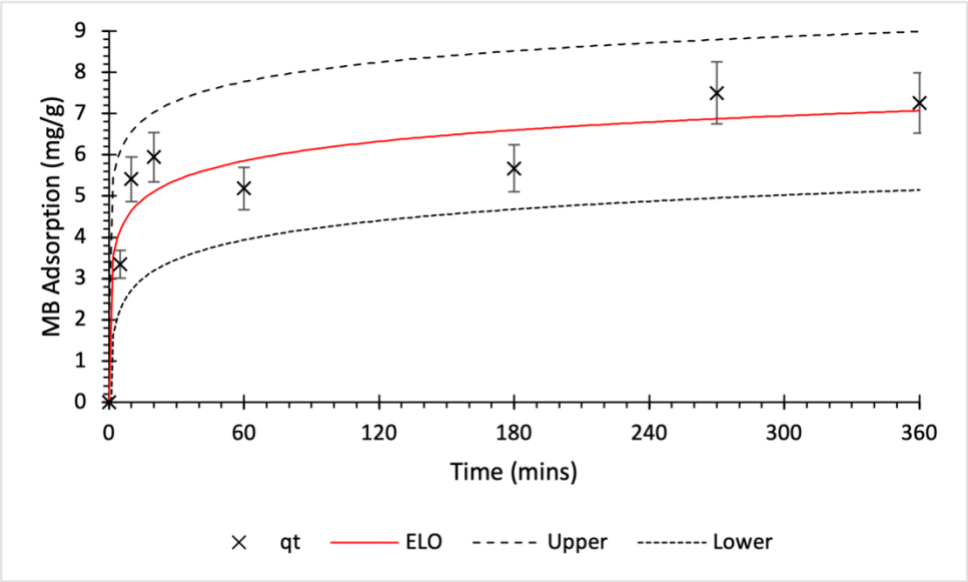

Figure 6.15 – Elovich model of methylene blue adsorption (C_i=100mg/l, pH=7) to biochar derived from mixed municipal discarded material pyrolyzed in a heat pipe reactor

Table 6.5 – Statistical analyses of kinetic models and experimental data for initial concentration of 100mg/l and initial pH of 7

Kinetic model		
Pseudo first order	**K_1**	0.1615
	q_e	6.388
	R^2	0.8988
	MSE	0.4563
	95% Confidence interval	2.024
Pseudo second order	**K_2**	0.0377
	q_e	6.719
	R^2	0.9055
	MSE	0.4793
	95% Confidence interval	1.956
Elovich	**A**	63.67
	B	1.476
	R^2	0.9090
	MSE	0.4617
	95% Confidence interval	1.920

6.2.1 Summary of Kinetic models

The kinetic models show that at initial methylene blue concentrations of 75mg/l and below the Elovich and pseudo second order kinetic models best describe the kinetic behaviour of methylene blue adsorption to MMDM biochar. Above an initial concentration of 75mg/l the kinetic models that best describe the adsorption of methylene blue to MMDM biochar become less easy to determine with similar R^2, MSE, and 95% confidence interval values. This

suggests that at concentrations greater than 75mg/l, the adsorption of methylene blue becomes more dependent on physical adsorption mechanisms and chemical adsorption mechanisms become less significant. The change in the best fitting kinetic models shows that multiple removal mechanisms likely occur between MMDM biochar and methylene blue. These may include various physical adsorption and chemical adsorption processes. These may include: π electron interactions between aromatic groups in the biochar and the methylene blue; hydrogen bonding between functional groups present in the biochar and methylene blue; and electrostatic interactions between the adsorbent and adsorbate. Partitioning mechanisms may also be significant with the low pyrolysis temperature leading to un-carbonised fractions remaining in the biochar material.

6.3 Diffusion Models

6.3.1 Intraparticle diffusion models

As is the case in copper adsorption, Weber-Morris plots of methylene blue adsorption to the biochar also revealed a multi-linear relationship. This shows that whilst the intraparticle model can describe the adsorption of methylene blue to MMDM biochar, it is not the only process involved in the adsorption of methylene blue to such biochar. Figure 6.16, Figure 6.17, Figure 6.18, Figure 6.19 and Figure 6.20 all show a rapid initial methylene blue uptake by the biochar material. This first phase likely represents the liquid film diffusion of methylene blue from bulk solution into the biochar material. The second linear stages likely represent the diffusion of methylene blue into medium-large pores, with diffusion into smaller pores being responsible for any additional linear stages [364,365].

The figures also show that as the initial concentration of methylene blue is increased, the determination of three distinct linearities in the Weber-Morris plots becomes more difficult. This shows that as initial concentration is increased, the adsorbent becomes saturated with methylene blue more rapidly.

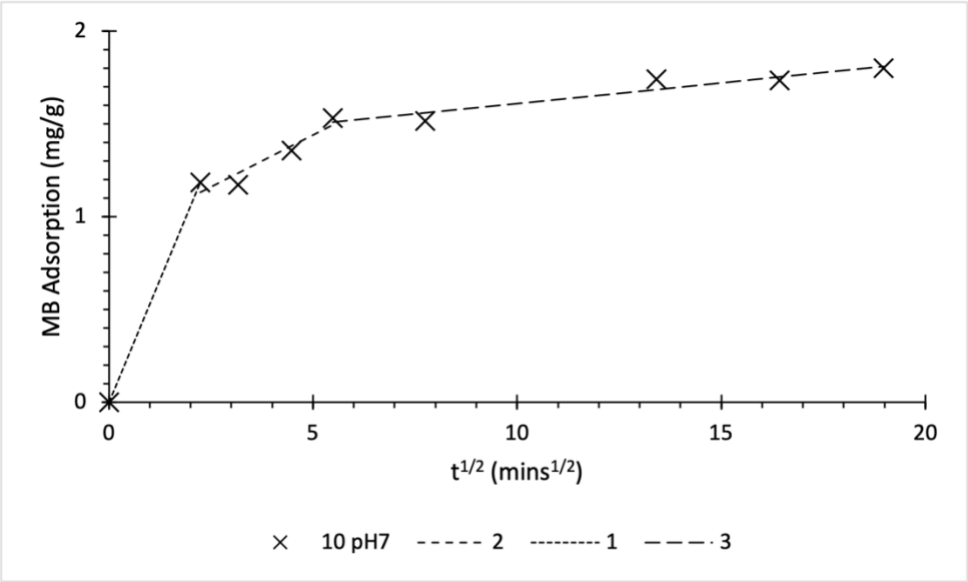

Figure 6.16 – Intraparticle model of methylene blue adsorption (C_i=10mg/l, pH=7) to biochar derived from mixed municipal discarded material pyrolyzed in a heat pipe reactor

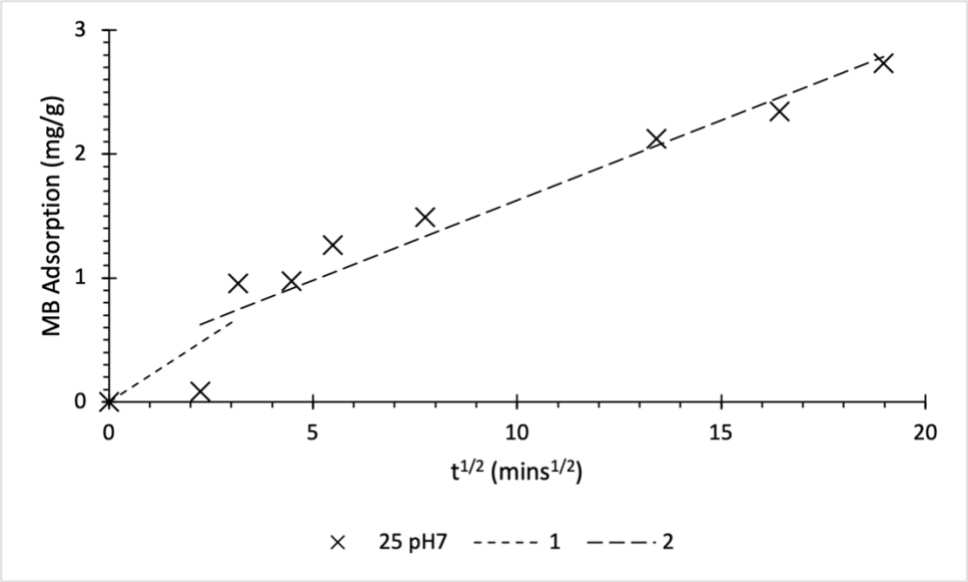

Figure 6.17 – Intraparticle model of methylene blue adsorption (C_i=25mg/l, pH=7) to biochar derived from mixed municipal discarded material pyrolyzed in a heat pipe reactor

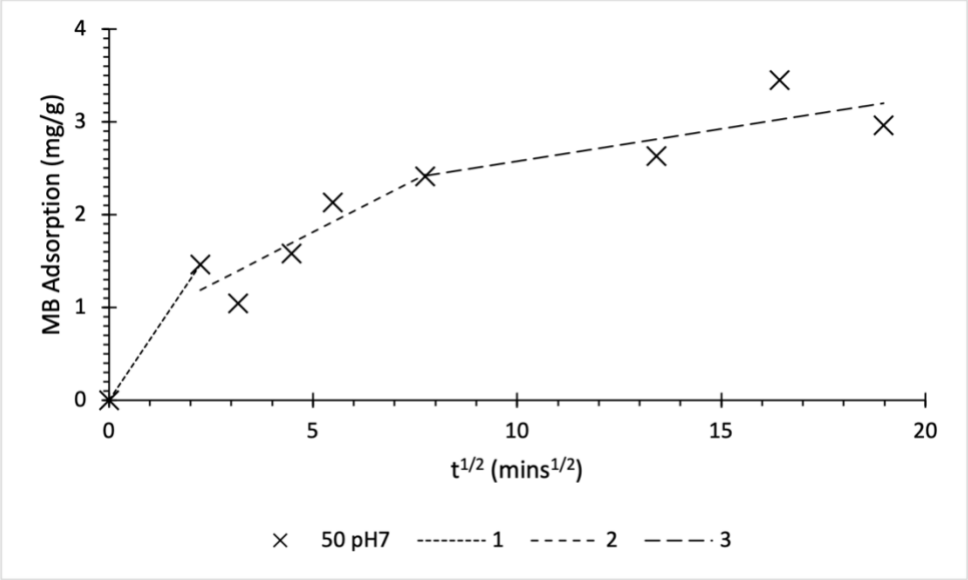

Figure 6.18 – Intraparticle model of methylene blue adsorption (C_i=50mg/l, pH=7) to biochar derived from mixed municipal discarded material pyrolyzed in a heat pipe reactor

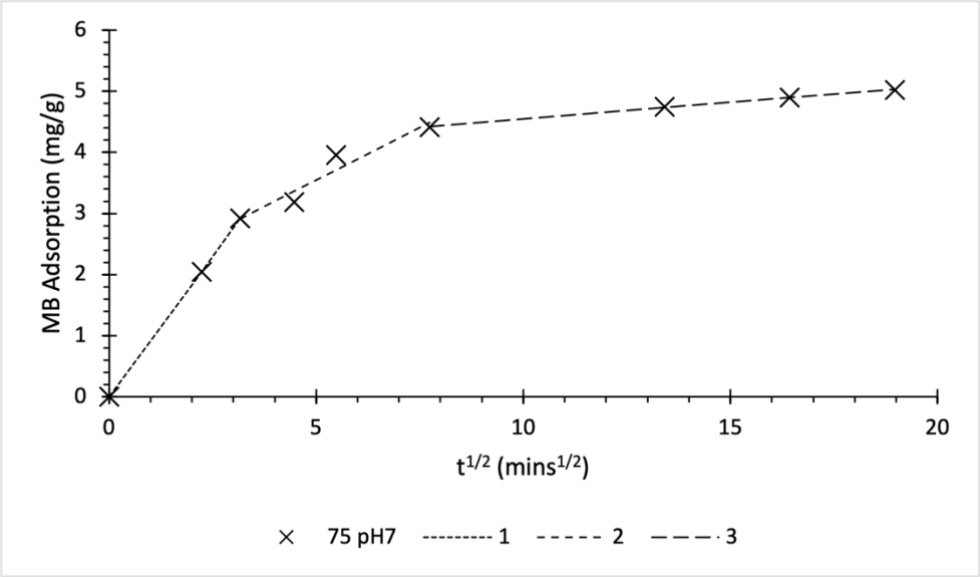

Figure 6.19 – Intraparticle model of methylene blue adsorption (C_i=75mg/l, pH=7) to biochar derived from mixed municipal discarded material pyrolyzed in a heat pipe reactor

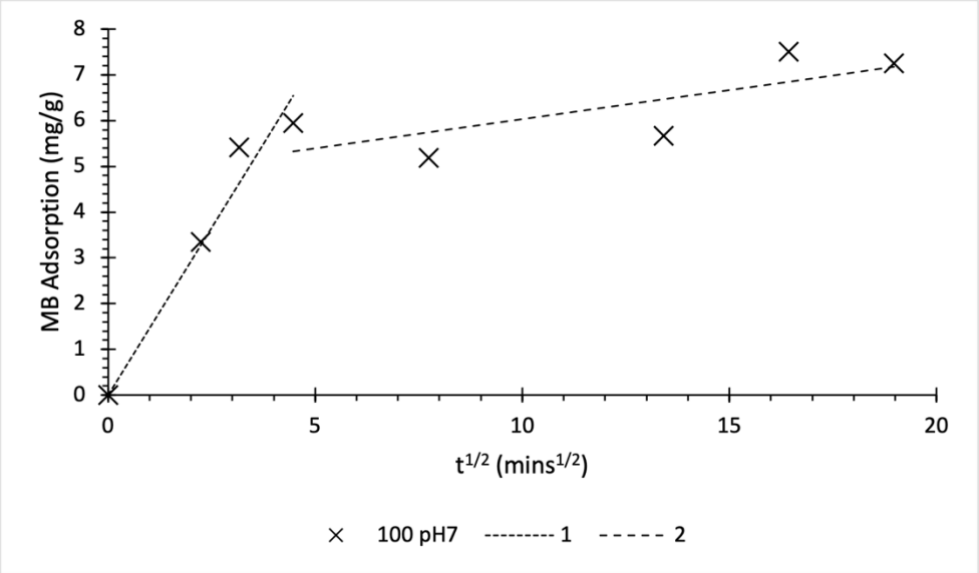

Figure 6.20 – Intraparticle model of methylene blue adsorption (C_i=100mg/l, pH=7) to biochar derived from mixed municipal discarded material pyrolyzed in a heat pipe reactor

6.3.2 Liquid film diffusion models

Figure 6.21, Figure 6.22, Figure 6.23, Figure 6.24 and Figure 6.25 show the Boyd plots of methylene blue adsorption to MMDM biochar. Table 6.6 shows the statistical analysis of methylene blue adsorption to MMDM biochar. The p values for initial methylene blue concentrations of 10mg/l to 75mg/l are all below 0.05 which shows that the line of best fit does not pass through the origin. This suggests that whilst intraparticle diffusion processes and other processes may occur as laid out in previous sections, liquid film diffusion is a significant process in the removal of methylene blue from water using MMDM biochar. The p-value for the Boyd plot concerning initial methylene blue concentrations of 100mg/l is slightly above 0.05, this could suggest that liquid film diffusion is not as significant as other processes. However, the p-value is still close to 0.05 which suggests that whilst liquid film diffusion is not as significant as in the lower initial methylene blue concentration, it is still a highly significant part of the methylene blue removal from water by MMDM biochar [366].

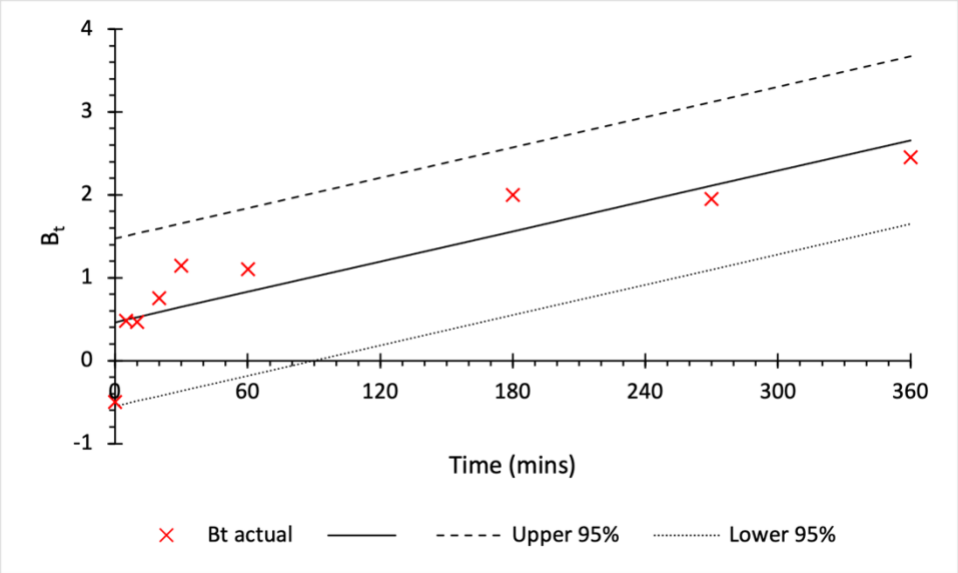

Figure 6.21 – Boyd plot of methylene blue adsorption to biochar derived from mixed municipal discarded material in a heat pipe reactor at initial pH7 and initial copper concentration of 10mg/l

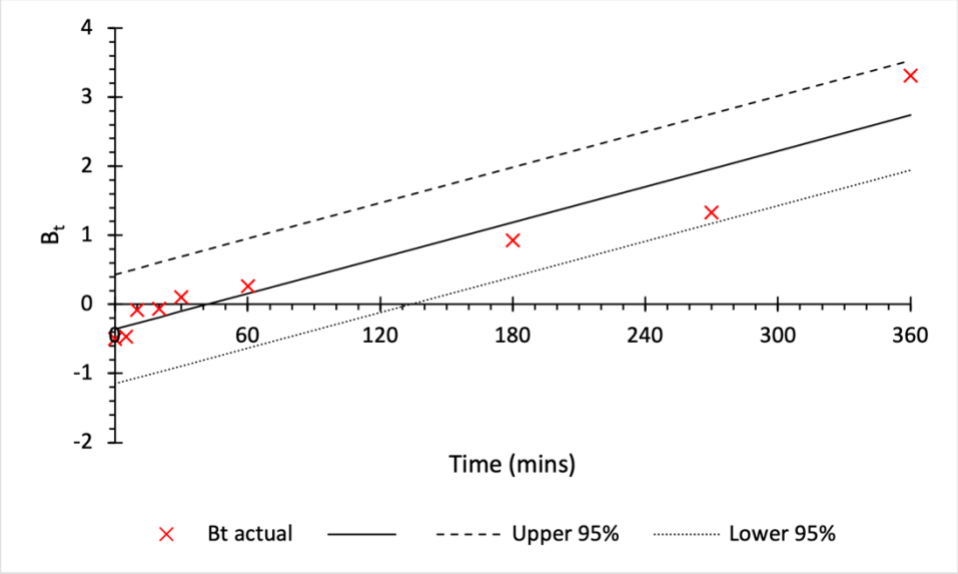

Figure 6.22 - Boyd plot of methylene blue adsorption to biochar derived from mixed municipal discarded material in a heat pipe reactor at initial pH7 and initial copper concentration of 25mg/l

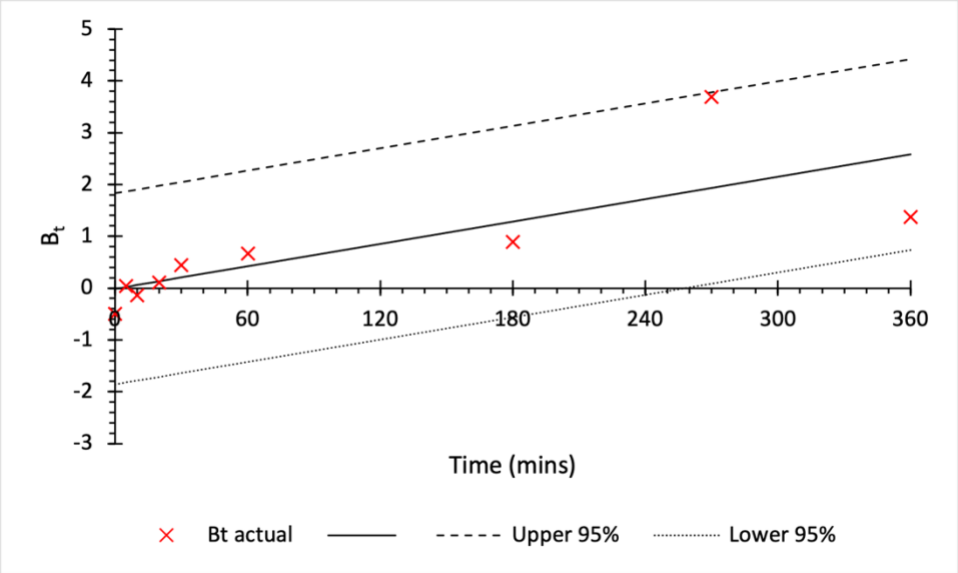

Figure 6.23 – Boyd plot of methylene blue adsorption to biochar derived from mixed municipal discarded material in a heat pipe reactor at initial pH7 and initial copper concentration of 50mg/l

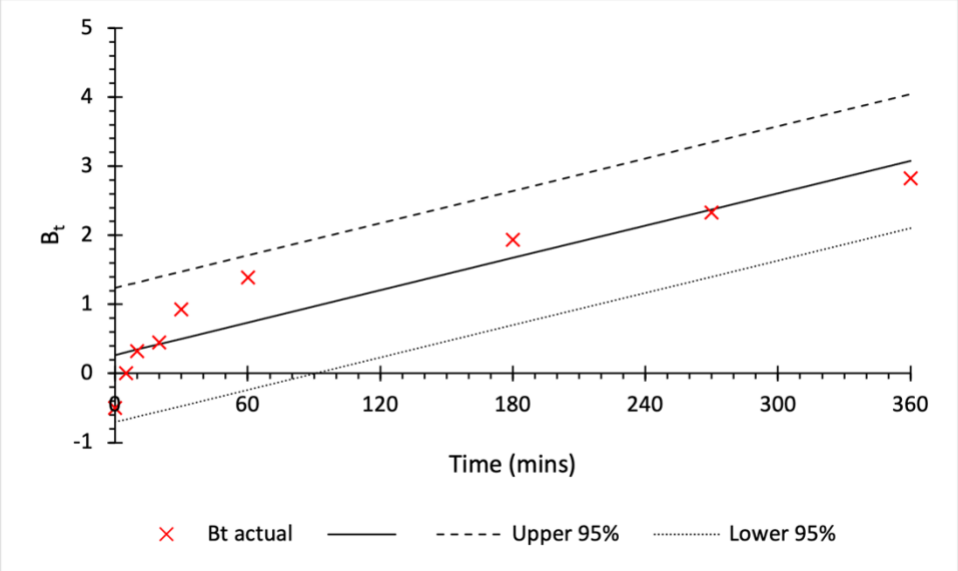

Figure 6.24 – Boyd plot of methylene blue adsorption to biochar derived from mixed municipal discarded material in a heat pipe reactor at initial pH7 and initial copper concentration of 75mg/l

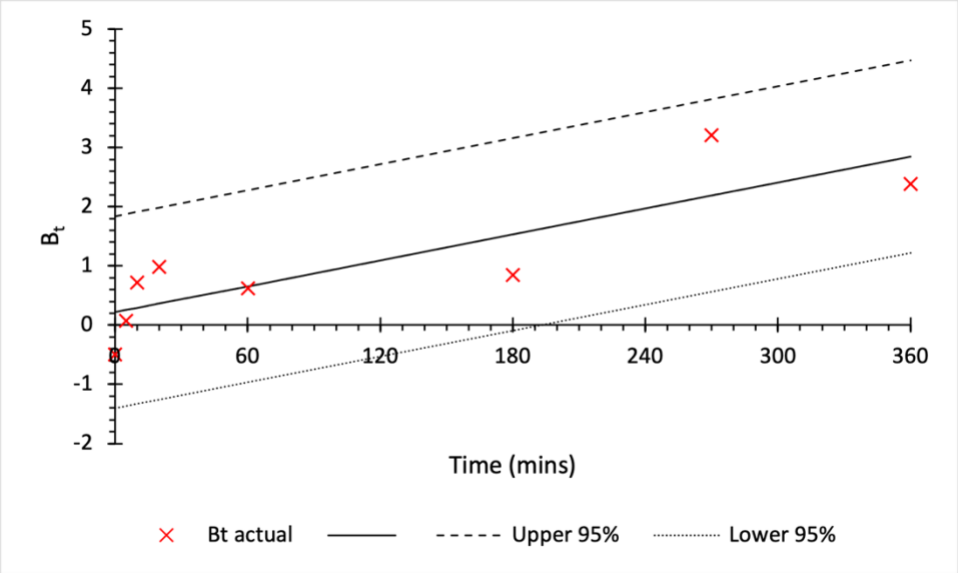

Figure 6.25 – Boyd plot of methylene blue adsorption to biochar derived from mixed municipal discarded material in a heat pipe reactor at initial pH7 and initial copper concentration of 100mg/l

Table 6.6 – Table showing statistical analysis for the Boyd plots in Figure 6.21, Figure 6.22, Figure 6.23, Figure 6.24 and Figure 6.25

Methylene Blue concentration	**R^2**	**MSE**	**p-value**
10mg/l, pH 7	0.858	0.231	0.0488
25mg/l, pH 7	0.852	0.351	0.0472
50mg/l, pH 7	0.601	0.507	0.0479
75mg/l, pH 7	0.859	0.158	0.0498
100mg/l, pH 7	0.674	0.357	0.0562

6.4 Methylene Blue Adsorption Isotherms

Adsorption isotherms reveal the nature of methylene blue adsorption to MMDM biochar. On inspection, the isotherm data displayed in Figure 6.26, Figure 6.27, Figure 6.30 and Figure 6.28 appears to follow an almost linear relationship. Figure 6.26 shows the Langmuir model fit to the collected adsorption data for methylene blue. It shows a very linear relationship under the experimental conditions used. This is confirmed in Table 6.7 where a low value for K_L and large value for Q_m which explain the apparent linearity of the Langmuir model under the experimental conditions used. Additionally, the value of the separation factor (R_L) is also shown to be close to 1, showing that whilst adsorption as predicted by the Langmuir model is favourable due to R_L lying between 0 and 1, it is nonetheless highly linear. This suggests that either the adsorption is dominated by partitioning mechanisms under the experimental conditions used; the adsorption of methylene blue has not significantly approached the maximum capacity (q_m); or the adsorption of methylene blue is best described by another

adsorption isotherm, despite the Langmuir model displaying the highest R^2 value in Table 6.11. The latter is likely the case where the Langmuir model displays the highest MSE value, and highest 95% confidence interval of both two parameter models (Langmuir and Freundlich).

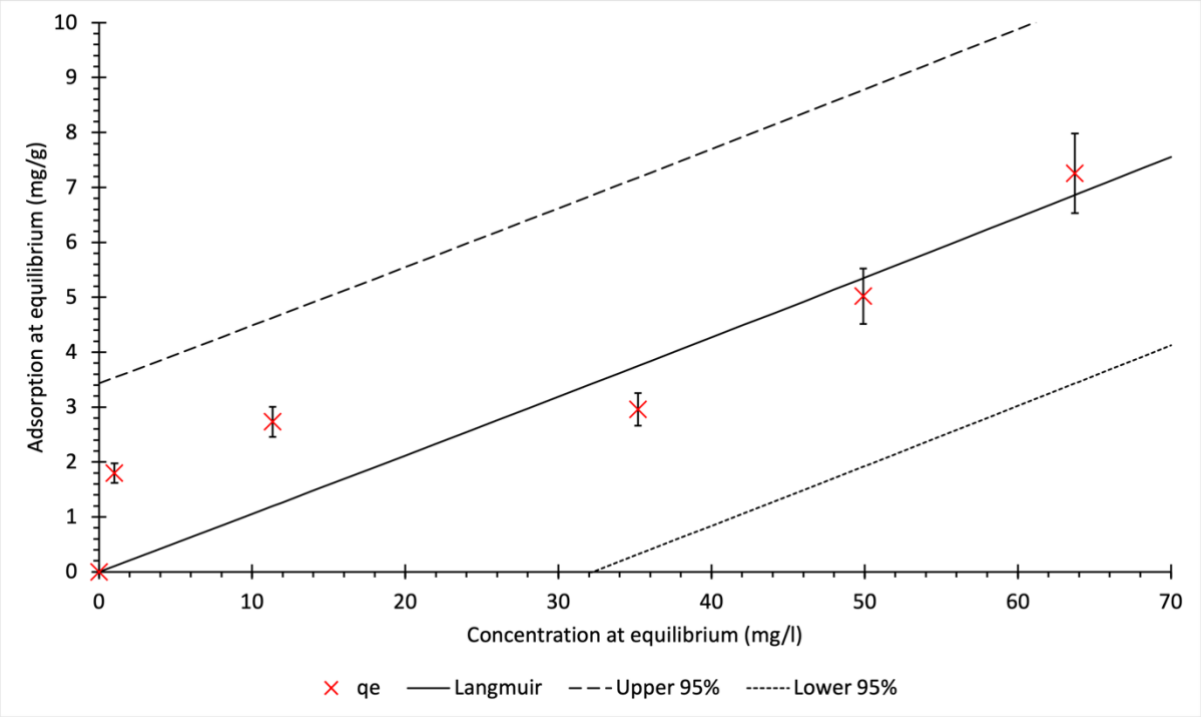

Figure 6.26 – Langmuir Model of methylene blue adsorption to biochar derived from MMDM

Table 6.7 – Langmuir isotherm coefficients

K_L (l/mg)	**Q_m (mg/g)**
0.000395	265.8
C_i (mg/l)	**R_L**
10	0.9960644
25	0.99021873
50	0.98062696
75	0.97121922
100	0.96199028

The Freundlich model is displayed in Figure 6.27 with the model coefficients shown in Table 6.8. The value of n being greater than 1 shows that adsorption to MMDM biochar is favourable [367]. Whilst the Freundlich model returns a lower R^2 model than the Langmuir model displayed in Table 6.11, it does return lower MSE value and 95% confidence intervals than the Langmuir model. This suggests that the Freundlich model better describes the adsorption compared with the calculated Langmuir adsorption. The Freundlich model suggests a heterogenous surface where multilayer adsorption can occur [368,369]. Therefore, the better fit of the Freundlich model suggests that MMDM biochar adsorbent has a heterogenous surface in terms of methylene blue adsorption. However, the apparent linearity of the adsorption isotherm on inspection cannot be ignored, this suggests that other processes may be responsible for the removal of methylene blue from solution by MMDM biochar.

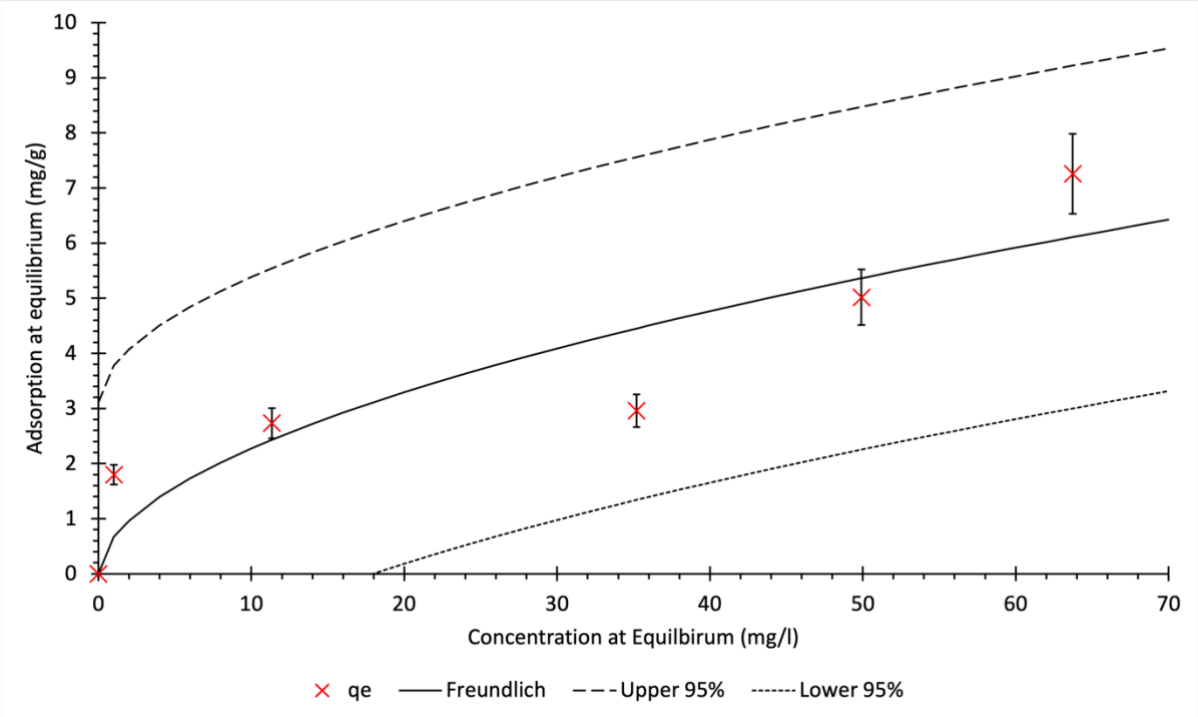

Figure 6.27 – Freundlich Model of methylene blue adsorption to biochar derived from MMDM

Table 6.8 – Freundlich model coefficients

K_F (l/g)	n
0.6657	1.874

The dual mode isotherm is shown in Figure 6.28, this isotherm contains three terms, and consists of two equations added together, with a non-linear Langmuir equation which describes the removal of methylene blue by adsorption processes, and a linear equation which describes the removal of methylene blue by partitioning processes. Of the two three term isotherms investigated (Dual mode and Sips model) the dual mode isotherm better describes the adsorption of methylene blue to MMDM biochar, with a higher R^2 value, and lower MSE value and 95% confidence interval than the Sips model. The R^2 value of the dual mode isotherm is slightly lower than the Langmuir model, but the MSE value is significantly lower than all of the other models. The 95% confidence interval is the third largest of the four isotherm models investigated. This is largely due to this model containing three different terms compared with the Langmuir and Freundlich models which only have two terms. This gives the Dual mode isotherm a degree of freedom 1 less than the two term models. Future experiments on this material with regards to removal of methylene blue dye using this material could mitigate this effect by taking a greater number of samples. For this reason, despite the 95% confidence interval being wider than the other models, the dual mode isotherm is the model that best describes adsorption to MMDM biochar produced in a heat pipe reactor.

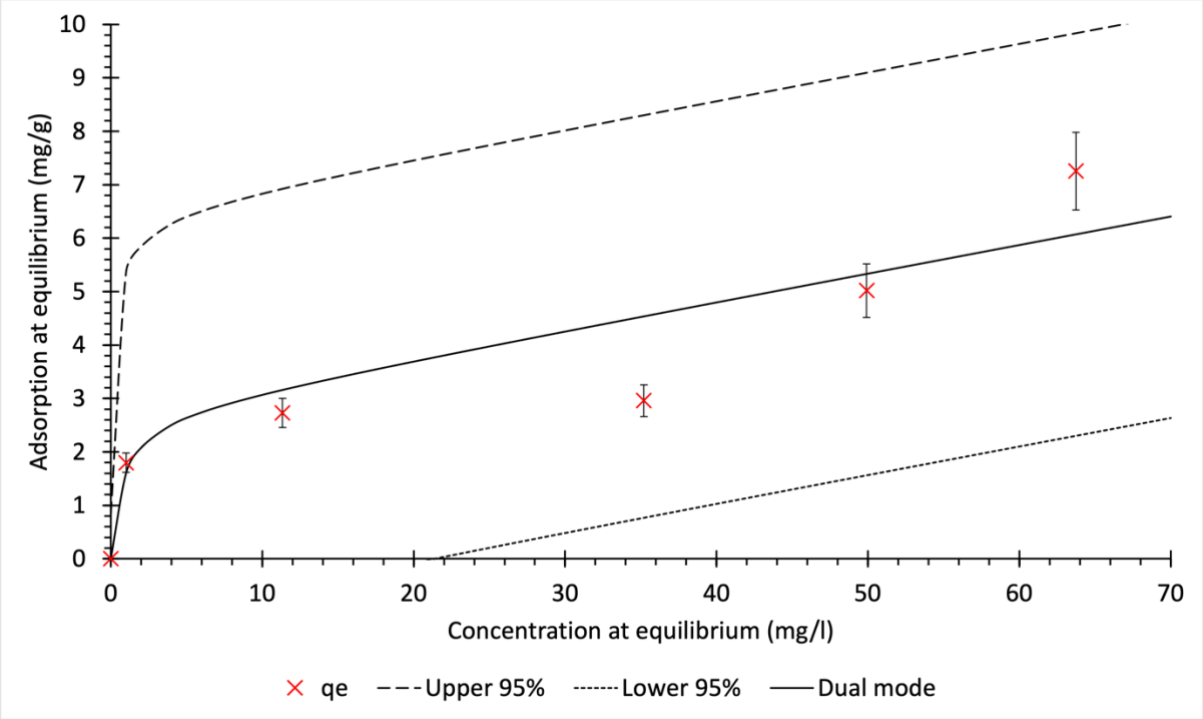

Figure 6.28 – Dual Mode Model of methylene blue adsorption to biochar derived from MMDM

Table 6.9 – Dual Mode isotherm model coefficients

$K_{DM,nl}$ (l/mg)	Q_m (mg/g)	$K_{DM,l}$ (l/g)
1.292	2.732	0.053

Figure 6.29 shows the dual mode isotherm separated out into the separate adsorption and partitioning equations. Partitioning is shown to overtake adsorption as the dominant mechanisms of methylene blue removal from solution at an equilibrium concentration of 50.89 mg/l. This suggests that at higher initial methylene blue concentrations, the non-carbonised parts of the MMDM biochar become more important to methylene blue removal from aqueous solution than adsorption of methylene blue to the carbonised portions of the MMDM biochar [298].

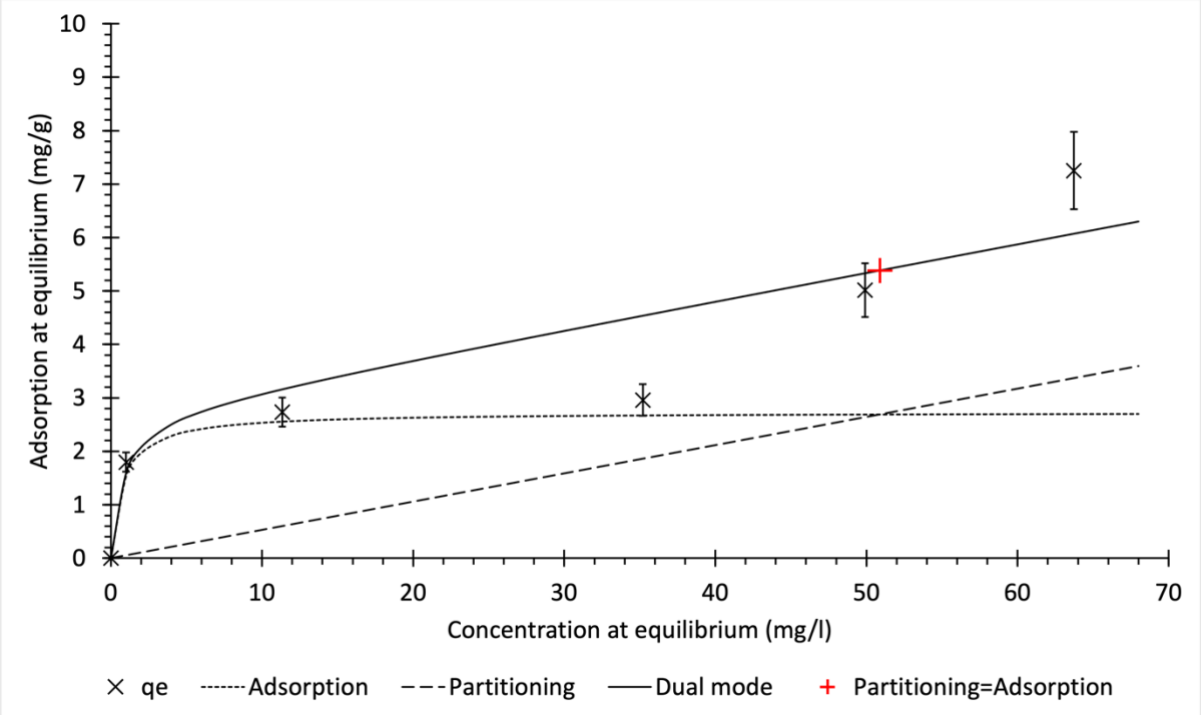

Figure 6.29 – Dual Mode model showing separate adsorption and partitioning mechanisms

The final adsorption isotherm investigated was the Sips model. This is a combined version of the Langmuir and Freundlich isothermal models. This makes it a three-term model. As is the case with the Dual mode isotherm, the 95% confidence intervals of the sips isotherm in future experiments could be decreased through increasing the number of samples collected with equilibrium concentrations between 0 and 50 mg/l. The Sips model is shown to have the

lowest R^2 value and highest 95% confidence interval of all the isothermal models analysed, however it has a lower MSE value than the Langmuir adsorption isotherm. This further confirms that despite its higher R^2 value, the Langmuir model does not necessarily describe the adsorption of methylene blue to MMDM biochar well. Most literature as stated previously is content with utilising the R^2 values calculated from linearised models of the adsorption isotherms to determine the best fitting adsorption isotherms. The statistical analysis of the non-linear methylene blue adsorption isotherms for MMDM biochar adsorption shows the folly of this method. It is consequently suggested that the method followed to produce the isothermal model data in this thesis is an improvement on that found in the majority of literature and is not much more difficult to carry out than the use of linearised isothermal models, with non-linear regression being possible in Microsoft Excel software through the use of the Solver add in.

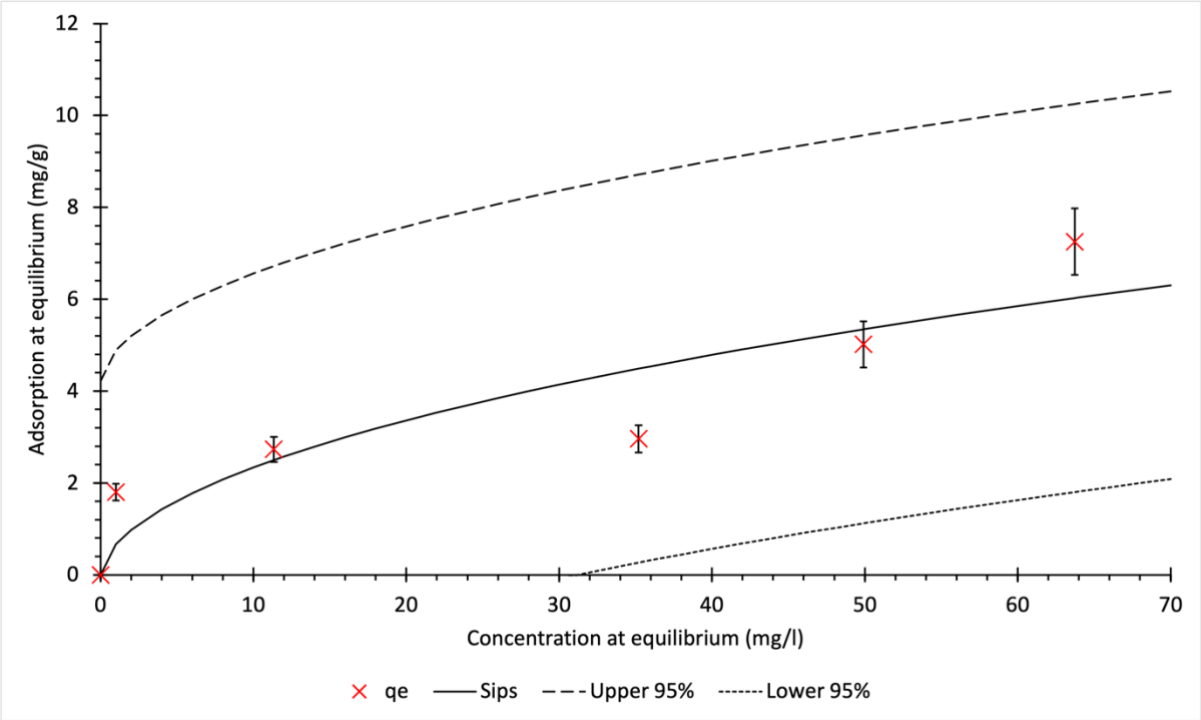

Figure 6.30 – Sips Model of methylene blue adsorption to biochar derived from MMDM

Table 6.10 – Sips model coefficients

K_s (l/mg)	Q_m (mg/g)	n
0.0149	45.52	1.786

Table 6.11 – Statistical analyses of isotherm models for methylene blue adsorption to MMDM biochar

Isothermal model	R^2	MSE	95% Confidence interval
Langmuir	0.8816	1.017	3.430
Freundlich	0.8522	0.8365	3.110
Sips	0.8434	0.8806	4.223
Dual mode	0.8742	0.7003	3.766

6.5 Methylene blue percentage removal

Figure 6.31 shows the percentage removal of methylene blue with increasing methylene blue concentration. At low concentration the removal percentage is highest, however the adsorption to the biochar is lowest. At initial concentration of 50mg/l the removal starts to increase gently towards 100mg/l, this suggests that up to an initial concentration of 50 mg/l there is an adsorption process that reaches saturation after 50mg/l. This is confirmed by the dual mode isotherm shown in Figure 6.29 where the adsorption is equal to partitioning at an equilibrium concentration of 50.9mg/l.

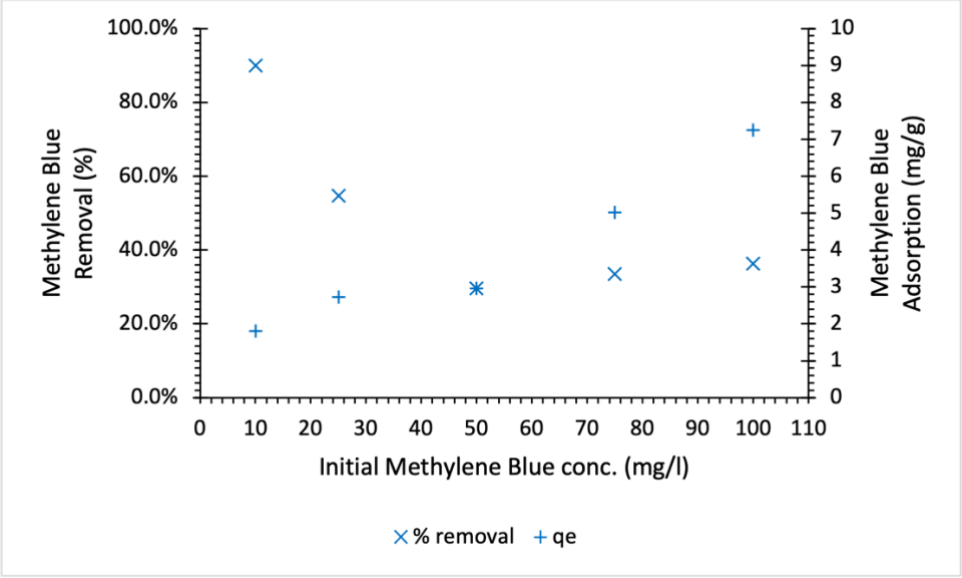

Figure 6.31 – Percentage removal of methylene blue from solution using biochar adsorbent derived from mixed municipal discarded material pyrolyzed in a heat pipe reactor, data labels show adsorption of methylene blue in mg/g

6.6 Discussion

Methylene blue is a common ingredient in several industries as identified in 6.1. This chapter shows that an adsorbent can be produced from MMDM using a heat pipe reactor to remove this pollutant from aqueous solution. As is the case with copper adsorption, other more efficacious adsorbents are produced in other studies, however these as is the case for the removal of copper from aqueous solution make use of specific feedstocks that are only available to specific businesses, or specific parts of the globe. MMDM is a material that is available the world over, with the majority of this material still being sent to landfill or being processed in incinerators [12].

Methylene blue assessed in this chapter can also be considered as an indicator of organic pollutant removal. Indeed, methylene blue contains a number of similar moieties to other organic pollutants of interest. These include aromatic groups present in some pesticides and pharmaceuticals which can participate in π electron interactions [370], as well as amine groups capable of participating in hydrogen bonding [371]. In this sense the adsorption of methylene blue can reflect the ability of this biochar to remove other such similar pollutants.

Table 6.12 shows a comparative table of the methylene blue adsorption in this chapter compared with methylene blue adsorption in some selected literature. What is first noticeable from the table is that methylene blue adsorption to MMDM biochar produced in a heat pipe reactor in this chapter is comparable to that of activated biochar produced from municipal solid waste, indeed the biochar used in this chapter may even outperform the activated biochar where the biochar dosage is higher in this work compared with that of Sumalinog et al. [372]. Furthermore, ball milling was found to significantly increase the adsorption capacity of biochar produced from sugarcane bagasse, hickory wood and bamboo, this was mainly attributed to surface aromatic and oxygen containing functional groups being more available in the ball milled biochar. Such a process was not applied in this thesis, however it's apparent positive impact in other literature shows that biochar produced from MMDM in heat pipe reactors could be vastly improved by an additional ball milling process [373].

The use of granulated MMDM biochar in this thesis does not remove methylene blue as well as in other studies that use more specific feedstocks or activating procedures. This means that it's uses as a specialist adsorbent similar to other granular activated carbon materials is

questionable. However the use of ball milling in other studies to produce powdered biochar produced an adsorbent that was vastly improved over its original granulated state [374]. This would likely improve the adsorption ability of materials produced using a heat pipe reactor, where the low temperatures used result in materials with greater amounts of functional groups as is evidenced in the biochar characterisation. This results in adsorbent materials that are very effective at removing polar organic pollutants such as methylene blue. Despite this, other non-polar pollutants will likely require an adsorbent produced at higher temperature, resulting in greater surface areas and aromatic groups capable of interacting with non-polar pollutants via π electron interactions as well as other processes [375].

Table 6.12 *– Comparison of collected methylene blue adsorption data and a selection of adsorption data from literature*

Feedstock	Adsorbent production	Biochar dosage (g/l)	Initial solution conc. (mg/l)	Initial solution pH	Adsorption (mg/g)	Source
Banana pseudo stem	Pyrolysis at 200°C	0.5	50	7	66	[376]
Banana pseudo stem	Pyrolysis at 300°C	0.5	50	7	40	[376]
Banana pseudo stem	Pyrolysis at 400°C	0.5	50	7	12	[376]
Banana pseudo stem	Pyrolysis at 500°C	0.5	50	7	16	[376]
Banana pseudo stem	Pyrolysis at 600°C	0.5	50	7	15	[376]
Lychee seeds	Pyrolysis at 700°C followed by KOH impregnation	0.6	50	7	122.96	[377]
Rice husk	Pyrolysis at 500°C for 3h	5	100	7	17.97	[378]
Cow dung	Pyrolysis at 500°C for 3h	5	100	7	17.50	[378]
Sludge	Pyrolysis at 500°C for 3h	5	100	7	19.21	[378]
Sugar cane bagasse	Pyrolysis at 300°C	0.16	50	Not stated	9.9	[373]
Sugar cane bagasse	Pyrolysis at 300°C followed by ball milling	0.16	50	Not stated	169	[373]
Hickory wood	Pyrolysis at 300°C	0.16	50	Not stated	7.9	[373]
Hickory wood	Pyrolysis at 300°C followed by ball milling	0.16	50	Not stated	114	[373]
Bamboo	Pyrolysis at 300°C	0.16	50	Not stated	9.2	[373]

Table 6.12 *Continued*

Bamboo	Pyrolysis at 300°C followed by ball milling	0.16	50	Not stated	202	[373]
Municipal solid waste	Pyrolyzed at 400-500°C and impregnated with potassium hydroxide	2	50	6.5	4.35	[372]
Pumpkin peel	Pyrolyzed at 250°C, then stirred with beetroot juice at 100°C	0.5	50	7	96.68	[15]
Pumpkin peel	Pyrolyzed at 250°C, then stirred with beetroot juice at 100°C	0.5	100	7	167.8	[15]
Pumpkin peel	Pyrolyzed at 250°C, then stirred with beetroot juice at 100°C	0.5	150	7	175.94	[15]
Pumpkin peel	Pyrolyzed at 250°C, then stirred with beetroot juice at 100°C	0.5	200	7	198.15	[15]
MMDM	Pyrolyzed at temperatures below 300°C	5	10	7	1.798	This chapter
MMDM	Pyrolyzed at temperatures below 300°C	5	25	7	2.732	This chapter
MMDM	Pyrolyzed at temperatures below 300°C	5	50	7	2.960	This chapter
MMDM	Pyrolyzed at temperatures below 300°C	5	75	7	5.019	This chapter
MMDM	Pyrolyzed at temperatures below 300°C	5	100	7	7.254	This chapter

6.6.1 Potential applications of MMDM biochar targeting dyes and pesticides

As is the case in copper adsorption to the same material, this material shows promise for use in the textile and pharmaceutical industries where methylene blue is used. However, unlike copper adsorption the methylene blue adsorption followed a more linear isothermal behaviour than copper adsorption, with the Dual-mode isotherm being the best fitting

isothermal model. **Table 6.12** shows the comparison with biochar produced in literature, the biochar produced in literature does seem to remove more methylene blue from aqueous solutions more efficiently than the biochar in this chapter. However, the biochar produced in this chapter is comparable to some biochar produced in similar ways in other literature. This suggests that whilst this material may not compete with commercial and experimental activated carbons for use in commercial water treatment processes it may be of interest to other applications such as in agricultural soils and sustainable urban drainage systems, where it could reduce the environmental impact of organic dyes and other similar compounds including organic pesticides. Indeed, similar material has been used in agricultural processes to remove pollutants similar to methylene blue [379,380]. Such material could be used in sustainable drainage systems such as managed wetlands. This would be particularly beneficial in areas with intense agricultural land use where pesticides are used extensively. The MMDM biochar produced in this study could be of particular interest in areas contaminated by polar organic contamination [381–383]. Using the MMDM derived biochar as a filter media in SuDS could result in the removal of some organic pollutants through biodegradation processes [337].

Such a system could include the sandwiching of an MMDM biochar adsorbent substrate between layers of mesh separating the adsorbent material from crushed rock drainage materials below and wetland soils and plants above, as illustrated in Figure 6.32. The water that percolates through the substrate columns consequently undergoes biological treatment processes in the soil layers, followed by adsorption of any persisting pollutants in the biochar substrate [384]. This is then drained through a crushed rock/sand layer and conveyed away by perforated pipework. This would enable biochar materials to be periodically replaced when the adsorbent becomes saturated.

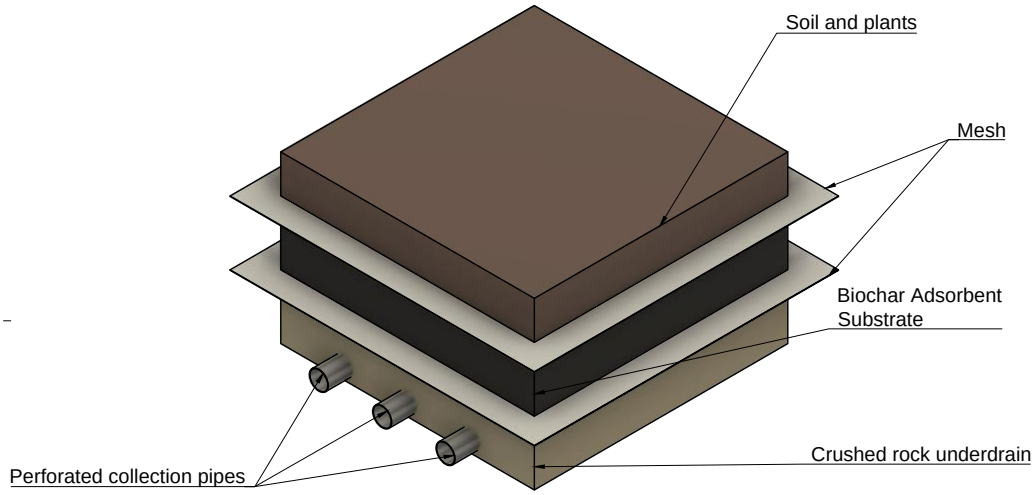

Figure 6.32 – Simple cross-section of a Sustainable drainage system including biochar adsorbent substrate

Areas where both polar and non-polar organic contaminants are present would benefit from a drainage system as shown in Figure 6.33, with alternating or mixed layers of biochar adsorbents produced at temperatures both below and above 500^{o}C. This would result in the removal of polar contaminants such as methylene blue by the biochar adsorbent produced at lower pyrolysis temperature, with non-polar contaminants being more greatly removed in biochar adsorbents produced at elevated pyrolysis temperature. This is due to the increased surface area and decreased polarity in higher temperature biochar, as is explained in the state of the art.

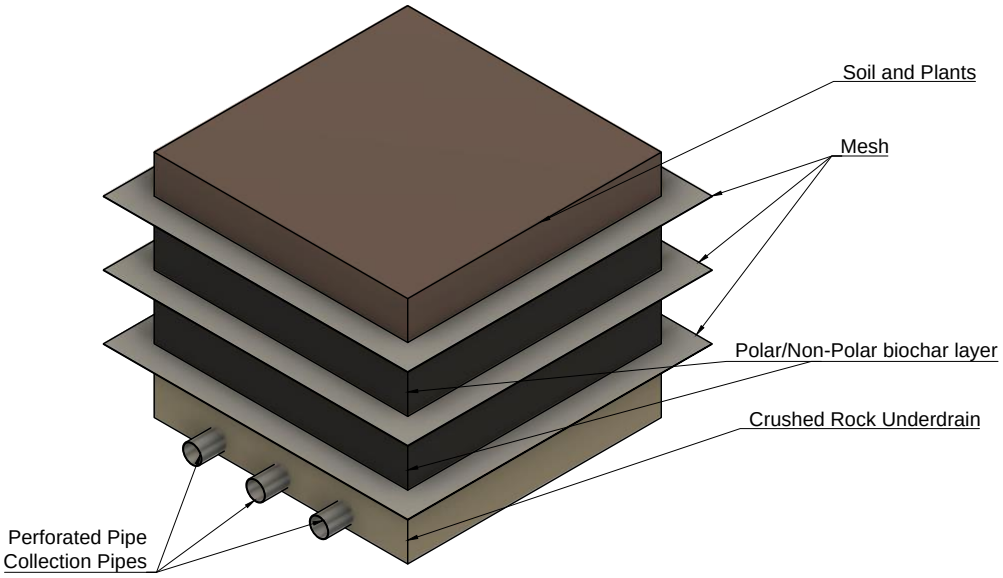

Figure 6.33 -Simple cross section of a multi-layer biochar sustainable drainage system

Ball milling shows great promise for improving the adsorption characteristics of other similar biochar produced at lower pyrolysis temperatures similar to those present in the heat pipe reactor used in this thesis. This suggests that powdering biochar produced from MMDM could increase the uptake of polar organic contaminants such as methylene blue [374]. Furthermore, the atmosphere in which MMDM biochar are milled in could also significantly impact the removal of organic contaminants. Both nitrogen and vacuum atmospheres are shown to improve the removal amount of reactive red more so than ball milling of biochar produced from hickory chips at 450^{o}C, this can be attributed to the smaller particle size, and thus greater surface area of adsorbent in these ball milling conditions [385]. Methylene blue adsorption is shown to increase after the ball milling of activated carbon, as well as being attributed to increased surface area, this may also be attributed to the increased exposure of functional groups to the bulk solution [386]. This phenomenon could be of particular interest with regards to biochar produced usi9ng MMDM which is shown by FTIR to contain such oxygen containing functional groups. Ball milling would therefore expose some of these functional groups that are not available as active sites for methylene blue adsorption interactions prior to ball milling. This suggests that ball milling could be used to produce powdered activated carbon from MMDM. This material could be used during the coagulation/flocculation stage of a water treatment plant to remove persistent organics such as pesticides and pharmaceutical products [261]. If such materials are to be used in drinking water treatment, care must be taken to produce them correctly ensuring that the powdered biochar does not introduce new impurities to the water. Furthermore, whilst milling can improve the adsorption characteristics of biochar, over milling of biochar can lead to the loss of this increased adsorption ability [387].

6.7 Summary

To summarise, at initial methylene blue concentrations of 75mg/l and below, the experimental methylene blue adsorption data fit the Elovich and pseudo second order models better than the pseudo first order models, this suggests that adsorption occurs in a heterogenous fashion across the MMDM biochar surface, being largely due to chemisorption processes with the biochar. However, at initial concentrations greater than 100mg/l the nature of adsorption seemed to change. The ability to distinguish which kinetic model best fit the data diminished, with the MSE value of the pseudo first order being the lowest of all three models despite the R^2 value of this model also being the lowest. This shows the importance

for research regarding adsorption to biochar and other similar materials to move away from simply using the R^2 value to determine the best fitting kinetic models. It also shows that as initial concentrations of methylene blue increase above 75mg/l, physical processes begin to become more dominant over chemical processes.

The best fitting isotherm inspecting only the R^2 values appears to be the Langmuir model. However, the MSE value was the largest of any of the analysed isotherms with the 95% confidence interval being the largest of the two term isotherms assessed. Using all three metrics as well as considering the degree of freedom, arguably the best fitting isotherm is the dual mode Langmuir isotherm. This had the lowest MSE value, and second highest R^2 value. This indicates that partitioning as well as adsorption processes occur in the biochar, with partitioning becoming the dominant mechanism at an equilibrium concentration of 50.89mg/l. This is consistent with the change in kinetic findings which indicated a change in the adsorption at initial concentrations greater than 75mg/l.

Liquid film diffusion was found to be a significant limiting step to methylene blue removal under all experimental conditions with p-values close to or below 0.05. This suggests that for methylene blue, intraparticle diffusion processes were less significant than the diffusion of methylene blue across the boundary the bulk solution and the MMDM biochar. This could be due to the reduced porosity and surface area of biochar produced at lower temperatures, with higher pyrolysis temperatures producing biochar with greater surface area over which methylene blue can diffuse. Nevertheless, the functional groups that remain in the MMDM biochar due to the lower pyrolysis temperature in the heat pipe reactor are significant for the removal of polar organic compounds such as methylene blue. The powdering/ball milling of MMDM heat pipe derived biochar could potentially produce an adsorbent material capable of being used in coagulation/flocculation processes for the removal of polar organic contaminants including some pesticides.

7 TETRACYCLINE ADSORPTION TO BIOCHAR DERIVED FROM MIXED MUNICIPAL DISCARDED MATERIAL IN A HEAT PIPE REACTOR

7.1 Tetracycline

Tetracycline is an antibiotic that is widely used in the agricultural industry due to its broad spectrum and relative ease of production [388]. Antibiotics have been instrumental in controlling disease in both humans and animals since their advent in the 20th century. However, in the 21st century, the issue of antibiotic resistance has become an area of particular concern. Antibiotic resistance develops in the environment due to the irresponsible emission of antibiotics from pharmaceutical and healthcare waste, as well as from surviving antibiotics in human and animal waste. These antibiotics can interact with bacteria in the environment causing their death, however more resistant strains either survive or develop, particularly in instances of prolonged, non-lethal antibiotic exposure [389]. Once these genes have developed, they can be passed on to the offspring of resistant bacteria, leading to the propagation of antibiotic resistant genes in the environment, this is known as vertical gene transfer. However, these genes can be taken up by bacteria via several horizontal gene transfer processes including conjugation, transformation and transduction [390]. Reducing antibiotic emissions to the environment is therefore highly important for mitigating the propagation of antibiotic resistant genes in the environment.

Antibiotics can be removed from water using different processes. These include modified micro and ultrafiltration membranes, nanofiltration [391], reverse osmosis, forward osmosis [392], distillation, adsorption [393], and advanced oxidation procedures including ozonation and catalytic processes [394,395]. Ozonation, nanofiltration and osmosis processes are highly effective in the reduction of tetracycline in aqueous solution. Membrane processes become less efficient over time as retained contaminants such as antibiotics contribute to membrane fouling, increasing the transmembrane pressure required to achieve the same output of water. Ozonation is also an expensive process where ozone needs to be produced on site, with aqueous conditions including pH also needing to be optimised to produce the important hydroxyl radical oxygen species as well as ozone. The fouling of membrane processes, and/or the consumption of oxidative species in advanced oxidation processes can be reduced by pre-treatment processes.

Adsorption is an attractive solution as a pre-treatment process for more effective/advanced technologies. However, some adsorbents whilst highly effective in tetracycline adsorption are

expensive to produce and are produced from feedstocks specific to certain localities, or are produced from non-renewable materials such as clay and fossil materials as stated in the previous chapter regarding methylene blue adsorption. The production of cheaper adsorbents for the removal of tetracycline is therefore an area of great interest. To this end, biochar is a material that is garnering increasing attention, particularly biochar produced from waste materials. Biochar derived from pharmaceutical sludge, tea waste and crayfish shell are shown to effectively remove tetracycline from aqueous solution [17,396–398]. Such feedstocks are readily available and cheap to the businesses that produce them. However, if they enter the municipal waste chain, sorting them can be a costly process both economically, and environmentally. As these materials may end up as a mixture in collected municipal waste, the study of adsorbent material produced using a mixture of different municipal wastes is an important research step towards the production of adsorbents capable of removing tetracycline as well as other antibiotics from aqueous solutions. Such adsorbents could be used as pre-treatments to more expensive treatment steps to reduce the stress antibiotics place on water treatment processes including nanofiltration, reverse osmosis, ozonation and other advanced oxidation techniques.

The emission of antibiotics such as tetracycline from the wastewater of pharmaceutical industries, hospitals and human excrement can be controlled fairly easily where these sources of antibiotic contamination are isolated from the environment in waste water conveyance and treatment systems [399]. However, conventional wastewater treatment plants are known to be ineffective in the removal of antibiotics resulting in sludge and to a lesser extent effluent that still contains antibiotics such as tetracyclines [400]. These solids are often used in agriculture as a soil additive, this represents a pathway through which antibiotics can enter the environment in non-lethal concentrations. Tetracycline can also find its way into the environment from veterinary and agricultural uses. In these uses excretion from animals is not as controlled as anthropogenic waste and, as a result, antibiotics used in animal related industries can find their way into surface waters from animal excretion. Adsorbents could be used in drainage systems near areas of dense animal populations such as farms or cities where livestock and pets are kept respectively to mitigate the problem of antibiotics entering the environment through such uses. Such systems include sustainable drainage systems designed to reduce pollution in the environment such as swales, retention ponds, and reed beds as a

few examples. The conditions in these drainage systems are not controlled as they are in conventional treatment plants, consequently the utilisation of specialist adsorbent materials such as activated carbons and clay mineral adsorbents in such systems is not necessarily ideal. This is due to the expense required to produce these materials, as well as the optimum conditions required for them to operate at maximum pollutant removal efficacy. There is clearly a market and need for cheaper adsorbents that can be utilised in applications such as sustainable drainage systems. One such source material for these adsorbents is municipal discarded material. Consequently, this chapter explores the use of heat-pipe derived MMDM biochar for the removal of tetracycline from water.

7.2 Adsorption kinetics

7.2.1 Introduction

The kinetic models are compared against experimental data, with statistical analyses of the models compared to the experimental data being undertaken to determine the best fitting models. The best fitting models determine the best way to describe the kinetic behaviour of tetracycline adsorption to MMDM biochar. The statistical analyses used to determine the best fitting kinetic and isothermal models are the coefficient of determination (R^2), mean squared error (MSE), and the 95% confidence intervals. Higher R^2 values and lower MSE and 95% confidence intervals mean that a kinetic or isothermal model has a better fit than another model with lower R^2 values and higher MSE and/or 95% confidence intervals.

7.2.2 Adsorption Kinetic results

Results from tetracycline adsorption experiments with initial concentration of 20mg/L and pH of 7 are discussed below. Figure 7.1, Figure 7.2 and Figure 7.3 show the pseudo first order, pseudo second order and Elovich kinetic models respectively. Table 7.1 shows the statistical analyses of the kinetic models compared with the experimental data. The R^2 values calculated follow the order Elovich > pseudo second order > pseudo first order, with MSE and 95% confidence intervals following the order pseudo first order > pseudo second order > Elovich. This means that the kinetic model that best describes tetracycline adsorption is the Elovich model, with the second and third best fitting models being the pseudo second order and pseudo first order models respectively. This shows that the adsorption of tetracycline to MMDM biochar is limited by chemisorption processes that occur in a heterogenous fashion across the biochar surface, as per the assumptions in the Elovich kinetic model.

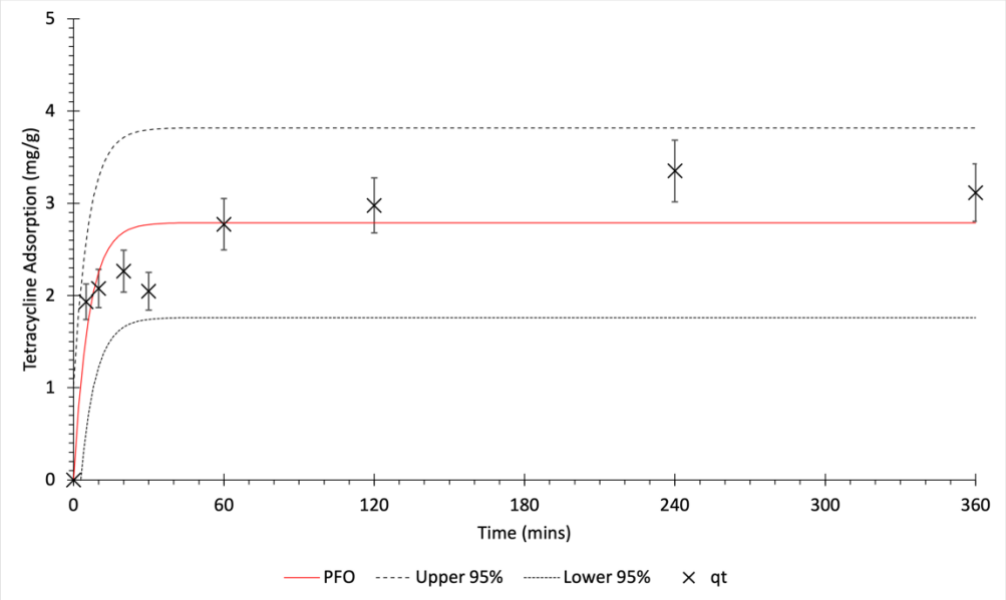

Figure 7.1 – Pseudo first order model of tetracycline adsorption (C_i=20mg/L, pH=7) to biochar derived from mixed municipal discarded material pyrolyzed in a heat pipe reactor, with q_t showing the experimental data, PFO showing the pseudo first order model, and upper 95% and lower 95% showing the 95% confidence intervals

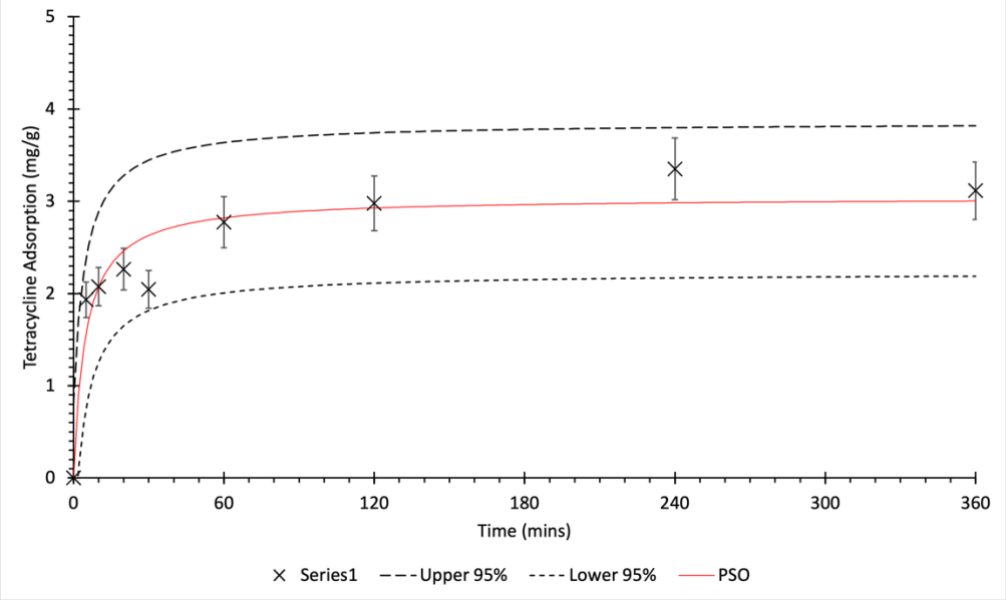

Figure 7.2 – Pseudo second order model of tetracycline adsorption (C_i=20mg/L, pH=7) to biochar derived from mixed municipal discarded material pyrolyzed in a heat pipe reactor, with q_t showing the experimental data, PSO showing the pseudo second order model, and upper 95% and lower 95% showing the 95% confidence intervals

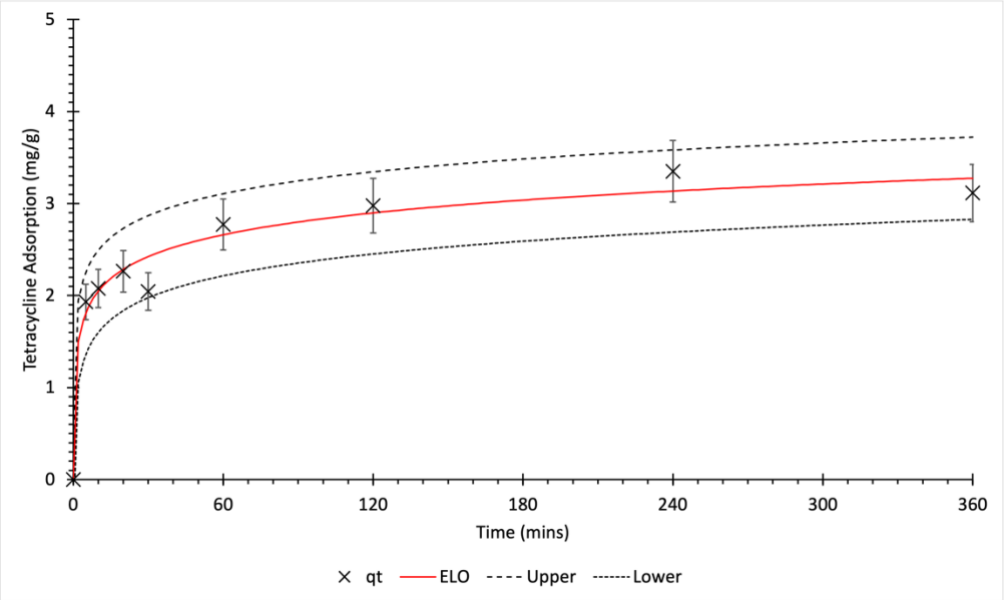

Figure 7.3 – Elovich model of tetracycline adsorption (C_i=20mg/L, pH=7) to biochar derived from mixed municipal discarded material pyrolyzed in a heat pipe reactor

Table 7.1 – Statistical analyses of kinetic models and experimental data for initial Tetracycline concentration of 20mg/L and initial pH of 7, with q_t showing the experimental data, ELO showing the Elovich model, and upper 95% and lower 95% showing the 95% confidence intervals

Kinetic model		
Pseudo first order	**K_1**	0.1644
	q_e	2.7891
	R^2	0.8354
	MSE	0.1472
	95% Confidence interval	1.029
Pseudo second order	**K_2**	0.0699
	q_e	3.0417
	R^2	0.9171
	MSE	0.0740
	95% Confidence interval	0.815
Elovich	**A**	13.3633
	B	2.9161
	R^2	0.9688
	MSE	0.0277
	95% Confidence interval	0.446

Results from tetracycline adsorption experiments with initial concentration of 40mg/L and pH of 7 are discussed below. Figure 7.4, Figure 7.5 and Figure 7.6 show the pseudo first order, pseudo second order and Elovich kinetic models respectively. Table 7.2 shows the statistical analyses of these kinetic models with the experimental data. R^2 values displayed in Table 7.2 follow the order Elovich > pseudo second order > pseudo first order, with MSE and 95% confidence intervals following the order pseudo first order > pseudo second order > Elovich.

These analyses show that the Elovich model best describes the adsorption kinetic data. This means that the adsorption of tetracycline with an initial concentration of 40mg/L to MMDM biochar is limited by chemical adsorption mechanisms that occur heterogeneously across the biochar surface, as per the assumptions in the Elovich kinetic model.

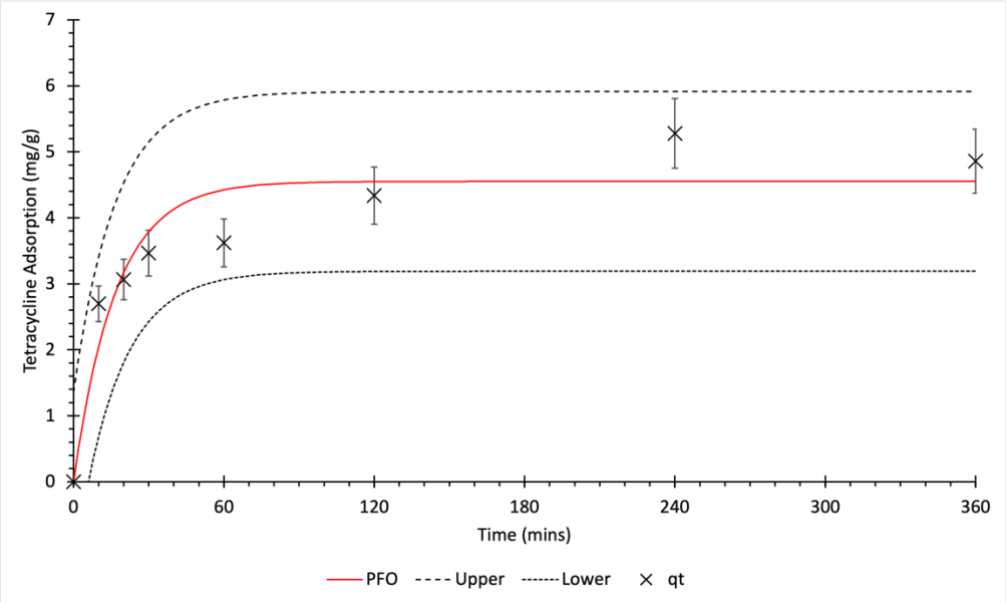

Figure 7.4 – Pseudo first order model of tetracycline adsorption (C_i=40mg/L, pH=7) to biochar derived from mixed municipal discarded material pyrolyzed in a heat pipe reactor, with q_t showing the experimental data, PFO showing the pseudo first order model, and upper 95% and lower 95% showing the 95% confidence intervals

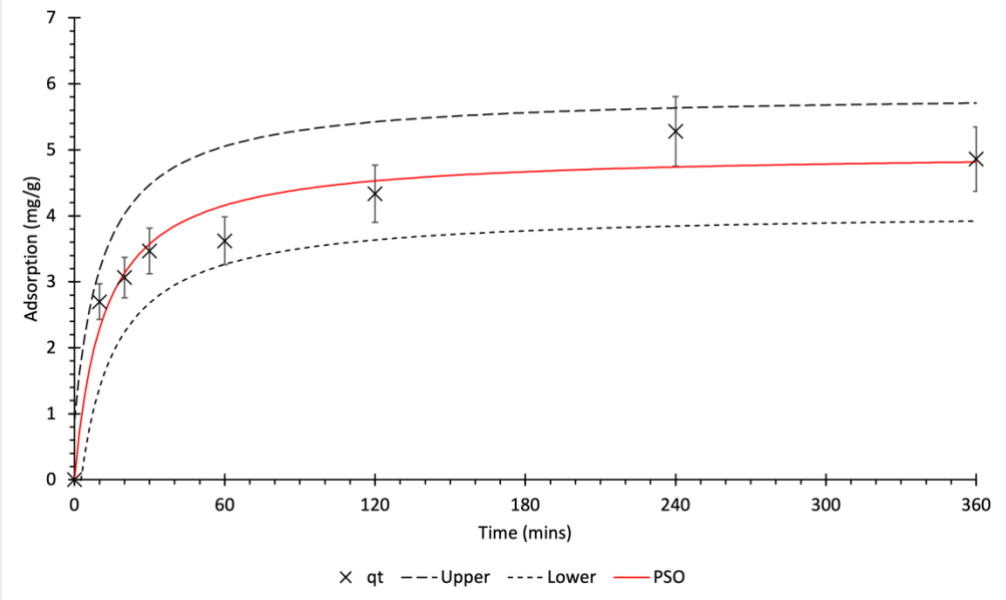

Figure 7.5 – Pseudo second order model of tetracycline adsorption (C_i=40mg/L, pH=7) to biochar derived from mixed municipal discarded material pyrolyzed in a heat pipe reactor, with q_t showing the experimental data, PSO showing the pseudo second order model, and upper 95% and lower 95% showing the 95% confidence intervals

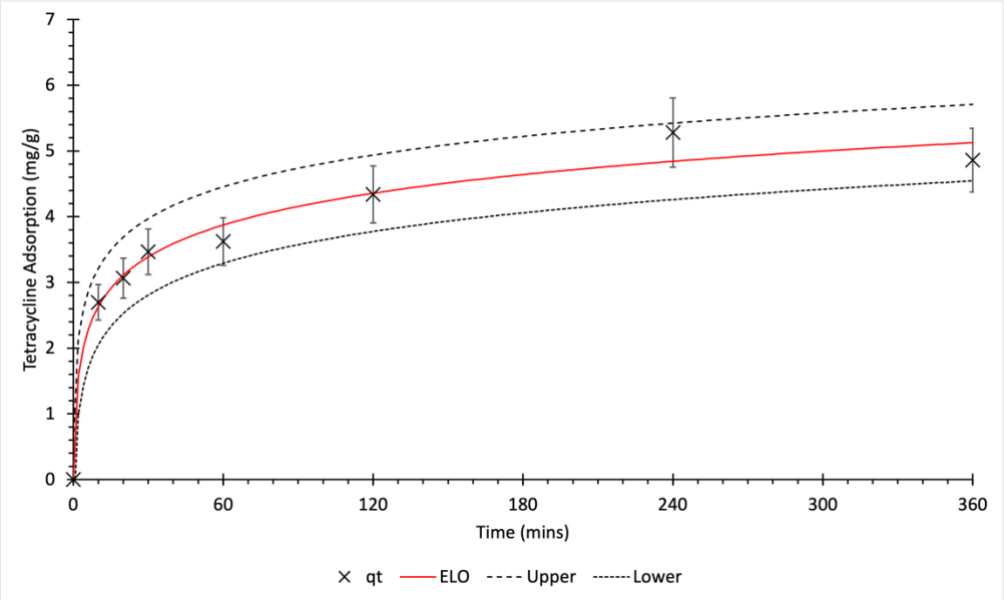

Figure 7.6 – Elovich model of tetracycline adsorption (C_i=40mg/L, pH=7) to biochar derived from mixed municipal discarded material pyrolyzed in a heat pipe reactor, with q_t showing the experimental data, ELO showing the Elovich model, and upper 95% and lower 95% showing the 95% confidence intervals

Table 7.2 – Statistical analyses of kinetic models and experimental data for initial Tetracycline concentration of 40mg/L and initial pH of 7

Kinetic model		
Pseudo first order	**K_1**	0.0595
	q_e	4.5516
	R^2	0.9035
	MSE	0.2322
	95% Confidence interval	1.361
Pseudo second order	**K_2**	0.0171
	q_e	4.9718
	R^2	0.9575
	MSE	0.1004
	95% Confidence interval	0.895
Elovich	**A**	2.9257
	B	1.4275
	R^2	0.9819
	MSE	0.0423
	95% Confidence interval	0.581

Results from tetracycline adsorption experiments with initial concentration of 60mg/L and pH of 7 are discussed below. Figure 7.7, Figure 7.8 and Figure 7.9 show the pseudo first order, pseudo second order and Elovich kinetic models respectively. Table 7.3 shows the statistical analyses of the respective kinetic models. R^2 values follow the order of Elovich > pseudo second order > pseudo first order, with MSE and 95% confidence intervals following the order

of pseudo first order > pseudo second order > Elovich. This shows that the Elovich and pseudo second order kinetic models describe the adsorption of tetracycline to MMDM biochar better than the pseudo first order kinetic model. This indicates that adsorption is limited by chemisorption occurring heterogeneously across the surface of the MMDM biochar when the initial concentration is 60mg/L and initial solution pH is 7, as per the assumptions in the Elovich kinetic model.

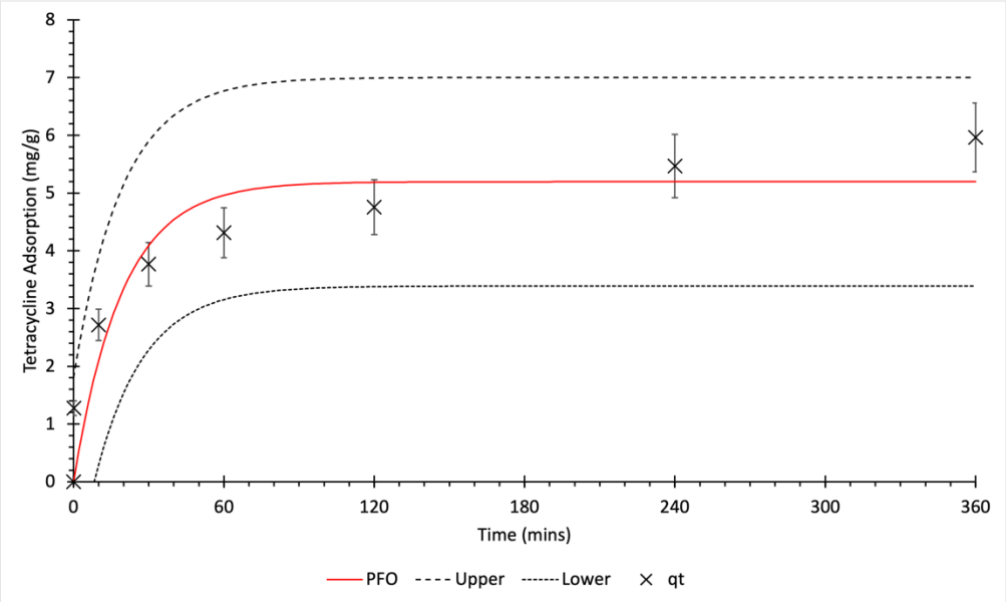

Figure 7.7 – Pseudo first order model of tetracycline adsorption (C_i=60mg/L, pH=7) to biochar derived from mixed municipal discarded material pyrolyzed in a heat pipe reactor, with q_t showing the experimental data, PFO showing the pseudo first order model, and upper 95% and lower 95% showing the 95% confidence intervals

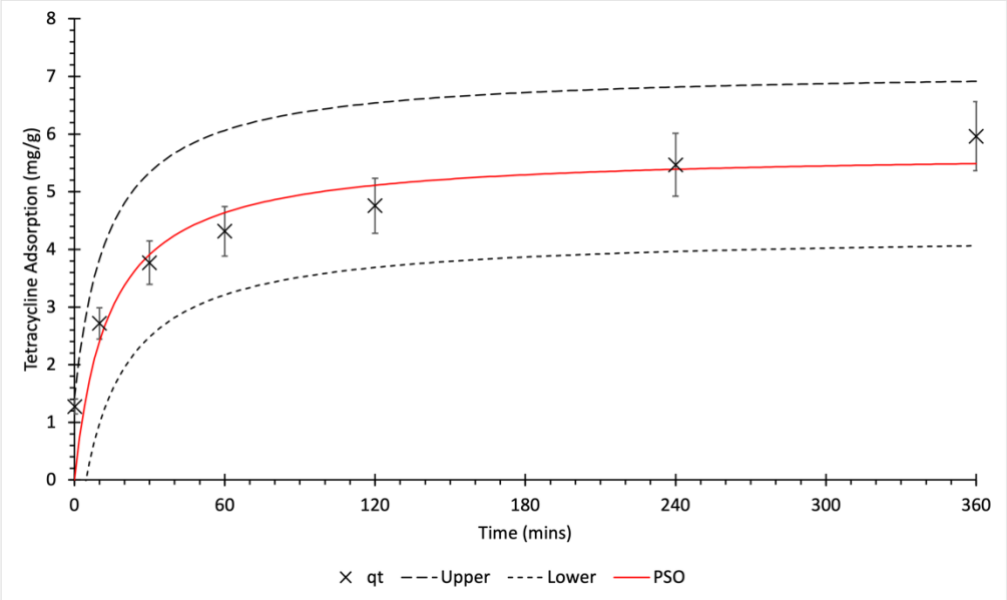

Figure 7.8 – Pseudo second order model of tetracycline adsorption (C_i=60mg/L, pH=7) to biochar derived from mixed municipal discarded material pyrolyzed in a heat pipe reactor, with q_t showing the experimental data, PSO showing the pseudo second order model, and upper 95% and lower 95% showing the 95% confidence intervals

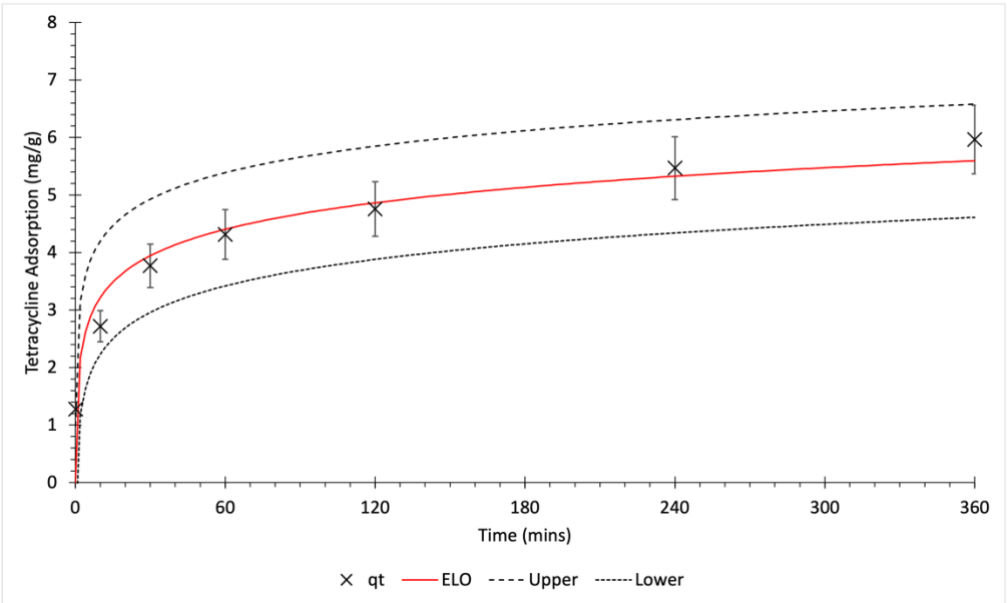

Figure 7.9 – Elovich model of tetracycline adsorption (C_i=60mg/L, pH=7) to biochar derived from mixed municipal discarded material pyrolyzed in a heat pipe reactor, with q_t showing the experimental data, ELO showing the Elovich model, and upper 95% and lower 95% showing the 95% confidence intervals

Table 7.3 – Statistical analyses of kinetic models and experimental data for initial Tetracycline concentration of 60mg/L and initial pH of 7

Kinetic model		
Pseudo first order	**K_1**	0.0516
	q_e	5.1964
	R^2	0.9228
	MSE	0.4090
	95% Confidence interval	1.807
Pseudo second order	**K_2**	0.0128
	q_e	5.6977
	R^2	0.9479
	MSE	0.2914
	95% Confidence interval	1.427
Elovich	**A**	8.2847
	B	1.5026
	R^2	0.9556
	MSE	0.1047
	95% Confidence interval	0.984

Results from tetracycline adsorption experiments with initial concentration of 80mg/L and pH of 7 are discussed below. Figure 7.10, Figure 7.11 and Figure 7.12 show the pseudo first order, pseudo second order and Elovich kinetic models respectively. Table 7.4 show the statistical analyses for these kinetic models. R^2 values follow the order Elovich > pseudo second order > pseudo first order, with MSE and 95% confidence intervals following the order pseudo first order > pseudo second order > Elovich. This shows that tetracycline adsorption is limited by heterogenous chemisorption processes rather than the physisorption processes described by the pseudo first order kinetic model.

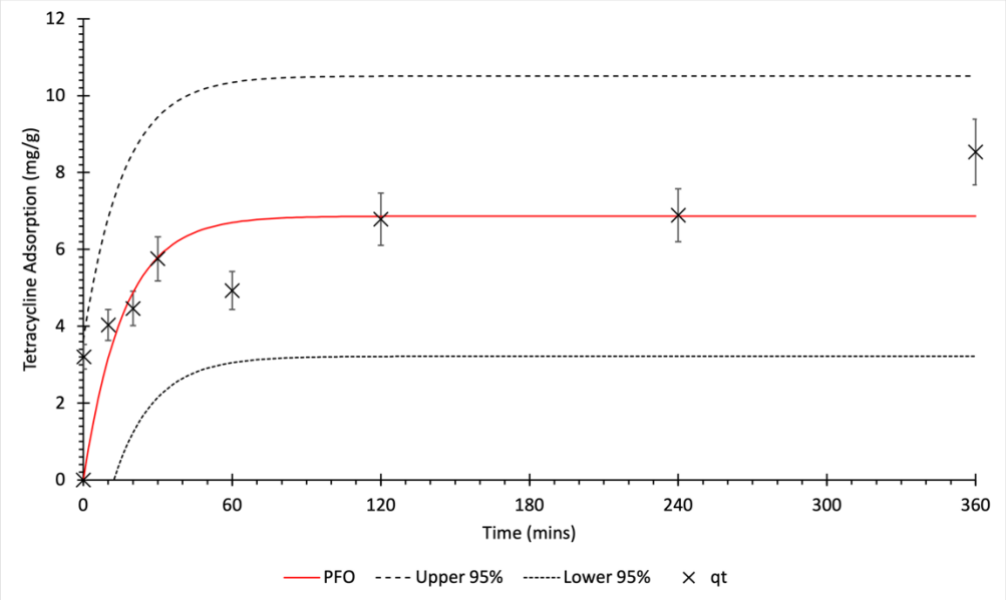

Figure 7.10 – Pseudo first order model of tetracycline adsorption (C_i=80mg/L, pH=7) to biochar derived from mixed municipal discarded material pyrolyzed in a heat pipe reactor, with q_t showing the experimental data, PFO showing the pseudo first order model, and upper 95% and lower 95% showing the 95% confidence intervals

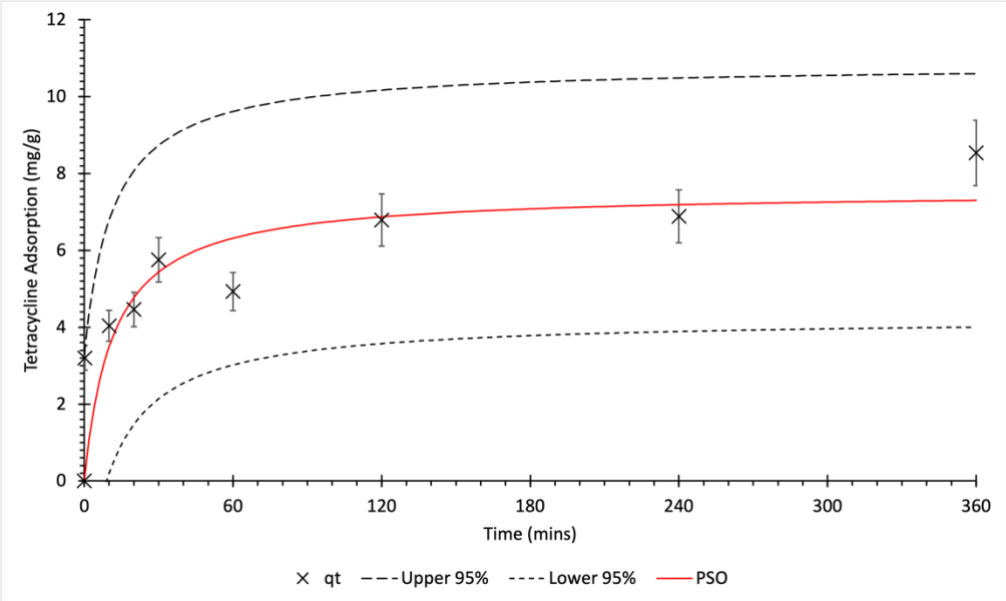

Figure 7.11 – Pseudo second order model of tetracycline adsorption (C_i=80mg/L, pH=7) to biochar derived from mixed municipal discarded material pyrolyzed in a heat pipe reactor, with q_t showing the experimental data, PSO showing the pseudo second order model, and upper 95% and lower 95% showing the 95% confidence intervals

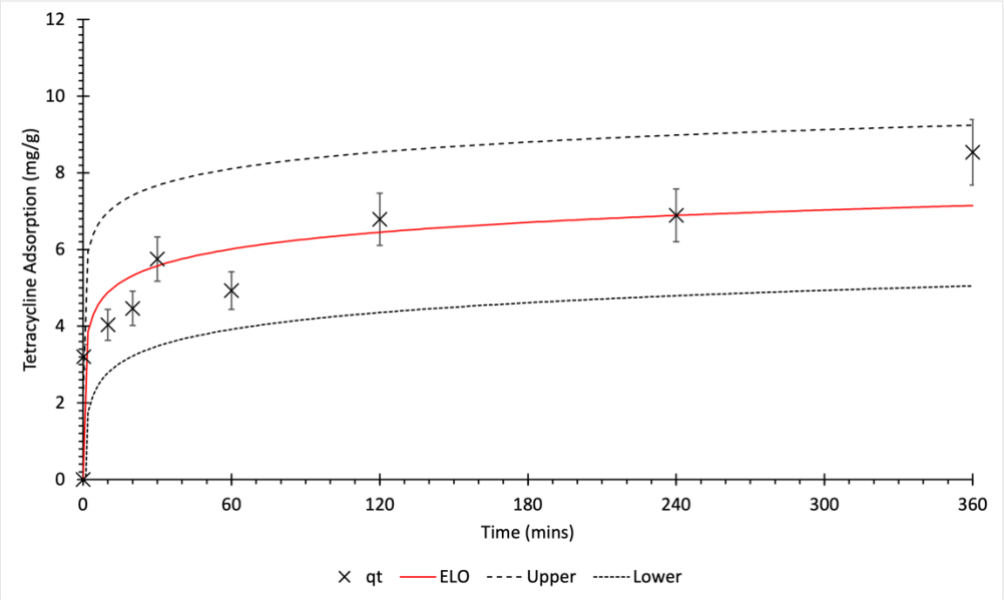

Figure 7.12 – Elovich model of tetracycline adsorption (C_i=80mg/L, pH=7) to biochar derived from mixed municipal discarded material pyrolyzed in a heat pipe reactor, with q_t showing the experimental data, ELO showing the Elovich model, and upper 95% and lower 95% showing the 95% confidence intervals

Table 7.4 – Statistical analyses of kinetic models and experimental data for initial Tetracycline concentration of 80mg/L and initial pH of 7

Kinetic model		
Pseudo first order	**K_1**	0.0620
	q_e	6.8644
	R^2	0.7634
	MSE	1.8506
	95% Confidence interval	3.648
Pseudo second order	**K_2**	0.0115
	q_e	7.5359
	R^2	0.8092
	MSE	1.5134
	95% Confidence interval	3.298
Elovich	**A**	140.6783
	B	1.5798
	R^2	0.8884
	MSE	0.6108
	95% Confidence interval	2.095

Results from tetracycline adsorption experiments with initial concentration of 100mg/L and pH of 7 are discussed below. Figure 7.13, Figure 7.14 and Figure 7.15 show the pseudo first order, pseudo second order and Elovich kinetic models of tetracycline adsorption to MMDM biochar respectively.

Table 7.5 shows the statistical analyses for the different kinetic models. R^2 values follow the

Kinetic model		
Pseudo first order	**K_1**	0.0990
	q_e	8.4901
	R^2	0.7731
	MSE	2.8044
	95% Confidence interval	4.4901
Pseudo second order	**K_2**	0.0189
	q_e	9.0509
	R^2	0.8102
	MSE	2.3599
	95% Confidence interval	4.1189
Elovich	**A**	940.2
	B	1.4347
	R^2	0.9557
	MSE	0.3531
	95% Confidence interval	1.5933

order Elovich > pseudo second order > pseudo first order. MSE and 95% confidence intervals follow the order pseudo first order > pseudo second order > Elovich. These analyses show that the Elovich and pseudo second order kinetic models both describe the tetracycline adsorption to MMDM biochar better than the pseudo first order kinetic model. Consequently, when the initial tetracycline concentration is 100mg/L and initial pH of 7, tetracycline adsorption is limited by chemisorption processes that occur in a heterogenous fashion across the biochar surface, as per the assumptions in the Elovich kinetic model.

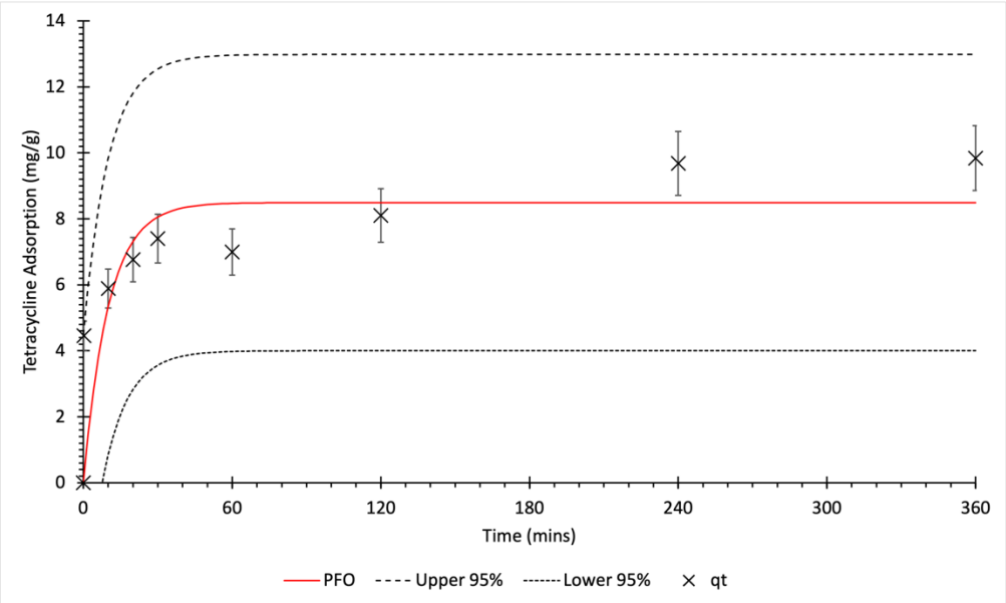

Figure 7.13 – Pseudo first order model of tetracycline adsorption (C_i=100mg/L, pH=7) to biochar derived from mixed municipal discarded material pyrolyzed in a heat pipe reactor, with q_t showing the

experimental data, PFO showing the pseudo first order model, and upper 95% and lower 95% showing the 95% confidence intervals

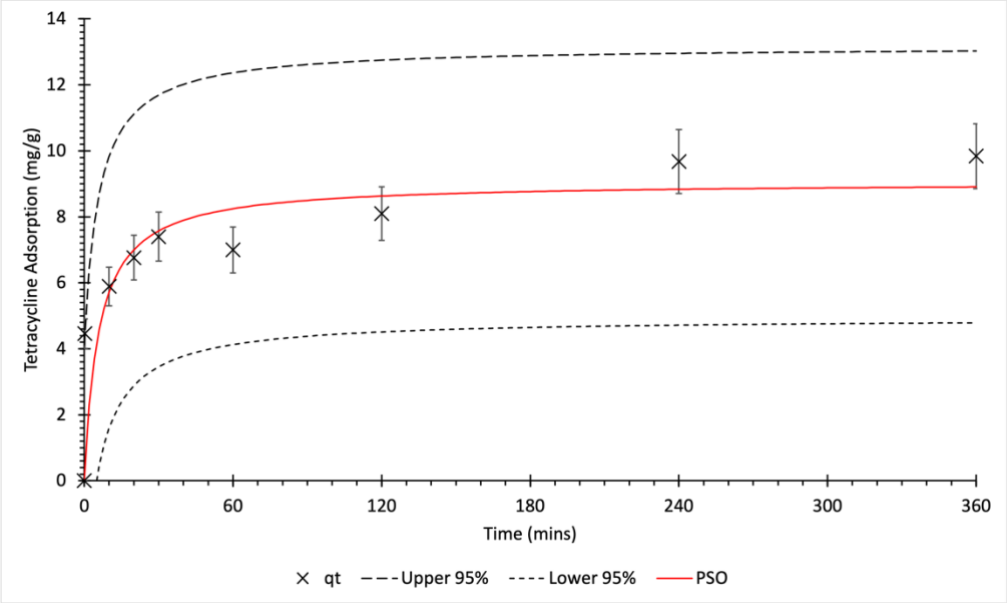

Figure 7.14 – Pseudo second order model of tetracycline adsorption (C_i=100mg/L, pH=7) to biochar derived from mixed municipal discarded material pyrolyzed in a heat pipe reactor, with q_t showing the experimental data, PSO showing the pseudo second order model, and upper 95% and lower 95% showing the 95% confidence intervals

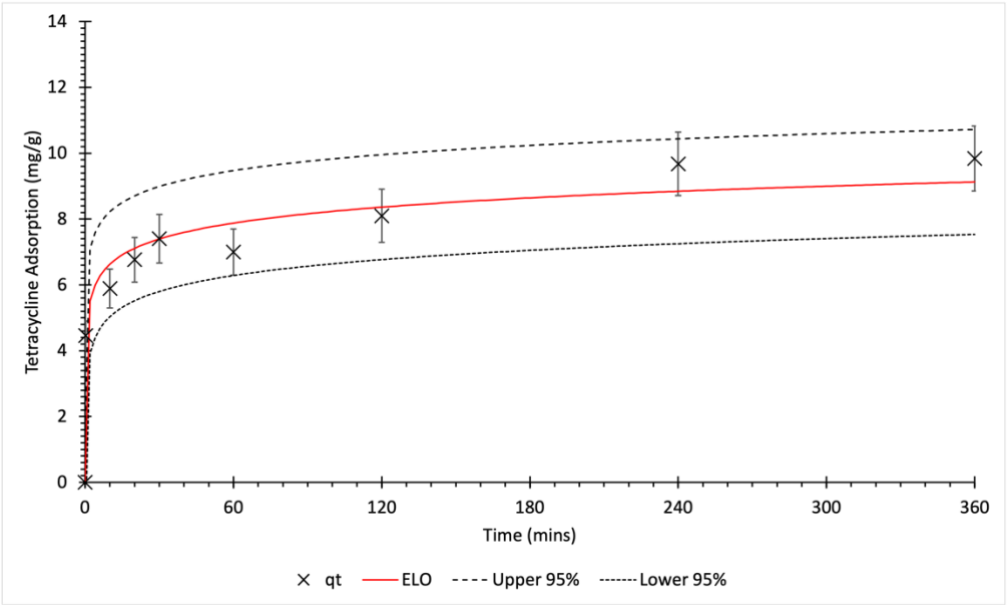

Figure 7.15 – Elovich model of tetracycline adsorption (C_i=100mg/L, pH=7) to biochar derived from mixed municipal discarded material pyrolyzed in a heat pipe reactor, with q_t showing the experimental data, ELO showing the Elovich model, and upper 95% and lower 95% showing the 95% confidence intervals

Table 7.5 – Statistical analyses of kinetic models and experimental data for initial Tetracycline concentration of 100mg/L and initial pH of 7

Kinetic model		
Pseudo first order	**K_1**	0.0990
	q_e	8.4901
	R^2	0.7731
	MSE	2.8044
	95% Confidence interval	4.4901
Pseudo second order	**K_2**	0.0189
	q_e	9.0509
	R^2	0.8102
	MSE	2.3599
	95% Confidence interval	4.1189
Elovich	**A**	940.2
	B	1.4347
	R^2	0.9557
	MSE	0.3531
	95% Confidence interval	1.5933

7.2.3 Summary of kinetic models

All of the tetracycline adsorption experiments were shown to fit the Elovich model most closely, followed by the pseudo second order, and lastly the pseudo first order models. This shows that under all conditions the removal of tetracycline by MMDM is heterogenous in fashion and is limited by chemisorption processes. This is unlike the methylene blue adsorption where adsorption kinetics were shown to change with increasing initial concentration. This suggests that for tetracycline adsorption, liquid film diffusion processes are not as significant as they are in methylene blue adsorption. This is potentially due to the neutral charge of the majority of tetracycline under the experimental conditions of initial pH, whereas methylene blue is a positively charged organic ion under the same conditions. As a result, there are lower repulsive forces between individual tetracycline molecules which results in lower repulsive forces between tetracycline molecules on either side of the film between the bulk solution and the biochar.

7.3 Diffusion Models

7.3.1 Intraparticle Diffusion Model

Figure 7.16, Figure 7.17, Figure 7.18, Figure 7.19 and Figure 7.20 show the Weber-Morris plots for the tetracycline adsorption experiments. Multi-linearity is displayed in all of the Weber-Morris plots, as is the case in both copper and methylene blue adsorption experiments. This shows that whilst intraparticle diffusion can be attributed as a governing process in

tetracycline removal from solution, it is not the only process at work. Indeed, the first stage of tetracycline removal from bulk solution would appear to be very rapid. This is indicative of the liquid film diffusion process that occurs between the bulk solution and biochar adsorbent. The second linear phase can be described by the diffusion of tetracycline into medium-large sized pores. The slower third linear phase probably represents the diffusion of tetracycline into smaller pores, as well as onto active sites where it is involved in chemisorption processes.

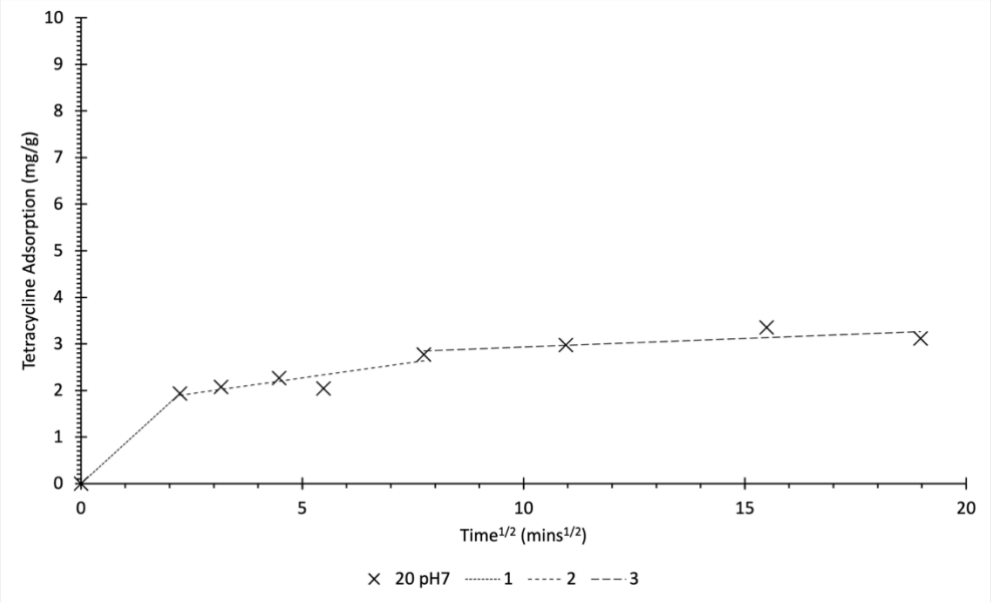

Figure 7.16 – Intraparticle model of Tetracycline adsorption (C_i=20mg/L, pH=7) to biochar derived from mixed municipal discarded material pyrolyzed in a heat pipe reactor

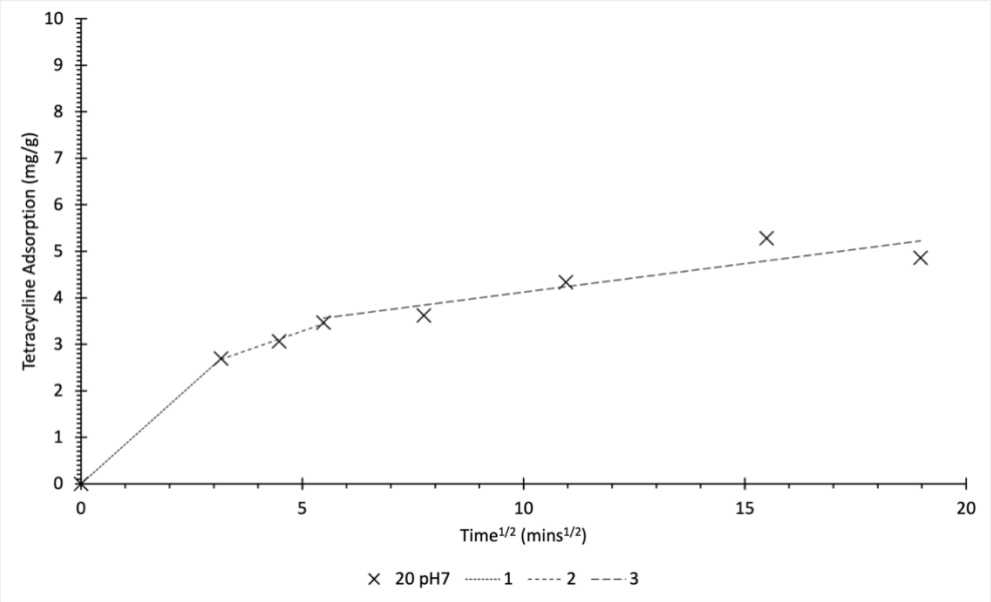

Figure 7.17 – Intraparticle model of Tetracycline adsorption (C_i=40mg/L, pH=7) to biochar derived from mixed municipal discarded material pyrolyzed in a heat pipe reactor

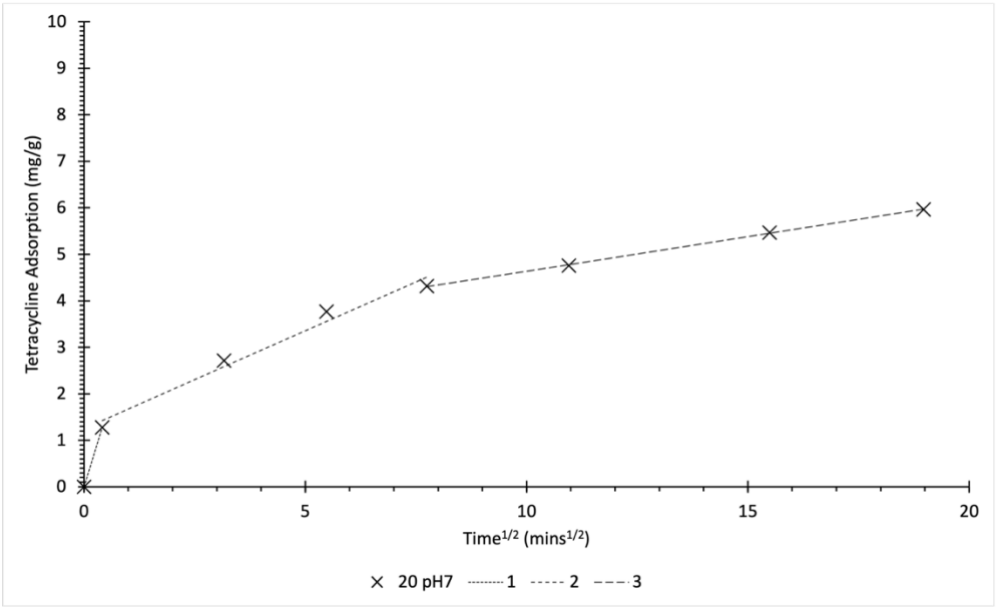

Figure 7.18 – Intraparticle model of Tetracycline adsorption (C_i=60mg/L, pH=7) to biochar derived from mixed municipal discarded material pyrolyzed in a heat pipe reactor

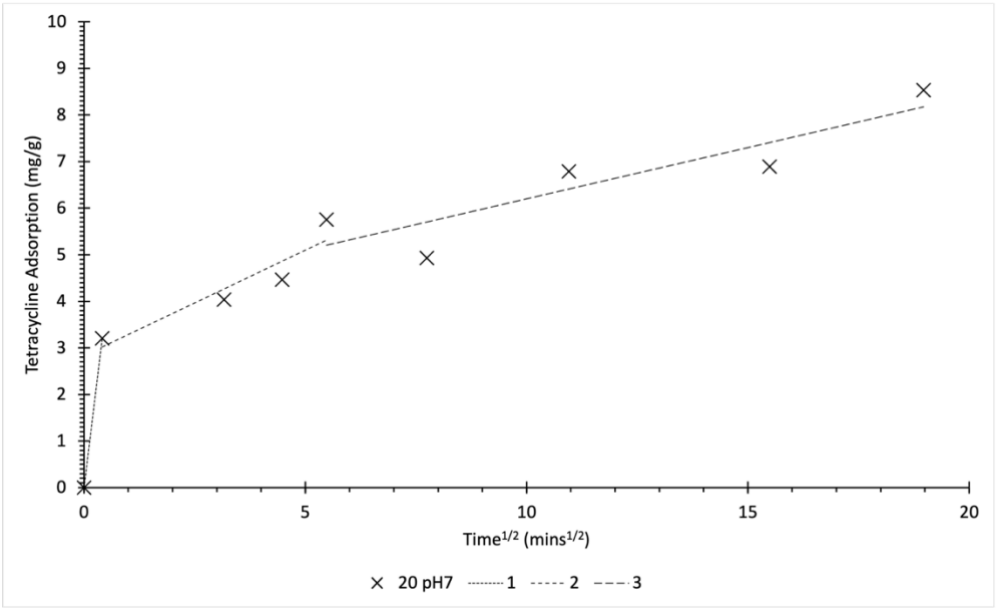

Figure 7.19 – Intraparticle model of Tetracycline adsorption (C_i=80mg/L, pH=7) to biochar derived from mixed municipal discarded material pyrolyzed in a heat pipe reactor

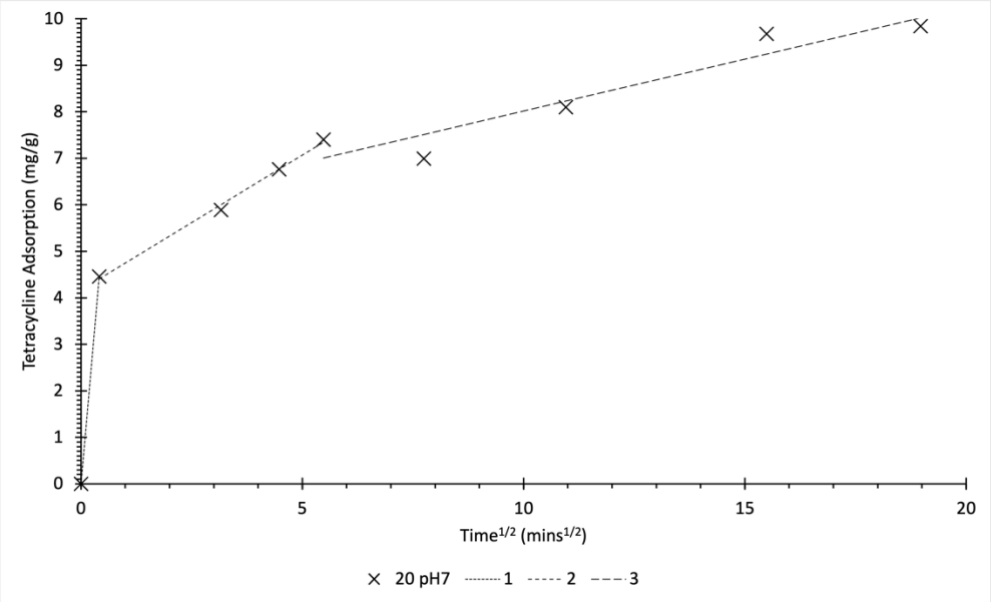

Figure 7.20 – Intraparticle model of Tetracycline adsorption (C_i=100mg/L, pH=7) to biochar derived from mixed municipal discarded material pyrolyzed in a heat pipe reactor

7.3.2 Liquid Film Diffusion Model

Figure 7.21, Figure 7.22, Figure 7.23, Figure 7.24 and Figure 7.25 show the Boyd plots for tetracycline adsorption to MMDM biochar, for initial tetracycline concentrations between 20mg/L and 100mg/L and initial solution pH of 7. Table 7.6 shows the statistical analysis for these Boyd plots. Apart from the adsorption experiment conducted using an initial tetracycline concentration of 40mg/L, the p-values for all of the Boyd plots were above 0.05. However, all of the calculated p-values are only slightly above or below 0.05. This suggests that liquid film is a large governing effect on the removal of tetracycline by MMDM biochar. However, the fact that most of the p-values are greater than 0.05 also suggests that other processes also limit the removal of tetracycline from solutions by MMDM biochar. As seen earlier, these may include intraparticle diffusion processes as well as heterogenous chemisorption processes described by the Elovich kinetic model.

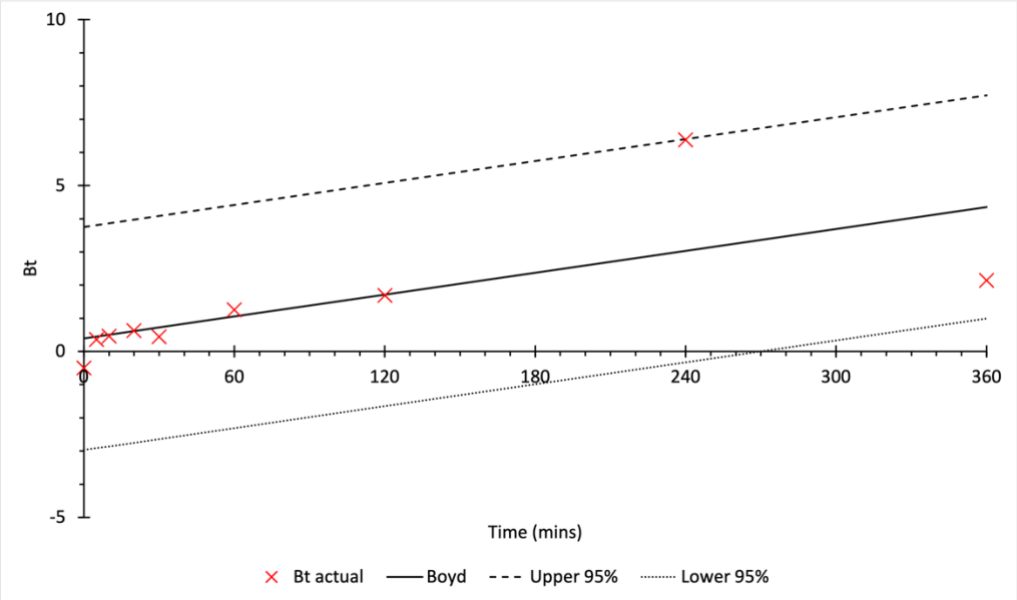

Figure 7.21 – Boyd plot of tetracycline adsorption to biochar derived from mixed municipal discarded material in a heat pipe reactor at initial pH7 and initial tetracycline concentration of 20mg/L

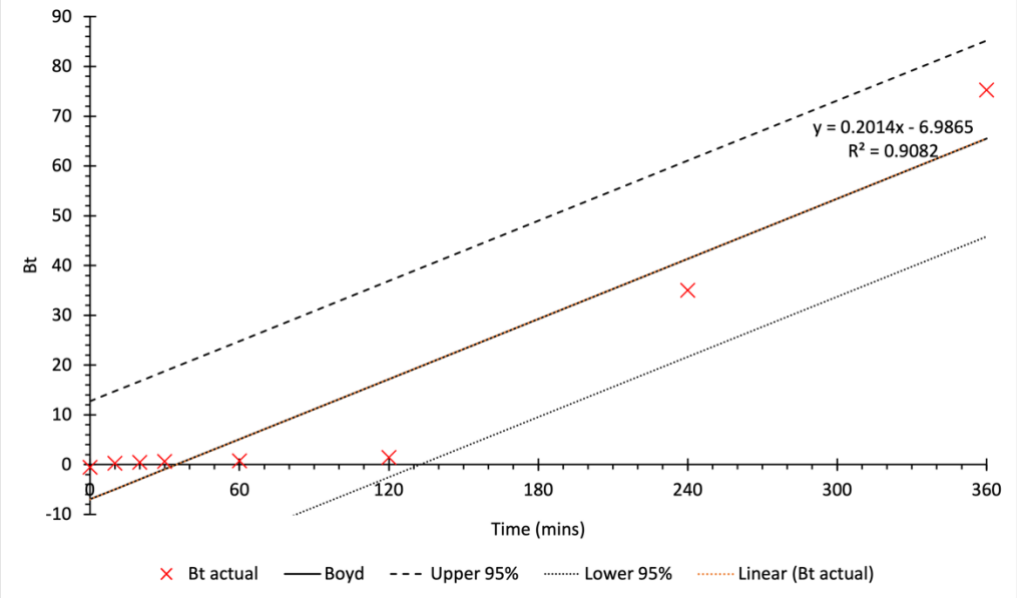

Figure 7.22 – Boyd plot of tetracycline adsorption to biochar derived from mixed municipal discarded material in a heat pipe reactor at initial pH7 and initial tetracycline concentration of 40mg/L

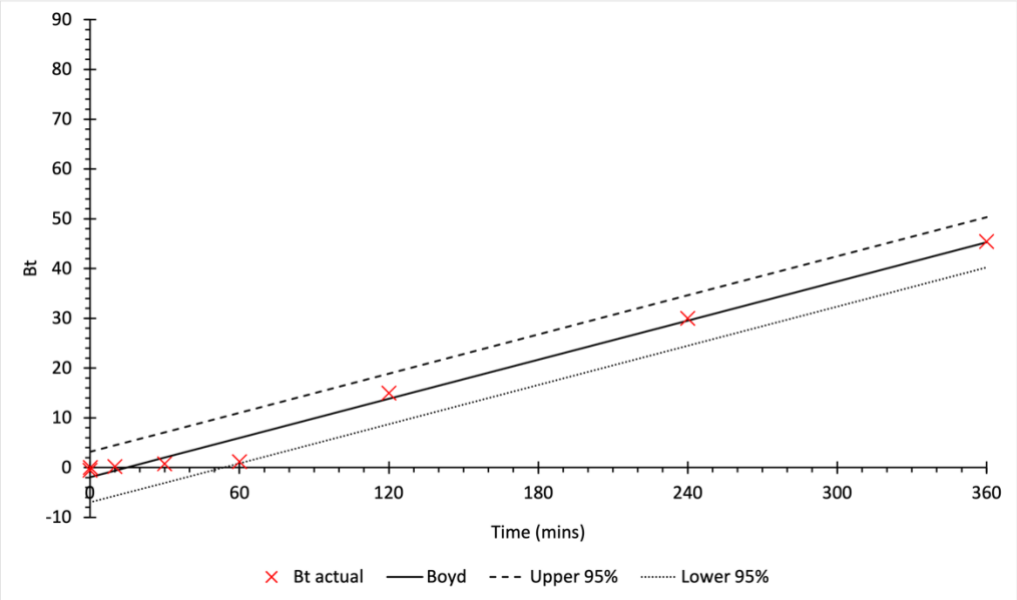

Figure 7.23 – Boyd plot of tetracycline adsorption to biochar derived from mixed municipal discarded material in a heat pipe reactor at initial pH7 and initial tetracycline concentration of 60mg/L

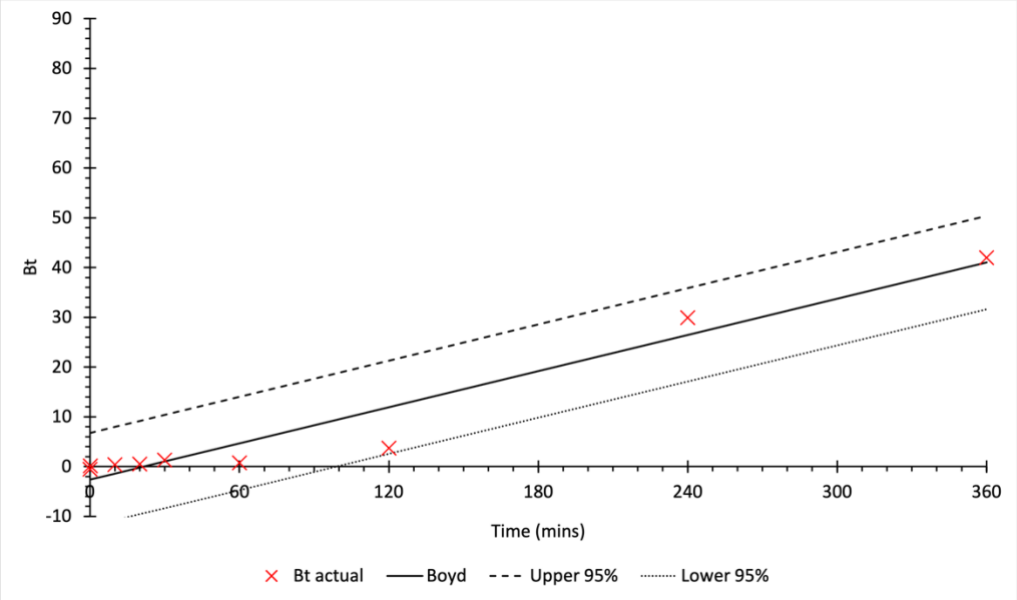

Figure 7.24 – Boyd plot of tetracycline adsorption to biochar derived from mixed municipal discarded material in a heat pipe reactor at initial pH7 and initial tetracycline concentration of 80mg/L

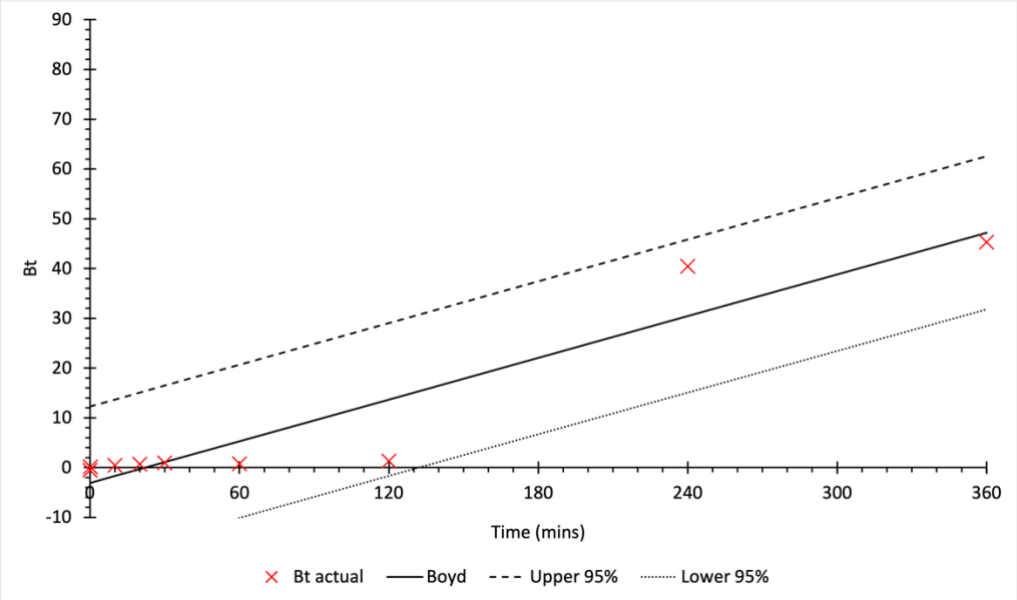

Figure 7.25 – Boyd plot of tetracycline adsorption to biochar derived from mixed municipal discarded material in a heat pipe reactor at initial pH7 and initial tetracycline concentration of 100mg/L

Table 7.6 - Table showing statistical analysis for the Boyd plots in Figure 7.21, Figure 7.22, Figure 7.23, Figure 7.24 and Figure 7.25

Tetracycline Blue concentration	R^2	MSE	p-value
20mg/L, pH 7	0.4767	1.891	0.0569
40mg/L, pH 7	0.9082	60.74	0.0431
60mg/L, pH 7	0.9849	4.020	0.0599
80mg/L, pH 7	0.9444	12.214	0.0519
100mg/L, pH 7	0.8931	33.271	0.0509

7.4 Adsorption Isotherms

Figure 7.26 shows the Langmuir isotherm model as calculated for the tetracycline adsorption to MMDM biochar. Under the experimental conditions used it can be seen that the Langmuir model is almost linear, indeed the R_L values shown in Table 7.7 are close to 1 which shows that the tetracycline removal by MMDM biochar follows an almost linear relationship when described by the Langmuir model. The statistical analysis displayed in Table 7.11 shows that the Langmuir model has the lowest R^2 value, and highest MSE and 95% confidence intervals when compared to the other isothermal models used. This means that the Langmuir model is not the best fitting isothermal model of the four different adsorption isotherms analysed.

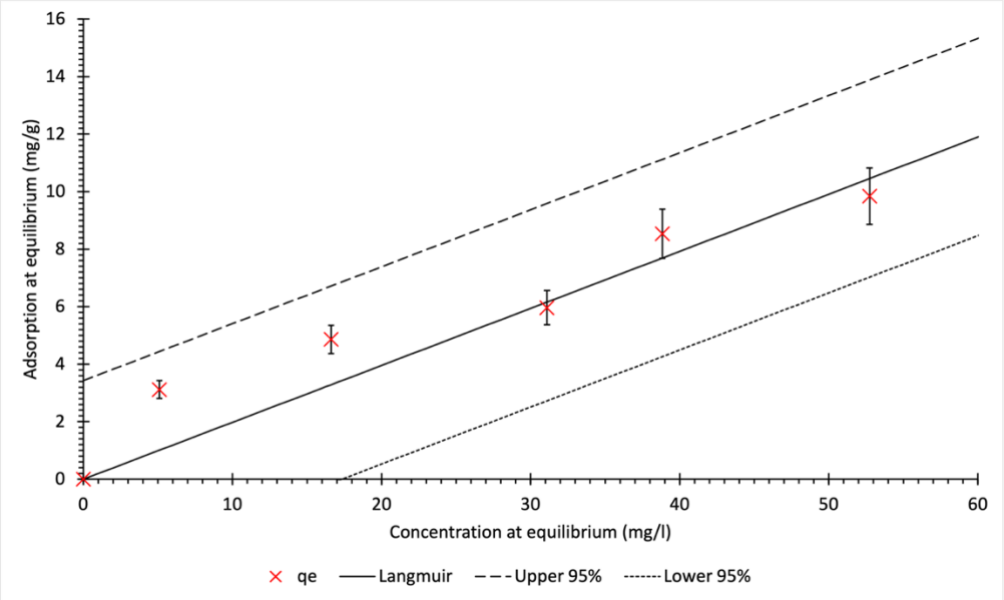

Figure 7.26 – Langmuir Model of Tetracycline adsorption to biochar derived from MMDM

Table 7.7 – Langmuir isotherm coefficients

K_L (l/mg)	**Q_m (mg/g)**
0.0000626	3157.7
C_i (mg/L)	**R_L**
20	0.99875036
40	0.99750385
60	0.99626044
80	0.99502012
100	0.99378289

Figure 7.27 shows the Freundlich isotherm model, with Table 7.8 showing the two coefficients involved in this model. The Freundlich model returns a non-linear relationship, with an n value of 1.7600. With n being greater than 1, adsorption of tetracycline to MMDM biochar is shown to be favourable. The R^2 value of the Freundlich model displayed in Table 7.11 is larger than the R^2 for the Langmuir model, with MSE and 95% confidence intervals for the Freundlich model also being lower than those calculated for the Langmuir mode, showing the Freundlich model is the best fitting two-term isotherm analysed. However, the R^2 value for the Freundlich model is lower than the R^2 values for both the Sips isotherm and dual mode

isotherm, with the MSE and 95% confidence intervals for these models being smaller than those of the Freundlich model.

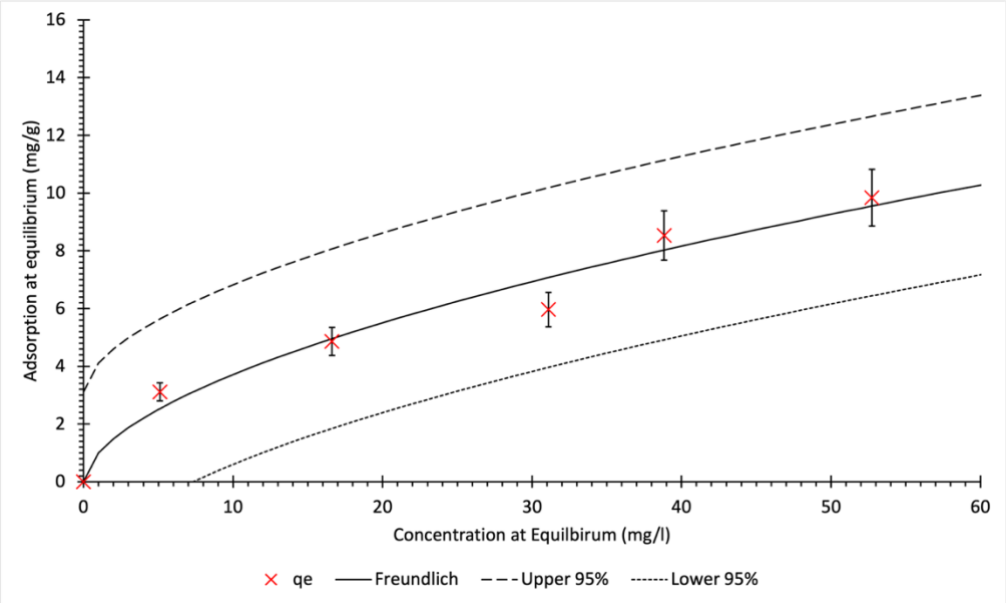

Figure 7.27 – Freundlich Model of Tetracycline adsorption to biochar derived from MMDM

Table 7.8 – Freundlich model coefficients

K_F (l/g)	n
1.0035	1.7600

Figure 7.28 shows the Sips model for tetracycline adsorption to MMDM biochar. Table 7.9 shows the Sips model coefficients. The n value being greater than 1 demonstrates that adsorption is a favourable mechanism as calculated by the Sips model. However, with Q_m being large compared to the tetracycline adsorption observed and K_s being very small, the adsorption behaviour under the experimental conditions is shown to be almost linear under the experimental conditions. Indeed, the R^2 value calculated for the Sips model is the second largest R^2 value of all the isothermal models, second only to the R^2 value calculated for the dual mode isotherm. The MSE value is shown to be larger than MSE values calculated for both the dual mode and Freundlich isotherms. Finally, the 95% confidence limit of the Sips model was larger than the 95% confidence interval calculated for the dual mode isotherm. This shows that the Sips model better describes tetracycline adsorption to MMDM biochar compared with the Freundlich and Langmuir models. However, the dual mode isotherm with

a larger R^2 value, and lower MSE and 95% confidence intervals fits the experimental data better than the Sips model.

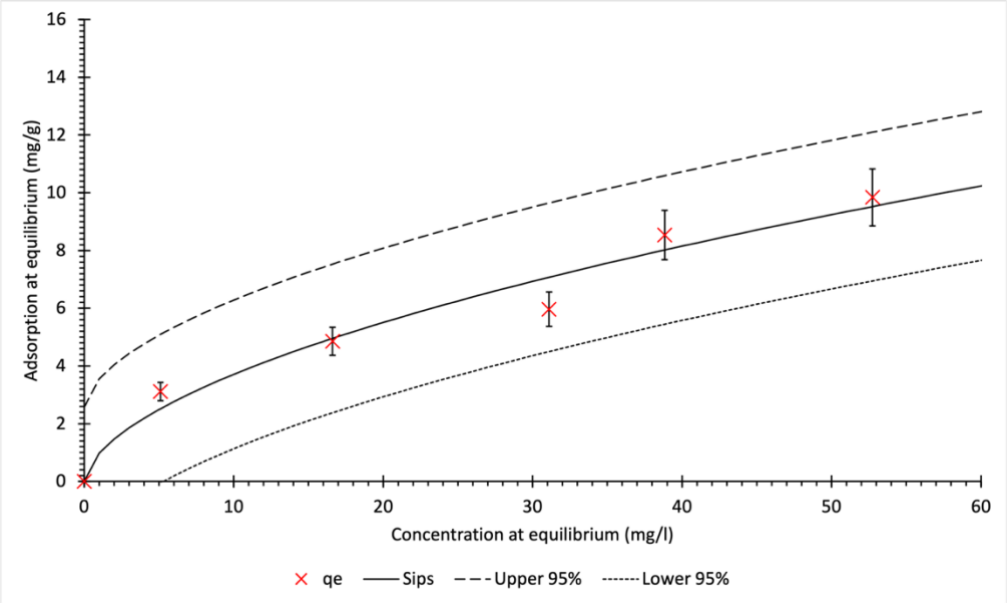

Figure 7.28 – Sips Model of Tetracycline adsorption to biochar derived from MMDM

Table 7.9 – Sips model coefficients

K_s (l/mg)	Q_m (mg/g)	n
0.00357	276.53	1.7224

Figure 7.29 shows the dual mode isotherm with Table 7.10 showing the coefficients for the dual mode isotherm. The statistical analyses in Table 7.11 shows that this model is the best fitting model of all the isotherms analysed, with the largest R^2 values and lowest MSE and 95% confidence intervals of all the isotherm models. This suggests that both adsorption and partitioning mechanisms are responsible for the removal of tetracycline from solution by biochar adsorbent, with the linear partitioning mechanism explaining the apparent linearity of the adsorption data plotted against the respective equilibrium concentrations.

Figure 7.30 shows the dual mode isotherm with the red cross indicating the point at which the removal of tetracycline from aqueous solution becomes dominated by partitioning mechanisms. At concentrations greater than 26.5mg/L partitioning of tetracycline into uncarbonized fractions of the biochar is the dominant mechanism, whilst at concentrations

below 26.5mg/L adsorption mechanisms such as hydrogen bonding, π electron interactions, electrostatic interactions etc. are the dominant mechanisms of tetracycline removal.

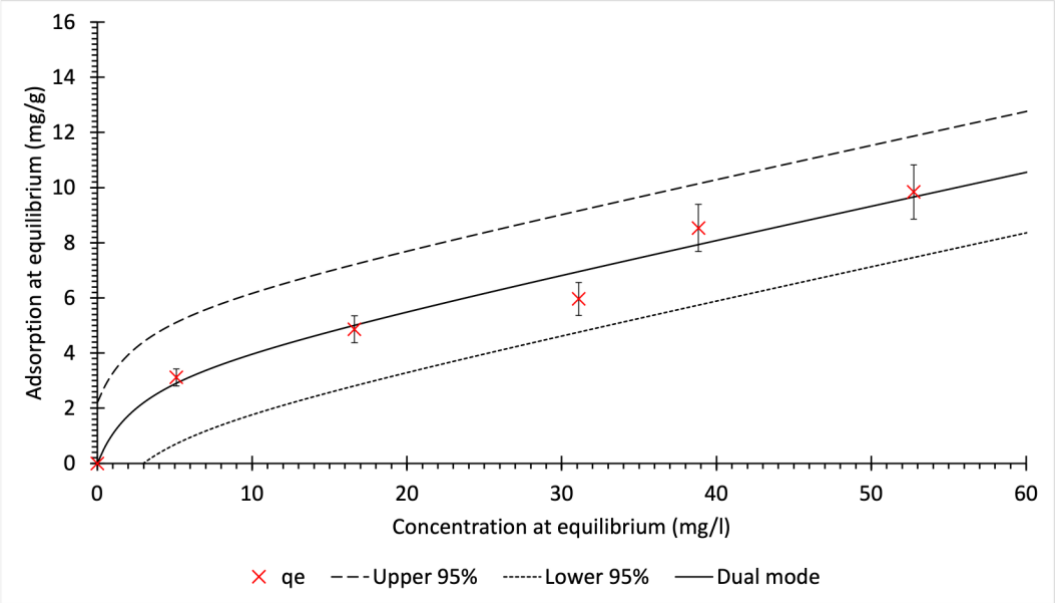

Figure 7.29 – Dual Mode Model of Tetracycline adsorption to biochar derived from MMDM

Table 7.10 – Dual Mode isotherm model coefficients

$K_{DM,nl}$ (l/mg)	Q_m (mg/g)	$K_{DM,l}$ (l/g)
0.3737	3.500	0.1201

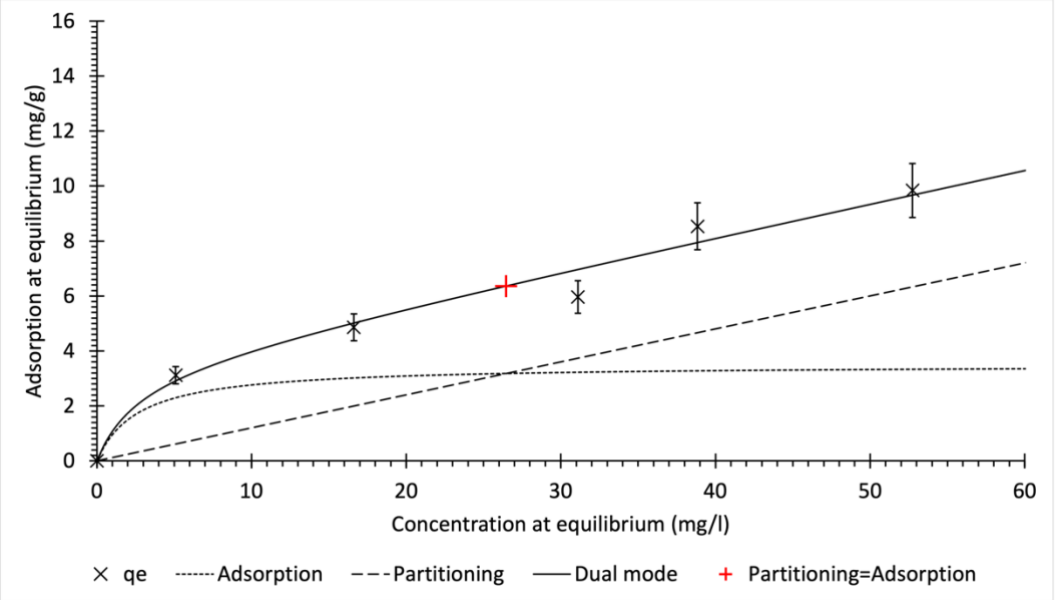

Figure 7.30 – Dual Mode model showing separate adsorption and partitioning mechanisms

Table 7.11 – Statistical analyses of isotherm models for Tetracycline adsorption to MMDM biochar

Kinetic model	R^2	MSE	95% Confidence interval
Langmuir	0.9363	1.403	3.4300
Freundlich	0.9705	0.3208	3.1101
Sips	0.9699	0.3272	2.5743
Dual mode	0.9827	0.2400	2.2051

7.5 Tetracycline Percentage removal

The percentage removal of tetracycline is shown in Figure 7.31. Percentage removal of tetracycline is highest at lower concentrations with the adsorption amount of tetracycline being highest at higher concentrations. As is the case in methylene blue adsorption, the tetracycline adsorption is shown to plateau when the initial concentration is between 40mg/L and 60mg/L. This could possibly be due to the exhaustion of "active sites" responsible for adsorption mechanisms at concentrations below these concentrations, leaving only partitioning mechanisms to remove tetracycline from aqueous solutions. Whilst the percentage removal of tetracycline is low compared with other such biochar, the successful removal of tetracycline by MMDM biochar is still demonstrated. Indeed, this material demonstrates 77.86% tetracycline removal for an initial tetracycline concentration of 20mg/L, decreasing to 49.20% tetracycline removal for an initial tetracycline concentration of 100mg/L. Whilst this shows that such an adsorbent cannot completely remove tetracycline from solution, it is shown that such an adsorbent could be used to reduce the burden that tetracycline has on more expensive water treatment methods including ozonation, membrane filtration, and further more expensive adsorbents. Furthermore, the concentrations of tetracycline and other antibiotics expected in environmental waters are low compared with the higher concentrations used in this study. This indicates that MMDM biochar could be implemented in drainage systems to reduce and manage levels of pharmaceutical contaminants such as tetracycline in the environment [401].

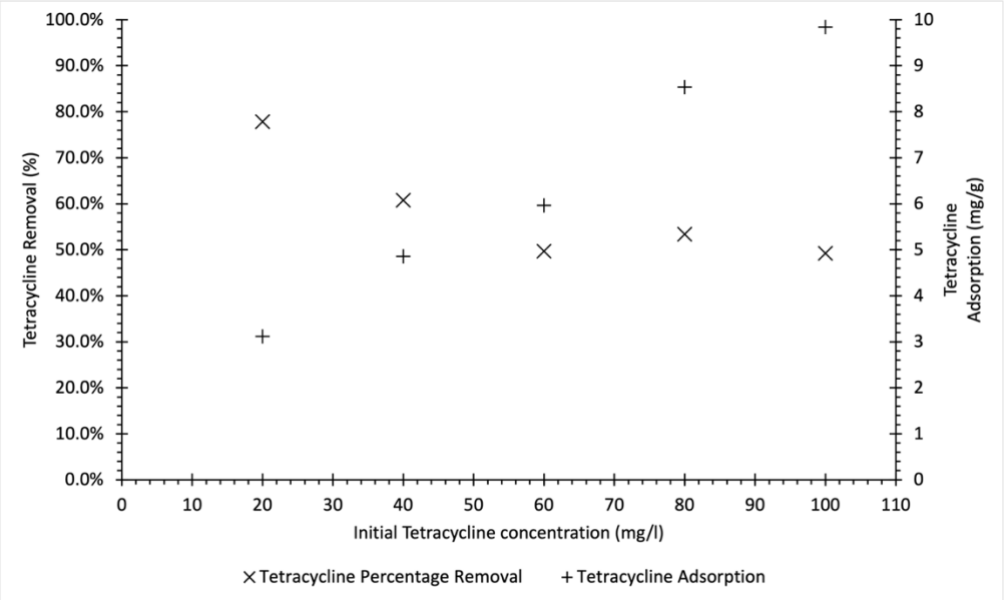

Figure 7.31 – Percentage removal of methylene blue from solution using biochar adsorbent derived from mixed municipal discarded material pyrolyzed in a heat pipe reactor, data labels show adsorption of methylene blue in mg/g

7.6 Discussion

As mentioned earlier, tetracycline as well as other antibiotics are a pollutant of global importance due to the proliferation of antibiotic resistance. This chapter shows that MMDM biochar produced in a heat pipe reactor can be used to remove tetracycline from aqueous solutions. As is the case for methylene blue, there are more efficacious adsorbents available for the removal of tetracycline from water. Similar to both the copper and methylene blue adsorption chapters prior to this, these adsorbents tend to be produced from specific feedstocks and are also subjected to further processes that improve the adsorption of tetracycline to the biochar adsorbents produced [17,402]. The purpose of this chapter was to prove that adsorbent material for the removal of aqueous tetracycline could be produced in a simple one-step process from MMDM material. In this regard it can be stated that the material produced from the heat pipe pyrolysis of MMDM is effective in the removal of tetracycline from solution. **Table 7.12** shows a selection of biochar material from literature, some of which outperforms MMDM biochar in tetracycline adsorption. On inspection however it can also be seen that MMDM biochar is comparable to some of the biochar adsorbents produced [397,402–404]. This can be stated as the adsorption of pollutants to biochar is known to decrease with increased biochar dosage; the biochar dosage used in this thesis was higher than that used in the studies displayed in **Table 7.12**.

Tetracycline adsorption by MMDM biochar could consequently be improved through the use of activating agents or procedures. Indeed, ball milling is one such simple mechanical procedure shown to significantly improve the tetracycline adsorption of wheat stalk biochar [402]. Ball milling could potentially be used to improve the tetracycline adsorption of MMDM biochar. This procedure reduces the particle size of the adsorbent, as well as causing it to fracture. This could increase the surface area of the MMDM biochar exposed to solution, further increasing the number of aromatic and oxygen containing moieties available for tetracycline adsorption in π electron interactions and hydrogen bonding respectively [398].

Tetracycline adsorption to MMDM biochar could also be improved through stirring it with aqueous or liquid organic extracts, in similar processes to the biochar derived from grapefruit peels in **Table 7.12** [404]. This method has been successfully utilised for improving methylene blue adsorption by pumpkin biochar [15]. Using methods of chemical improvement with MMDM biochar however could be hazardous due to the potential for MMDM to introduce hazardous compounds to water. These may include some heavy metals and organic compounds already present in mixed discarded materials and, additionally, PAHs and dioxins can also be present in biochar due to their production during pyrolysis. PAHs and dioxins are however reduced through the use of lower pyrolysis temperatures in the heat pipe reactor [344,405]. The presence of hazardous materials in MMDM biochar could be mitigated through introducing household/consumer sorting practises prior to waste collection, where specific bins are used for discarded food, paper, plastics, and non-organics, thus minimising the presence of heavy metals and other unwanted substances originating from some feedstocks in the final biochar adsorbent. This could for example mean reducing or eliminating discarded plastics used in feedstocks used for adsorbent production, consequently reducing the amount of polycyclic aromatic hydrocarbons produced by the pyrolysis of such materials [405]. The discarded food and paper materials could then be used to produce adsorbents as well as aqueous/liquid extracts for functionalising later MMDM biochar, with these feedstocks being less likely to contain or produce toxins due to standards surrounding their initial use [406].

Table 7.12 *– Comparison of collected tetracycline adsorption data and a selection of adsorption data from literature*

Feedstock	Adsorbent production	Biochar dosage (g/L)	Initial solution conc. (mg/L)	Initial solution pH	Adsorption (mg/g)	Source
Cassava ethanol sludge	Impregnated with sodium bicarbonate prior to Pyrolysis at 800°C	1	20	4	17.38	[407]
Cassava ethanol sludge	Impregnated with sodium bicarbonate prior to Pyrolysis at 800°C	1	50	4	43.04	[407]
Cassava ethanol sludge	Impregnated with sodium bicarbonate prior to Pyrolysis at 800°C	1	80	4	68.74	[407]
Spent coffee grounds	Pyrolysis at 500°C	0.1	100	7	39.22	[397]
Spent coffee grounds	Dried, then impregnated with sodium hydroxide prior to Pyrolysis at 500°C	0.1	100	7	113.64	[397]
Date palm leaves	Pyrolysis at 500°C, oxidised and sonicated with H_2O_2, activated with cyanuric chloride and triethylamine, refluxed with vitamin B6	1	60	7	55.86	[408]
Wheat stalk	Pyrolyzed at 300°C	0.2	25	7	21.67	[402]
Wheat stalk	Pyrolyzed at 300°C, Ball milled	0.2	25	7	50.58	[402]
Wheat stalk	Pyrolyzed at 450°C	0.2	25	7	25.00	[402]
Wheat stalk	Pyrolyzed at 450°C, Ball milled	0.2	25	7	81.97	[402]
Wheat stalk	Pyrolyzed at 600°C	0.2	25	7	28.64	[402]
Wheat stalk	Pyrolyzed at 600°C, Ball milled	0.2	25	7	84.55	[402]
Pomelo peels	Pyrolyzed at 400°C	0.2	10	7	8.94	[403]
Pomelo peels	Pyrolyzed at 600°C	0.2	10	7	14.42	[403]
Pomelo peels	Pyrolyzed at 400°C, impregnated with KOH and pyrolyzed at 600°C	0.08	10	7	124.95	[403]
Grapefruit peel	Pyrolyzed at 600°C	0.5	50	6.17	15.31	[404]
Grapefruit peel	Pyrolyzed at 600°C and mixed with grapefruit extract (solid:liquid 1:10)	0.5	50	6.17	19.51	[404]

***Table 7.12** Continued*

Grapefruit peel	Pyrolyzed at 600°C and mixed with grapefruit extract (solid:liquid 1:20)	0.5	50	6.17	32.46	[404]
Grapefruit peel	Pyrolyzed at 600°C and mixed with grapefruit extract (solid:liquid 1:30)	0.5	50	6.17	27.74	[404]
Crayfish shell	Pyrolyzed at 400°C	1.25	100	7	17.8	[398]
Crayfish shell	Pyrolyzed at 400°C, ball milled	1.25	100	7	40.0	[398]
Crayfish shell	Pyrolyzed at 600°C	1.25	100	7	30.1	[398]
Crayfish shell	Pyrolyzed at 600°C, ball milled	1.25	100	7	44.8	[398]
Crayfish shell	Pyrolyzed at 800°C	1.25	100	7	41.0	[398]
Crayfish shell	Pyrolyzed at 800°C, ball milled	1.25	100	7	56.9	[398]
Mixed municipal discarded material	Pyrolyzed below 300°C	5	20	7	3.11	This thesis
Mixed municipal discarded material	Pyrolyzed below 300°C	5	40	7	4.86	This thesis
Mixed municipal discarded material	Pyrolyzed below 300°C	5	60	7	5.96	This thesis
Mixed municipal discarded material	Pyrolyzed below 300°C	5	80	7	8.54	This thesis
Mixed municipal discarded material	Pyrolyzed below 300°C	5	100	7	9.84	This thesis

A mixture of the processes used in **Table 7.12** could consequently result in an adsorbent comparable to commercial powdered activated carbons using MMDM as a feedstock for heat pipe pyrolysis. As stated previously this could be utilised in the sedimentation and/or coagulation-flocculation stages of water treatment plants, where the powdered activated carbon is known to assist in the removal of low molar mass aqueous organic compounds such as tetracycline [409]. The removal of tetracycline from water using powdered biochar presents a problem of itself, however as it results in a sludge contaminated with removed antibiotics. One study has shown that this adsorbed tetracycline can be almost completely

degraded using a further ball-milling step, with or without the use of additional quartz material [410]. Another method for removing antibiotics from powdered biochar is regeneration. These typically involve immersing the spent biochar in a solution containing an eluent. Indeed, sodium hydroxide has been shown to effectively desorb tetracycline from similar biochar adsorbents, allowing them to be reused a number of times [398]. This process does however result in a solution containing tetracycline, and/or other antibiotics that require further treatment to remove antibiotics from the aqueous waste stream [411]. Further pyrolysis using intermediate temperatures (400-700^{o}C) could also result in the degradation of tetracycline captured on the biochar surface [412]. This would also result in the production of a further adsorbent material containing more aromatic groups, greater surface area, and fewer functional groups, thus producing a biochar more suited to non-polar contaminants. Re-pyrolysis at greater temperatures could therefore extend the life of the MMDM biochar produced in this thesis as an alternative to commercial powdered activated carbons.

An alternative use for MMDM biochar could be to use it in drainage systems around areas where antibiotic contamination is expected. This kind of application is identified in the previous chapter on methylene blue adsorption, where layers of this material could be used in constructed wetlands to reduce concentrations of unwanted organic contaminants such as antibiotics [384]. Some antibiotics are known to adsorb to soils and are consequently not detected in water samples taken from environmental surface water [413]. The use of managed engineered soil materials containing a mixture of, or completely comprised of, MMDM biochar could therefore be used to reduce the presence of antibiotics such as tetracyclines in agricultural soils. Regularly replacing these adsorbent materials could therefore represent a method which large agricultural enterprises could use to reduce their antibiotic as well as pesticide footprint. The benefit of using MMDM biochar is that it is a very cheap adsorbent to produce due to the feedstock being found wherever there is human activity. This makes it an attractive adsorbent for use in sustainable drainage systems which target persistent pharmaceuticals, where the use of specialist adsorbents would be wasteful as conditions are not closely monitored and maintained, as they are in water treatment plants where commercial adsorbents are typically used. Furthermore, antibiotic emission to the environment tends to be intermittent. This further highlights the benefit of using a cheaper adsorbent in environmental systems, reserving the specialist/commercial adsorbents for use

in systems where more elevated levels of tetracycline and other antibiotics are expected [414]. Once MMDM biochar has reached the end of its useful life as an adsorbent of antibiotics and other similar pharmaceuticals, it can be further used as an aggregate in concrete/cement materials [415]. This locks the carbon content of the biochar away in a carbon sink and also improves the sustainability of the concrete material.

Whilst biochar produced from MMDM can reduce concentrations of aqueous tetracycline, it is possible that their application in drainage systems could introduce antibiotic resistance genes to the environment with some feedstocks such as sewage sludge containing these contaminants [416]. Furthermore, the application of biochar to soils or in drainage systems may assist in the proliferation of antibiotic resistance genes in the environment, increasing the viability of certain bacterial communities over others in soils and drainage systems such as wetlands [417,418]. In some systems the introduction of biochar can actually inhibit the growth of antibiotic resistance genes through promoting the growth of bacteria that are not sensitive to the contaminating antibiotics, potentially also promoting the growth of bacteria capable of degrading the contaminating antibiotics [384]. However, whilst MMDM biochar shows promise as an adsorbent substrate, more work is required towards the use of MMDM biochar as an environmental adsorbent substrate before it can be used in full scale applications.

7.7 Summary

In summary, the removal of tetracycline from aqueous solutions follows the Elovich and pseudo second order kinetics more closely than the pseudo first order kinetic. This shows that the adsorption of tetracycline to heat pipe derived MMDM biochar is limited by chemisorption mechanisms that occur heterogeneously across the surface of the biochar. The best fitting isotherm was found to be the dual mode isotherm with the highest R^2 value, and lowest MSE and 95% confidence interval values. The best fitting isothermal model was easier to determine for the removal of tetracycline compared with the removal of methylene blue from solution. This could potentially be due to tetracycline predominantly existing as a neutral species under the experimental pH conditions. This would lead to reduced “resistance” to tetracycline movement across the liquid film compared with that of methylene blue which exists as a positively charged ion under the same conditions of pH. Indeed, the liquid film diffusion model for tetracycline removal produced p-values for B_t plotted against t that were

almost all greater than 0.05, albeit still close to this value. This shows that whilst liquid film diffusion is a significant process limiting the movement of tetracycline into the MMDM biochar from the aqueous solution, it is not the most significant mechanism, with intraparticle diffusion processes as well as adsorption mechanisms also limiting the movement of tetracycline into the biochar material. The best fitting isotherm was the dual mode isotherm. This shows that both adsorption and partitioning processes are responsible for tetracycline removal. Adsorption is found to be the dominant removal mechanism below equilibrium concentrations of 26.5mg/L, with partitioning being the dominant removal process above this concentration. This means that under expected environmental concentrations of antibiotics, adsorption to MMDM will be the predominant mechanism for tetracycline removal. However, it is possible that in industrial applications such as pharmaceutical and hospital wastewater, antibiotic concentrations may be higher, meaning partitioning becomes a more significant tetracycline removal mechanism.

Higher percentage removal of tetracycline was observed at lower initial concentrations, with the maximum observed percentage removal being 77.86% at an initial tetracycline concentration of 20mg/L. Whilst complete removal is not achieved, this result is still promising as it shows that useful tetracycline/antibiotic adsorbents can be produced from MMDM in the heat pipe reactor. These could be used in conjunction with current commercial adsorbents such as clay minerals and activated carbons to increase the useful life of these more expensive adsorbent materials.

Biochar produced from MMDM could undergo some further processes to improve the adsorption characteristics, with studies showing that tetracycline adsorption is enhanced by the ball milling biochar produced from similar biomass under similar pyrolysis conditions to those used for MMDM in this thesis. Other studies show that it is possible to produce an aqueous or liquid extract from biomass prior to the pyrolysis of the remaining solids; this liquid can then be used to functionalise biochar after it has been produced, improving tetracycline removal. It is reasonable to conclude that these processes would also improve the MMDM biochar due to the feedstocks and pyrolysis procedures being similar in the assessed literature to those used to produce heat pipe derived MMDM biochar. Chemically treated ball milled MMDM biochar could be used to reduce the requirement for more expensive powdered activated carbons in water treatment. However, further work is needed

to conclusively prove that this material is safe for use in drinking water applications.

The MMDM biochar could also feasibly be used in drainage systems to remove antibiotic contamination in agricultural as well as urban settings. This includes the use of the material in managed soils and wetlands where it can remove antibiotics released to the environment through veterinary and agricultural processes. In such applications, the use of biochar in sustainable drainage systems can remove antibiotics through adsorption processes similar to those seen in this chapter. Further studies are required into the use of heat pipe derived MMDM biochar in constructed wetlands to determine whether the use of this material results in the removal/degradation of antibiotics in these drainage systems, as well as how this material might affect the prevalence of antibiotic resistant genes in the environment.

Finally, this chapter shows that the heat pipe pyrolysis of MMDM can produce an effective material for tetracycline removal, comparable to other biochar adsorbents produced in literature. This material could be further improved through a mixture of mechanochemical processes such as ball-milling, and pre/post pyrolysis chemical activation/functionalisation.

8 CONCLUSIONS AND RECOMMENDATIONS FOR FUTURE WORK

The main objective of this thesis was to investigate the use of MMDM biochar adsorbents, and to identify possible applications where such materials may be used. The literature review presented in chapter 2 shows the current membrane and granular materials used to filter and treat water. This review revealed that these processes are effective in the removal of water contaminants they target. However, combinations of these processes are required to fully treat water to the required standards. The literature review also found that membrane processes such as reverse osmosis and nanofiltration particularly can suffer from reductions in process efficiency due to membrane fouling, as a result these processes are often used in conjunction with other treatment processes including the use of adsorbents to remove pollution prior to these processes. This reduces membrane fouling, this maintains the output of water for a given transmembrane pressure, where membranes without sufficient pre-treatment suffer drops in water output at constant transmembrane pressures. The literature review also showed that reverse osmosis, nanofiltration and some ultrafiltration membranes require advanced technologies and processes including interfacial polymerisation to produce. Furthermore, these membranes can be both fragile and expensive. This means that these water treatment processes are only applicable in areas where they are a necessity, for example in areas where saline water is the major source of drinking water. In areas where non-saline surface water is available, drinking water treatment plants may only need screening, sedimentation, coagulation/flocculation, membrane/granular filtration, adsorption and disinfection to achieve satisfactory water quality. The state-of-the-art chapter also shows that these processes don't remove all contaminants, hence the use of multiple processes to fully treat the water. Many adsorbents are shown by the literature review to be versatile in contamination removal, with aqueous concentrations of heavy metals, and persistent organics including pesticides and pharmaceutical compounds all being reduced by adsorbents. Biochar and activated carbon adsorbents are commonly produced at temperatures in excess of 400^{o}C promoting the development of surface area in the adsorbent material. This however is shown in the literature review to reduce oxygen containing functional groups. These are important for some adsorption mechanisms including outer and inner sphere complexation with dissolved heavy metals, and hydrogen bonding interactions between aqueous organic compounds and adsorbents. These adsorbents are also often produced from specific discarded materials used as feedstocks. This reveals the research gaps

this thesis aimed to address. The production and use of biochar produced at low temperature for use as an adsorbent, using municipal mixed discarded material as a feedstock, and using a novel heat pipe reactor to produce this adsorbent are the three main research gaps.

8.1 Biochar characterisation

The produced biochar had different physical characteristics dependent on the feedstock used. Biochar produced in the heat pipe reactor from plastic feedstock was shown by scanning electron microscopy to have a surface morphology lacking in pores compared to biochar produced from discarded food materials. Paper and cardboard biochar kept its original structure with fibres remaining intact, this is due to the pyrolysis temperature used being lower than the thermal decomposition temperature of cellulose, the predominant material present in paper and cardboard. Energy dispersive x-ray analysis also showed differences in the elemental composition of the biochar produced from different feedstocks. The major element present in all of the biochar materials produced was carbon. However, both discarded plastic and paper/cardboard materials contained large amounts of calcium and oxygen, dispersed heterogeneously across the surface and plastic containing higher amounts of calcium and oxygen than is the case for biochar derived from discarded food material which contains larger amounts of sodium, potassium and chlorine than discarded paper and plastic biochar. The calcium and oxygen content of the plastic and paper biochar is due to the presence of calcite in these biochar materials. The presence of calcite in biochar derived from discarded paper and plastic is further confirmed by FTIR analysis. FTIR confirms the presence of C=O, O-H, C-O, C-H and aromatic C=C functional groups in biochar derived from discarded food and paper. Some of these groups are also shown to be present in biochar derived from plastic. However, aromatic C=C and C-H groups are less abundant in discarded plastic biochar, with the FTIR peaks for these groups being less intense for this biochar material. Greater amounts of nitrogen containing functional groups were also present in plastic biochar that were not present in discarded paper or food biochar, with the FTIR peak at 1576cm^{-1} only being present in plastic biochar, showing the presence of in plane bending of N-H bonds and stretching of C-N bonds. Carbonates are shown to be present in all biochar materials analysed by FTIR spectroscopy. XRD spectra of the combined biochar material confirms the presence of materials suspected to be present in the biochar due to SEM, EDAX and FTIR analysis. XRD confirms the presence of carbonate in all biochar materials, as well as the presence of both sodium and potassium chloride present in the discarded food biochar. Finally, Raman spectra

of the mixed biochar material confirms the presence of aromatic groups in the biochar, present in both the disordered form and ordered graphitic form, amorphous carbon is also present, with the trough between the disordered and ordered peaks being shallow. The functional groups and mineral contents of the MMDM biochar are important for the removal of heavy metals such as copper from water, giving these biochar adsorbents the ability to adsorb copper from water via outer and inner sphere complexation, as well as through precipitation and ion exchange with the minerals present in the biochar. The oxygen containing functional groups, particularly alcohol groups interact with organic pollutants containing the same groups in hydrogen bonding. Additionally, the aromatic groups present in the biochar can interact with the same groups in contaminants containing aromatic groups in π-π stacking interactions, with the biochar also participating as a π electron acceptor.

8.2 Adsorption experiments

8.2.1 Copper adsorption

Copper adsorption reached a maximum of 6.28mg/g at an initial copper concentration of 100mg/l and initial solution pH of 5. Maximum total copper removal was achieved with an initial solution pH of 6 and initial copper concentration of 150mg/l, with a removal percentage of 92.73%. 79.29% of this removal can be attributed to copper hydroxide solid forming in solution, with the remaining 13.44% of removal being attributed to the removal of dissolved Cu^{2+} and $CuOH^{+}$ ions in solution by adsorption to the MMDM biochar. The increase of pH from 3 to 5.5 resulted in an increase in adsorption of copper to biochar. The increase in adsorption was due to the deprotonation of “active sites” on the biochar surface. The decrease in adsorption from pH 5.5 to 6 was due to the decrease in aqueous copper concentration between these pH values. The removal percentage of copper due to adsorption was also shown to decrease with increasing copper concentration, from a value of 34.09% for initial copper concentrations of 50mg/L at pH 5, to a value of 10.04% for initial copper concentrations 250mg/L at pH 5. At a pH of 6 and initial copper concentration of 150mg/L, discounting the copper removed by precipitation, the removal of aqueous copper reached a removal percentage of 64.92%. This shows that copper removal percentage by MMDM will increase under decreasing concentrations of copper. Copper adsorption was shown to fit the Elovich and pseudo second order kinetic models more closely than the pseudo first order kinetic model, however as initial copper concentration increased, the Elovich model became less closely fitting, with the pseudo first order model being the most closely fitting model at

higher initial copper concentrations. This shows that as copper concentrations increase, physical phenomena such as film diffusion and intraparticle diffusion begin to limit the removal of copper from solution by MMDM biochar more than chemisorption processes do. Weber-Morris plots showed multi-linear behaviour, indicating that different processes are more responsible for the removal of copper from solution at different times. The film diffusion process plotted in the Boyd plots was shown to not be a significant limiting factor in the removal of copper from solution, with p-values for B_t plotted against time all being greater than 0.05. This means that other processes including intraparticle diffusion and chemisorption are more significant limiting factors of copper removal by MMDM biochar produced in a heat pipe reactor. The closest fitting isotherm for copper adsorption was determined as the Langmuir isothermal model. Copper adsorption occurring in a monolayer fashion across the MMDM biochar surface is therefore the best description of the adsorption process that can be determined from the data collected. EDAX analysis after copper adsorption experiments for food and paper showed that copper was fairly evenly distributed across the biochar surface, with no statistically significant relationships between copper or any other detected element. This shows that copper adsorption is fairly homogenous across the surface of these adsorbents, with multiple mechanisms being responsible for copper adsorption including outer and inner sphere complexation, electrostatic interaction, precipitation, and ion exchange. However, the opposite was true for copper concentrations in the biochar derived from discarded plastics. In this instance, copper was found to exist in greater amounts where mixtures of oxygen, positively charged ions, and negatively charged ions were present, with this relationship found to be statistically significant. Copper adsorption to biochar derived from discarded plastic is therefore more heavily reliant on precipitation, ion exchange, and electrostatic interaction mechanisms than is the case for copper adsorption to biochar derived from discarded food and paper.

8.2.2 Methylene blue adsorption

Methylene blue adsorption reached a maximum value of 7.25mg/g at an initial methylene blue concentration of 100mg/L and an initial pH of 7. Methylene blue percentage removal reached a maximum of 89.92% for an initial methylene blue concentration of 10mg/l and initial pH of 7, with the percentage removal decreasing to 33.67% for an initial methylene blue concentration of 50mg/L and pH of 7, the percentage removal then slowly increased from this

value to 41.26% for an initial methylene blue concentration of 100mg/L and pH of 7. This shows that between initial methylene blue concentrations of 0 and 50mg/L one or several similar removal mechanisms are largely responsible for the removal of methylene blue. These however reach their maximum capacity after an initial methylene blue concentration of 50mg/L, with one or several other removal mechanisms becoming more significant at these elevated initial methylene blue concentrations. Methylene blue removal was shown to be best described by the Elovich and pseudo second order kinetic models at initial methylene blue concentrations below 75mg/L and initial pH of 7. However, at initial methylene blue concentrations greater than 75mg/L, the best fitting adsorption model becomes less clear with all kinetic models producing similar R^2, MSE, and 95% confidence intervals. This suggests that at these elevated concentrations, physical processes such as intraparticle diffusion and liquid film diffusion become more significant limiting factors to methylene blue removal than they are at concentrations below 75mg/L. The kinetic model results suggest that multiple mechanisms are responsible for methylene blue removal by biochar, with complexation and electrostatic interactions between the positively charged methylene blue molecule, and the deprotonated C-O-H groups known to exist on the biochar surface. Other interactions such as hydrogen bonding and π electron interactions are also responsible for the removal of methylene blue from solution. Weber-Morris plots of methylene blue removal by MMDM biochar also result in multi-linearity. Boyd plots of methylene blue adsorption to biochar produce p-values of B_t against t that are below or are very close to 0.05. This means that methylene blue removal by MMDM biochar is significantly limited by the liquid film diffusion process. However, the closeness of the p-value to 0.05 suggests that it is not the only process limiting the removal of methylene blue, despite being the most significant. The multi-linearity of the Weber-Morris plots, and closer fit of the Elovich and pseudo second order models also show that intraparticle and chemisorption processes also limit the removal of methylene blue by MMDM biochar derived in a heat pipe reactor. The best fitting isothermal model of methylene blue removal was the dual mode isotherm. This means that both adsorption mechanisms and partitioning mechanisms are responsible for the removal of methylene blue from aqueous solutions. Indeed, at an equilibrium concentration of 50.89mg/L, partitioning becomes the dominant mechanism of methylene blue removal, this explains why the removal percentage of methylene blue by MMDM biochar appears to plateau after an initial methylene blue concentration of 50mg/L, where the sites responsible for adsorption have

become largely saturated, whilst partitioning can still occur at these elevated initial methylene blue concentrations.

8.2.3 Tetracycline adsorption

Tetracycline removal by MMDM biochar reaches a maximum value of 9.84mg/g at an initial tetracycline concentration of 100mg/L and initial pH of 7. The maximum observed percentage removal of tetracycline was 77.86% for an initial tetracycline concentration of 20mg/L and initial pH of 7, with this decreasing to 55.96% for an initial tetracycline concentration of 100mg/L and initial pH of 7. The percentage removal of tetracycline also seemed to decrease towards a plateau starting at an initial concentration of 60mg/L. This again suggests that tetracycline removal at lower concentrations is more attributed to processes that become saturated at, or around initial tetracycline concentrations of 60mg/L. Tetracycline removal was found to be best described by the Elovich model, followed by the pseudo second order and finally the pseudo first order kinetic model. This suggests that chemisorption processes are the limiting factor of tetracycline removal by MMDM biochar rather than the physisorption processes described by pseudo first order. Furthermore, the kinetic models are easily distinguishable for all initial concentrations up to 100mg/L. This is unlike the opposite phenomenon observed in methylene blue adsorption where increasing the initial methylene blue concentration led to a decrease in the distinguishability between the different kinetic models. This is explained by the dominant ionic species of tetracycline at pH 7 being a neutral ion, whereas the methylene blue species dominant at this pH value is a positive ion. Consequently, tetracycline that has diffused into the MMDM biochar offers less resistance to the liquid film and intraparticle diffusion of further tetracycline molecules. Conversely, methylene blue with its positive charge repels other similarly charged methylene blue ions resulting in resistance to the diffusion of more methylene blue molecules, with this effect being more significant as initial methylene blue concentrations increase. The removal mechanisms largely responsible for tetracycline removal by MMDM biochar are hydrogen bonding between C-O-H groups present on the biochar surface and similar groups present in the tetracycline, and π-bonding interactions between the tetracycline and the biochar, with covalent bonding also potentially occurring.

Weber-Morris plots for tetracycline removal also revealed apparent multi-linearity of these plots, with three distinct linear stages clear in each of the plots for every initial tetracycline

concentration. The best fitting kinetic models of adsorption show that chemisorption processes do occur and do limit the adsorption of tetracycline to MMDM biochar. Boyd plots of tetracycline removal produce p-values for B_t plotted against time that are mainly above, but close to 0.05. This shows that whilst liquid film diffusion is not the most significant process limiting the removal of tetracycline by biochar, it does nonetheless partially limit the removal of tetracycline by MMDM biochar.

As is the case for methylene blue removal, the isothermal model that best describes tetracycline removal is also the dual mode model. This means that partitioning as well as adsorption mechanisms are also active in the removal of tetracycline by MMDM biochar. Partitioning becomes the dominant removal mechanism at equilibrium concentrations greater than 26.47mg/L. This explains the apparent plateau in the percentage removal graph, where the adsorption sites responsible for tetracycline removal are almost completely saturated when the initial concentration is 60mg/L or above, with the linear partitioning removal still occurring at these higher tetracycline concentrations.

8.2.4 Contributions to knowledge

To summarise, this thesis contributes to the knowledge of biochar adsorbents produced at temperatures below 300 ^{o}C. it highlights the ability of this biochar to remove different types of pollutants from aqueous solution.

- Copper, methylene blue and tetracycline can all be removed from solution using adsorbent materials pyrolyzed at temperatures between 250 – 300 ^{o}C not commonly considered in literature. This suggests that other pollutants could be removed by the same and similar materials produced at these lower pyrolysis temperatures.
- Mixed feedstocks have been successfully pyrolyzed to produce adsorbent materials. This shows that mixed materials should be considered to produce adsorbent materials, where literature typically focuses on the use of specific feedstocks.
- Non-linear regression techniques can be applied to reduce the errors introduced by linearised equations for kinetic, diffusion and isothermal modelling. This can be achieved using accessible statistical modelling software such as SAS University edition or Microsoft Excel using the solver add-in. With non-linear regression being more accessible due to modern computing, future research could apply similar techniques to avoid the use of linearised models.

8.3 Comments and recommendations for future research

8.3.1 Improvements to research methodology

If this research was to be conducted again, it would be beneficial to conduct studies into the competitive adsorption between the three pollutants and the biochar. This would further increase the impact of the thesis providing further information on its capabilities, as well as the impact of a mixed pollutant matrix on the removal of other pollutants. Purchasing commercial activated carbons as well as sourcing other biochar materials to test under the same experimental conditions as the produced biochar would also improve the experimental methodology as comparisons with other adsorbents could be drawn from experimental data as well as from available literature.

8.3.2 Potential future research

Firstly, this thesis shows that it is possible for researchers to make use of non-linear kinetic and isothermal models using statistical modelling software. Linear models have been commonly used in adsorbent research to model the adsorption of contaminants in batch adsorption experiments. This was originally done to reduce the computation time needed to determine which models best fit the adsorption data. It is no longer necessary to use the linearised models of adsorption kinetics and isotherms where non-linear regression can be computed quickly using statistical software such as SAS or through the use of the solver add-in in Microsoft Excel. This means that statistical analyses of adsorption kinetics and isotherms can be produced and compared on the same scales. Similar methodologies could be adopted easily by future research.

The ability of MMDM biochar produced at low temperatures using a heat pipe reactor is shown to be at least comparable with regards to the adsorption of copper, methylene blue and tetracycline to pristine biochar produced in other studies. This shows that municipal waste could be used to produce a valuable adsorbent capable of removing a range of contaminants from water. This material could potentially be used in sustainable drainage systems to reduce the contamination of water in the environment. This use would have the added benefit of being a carbon sink, where discarded food and paper materials is made more stable through pyrolysis and buried. Discarded food and paper would otherwise produce greenhouse gases either through their incineration or decomposition in landfill. This thesis therefore shows that this material is a promising adsorbent that could potentially be used in

sustainable drainage systems. More research is however required to ensure that these biochar adsorbents do not release harmful contaminants above permitted standards to environmental water when used in this way.

Comparing the adsorption of copper, methylene blue and tetracycline observed in this thesis to that observed in other literature reveals that the MMDM biochar could be further processed to improve its adsorption of these pollutants. Ball milling for example could be investigated to produce a powder from MMDM biochar that could be implemented in the coagulation-flocculation stage of drinking water treatment, either in place of or alongside commercial powdered activated carbon. This could potentially result in the reduced burden on downstream processes such as commercial granular activated carbon filters, and filtration membranes, where some of the contamination targeted by these processes has already been removed in pre-treatment by powdered MMDM biochar. Other methods of improving the adsorption capabilities of biochar, such as impregnation with potassium hydroxide before pyrolysis, or functionalising the MMDM biochar with liquids after pyrolysis could also be investigated to produce an adsorbent of even greater quality than that produced in this thesis.

Further work on this material is therefore of high importance, as a commercially and ecologically valuable material could be produced using material commonly found in the discarded materials from domestic and businesses.

REFERENCES

[1] Tan X, Liu S, Liu Y, Gu Y, Zeng G, Hu X, et al. Biochar as potential sustainable precursors for activated carbon production: Multiple applications in environmental protection and energy storage. Bioresource Technology 2017;227:359–72. https://doi.org/https://doi.org/10.1016/j.biortech.2016.12.083.

[2] Wang Q, Lai Z, Mu J, Chu D, Zang X. Converting industrial waste cork to biochar as Cu (II) adsorbent via slow pyrolysis. Waste Management 2020;105:102–9. https://doi.org/https://doi.org/10.1016/j.wasman.2020.01.041.

[3] Hassan M, Liu Y, Naidu R, Parikh SJ, Du J, Qi F, et al. Influences of feedstock sources and pyrolysis temperature on the properties of biochar and functionality as adsorbents: A meta-analysis. Science of the Total Environment 2020;744:140714. https://doi.org/https://doi.org/10.1016/j.scitotenv.2020.140714.

[4] Qiu B, Tao X, Wang H, Li W, Ding X, Chu H. Biochar as a low-cost adsorbent for aqueous heavy metal removal: A review. Journal of Analytical and Applied Pyrolysis 2021;155:105081. https://doi.org/https://doi.org/10.1016/j.jaap.2021.105081.

[5] Luo C, Routh J, Dario M, Sarkar S, Wei L, Luo D, et al. Distribution and mobilization of heavy metals at an acid mine drainage affected region in South China, a post-remediation study. Science of the Total Environment 2020;724:138122. https://doi.org/https://doi.org/10.1016/j.scitotenv.2020.138122.

[6] Zhou Q, Yang N, Li Y, Ren B, Ding X, Bian H, et al. Total concentrations and sources of heavy metal pollution in global river and lake water bodies from 1972 to 2017. Global Ecology and Conservation 2020;22:e00925. https://doi.org/https://doi.org/10.1016/j.gecco.2020.e00925.

[7] Xiong J, Li H, Ma X, Tan B, You J. A new configuration of polar organic chemical integrative sampler with nylon membranes to monitor emerging organophosphate ester contaminants in urban surface water. Ecotoxicology and Environmental Safety 2020;202:110891. https://doi.org/https://doi.org/10.1016/j.ecoenv.2020.110891.

[8] Delgado N, Capparelli A, Navarro A, Marino D. Pharmaceutical emerging pollutants removal from water using powdered activated carbon: Study of kinetics and adsorption equilibrium. Journal of Environmental Management 2019;236:301–8. https://doi.org/https://doi.org/10.1016/j.jenvman.2019.01.116.

[9] Oskarsson A, Rosenmai AK, Mandava G, Johannisson A, Holmes A, Tröger R, et al. Assessment of source and treated water quality in seven drinking water treatment plants by in vitro bioassays – Oxidative stress and antiandrogenic effects after artificial infiltration. Science of the Total Environment 2021;758:144001. https://doi.org/https://doi.org/10.1016/j.scitotenv.2020.144001.

[10] Bakaraki Turan N, Sari Erkan H, Onkal Engin G. Microplastics in wastewater treatment plants: Occurrence, fate and identification. Process Safety and Environmental Protection 2021;146:77–84. https://doi.org/https://doi.org/10.1016/j.psep.2020.08.039.

[11] Teodosiu C, Gilca A-F, Barjoveanu G, Fiore S. Emerging pollutants removal through advanced drinking water treatment: A review on processes and environmental performances assessment. Journal of Cleaner Production 2018;197:1210–21. https://doi.org/https://doi.org/10.1016/j.jclepro.2018.06.247.

[12] Kaza S, Yao L, Bhada-Tata P, Van Woerden F. What a Waste 2.0: A Global Snapshot of Solid Waste Management to 2050. Washington D.C.: The World Bank; 2018. https://doi.org/10.1596/978-1-4648-1329-0.

[13] Giwa AS, Xu H, Chang F, Zhang X, Ali N, Yuan J, et al. Pyrolysis coupled anaerobic digestion process for food waste and recalcitrant residues: Fundamentals, challenges, and considerations. Energy Science and Engineering 2019;7:2250–64. https://doi.org/https://doi.org/10.1002/ese3.503.

[14] Jouhara H, Nannou TK, Anguilano L, Ghazal H, Spencer N. Heat pipe based municipal waste treatment unit for home energy recovery. Energy 2017;139:1210–30. https://doi.org/https://doi.org/10.1016/j.energy.2017.02.044.

[15] Rashid J, Tehreem F, Rehman A, Kumar R. Synthesis using natural functionalization of activated carbon from pumpkin peels for decolourization of aqueous methylene blue. Science of the Total Environment 2019;671:369–76. https://doi.org/https://doi.org/10.1016/j.scitotenv.2019.03.363.

[16] Kwak J-H, Islam MS, Wang S, Messele SA, Naeth MA, El-Din MG, et al. Biochar properties and lead(II) adsorption capacity depend on feedstock type, pyrolysis temperature, and steam activation. Chemosphere 2019;231:393–404. https://doi.org/https://doi.org/10.1016/j.chemosphere.2019.05.128.

[17] Li B, Zhang Y, Xu J, Xie Z, Tang J, Li X, et al. Simultaneous carbonization, activation, and magnetization for producing tea waste biochar and its application in tetracycline removal from the aquatic environment.

Journal of Environmental Chemical Engineering 2021:105324. https://doi.org/https://doi.org/10.1016/j.jece.2021.105324.
[18] Gleick PH. World fresh water resources. New York: Oxford University Press; 1993.
[19] Fund) S (Sustainable DG. Clean water and sanitation 2015. http://www.sdgfund.org/goal-6-clean-water-and-sanitation (accessed March 13, 2018).
[20] World Health Organisation. WHO Joint monitoring programme 2017. https://washdata.org/ (accessed January 11, 2018).
[21] Pascoal R, Rocha H. Inequality measures for wealth distribution: Population vs individuals perspective. Physica A: Statistical Mechanics and its Applications 2018;492:1317–26. https://doi.org/https://doi.org/10.1016/j.physa.2017.11.059.
[22] Majuru B, Jagals P, Hunter PR. Assessing rural small community water supply in Limpopo, South Africa: Water service benchmarks and reliability. Science of the Total Environment 2012;435–436:479–86. https://doi.org/https://doi.org/10.1016/j.scitotenv.2012.07.024.
[23] Ritchie H, Roser M. Urbanization. Our World Data 2020.
[24] How much will your pump really cost you? Water Wastewater Treatment 2016. https://wwtonline.co.uk/features/how-much-will-your-pump-really-cost-you- (accessed January 9, 2020).
[25] Stauffer B, Spuhler D. Pumping stations. Furth Resour Water Distrib 2019.
[26] DEFRA, Government W. Water Framework Directive implementation in England and Wales: new and updated standards to protect the water environment United Kingdom: Crown Copyright; 2014.
[27] WHO. Guidelines for Drinking-Water Quality. Geneva: 2017.
[28] Liu A, Ren F, Lin WY, Wang J-Y. A review of municipal solid waste environmental standards with a focus on incinerator residues. International Journal of Sustainable Built Environment 2015;4:165–88. https://doi.org/https://doi.org/10.1016/j.ijsbe.2015.11.002.
[29] Aguilar FX. Spatial econometric analysis of location drivers in a renewable resource-based industry: The U.S. South Lumber Industry. Forest Policy and Economics 2009;11:184–93. https://doi.org/https://doi.org/10.1016/j.forpol.2009.02.006.
[30] Wu S, Yang Z. Optimizing location of manufacturing industries in the context of economic globalization: A bi-level model based approach. Physica A: Statistical Mechanics and its Applications 2018;501:327–37. https://doi.org/https://doi.org/10.1016/j.physa.2018.02.042.
[31] Behrens K, Bougna T. An anatomy of the geographical concentration of Canadian manufacturing industries. Regional Science and Urban Economics 2015;51:47–69. https://doi.org/https://doi.org/10.1016/j.regsciurbeco.2015.01.002.
[32] Odume ON. Searching for urban pollution signature and sensitive macroinvertebrate traits and ecological preferences in a river in the Eastern Cape of South Africa. Ecological Indicators 2020;108:105759. https://doi.org/https://doi.org/10.1016/j.ecolind.2019.105759.
[33] Geedicke I, Oldeland J, Leishman MR. Urban stormwater run-off promotes compression of saltmarshes by freshwater plants and mangrove forests. Science of the Total Environment 2018;637–638:137–44. https://doi.org/https://doi.org/10.1016/j.scitotenv.2018.04.357.
[34] Martinho VJPD. Best management practices from agricultural economics: Mitigating air, soil and water pollution. Science of the Total Environment 2019;688:346–60. https://doi.org/https://doi.org/10.1016/j.scitotenv.2019.06.199.
[35] Lai W. Pesticide use and health outcomes: Evidence from agricultural water pollution in China. Journal of Environmental Economics and Management 2017;86:93–120. https://doi.org/https://doi.org/10.1016/j.jeem.2017.05.006.
[36] Knobeloch L, Salna B, Hogan A, Postle J, Anderson H. Blue Babies and Nitrate-Contaminated Well Water. Environmental Health Perspectives 2000;108:675–8. https://doi.org/10.1289/ehp.00108675.
[37] de Melo Filho MES, Owatari MS, Mouriño JLP, Lapa KR, Soares HM. Application of nitrification and denitrification processes in a direct water reuse system for pacific white shrimp farmed in biofloc system. Aquacultural Engineering 2020;88:102043. https://doi.org/https://doi.org/10.1016/j.aquaeng.2020.102043.
[38] Huang J, Xu C, Ridoutt BG, Wang X, Ren P. Nitrogen and phosphorus losses and eutrophication potential associated with fertilizer application to cropland in China. Journal of Cleaner Production 2017;159:171–9. https://doi.org///doi.org/10.1016/j.jclepro.2017.05.008.
[39] Glibert PM. Eutrophication, harmful algae and biodiversity — Challenging paradigms in a world of complex nutrient changes. Marine Pollution Bulletin 2017;124:591–606. https://doi.org///doi.org/10.1016/j.marpolbul.2017.04.027.

[40] Álvarez X, Valero E, Santos RMB, Varandas SGP, Sanches Fernandes LF, Pacheco FAL. Anthropogenic nutrients and eutrophication in multiple land use watersheds: Best management practices and policies for the protection of water resources. Land Use Policy 2017;69:1–11. https://doi.org///doi.org/10.1016/j.landusepol.2017.08.028.

[41] Rajendran V, Nirmaladevi D S, Srinivasan B, Rengaraj C, Mariyaselvam S. Quality assessment of pollution indicators in marine water at critical locations of the Gulf of Mannar Biosphere Reserve, Tuticorin. Marine Pollution Bulletin 2018;126:236–40. https://doi.org///doi.org/10.1016/j.marpolbul.2017.10.091.

[42] Hou W, Sun S, Wang M, Li X, Zhang N, Xin X, et al. Assessing water quality of five typical reservoirs in lower reaches of Yellow River, China: Using a water quality index method. Ecological Indicators 2016;61:309–16. https://doi.org/https://doi.org/10.1016/j.ecolind.2015.09.030.

[43] Chollom MN, Pikwa K, Rathilal S, Pillay VL. Fouling mitigation on a woven fibre microfiltration membrane for the treatment of raw water. South African Journal of Chemical Engineering 2017;23:1–9. https://doi.org///doi.org/10.1016/j.sajce.2016.12.003.

[44] AWWA. Nitrification. Washington DC: U.S. Environmental Protection Agency Office of Ground Water and Drinking Water Standards and Risk Management Division; 2017.

[45] Bruni M, Spuhler D. Slow Sand Filtration 2012;2017. https://www.sswm.info/category/implementation-tools/water-purification/hardware/semi-centralised-drinking-water-treatmen-2.

[46] Paul D. Research on heavy metal pollution of river Ganga: A review. Annals of Agrarian Science 2017;15:278–86. https://doi.org///doi.org/10.1016/j.aasci.2017.04.001.

[47] Cooper Z, Bringolf R, Cooper R, Loftis K, Bryan AL, Martin JA. Heavy metal bioaccumulation in two passerines with differing migration strategies. Science of the Total Environment 2017;592:25–32. https://doi.org///doi.org/10.1016/j.scitotenv.2017.03.055.

[48] Goretti E, Pallottini M, Ricciarini MI, Selvaggi R, Cappelletti D. Heavy metals bioaccumulation in selected tissues of red swamp crayfish: An easy tool for monitoring environmental contamination levels. Science of the Total Environment 2016;559:339–46. https://doi.org///doi.org/10.1016/j.scitotenv.2016.03.169.

[49] Liu J, Cao L, Dou S. Bioaccumulation of heavy metals and health risk assessment in three benthic bivalves along the coast of Laizhou Bay, China. Marine Pollution Bulletin 2017;117:98–110. https://doi.org///doi.org/10.1016/j.marpolbul.2017.01.062.

[50] ZHAO M, ZHANG C, ZENG G, HUANG D, CHENG M. Toxicity and bioaccumulation of heavy metals in Phanerochaete chrysosporium. Transactions of Nonferrous Metals Society of China 2016;26:1410–8. https://doi.org///doi.org/10.1016/S1003-6326(16)64245-0.

[51] Howladar MF. An assessment of surface water chemistry with its possible sources of pollution around the Barapukuria Thermal Power Plant impacted area, Dinajpur, Bangladesh. Groundwater for Sustainable Development 2017;5:38–48. https://doi.org///doi.org/10.1016/j.gsd.2017.03.004.

[52] Sounthararajah DP, Loganathan P, Kandasamy J, Vigneswaran S. Adsorptive removal of heavy metals from water using sodium titanate nanofibres loaded onto GAC in fixed-bed columns. Journal of Hazardous Materials 2015;287:306–16. https://doi.org///doi.org/10.1016/j.jhazmat.2015.01.067.

[53] Vital B, Bartacek J, Ortega-Bravo JC, Jeison D. Treatment of acid mine drainage by forward osmosis: Heavy metal rejection and reverse flux of draw solution constituents. Chemical Engineering Journal 2018;332:85–91. https://doi.org///doi.org/10.1016/j.cej.2017.09.034.

[54] Lam B, Déon S, Morin-Crini N, Crini G, Fievet P. Polymer-enhanced ultrafiltration for heavy metal removal: Influence of chitosan and carboxymethyl cellulose on filtration performances. Journal of Cleaner Production 2018;171:927–33. https://doi.org///doi.org/10.1016/j.jclepro.2017.10.090.

[55] Maher A, Sadeghi M, Moheb A. Heavy metal elimination from drinking water using nanofiltration membrane technology and process optimization using response surface methodology. Desalination 2014;352:166–73. https://doi.org///doi.org/10.1016/j.desal.2014.08.023.

[56] WHO. Guidelines for Drinking-Water Quality. Geneva: 2017.

[57] Lin W-S, Lee M, Huang Y-C, Den W. Identifying water recycling strategy using multivariate statistical analysis for high-tech industries in Taiwan. Resources, Conservation and Recycling 2015;94:35–42. https://doi.org/https://doi.org/10.1016/j.resconrec.2014.11.007.

[58] Yang L, She Q, Wan MP, Wang R, Chang VW-C, Tang CY. Removal of haloacetic acids from swimming pool water by reverse osmosis and nanofiltration. Water Research 2017;116:116–25. https://doi.org/https://doi.org/10.1016/j.watres.2017.03.025.

[59] Industries F. Autotrophic vs. Heterotrophic Bacteria 2001;2017. http://www.bioconlabs.com/autoheterobac.html.

[60] Agency MPC. Phosphorus Treatment and Removal Technologies 2006;2017.

https://www.pca.state.mn.us/sites/default/files/wq-wwtp9-02.pdf.

[61] Keene NA, Reusser SR, Scarborough MJ, Grooms AL, Seib M, Santo Domingo J, et al. Pilot plant demonstration of stable and efficient high rate biological nutrient removal with low dissolved oxygen conditions. Water Research 2017;121:72–85. https://doi.org///doi.org/10.1016/j.watres.2017.05.029.

[62] Moussa DT, El-Naas MH, Nasser M, Al-Marri MJ. A comprehensive review of electrocoagulation for water treatment: Potentials and challenges. Journal of Environmental Management 2017;186:24–41. https://doi.org///doi.org/10.1016/j.jenvman.2016.10.032.

[63] Sillanpää M, Ncibi MC, Matilainen A, Vepsäläinen M. Removal of natural organic matter in drinking water treatment by coagulation: A comprehensive review. Chemosphere 2018;190:54–71. https://doi.org///doi.org/10.1016/j.chemosphere.2017.09.113.

[64] Lagaly G, Ziesmer S. Colloid chemistry of clay minerals: the coagulation of montmorillonite dispersions. Advances in Colloid and Interface Science 2003;100–102:105–28. https://doi.org///doi.org/10.1016/S0001-8686(02)00064-7.

[65] Su Z, Liu T, Yu W, Li X, Graham NJD. Coagulation of surface water: Observations on the significance of biopolymers. Water Research 2017;126:144–52. https://doi.org///doi.org/10.1016/j.watres.2017.09.022.

[66] McKie MJ, Taylor-Edmonds L, Andrews SA, Andrews RC. Engineered biofiltration for the removal of disinfection by-product precursors and genotoxicity. Water Research 2015;81:196–207. https://doi.org///doi.org/10.1016/j.watres.2015.05.034.

[67] Ebeling JM, Sibrell PL, Ogden SR, Summerfelt ST. Evaluation of chemical coagulation–flocculation aids for the removal of suspended solids and phosphorus from intensive recirculating aquaculture effluent discharge. Aquacultural Engineering 2003;29:23–42. https://doi.org///doi.org/10.1016/S0144-8609(03)00029-3.

[68] Jeon S-B, Kim S, Park S-J, Seol M-L, Kim D, Chang YK, et al. Self-powered electro-coagulation system driven by a wind energy harvesting triboelectric nanogenerator for decentralized water treatment. Nano Energy 2016;28:288–95. https://doi.org///doi.org/10.1016/j.nanoen.2016.08.051.

[69] Malakootian M, Mansoorian HJ, Moosazadeh M. Performance evaluation of electrocoagulation process using iron-rod electrodes for removing hardness from drinking water. Desalination 2010;255:67–71. https://doi.org///doi.org/10.1016/j.desal.2010.01.015.

[70] Krystynik P, Tito DN. Key process parameters affecting performance of electro-coagulation. Chemical Engineering and Processing: Process Intensification 2017;117:106–12. https://doi.org///doi.org/10.1016/j.cep.2017.03.022.

[71] Tito DN, Krystynik P, Kluson P. Notes on process and data analysis in electro-coagulation—The importance of standardisation and clarity. Chemical Engineering and Processing: Process Intensification 2016;104:22–8. https://doi.org///doi.org/10.1016/j.cep.2016.02.011.

[72] Engineering GP. Membrane Filtration: Reverse Osmosis, Nanofiltration, Ultrafiltration and Microfiltration 2012:1–12. https://www.gea.com/en/binaries/membrane-filtration-ultrafiltration-nanofiltration-microfiltration-reverse-osmosis-gea_tcm11-34841.pdf (accessed December 21, 2017).

[73] Mouiya M, Abourriche A, Bouazizi A, Benhammou A, El Hafiane Y, Abouliatim Y, et al. Flat ceramic microfiltration membrane based on natural clay and Moroccan phosphate for desalination and industrial wastewater treatment. Desalination 2018;427:42–50. https://doi.org/https://doi.org/10.1016/j.desal.2017.11.005.

[74] Waszak M, Gryta M. The ultrafiltration ceramic membrane used for broth separation in membrane bioreactor. Chemical Engineering Journal 2016;305:129–35. https://doi.org/https://doi.org/10.1016/j.cej.2015.11.058.

[75] Ko K, Yu Y, Kim M-J, Kweon J, Chung H. Improvement in fouling resistance of silver-graphene oxide coated polyvinylidene fluoride membrane prepared by pressurized filtration. Separation and Purification Technology 2018;194:161–9. https://doi.org/https://doi.org/10.1016/j.seppur.2017.11.016.

[76] Chatterjee S, De S. Adsorptive removal of arsenic from groundwater using chemically treated iron ore slime incorporated mixed matrix hollow fiber membrane. Separation and Purification Technology 2017;179:357–68. https://doi.org/https://doi.org/10.1016/j.seppur.2017.02.019.

[77] Manouchehri M, Kargari A. Water recovery from laundry wastewater by the cross flow microfiltration process: A strategy for water recycling in residential buildings. Journal of Cleaner Production 2017;168:227–38. https://doi.org///doi.org/10.1016/j.jclepro.2017.08.211.

[78] Gwenaelle MPO, Jung J, Choi Y, Lee S. Effect of microbubbles on microfiltration pretreatment for seawater reverse osmosis membrane. Desalination 2017;403:153–60. https://doi.org///doi.org/10.1016/j.desal.2016.06.012.

[79] Jamaly S, Darwish NN, Ahmed I, Hasan SW. A short review on reverse osmosis pretreatment technologies. Desalination 2014;354:30–8. https://doi.org/10.1016/j.desal.2014.09.017.

[80] Suresh K, Pugazhenthi G. Cross flow microfiltration of oil-water emulsions using clay based ceramic membrane support and TiO2 composite membrane. Egyptian Journal of Petroleum 2017;26:679–94. https://doi.org/https://doi.org/10.1016/j.ejpe.2016.10.007.

[81] Carpintero-Tepole V, Brito-de la Fuente E, Torrestiana-Sánchez B. Microfiltration of oil in water (O/W) emulsions: Effect of membrane microstructure and surface properties. Chemical Engineering Research and Design 2017;126:286–96. https://doi.org/https://doi.org/10.1016/j.cherd.2017.08.023.

[82] Hung MT, Liu JC. Microfiltration of microalgae in the presence of rigid particles. Separation and Purification Technology 2016. https://doi.org/https://doi.org/10.1016/j.seppur.2016.10.063.

[83] Suresh K, Pugazhenthi G, Uppaluri R. Fly ash based ceramic microfiltration membranes for oil-water emulsion treatment: Parametric optimization using response surface methodology. Journal of Water Process Engineering 2016;13:27–43. https://doi.org/https://doi.org/10.1016/j.jwpe.2016.07.008.

[84] Monash P, Pugazhenthi G. Effect of TiO2 addition on the fabrication of ceramic membrane supports: A study on the separation of oil droplets and bovine serum albumin (BSA) from its solution. Desalination 2011;279:104–14. https://doi.org/https://doi.org/10.1016/j.desal.2011.05.065.

[85] Sutherland K. What is nanofiltration? 2009;2017. http://www.filtsep.com/water-and-wastewater/features/what-is-nanofiltration/.

[86] Li Z, Feng X, Li G, Bi X, Zhu J, Qin H, et al. Distributions, sources and pollution status of 17 trace metal/metalloids in the street dust of a heavily industrialized city of central China. Environmental Pollution 2013;182:408–16. https://doi.org/https://doi.org/10.1016/j.envpol.2013.07.041.

[87] SAMCO. Reverse Osmosis vs Nanofiltration Membrane Process: What Is the Difference? 2017;2017. https://www.samcotech.com/reverse-osmosis-vs-nanofiltration-membrane-process-what-is-the-difference/.

[88] Yorgun MS, Balcioglu IA, Saygin O. Performance comparison of ultrafiltration, nanofiltration and reverse osmosis on whey treatment. Desalination 2008;229:204–16. https://doi.org///doi.org/10.1016/j.desal.2007.09.008.

[89] Yoon Y, Westerhoff P, Snyder SA, Wert EC, Yoon J. Removal of endocrine disrupting compounds and pharmaceuticals by nanofiltration and ultrafiltration membranes. Desalination 2007;202:16–23. https://doi.org///doi.org/10.1016/j.desal.2005.12.033.

[90] Yoon J, Amy G, Chung J, Sohn J, Yoon Y. Removal of toxic ions (chromate, arsenate, and perchlorate) using reverse osmosis, nanofiltration, and ultrafiltration membranes. Chemosphere 2009;77:228–35. https://doi.org///doi.org/10.1016/j.chemosphere.2009.07.028.

[91] American Membrane Technology Association (AMTA). Membrane Desalination Power Usage Put in Perspective 2009;2017. https://www.amtaorg.com/wp-content/uploads/7_MembraneDesalinationPowerUsagePutInPerspective.pdf.

[92] Blanco-Marigorta AM, Lozano-Medina A, Marcos JD. A critical review of definitions for exergetic efficiency in reverse osmosis desalination plants. Energy 2017;137:752–60. https://doi.org///doi.org/10.1016/j.energy.2017.05.136.

[93] Bartholomew T V, Mey L, Arena JT, Siefert NS, Mauter MS. Osmotically assisted reverse osmosis for high salinity brine treatment. Desalination 2017;421:3–11. https://doi.org///doi.org/10.1016/j.desal.2017.04.012.

[94] Lotfi F, Chekli L, Phuntsho S, Hong S, Choi JY, Shon HK. Understanding the possible underlying mechanisms for low fouling tendency of the forward osmosis and pressure assisted osmosis processes. Desalination 2017;421:89–98. https://doi.org///doi.org/10.1016/j.desal.2017.01.037.

[95] Kim JE, Phuntsho S, Ali SM, Choi JY, Shon HK. Forward osmosis membrane modular configurations for osmotic dilution of seawater by forward osmosis and reverse osmosis hybrid system. Water Research 2018;128:183–92. https://doi.org/https://doi.org/10.1016/j.watres.2017.10.042.

[96] Qasim M, Mohammed F, Aidan A, Darwish NA. Forward osmosis desalination using ferric sulfate draw solute. Desalination 2017;423:12–20. https://doi.org///doi.org/10.1016/j.desal.2017.08.019.

[97] Shaaban S, Yahya H. Detailed analysis of reverse osmosis systems in hot climate conditions. Desalination 2017;423:41–51. https://doi.org///doi.org/10.1016/j.desal.2017.09.002.

[98] Monnot M, Nguyên HTK, Laborie S, Cabassud C. Seawater reverse osmosis desalination plant at community-scale: Role of an innovative pretreatment on process performances and intensification. Chemical Engineering and Processing: Process Intensification 2017;113:42–55. https://doi.org///doi.org/10.1016/j.cep.2016.09.020.

[99] Roy D, Gherrou A, Pierre P, Landry D, Yargeau V. Reverse osmosis applied to soil remediation

wastewater: Comparison between bench-scale and pilot-scale results. Journal of Water Process Engineering 2017;16:115–22. https://doi.org///doi.org/10.1016/j.jwpe.2016.12.013.

[100] Wu B, Suwarno SR, Tan HS, Kim LH, Hochstrasser F, Chong TH, et al. Gravity-driven microfiltration pretreatment for reverse osmosis (RO) seawater desalination: Microbial community characterization and RO performance. Desalination 2017;418:1–8. https://doi.org///doi.org/10.1016/j.desal.2017.05.024.

[101] Zhang Y, Wan Y, Pan G, Shi H, Yan H, Xu J, et al. Surface modification of polyamide reverse osmosis membrane with sulfonated polyvinyl alcohol for antifouling. Applied Surface Science 2017;419:177–87. https://doi.org///doi.org/10.1016/j.apsusc.2017.05.047.

[102] Víctor-Ortega MD, Ratnaweera HC. Double filtration as an effective system for removal of arsenate and arsenite from drinking water through reverse osmosis. Process Safety and Environmental Protection 2017;111:399–408. https://doi.org/https://doi.org/10.1016/j.psep.2017.08.001.

[103] Baudequin C, Couallier E, Rakib M, Deguerry I, Severac R, Pabon M. Purification of firefighting water containing a fluorinated surfactant by reverse osmosis coupled to electrocoagulation–filtration. Separation and Purification Technology 2011;76:275–82. https://doi.org/https://doi.org/10.1016/j.seppur.2010.10.016.

[104] Boddu VM, Paul T, Page MA, Byl C, Ward L, Ruan J. Gray water recycle: Effect of pretreatment technologies on low pressure reverse osmosis treatment. Journal of Environmental Chemical Engineering 2016;4:4435–43. https://doi.org/https://doi.org/10.1016/j.jece.2016.09.031.

[105] Vatanpour V, Safarpour M, Khataee A, Zarrabi H, Yekavalangi ME, Kavian M. A thin film nanocomposite reverse osmosis membrane containing amine-functionalized carbon nanotubes. Separation and Purification Technology 2017;184:135–43. https://doi.org/https://doi.org/10.1016/j.seppur.2017.04.038.

[106] Häyrynen K, Pongrácz E, Väisänen V, Pap N, Mänttäri M, Langwaldt J, et al. Concentration of ammonium and nitrate from mine water by reverse osmosis and nanofiltration. Desalination 2009;240:280–9. https://doi.org/https://doi.org/10.1016/j.desal.2008.02.027.

[107] LIU F, ZHANG G, MENG Q, ZHANG H. Performance of Nanofiltration and Reverse Osmosis Membranes in Metal Effluent Treatment* *Supported by the National Natural Science Foundation of China (20476096, 20776133), Zhejiang Provincial Bureau of Science & Technology (2005C33040) and Bureau of Edu. Chinese Journal of Chemical Engineering 2008;16:441–5. https://doi.org/https://doi.org/10.1016/S1004-9541(08)60102-0.

[108] Bi F, Zhao H, Zhou Z, Zhang L, Chen H, Gao C. Optimal design of nanofiltration system for surface water treatment. Chinese Journal of Chemical Engineering 2016;24:1674–9. https://doi.org///doi.org/10.1016/j.cjche.2016.05.012.

[109] Hedayatipour M, Jaafarzadeh N, Ahmadmoazzam M. Removal optimization of heavy metals from effluent of sludge dewatering process in oil and gas well drilling by nanofiltration. Journal of Environmental Management 2017;203:151–6. https://doi.org/https://doi.org/10.1016/j.jenvman.2017.07.070.

[110] Masindi V, Osman MS, Abu-Mahfouz AM. Integrated treatment of acid mine drainage using BOF slag, lime/soda ash and reverse osmosis (RO): Implication for the production of drinking water. Desalination 2017;424:45–52. https://doi.org/https://doi.org/10.1016/j.desal.2017.10.002.

[111] (Association) MRW. Membrane Filtration n.d.:1–12. https://www.mrwa.com/WaterWorksMnl/Chapter 19 Membrane Filtration.pdf (accessed January 8, 2018).

[112] Hydranautics. Commercial RO Technology 2001:1–6. http://www.membranes.com/docs/trc/commerc.pdf (accessed January 8, 2018).

[113] Ortega Sandoval AD, Barbosa Brião V, Cartana Fernandes VM, Hemkemeier A, Friedrich MT. Stormwater management by microfiltration and ultrafiltration treatment. Journal of Water Process Engineering 2017. https://doi.org///doi.org/10.1016/j.jwpe.2017.07.018.

[114] Bogler A, Lin S, Bar-Zeev E. Biofouling of membrane distillation, forward osmosis and pressure retarded osmosis: Principles, impacts and future directions. Journal of Membrane Science 2017;542:378–98. https://doi.org/https://doi.org/10.1016/j.memsci.2017.08.001.

[115] Staff A. Reverse Osmosis and Nanofiltration, (M46). American Water Works Association; 2011.

[116] van der Laan H, van Halem D, Smeets PWMH, Soppe AIA, Kroesbergen J, Wubbels G, et al. Bacteria and virus removal effectiveness of ceramic pot filters with different silver applications in a long term experiment. Water Research 2014;51:47–54. https://doi.org/https://doi.org/10.1016/j.watres.2013.11.010.

[117] PureMadi. The Manufacturing Process 2014. http://www.puremadi.org/science-overview/ (accessed

January 15, 2018).
[118] CAWST. Ceramic Pot Filter 2017.
[119] Peter-Varbanets M, Zurbrügg C, Swartz C, Pronk W. Decentralized systems for potable water and the potential of membrane technology. Water Research 2009;43:245–65. https://doi.org///doi.org/10.1016/j.watres.2008.10.030.
[120] Ja-Young K, Nowon K. Composite polyamide reverse osmosis membrane and method of producing the same. US6015495A, 1998.
[121] Yu C, Li H, Zhang X, Lü Z, Yu S, Liu M, et al. Polyamide thin-film composite membrane fabricated through interfacial polymerization coupled with surface amidation for improved reverse osmosis performance. Journal of Membrane Science 2018;566:87–95. https://doi.org/https://doi.org/10.1016/j.memsci.2018.09.012.
[122] Park S-J, Kwon SJ, Kwon H-E, Shin MG, Park S-H, Park H, et al. Aromatic solvent-assisted interfacial polymerization to prepare high performance thin film composite reverse osmosis membranes based on hydrophilic supports. Polymer (Guildf) 2018;144:159–67. https://doi.org/https://doi.org/10.1016/j.polymer.2018.04.060.
[123] Hailemariam RH, Woo YC, Damtie MM, Kim BC, Park K-D, Choi J-S. Reverse osmosis membrane fabrication and modification technologies and future trends: A review. Advances in Colloid and Interface Science 2020;276:102100. https://doi.org/https://doi.org/10.1016/j.cis.2019.102100.
[124] Van Wagner EM, Sagle AC, Sharma MM, Freeman BD. Effect of crossflow testing conditions, including feed pH and continuous feed filtration, on commercial reverse osmosis membrane performance. Journal of Membrane Science 2009;345:97–109. https://doi.org/https://doi.org/10.1016/j.memsci.2009.08.033.
[125] Management SS and W. Rapid Sand Filtration 2012;2017. https://www.sswm.info/category/implementation-tools/water-purification/hardware/semi-centralised-drinking-water-treatme-14.
[126] Han S, Fitzpatrick CSB, Wetherill A. The impact of flow surges on rapid gravity filtration. Water Research 2009;43:1171–8. https://doi.org///doi.org/10.1016/j.watres.2008.12.003.
[127] Marín Galvín R. Ripening of silica sand used for filtration. Water Research 1992;26:683–8. https://doi.org///doi.org/10.1016/0043-1354(92)90245-Y.
[128] Vries D, Bertelkamp C, Schoonenberg Kegel F, Hofs B, Dusseldorp J, Bruins JH, et al. Iron and manganese removal: Recent advances in modelling treatment efficiency by rapid sand filtration. Water Research 2017;109:35–45. https://doi.org///doi.org/10.1016/j.watres.2016.11.032.
[129] Gude JCJ, Rietveld LC, van Halem D. Biological As(III) oxidation in rapid sand filters. Journal of Water Process Engineering 2018;21:107–15. https://doi.org/https://doi.org/10.1016/j.jwpe.2017.12.003.
[130] Huangfu X, Ma C, Ma J, He Q, Yang C, Zhou J, et al. Effective removal of trace thallium from surface water by nanosized manganese dioxide enhanced quartz sand filtration. Chemosphere 2017;189:1–9. https://doi.org/https://doi.org/10.1016/j.chemosphere.2017.09.039.
[131] Gude JCJ, Joris K, Huysman K, Rietveld LC, van Halem D. Effect of supernatant water level on As removal in biological rapid sand filters. Water Research X 2018;1:100013. https://doi.org/https://doi.org/10.1016/j.wroa.2018.100013.
[132] Ranjan R, Megarajan S, Xavier B, Raju SS, Ghosh S, Gopalakrishnan A. Design and performance of recirculating aquaculture system for marine finfish broodstock development. Aquacultural Engineering 2019;85:90–7. https://doi.org/https://doi.org/10.1016/j.aquaeng.2019.03.002.
[133] Bland Alvarez, Claudia , Kim, Young-Gurl , Mitchell, TJ , Ruiz, Javier , Soberanis, Luis , Young, Preston L. Sustainable Community Development – Water Slow-Sand Filtration 2008;2017. https://cfpub.epa.gov/ncer_abstracts/index.cfm/fuseaction/display.highlight/abstract/8625/report/.
[134] Muhammad N. Removal of heavy metals by slow sand filtration. Loughborough University, 1998.
[135] Husiman L, Wood WE. Slow Sand Filtration. Geneva: World Health Organisation; 1974.
[136] Schmidt K. Behaviour of special pollutants in slow sand filters used in artificial recharge of ground-water 1977.
[137] D'Alessio M, Yoneyama B, Kirs M, Kisand V, Ray C. Pharmaceutically active compounds: Their removal during slow sand filtration and their impact on slow sand filtration bacterial removal. Science of the Total Environment 2015;524–525:124–35. https://doi.org/10.1016/j.scitotenv.2015.04.014.
[138] Khengaoui K, Mahammed MH, Touil Y, Amrane A. Influence of Secondary Salinity Wastewater on the Efficiency of Biological Treatment of Sand Filter. Energy Procedia 2015;74:398–403. https://doi.org/10.1016/j.egypro.2015.07.636.
[139] Eisazadeh A, Eisazadeh H, Kassim KA. Removal of Pb(II) using polyaniline composites and iron oxide

coated natural sand and clay from aqueous solution. Synthetic Metals 2013;171:56–61. https://doi.org/https://doi.org/10.1016/j.synthmet.2013.03.014.

[140] Smith K, Li Z, Chen B, Liang H, Zhang X, Xu R, et al. Comparison of sand-based water filters for point-of-use arsenic removal in China. Chemosphere 2017;168:155–62. https://doi.org/https://doi.org/10.1016/j.chemosphere.2016.10.021.

[141] Chaudhry SA, Khan TA, Ali I. Equilibrium, kinetic and thermodynamic studies of Cr(VI) adsorption from aqueous solution onto manganese oxide coated sand grain (MOCSG). Journal of Molecular Liquids 2017;236:320–30. https://doi.org/https://doi.org/10.1016/j.molliq.2017.04.029.

[142] Wang W, Shao Z, Liu Y, Wang G. Removal of multi-heavy metals using biogenic manganese oxides generated by a deep-sea sedimentary bacterium – Brachybacterium sp. strain Mn32. Microbiology 2009;155:1989–96. https://doi.org/https://doi.org/10.1099/mic.0.024141-0.

[143] Elliott MA, Stauber CE, Koksal F, DiGiano FA, Sobsey MD. Reductions of E. coli, echovirus type 12 and bacteriophages in an intermittently operated household-scale slow sand filter. Water Research 2008;42:2662–70. https://doi.org/https://doi.org/10.1016/j.watres.2008.01.016.

[144] Sabogal-Paz LP, Campos LC, Bogush A, Canales M. Household slow sand filters in intermittent and continuous flows to treat water containing low mineral ion concentrations and Bisphenol A. Science of the Total Environment 2020;702:135078. https://doi.org/https://doi.org/10.1016/j.scitotenv.2019.135078.

[145] Sizirici B, Yildiz I, AlAli A, Alkhemeiri A, Alkhoori A, Bufalasa F, et al. Modified biosand filters enriched with iron oxide coated gravel to remove chemical, organic and bacteriological contaminants. Journal of Water Process Engineering 2019;27:110–9. https://doi.org/https://doi.org/10.1016/j.jwpe.2018.11.015.

[146] Maeng M, Choi E, Dockko S. Reduction of organic matter in drinking water using a hybrid system combined with a rock biofilter and membrane in developing countries. Int Biodeterior Biodegradation 2015;102:223–30. https://doi.org/https://doi.org/10.1016/j.ibiod.2015.02.005.

[147] Li J, Zhou Q, Campos LC. The application of GAC sandwich slow sand filtration to remove pharmaceutical and personal care products. Science of the Total Environment 2018;635:1182–90. https://doi.org/https://doi.org/10.1016/j.scitotenv.2018.04.198.

[148] Grace MA, Healy MG, Clifford E. Performance and surface clogging in intermittently loaded and slow sand filters containing novel media. Journal of Environmental Management 2016;180:102–10. https://doi.org/https://doi.org/10.1016/j.jenvman.2016.05.018.

[149] Shin G-A, Kim T-Y, Kim H-S, Maeng M-S, Dockko S. Membrane hybrid system combined with a trickling filter and a thin layer of biosand to reduce high levels of organic matter in drinking water in developing countries. Process Safety and Environmental Protection 2016;104:541–8. https://doi.org/https://doi.org/10.1016/j.psep.2016.06.032.

[150] West J. Extractable global resources and the future availability of metal stocks: “Known Unknowns” for the foreseeable future. Resources Policy 2020;65:101574. https://doi.org/https://doi.org/10.1016/j.resourpol.2019.101574.

[151] Schrijvers D, Hool A, Blengini GA, Chen W-Q, Dewulf J, Eggert R, et al. A review of methods and data to determine raw material criticality. Resources, Conservation and Recycling 2020;155:104617. https://doi.org/https://doi.org/10.1016/j.resconrec.2019.104617.

[152] Altmann J, Rehfeld D, Traeder K, Sperlich A, Jekel M. Combination of granular activated carbon adsorption and deep-bed filtration as a single advanced wastewater treatment step for organic micropollutant and phosphorus removal. Water Research 2016;92:131–9. https://doi.org/10.1016/j.watres.2016.01.051.

[153] Genç-Fuhrman H, Bregnhøj H, McConchie D. Arsenate removal from water using sand–red mud columns. Water Research 2005;39:2944–54. https://doi.org/https://doi.org/10.1016/j.watres.2005.04.050.

[154] Genç-Fuhrman H, Mikkelsen PS, Ledin A. Simultaneous removal of As, Cd, Cr, Cu, Ni and Zn from stormwater: Experimental comparison of 11 different sorbents. Water Research 2007;41:591–602. https://doi.org/https://doi.org/10.1016/j.watres.2006.10.024.

[155] Arena N, Lee J, Clift R. Life Cycle Assessment of activated carbon production from coconut shells. Journal of Cleaner Production 2016;125:68–77. https://doi.org///doi.org/10.1016/j.jclepro.2016.03.073.

[156] De Silva F. Activated Carbon Filtration 2000;2017. http://www.watertreatmentguide.com/activated_carbon_filtration.htm.

[157] EPA US. Granular Activated Carbon 2011;2017. https://iaspub.epa.gov/tdb/pages/treatment/treatmentOverview.do?treatmentProcessId=2074826383.

[158] Shanmuganathan S, Loganathan P, Kazner C, Johir MAH, Vigneswaran S. Submerged membrane filtration adsorption hybrid system for the removal of organic micropollutants from a water reclamation plant reverse osmosis concentrate. Desalination 2017;401:134–41. https://doi.org///doi.org/10.1016/j.desal.2016.07.048.

[159] Yang Y, Zhang Y, Li Z, Zhao Z, Quan X, Zhao Z. Adding granular activated carbon into anaerobic sludge digestion to promote methane production and sludge decomposition. Journal of Cleaner Production 2017;149:1101–8. https://doi.org///doi.org/10.1016/j.jclepro.2017.02.156.

[160] Zhang J, Zhang L, Loh K-C, Dai Y, Tong YW. Enhanced anaerobic digestion of food waste by adding activated carbon: Fate of bacterial pathogens and antibiotic resistance genes. Biochemical Engineering Journal 2017;128:19–25. https://doi.org///doi.org/10.1016/j.bej.2017.09.004.

[161] Mamun MR Al, Karim MR, Rahman MM, Asiri AM, Torii S. Methane enrichment of biogas by carbon dioxide fixation with calcium hydroxide and activated carbon. Journal of the Taiwan Institute of Chemical Engineers 2016;58:476–81. https://doi.org///doi.org/10.1016/j.jtice.2015.06.029.

[162] Zietzschmann F, Stuetzer C, Jekel M. Granular activated carbon adsorption of organic micro-pollutants in drinking water and treated wastewater - Aligning breakthrough curves and capacities. Water Research 2016;92:180–7. https://doi.org/10.1016/j.watres.2016.01.056.

[163] Monnot M, Laborie S, Cabassud C. Granular activated carbon filtration plus ultrafiltration as a pretreatment to seawater desalination lines: Impact on water quality and UF fouling. Desalination 2016;383:1–11. https://doi.org/10.1016/j.desal.2015.12.010.

[164] Mazarji M, Aminzadeh B, Baghdadi M, Bhatnagar A. Removal of nitrate from aqueous solution using modified granular activated carbon. Journal of Molecular Liquids 2017;233:139–48. https://doi.org/https://doi.org/10.1016/j.molliq.2017.03.004.

[165] AbuDalo MA, Nevostrueva S, Hernandez MT. Enhanced Copper (II) Removal from Acidic Water By Granular Activated Carbon Impregnated with Carboxybenzotriazole. APCBEE Procedia 2013;5:64–8. https://doi.org/https://doi.org/10.1016/j.apcbee.2013.05.012.

[166] Enniya I, Rghioui L, Jourani A. Adsorption of hexavalent chromium in aqueous solution on activated carbon prepared from apple peels. Sustainable Chemistry and Pharmacy 2018;7:9–16. https://doi.org/https://doi.org/10.1016/j.scp.2017.11.003.

[167] Renu MA, Singh K, Upadhyaya S, Dohare RK. Removal of heavy metals from wastewater using modified agricultural adsorbents. Materials Today Proceedings 2017;4:10534–8. https://doi.org/https://doi.org/10.1016/j.matpr.2017.06.415.

[168] Guo Z, Zhang J, Kang Y, Liu H. Rapid and efficient removal of Pb(II) from aqueous solutions using biomass-derived activated carbon with humic acid in-situ modification. Ecotoxicology and Environmental Safety 2017;145:442–8. https://doi.org/https://doi.org/10.1016/j.ecoenv.2017.07.061.

[169] Kårelid V, Larsson G, Björlenius B. Pilot-scale removal of pharmaceuticals in municipal wastewater: Comparison of granular and powdered activated carbon treatment at three wastewater treatment plants. Journal of Environmental Management 2017;193:491–502. https://doi.org/https://doi.org/10.1016/j.jenvman.2017.02.042.

[170] Song JY, Bhadra BN, Jhung SH. Contribution of H-bond in adsorptive removal of pharmaceutical and personal care products from water using oxidized activated carbon. Microporous and Mesoporous Materials 2017;243:221–8. https://doi.org/https://doi.org/10.1016/j.micromeso.2017.02.024.

[171] Katsigiannis A, Noutsopoulos C, Mantziaras J, Gioldasi M. Removal of emerging pollutants through Granular Activated Carbon. Chemical Engineering Journal 2015;280:49–57. https://doi.org/https://doi.org/10.1016/j.cej.2015.05.109.

[172] Aqsolutions. 300 Liter per Day Water Treatment System 2016:1–12. http://www.aqsolutions.org/images/2016/02/blue-barrel-system-manual-English.pdf (accessed January 12, 2018).

[173] Ni B-J, Huang Q-S, Wang C, Ni T-Y, Sun J, Wei W. Competitive adsorption of heavy metals in aqueous solution onto biochar derived from anaerobically digested sludge. Chemosphere 2019;219:351–7. https://doi.org/https://doi.org/10.1016/j.chemosphere.2018.12.053.

[174] Xiao F, Cheng J, Cao W, Yang C, Chen J, Luo Z. Removal of heavy metals from aqueous solution using chitosan-combined magnetic biochars. Journal of Colloid and Interface Science 2019;540:579–84. https://doi.org/https://doi.org/10.1016/j.jcis.2019.01.068.

[175] Wang Y, Liu R. H2O2 treatment enhanced the heavy metals removal by manure biochar in aqueous solutions. Science of the Total Environment 2018;628–629:1139–48. https://doi.org/https://doi.org/10.1016/j.scitotenv.2018.02.137.

[176] Yang J, Li H, Zhang D, Wu M, Pan B. Limited role of biochars in nitrogen fixation through nitrate

adsorption. Science of the Total Environment 2017;592:758–65. https://doi.org/https://doi.org/10.1016/j.scitotenv.2016.10.182.

[177] Yin Q, Ren H, Wang R, Zhao Z. Evaluation of nitrate and phosphate adsorption on Al-modified biochar: Influence of Al content. Science of the Total Environment 2018;631–632:895–903. https://doi.org/https://doi.org/10.1016/j.scitotenv.2018.03.091.

[178] Cederlund H, Börjesson E, Stenström J. Effects of a wood-based biochar on the leaching of pesticides chlorpyrifos, diuron, glyphosate and MCPA. Journal of Environmental Management 2017;191:28–34. https://doi.org/https://doi.org/10.1016/j.jenvman.2017.01.004.

[179] Kim S, Park CM, Jang A, Jang M, Hernández-Maldonado AJ, Yu M, et al. Removal of selected pharmaceuticals in an ultrafiltration-activated biochar hybrid system. Journal of Membrane Science 2019;570–571:77–84. https://doi.org/https://doi.org/10.1016/j.memsci.2018.10.036.

[180] Lau AYT, Tsang DCW, Graham NJD, Ok YS, Yang X, Li X. Surface-modified biochar in a bioretention system for Escherichia coli removal from stormwater. Chemosphere 2017;169:89–98. https://doi.org/https://doi.org/10.1016/j.chemosphere.2016.11.048.

[181] Wang L, Wang Y, Ma F, Tankpa V, Bai S, Guo X, et al. Mechanisms and reutilization of modified biochar used for removal of heavy metals from wastewater: A review. Science of the Total Environment 2019;668:1298–309. https://doi.org/https://doi.org/10.1016/j.scitotenv.2019.03.011.

[182] Xu D, Cao J, Li Y, Howard A, Yu K. Effect of pyrolysis temperature on characteristics of biochars derived from different feedstocks: A case study on ammonium adsorption capacity. Waste Management 2019;87:652–60. https://doi.org/https://doi.org/10.1016/j.wasman.2019.02.049.

[183] Zhang P, Li Y, Cao Y, Han L. Characteristics of tetracycline adsorption by cow manure biochar prepared at different pyrolysis temperatures. Bioresource Technology 2019;285:121348. https://doi.org/https://doi.org/10.1016/j.biortech.2019.121348.

[184] Sewu DD, Jung H, Kim SS, Lee DS, Woo SH. Decolorization of cationic and anionic dye-laden wastewater by steam-activated biochar produced at an industrial-scale from spent mushroom substrate. Bioresource Technology 2019;277:77–86. https://doi.org/https://doi.org/10.1016/j.biortech.2019.01.034.

[185] Chen S, Qin C, Wang T, Chen F, Li X, Hou H, et al. Study on the adsorption of dyestuffs with different properties by sludge-rice husk biochar: Adsorption capacity, isotherm, kinetic, thermodynamics and mechanism. Journal of Molecular Liquids 2019;285:62–74. https://doi.org/https://doi.org/10.1016/j.molliq.2019.04.035.

[186] Cataldo S, Chiodo V, Crea F, Maisano S, Milea D, Pettignano A. Biochar from byproduct to high value added material – A new adsorbent for toxic metal ions removal from aqueous solutions. Journal of Molecular Liquids 2018;271:481–9. https://doi.org/https://doi.org/10.1016/j.molliq.2018.09.009.

[187] Li L, Zou D, Xiao Z, Zeng X, Zhang L, Jiang L, et al. Biochar as a sorbent for emerging contaminants enables improvements in waste management and sustainable resource use. Journal of Cleaner Production 2019;210:1324–42. https://doi.org/https://doi.org/10.1016/j.jclepro.2018.11.087.

[188] R. S, K. R. Influence of temperature on yield, composition and properties of the sub-fractions derived from slow pyrolysis of Calophyllum inophyllum de-oiled cake. Journal of Analytical and Applied Pyrolysis 2017;127:159–69. https://doi.org/https://doi.org/10.1016/j.jaap.2017.08.012.

[189] Zhang H, Chen C, Gray EM, Boyd SE. Effect of feedstock and pyrolysis temperature on properties of biochar governing end use efficacy. Biomass and Bioenergy 2017;105:136–46. https://doi.org/https://doi.org/10.1016/j.biombioe.2017.06.024.

[190] Sfakiotakis S, Vamvuka D. Thermal decomposition behavior, characterization and evaluation of pyrolysis products of agricultural wastes. Journal of the Energy Institute 2018;91:951–61. https://doi.org/https://doi.org/10.1016/j.joei.2017.09.001.

[191] Liu R, Liu G, Yousaf B, Abbas Q. Operating conditions-induced changes in product yield and characteristics during thermal-conversion of peanut shell to biochar in relation to economic analysis. Journal of Cleaner Production 2018;193:479–90. https://doi.org/https://doi.org/10.1016/j.jclepro.2018.05.034.

[192] Ibn Ferjani A, Jeguirim M, Jellali S, Limousy L, Courson C, Akrout H, et al. The use of exhausted grape marc to produce biofuels and biofertilizers: Effect of pyrolysis temperatures on biochars properties. Renewable and Sustainable Energy Reviews 2019;107:425–33. https://doi.org/https://doi.org/10.1016/j.rser.2019.03.034.

[193] Zhu K, Wang X, Geng M, Chen D, Lin H, Zhang H. Catalytic oxidation of clofibric acid by peroxydisulfate activated with wood-based biochar: Effect of biochar pyrolysis temperature, performance and mechanism. Chemical Engineering Journal 2019;374:1253–63.

https://doi.org/https://doi.org/10.1016/j.cej.2019.06.006.
[194] Zhang Y, Xu X, Cao L, Ok YS, Cao X. Characterization and quantification of electron donating capacity and its structure dependence in biochar derived from three waste biomasses. Chemosphere 2018;211:1073–81. https://doi.org/https://doi.org/10.1016/j.chemosphere.2018.08.033.
[195] Chu G, Zhao J, Liu Y, Lang D, Wu M, Pan B, et al. The relative importance of different carbon structures in biochars to carbamazepine and bisphenol A sorption. Journal of Hazardous Materials 2019;373:106–14. https://doi.org/https://doi.org/10.1016/j.jhazmat.2019.03.078.
[196] Zhang C, Shan B, Jiang S, Tang W. Effects of the pyrolysis temperature on the biotoxicity of Phyllostachys pubescens biochar in the aquatic environment. Journal of Hazardous Materials 2019;376:48–57. https://doi.org/https://doi.org/10.1016/j.jhazmat.2019.05.010.
[197] Jung K-W, Kim K, Jeong T-U, Ahn K-H. Influence of pyrolysis temperature on characteristics and phosphate adsorption capability of biochar derived from waste-marine macroalgae (Undaria pinnatifida roots). Bioresource Technology 2016;200:1024–8. https://doi.org/https://doi.org/10.1016/j.biortech.2015.10.016.
[198] Li J, Cao L, Yuan Y, Wang R, Wen Y, Man J. Comparative study for microcystin-LR sorption onto biochars produced from various plant- and animal-wastes at different pyrolysis temperatures: Influencing mechanisms of biochar properties. Bioresource Technology 2018;247:794–803. https://doi.org/https://doi.org/10.1016/j.biortech.2017.09.120.
[199] Li S, Chen G. Thermogravimetric, thermochemical, and infrared spectral characterization of feedstocks and biochar derived at different pyrolysis temperatures.Waste Management 2018;78:198–207. https://doi.org/https://doi.org/10.1016/j.wasman.2018.05.048.
[200] Chandra S, Bhattacharya J. Influence of temperature and duration of pyrolysis on the property heterogeneity of rice straw biochar and optimization of pyrolysis conditions for its application in soils. Journal of Cleaner Production 2019;215:1123–39. https://doi.org/https://doi.org/10.1016/j.jclepro.2019.01.079.
[201] Zhang J, Liu J, Liu R. Effects of pyrolysis temperature and heating time on biochar obtained from the pyrolysis of straw and lignosulfonate. Bioresource Technology 2015;176:288–91. https://doi.org/https://doi.org/10.1016/j.biortech.2014.11.011.
[202] Huang H, Yao W, Li R, Ali A, Du J, Guo D, et al. Effect of pyrolysis temperature on chemical form, behavior and environmental risk of Zn, Pb and Cd in biochar produced from phytoremediation residue. Bioresource Technology 2018;249:487–93. https://doi.org/https://doi.org/10.1016/j.biortech.2017.10.020.
[203] Chen G, Zhang Z, Zhang Z, Zhang R. Redox-active reactions in denitrification provided by biochars pyrolyzed at different temperatures. Science of the Total Environment 2018;615:1547–56. https://doi.org/https://doi.org/10.1016/j.scitotenv.2017.09.125.
[204] Chen T, Zhang Y, Wang H, Lu W, Zhou Z, Zhang Y, et al. Influence of pyrolysis temperature on characteristics and heavy metal adsorptive performance of biochar derived from municipal sewage sludge. Bioresource Technology 2014;164:47–54. https://doi.org/https://doi.org/10.1016/j.biortech.2014.04.048.
[205] Tag AT, Duman G, Ucar S, Yanik J. Effects of feedstock type and pyrolysis temperature on potential applications of biochar. Journal of Analytical and Applied Pyrolysis 2016;120:200–6. https://doi.org/https://doi.org/10.1016/j.jaap.2016.05.006.
[206] Pröll T, Afif R Al, Schaffer S, Pfeifer C. Reduced Local Emissions and Long-term Carbon Storage through Pyrolysis of Agricultural Waste and Application of Pyrolysis Char for Soil Improvement. Energy Procedia 2017;114:6057–66. https://doi.org/https://doi.org/10.1016/j.egypro.2017.03.1742.
[207] Ma Z, Yang Y, Ma Q, Zhou H, Luo X, Liu X, et al. Evolution of the chemical composition, functional group, pore structure and crystallographic structure of bio-char from palm kernel shell pyrolysis under different temperatures. Journal of Analytical and Applied Pyrolysis 2017;127:350–9. https://doi.org/https://doi.org/10.1016/j.jaap.2017.07.015.
[208] Li M, Tang Y, Ren N, Zhang Z, Cao Y. Effect of mineral constituents on temperature-dependent structural characterization of carbon fractions in sewage sludge-derived biochar. Journal of Cleaner Production 2018;172:3342–50. https://doi.org/https://doi.org/10.1016/j.jclepro.2017.11.090.
[209] Qian L, Chen B. Interactions of Aluminum with Biochars and Oxidized Biochars: Implications for the Biochar Aging Process. Journal of Agricultural and Food Chemistry 2014;62:373–80. https://doi.org/10.1021/jf404624h.
[210] Zhang J, Fu H, Lv X, Tang J, Xu X. Removal of Cu(II) from aqueous solution using the rice husk carbons prepared by the physical activation process. Biomass and Bioenergy 2011;35:464–72.

https://doi.org/https://doi.org/10.1016/j.biombioe.2010.09.002.
[211] Vithanage M, Ashiq A, Ramanayaka S, Bhatnagar A. Implications of layered double hydroxides assembled biochar composite in adsorptive removal of contaminants: Current status and future perspectives. Science of the Total Environment 2020;737:139718. https://doi.org/https://doi.org/10.1016/j.scitotenv.2020.139718.
[212] Khan ZH, Gao M, Qiu W, Song Z. Properties and adsorption mechanism of magnetic biochar modified with molybdenum disulfide for cadmium in aqueous solution. Chemosphere 2020;255:126995. https://doi.org/https://doi.org/10.1016/j.chemosphere.2020.126995.
[213] Varela-Álvarez A, Haines BE, Musaev DG. Key mechanistic insights into the intramolecular C-H bond amination and double bond aziridination in sulfamate esters catalyzed by dirhodium tetracarboxylate complexes. Journal of Organometallic Chemistry 2018;867:183–92. https://doi.org/https://doi.org/10.1016/j.jorganchem.2017.12.013.
[214] Zhuang W-R, Wang Y, Cui P-F, Xing L, Lee J, Kim D, et al. Applications of π-π stacking interactions in the design of drug-delivery systems. Journal of Controlled Release 2019;294:311–26. https://doi.org/https://doi.org/10.1016/j.jconrel.2018.12.014.
[215] Kazak O, Eker YR, Akin I, Bingol H, Tor A. A novel red mud@sucrose based carbon composite: Preparation, characterization and its adsorption performance toward methylene blue in aqueous solution. Journal of Environmental Chemical Engineering 2017;5:2639–47. https://doi.org/https://doi.org/10.1016/j.jece.2017.05.018.
[216] Zhao Z, Zhou W. Insight into interaction between biochar and soil minerals in changing biochar properties and adsorption capacities for sulfamethoxazole. Environmental Pollution 2019;245:208–17. https://doi.org/https://doi.org/10.1016/j.envpol.2018.11.013.
[217] Zhang H, Yue X, Li F, Xiao R, Zhang Y, Gu D. Preparation of rice straw-derived biochar for efficient cadmium removal by modification of oxygen-containing functional groups. Science of the Total Environment 2018;631–632:795–802. https://doi.org/https://doi.org/10.1016/j.scitotenv.2018.03.071.
[218] Hu X, Zhang X, Ngo HH, Guo W, Wen H, Li C, et al. Comparison study on the ammonium adsorption of the biochars derived from different kinds of fruit peel. Science of the Total Environment 2020;707:135544. https://doi.org/https://doi.org/10.1016/j.scitotenv.2019.135544.
[219] Fan Q, Sun J, Chu L, Cui L, Quan G, Yan J, et al. Effects of chemical oxidation on surface oxygen-containing functional groups and adsorption behavior of biochar. Chemosphere 2018;207:33–40. https://doi.org/https://doi.org/10.1016/j.chemosphere.2018.05.044.
[220] Wu Y, Chen B. Effect of fulvic acid coating on biochar surface structure and sorption properties towards 4-chlorophenol. Science of the Total Environment 2019;691:595–604. https://doi.org/https://doi.org/10.1016/j.scitotenv.2019.06.501.
[221] Tan Z, Yuan S, Hong M, Zhang L, Huang Q. Mechanism of negative surface charge formation on biochar and its effect on the fixation of soil Cd. Journal of Hazardous Materials 2020;384:121370. https://doi.org/https://doi.org/10.1016/j.jhazmat.2019.121370.
[222] Dai L, Zhu W, He L, Tan F, Zhu N, Zhou Q, et al. Calcium-rich biochar from crab shell: An unexpected super adsorbent for dye removal. Bioresource Technology 2018;267:510–6. https://doi.org/https://doi.org/10.1016/j.biortech.2018.07.090.
[223] Plappally AK, Lienhard JH. Costs for water supply, treatment, end-use and reclamation. Desalin. Water Treat., Taylor & Francis Group; 2012, p. 1–33. https://doi.org/https://doi.org/10.1080/19443994.2012.708996.
[224] Guo Y, Niu G, Starman T, Volder A, Gu M. Poinsettia Growth and Development Response to Container Root Substrate with Biochar. Horticulturae 2018;4:1–14. https://doi.org/https://doi:10.3390/horticulturae4010001.
[225] Gwenzi W, Chaukura N, Noubactep C, Mukome FND. Biochar-based water treatment systems as a potential low-cost and sustainable technology for clean water provision. Journal of Environmental Management 2017;197:732–49. https://doi.org/https://doi.org/10.1016/j.jenvman.2017.03.087.
[226] Jirka S (International biochar initiaitve), Tomlinson T (International biochar initiative). 2013 State of the Biochar Industry. 2014.
[227] Mohan D, Kumar H, Sarswat A, Alexandre-Franco M, Pittman CU. Cadmium and lead remediation using magnetic oak wood and oak bark fast pyrolysis bio-chars. Chemical Engineering Journal 2014;236:513–28. https://doi.org/https://doi.org/10.1016/j.cej.2013.09.057.
[228] Kate S, Shuming L. Energy for Conventional Water Supply and Wastewater Treatment in Urban China: A Review. Glob Challenges 2017;1:1600016. https://doi.org/10.1002/gch2.201600016.
[229] Copeland C (Congressional RS, Carter NT (Congressional RS. Energy-Water Nexus: The Water Sector's

Energy Use. 2017.
[230] EEA. Performance of water utilities beyond compliance. 2014.
[231] Bartels CR, Andes K. Consideration of energy savings in SWRO. Desalination and Water Treatment 2013;51:717–25. https://doi.org/10.1080/19443994.2012.700038.
[232] Dore MHI, Singh RG, Khaleghi-Moghadam A, Achari G. Cost differentials and scale for newer water treatment technologies. International Journal of Water Resources and Environmental Engineering 2013;5:100–9. https://doi.org/https://doi.org/10.5897/IJWREE12.103.
[233] Bick A, Gillerman L, Manor Y, Oron G. Economic Assessment of an Integrated Membrane System for Secondary Effluent Polishing for Unrestricted Reuse. Water 2012;4:219–36. https://doi.org/https://doi.org/10.3390/w4010219.
[234] Banat F. Economic and Technical Assessment of Desalination Technologies n.d. https://www.desline.com/Geneva/Banat.pdf (accessed January 19, 2018).
[235] Energy and Capital. Water Desalination Investments 2009. https://www.energyandcapital.com/report/water-desalination-investments/426 (accessed January 19, 2018).
[236] Center for Disease Control and Prevention (CDC). Slow sand filtration 2014. https://www.cdc.gov/safewater/sand-filtration.html (accessed January 19, 2018).
[237] Moreira Neto RF, Calijuri ML, Carvalho I de C, Santiago A da F. Rainwater treatment in airports using slow sand filtration followed by chlorination: Efficiency and costs. Resources, Conservation and Recycling 2012;65:124–9. https://doi.org/https://doi.org/10.1016/j.resconrec.2012.06.001.
[238] Sanchez LD, Marin LM, Visscher JT, Rietveld LC. Low-cost multi-stage filtration enhanced by coagulation-flocculation in upflow gravel filtration. Drinking Water Engineering and Science 2012;5:73–85. https://doi.org/https://doi.org/10.5194/dwes-5-73-2012.
[239] Heinonen-Tanski H, Juntunen P, Haume E, Rajala R, Niemelä A. Costs of tertiary treatment of municipal wastewater by rapid sand filter with coagulants and UV. Water Sci Technol Water Supply 2003;3:145–52. https://doi.org/doi:10.1016/j.desal.2009.02.008.
[240] Mulder M. Costs of Removal of Micropollutants from Effluents of Municipal Wastewater Treatment Plants 2015:2–50. http://www.tapes-interreg.eu/uploads/Stowa TAPES Final report.pdf (accessed January 19, 2018).
[241] Ciabattia I, Cesaro F, Faralli L, Fatarella E, Tognotti F. Demonstration of a treatment system for purification and reuse of laundry wastewater. Desalination 2009;245:451–9. https://doi.org/https://doi.org/10.1016/j.desal.2009.02.008.
[242] Odonkor ST, Frimpong K, Kurantin N. An assessment of house-hold solid waste management in a large Ghanaian district. Heliyon 2020;6:e03040. https://doi.org/https://doi.org/10.1016/j.heliyon.2019.e03040.
[243] Stürmer B. Feedstock change at biogas plants – Impact on production costs. Biomass and Bioenergy 2017;98:228–35. https://doi.org/https://doi.org/10.1016/j.biombioe.2017.01.032.
[244] Mächtig T, Moschner CR, Hartung E. Monitoring the efficiency of biogas plants – Correlation between gross calorific value and anaerobically non-degradable organic matter of digestates. Biomass and Bioenergy 2019;130:105389. https://doi.org/https://doi.org/10.1016/j.biombioe.2019.105389.
[245] Yang L, Huang Y, Zhao M, Huang Z, Miao H, Xu Z, et al. Enhancing biogas generation performance from food wastes by high-solids thermophilic anaerobic digestion: Effect of pH adjustment. Int Biodeterior Biodegradation 2015;105:153–9. https://doi.org/https://doi.org/10.1016/j.ibiod.2015.09.005.
[246] Pramanik SK, Suja FB, Zain SM, Pramanik BK. The anaerobic digestion process of biogas production from food waste: Prospects and constraints. Bioresource Technology Reports 2019;8:100310. https://doi.org/https://doi.org/10.1016/j.biteb.2019.100310.
[247] Liu Z, Wang X, Wang F, Bai Z, Chadwick D, Misselbrook T, et al. The progress of composting technologies from static heap to intelligent reactor: Benefits and limitations. Journal of Cleaner Production 2020:122328. https://doi.org/https://doi.org/10.1016/j.jclepro.2020.122328.
[248] Yang Y, Kumar Awasthi M, bao H, Bie J, Lei S, Lv J. Exploring the microbial mechanisms of organic matter transformation during pig manure composting amended with bean dregs and biochar. Bioresource Technology 2020:123647. https://doi.org/https://doi.org/10.1016/j.biortech.2020.123647.
[249] Tai H-S, He W-H. A novel composting process for plant wastes in Taiwan military barracks. Resources, Conservation and Recycling 2007;51:408–17. https://doi.org/https://doi.org/10.1016/j.resconrec.2006.10.006.
[250] Chen X, Zhao Y, Zhao X, Wu J, Zhu L, Zhang X, et al. Selective pressures of heavy metals on microbial community determine microbial functional roles during composting: Sensitive, resistant and actor.

Journal of Hazardous Materials 2020;398:122858. https://doi.org/https://doi.org/10.1016/j.jhazmat.2020.122858.

[251] Storino F, Arizmendiarrieta JS, Irigoyen I, Muro J, Aparicio-Tejo PM. Meat waste as feedstock for home composting: Effects on the process and quality of compost.Waste Management 2016;56:53–62. https://doi.org/https://doi.org/10.1016/j.wasman.2016.07.004.

[252] Ashraf MS, Ghouleh Z, Shao Y. Production of eco-cement exclusively from municipal solid waste incineration residues. Resources, Conservation and Recycling 2019;149:332–42. https://doi.org/https://doi.org/10.1016/j.resconrec.2019.06.018.

[253] Neehaul N, Jeetah P, Deenapanray P. Energy recovery from municipal solid waste in Mauritius: Opportunities and challenges. Environmental Development 2020;33:100489. https://doi.org/https://doi.org/10.1016/j.envdev.2019.100489.

[254] Li H-Y, Gao P-P, Ni H-G. Emission characteristics of parent and halogenated PAHs in simulated municipal solid waste incineration. Science of the Total Environment 2019;665:11–7. https://doi.org/https://doi.org/10.1016/j.scitotenv.2019.02.002.

[255] Tong H, Shen Y, Zhang J, Wang C-H, Ge TS, Tong YW. A comparative life cycle assessment on four waste-to-energy scenarios for food waste generated in eateries. Applied Energy 2018;225:1143–57. https://doi.org/https://doi.org/10.1016/j.apenergy.2018.05.062.

[256] Bai X, Wang G, Zhu Z, Cai C, Wang Z, Wang D. Investigation of improving the yields and qualities of pyrolysis products with combination rod-milled and torrefaction pretreatment. Renewable Energy 2020;151:446–53. https://doi.org/https://doi.org/10.1016/j.renene.2019.11.040.

[257] Wang T, Li Y, Zhi D, Lin Y, He K, Liu B, et al. Assessment of combustion and emission behavior of corn straw biochar briquette fuels under different temperatures. Journal of Environmental Management 2019;250:109399. https://doi.org/https://doi.org/10.1016/j.jenvman.2019.109399.

[258] Rafiq MK, Bai Y, Aziz R, Rafiq MT, Mašek O, Bachmann RT, et al. Biochar amendment improves alpine meadows growth and soil health in Tibetan plateau over a three year period. Science of the Total Environment 2020;717:135296. https://doi.org/https://doi.org/10.1016/j.scitotenv.2019.135296.

[259] Dai Q, Jiang X, Jiang Y, Jin Y, Wang F, Chi Y, et al. Formation of PAHs during the pyrolysis of dry sewage sludge. Fuel 2014;130:92–9. https://doi.org/https://doi.org/10.1016/j.fuel.2014.04.017.

[260] Huang X, Wan Y, Shi B, Shi J. Effects of powdered activated carbon on the coagulation-flocculation process in humic acid and humic acid-kaolin water treatment. Chemosphere 2020;238:124637. https://doi.org/https://doi.org/10.1016/j.chemosphere.2019.124637.

[261] Sánchez López S, MacAdam J, Biddle M, Jarvis P. The impact of dosing sequence on the removal of the persistent pesticide metaldehyde using powdered activated carbon with coagulation and clarification. Journal of Water Process Engineering 2021;39:101756. https://doi.org/https://doi.org/10.1016/j.jwpe.2020.101756.

[262] Bukhary S, Batista J, Ahmad S. Design Aspects, Energy Consumption Evaluation, and Offset for Drinking Water Treatment Operation. Water 2020;12. https://doi.org/10.3390/w12061772.

[263] Buss W, Graham MC, MacKinnon G, Mašek O. Strategies for producing biochars with minimum PAH contamination. Journal of Analytical and Applied Pyrolysis 2016;119:24–30. https://doi.org/https://doi.org/10.1016/j.jaap.2016.04.001.

[264] Lyu H, He Y, Tang J, Hecker M, Liu Q, Jones PD, et al. Effect of pyrolysis temperature on potential toxicity of biochar if applied to the environment. Environmental Pollution 2016;218:1–7. https://doi.org/https://doi.org/10.1016/j.envpol.2016.08.014.

[265] Zhou H, Wu C, Onwudili JA, Meng A, Zhang Y, Williams PT. Influence of process conditions on the formation of 2–4 ring polycyclic aromatic hydrocarbons from the pyrolysis of polyvinyl chloride. Fuel Processing Technology 2016;144:299–304. https://doi.org/https://doi.org/10.1016/j.fuproc.2016.01.013.

[266] Group WB. Waste Composition 2012;2017. http://siteresources.worldbank.org/INTURBANDEVELOPMENT/Resources/336387-1334852610766/Chap5.pdf.

[267] Czech B, Kończak M, Rakowska M, Oleszczuk P. Engineered biochars from organic wastes for the adsorption of diclofenac, naproxen and triclosan from water systems. Journal of Cleaner Production 2021;288:125686. https://doi.org/https://doi.org/10.1016/j.jclepro.2020.125686.

[268] Kumar A, Singh E, Khapre A, Bordoloi N, Kumar S. Sorption of volatile organic compounds on non-activated biochar. Bioresource Technology 2020;297:122469. https://doi.org/https://doi.org/10.1016/j.biortech.2019.122469.

[269] Pan M, Lin X, Xie J, Huang X. Kinetic, equilibrium and thermodynamic studies for phosphate adsorption

on aluminum hydroxide modified palygorskite nano-composites. RSC Advances 2017;7:4492–500. https://doi.org/10.1039/C6RA26802A.

[270] Salam M, El-Shishtawy R, Obaid A. Synthesis of magnetic multi-walled carbon nanotubes/magnetite/chitin magnetic nanocomposite for the removal of Rose Bengal from real and model solution. Journal of Industrial and Engineering Chemistry 2014;20:3559–67. https://doi.org/10.1016/j.jiec.2013.12.049.

[271] Igwe JC, Mbonu OF, Abia AA. Sorption Kinetics, Intraparticle Diffusion and Equilibrium Partitioning of Azo Dyes on Great Millet (Andropogon sorghum) Waste Biomass. Journal of Applied Sciences 2007;7:2840–7. https://doi.org/10.3923/jas.2007.2840.2847.

[272] Patiha, Firdaus M, Wahyuningsih S, Nugrahaningtyas KD, Hidayat Y. Derivation and constants determination of the Freundlich and (fractal) Langmuir adsorption isotherms from kinetics. IOP Conference Series: Materials Science and Engineering 2018;333:12010. https://doi.org/10.1088/1757-899x/333/1/012010.

[273] Huang Y-T, Lee L-C, Shih M-C, Huang W-T. Introductory of Excel Spreadsheet for comparative analysis of linearized expressions of Langmuir isotherm for methylene blue onto rice husk. International Journal of Scientific and Research Publications 2019;9:p8587. https://doi.org/10.29322/IJSRP.9.01.2019.p8587.

[274] Santos P, Vicente K, Reis L, Marquardt L, Antonini Alves T. Modeling and experimental tests of a copper thermosyphon. Acta Scientiarum Technology 2017;39:59–68. https://doi.org/10.4025/actascitechnol.v39i1.28957.

[275] Yang H, Yan R, Chen H, Lee DH, Zheng C. Characteristics of hemicellulose, cellulose and lignin pyrolysis. Fuel 2007;86:1781–8. https://doi.org/https://doi.org/10.1016/j.fuel.2006.12.013.

[276] Jo J-H, Kim S-S, Shim J-W, Lee Y-E, Yoo Y-S. Pyrolysis Characteristics and Kinetics of Food Wastes. Energies 2017;10. https://doi.org/10.3390/en10081191.

[277] Vamvuka D, Dermitzakis S, Pentari D, Sfakiotakis S. Valorization of Meat and Bone Meal through pyrolysis for soil amendment or lead adsorption from wastewaters. Food and Bioproducts Processing 2018;109:148–57. https://doi.org/https://doi.org/10.1016/j.fbp.2018.04.002.

[278] Europlas. How does calcium carbonate filler benefit to the plastic industry? 2019. https://europlas.com.vn/calcium-carbonate-filler-benefit-plastic-industry/ (accessed February 8, 2021).

[279] Tyuftin AA, Kerry JP. Review of surface treatment methods for polyamide films for potential application as smart packaging materials: surface structure, antimicrobial and spectral properties. Food Packag Shelf Life 2020;24:100475. https://doi.org/https://doi.org/10.1016/j.fpsl.2020.100475.

[280] Seo YB, Ahn JH, Lee HL. Upgrading waste paper by in-situ calcium carbonate formation. Journal of Cleaner Production 2017;155:212–7. https://doi.org/https://doi.org/10.1016/j.jclepro.2016.09.003.

[281] Naijian F, Rudi H, Resalati H, Torshizi HJ. Application of bio-based modified kaolin clay engineered as papermaking additive for improving the properties of filled recycled papers. Applied Clay Science 2019;182:105258. https://doi.org/https://doi.org/10.1016/j.clay.2019.105258.

[282] Tomczyk A, Sokołowska Z, Boguta P. Biochar physicochemical properties: pyrolysis temperature and feedstock kind effects. Rev Environ Sci Bio/Technology 2020;19:191–215. https://doi.org/10.1007/s11157-020-09523-3.

[283] Štefušová K, Lovas M, Zubrik A, Matik M, Vaclavikova M. Removal of Cd2+ And Pb2+ from Aqueous Solutions Using Bio-Char Residues. Nova Biotechnologica et Chimica 2012;11:139–46. https://doi.org/10.2478/v10296-012-0016-x.

[284] Aracri E, Díaz Blanco C, Tzanov T. An enzymatic approach to develop a lignin-based adhesive for wool floor coverings. Green Chemistry 2014;16:2597–603. https://doi.org/10.1039/C4GC00063C.

[285] Michalak I, Baśladyńska S, Mokrzycki J, Rutkowski P. Biochar from A Freshwater Macroalga as A Potential Biosorbent for Wastewater Treatment. Water 2019;11. https://doi.org/10.3390/w11071390.

[286] Vagenas N V, Gatsouli A, Kontoyannis CG. Quantitative analysis of synthetic calcium carbonate polymorphs using FT-IR spectroscopy. Talanta 2003;59:831–6. https://doi.org/https://doi.org/10.1016/S0039-9140(02)00638-0.

[287] Liu S, Huang B, Chai L, Liu Y, Zeng G, Wang X, et al. Enhancement of As(v) adsorption from aqueous solution by a magnetic chitosan/biochar composite. RSC Advances 2017;7:10891–900. https://doi.org/10.1039/C6RA27341F.

[288] Philippou K, Konstantinou A, Pashalidis I. Thorium adsorption by oxidized biochar pine needles - the effect of particle size. Desalination and Water Treatment 2020;194:411–6. https://doi.org/10.5004/dwt.2020.25445.

[289] Xia S, Huang Y, Tang J, Wang L. Preparation of various thiol-functionalized carbon-based materials for enhanced removal of mercury from aqueous solution. Environmental Science and Pollution Research

2019;26:8709–20. https://doi.org/10.1007/s11356-019-04320-0.
[290] Ni M, Ratner BD. Differentiation of Calcium Carbonate Polymorphs by Surface Analysis Techniques - An XPS and TOF-SIMS study. Surface and Interface Analysis 2008;40:1356–61. https://doi.org/10.1002/sia.2904.
[291] Song X, Cao Y, Bu X, Luo X. Porous vaterite and cubic calcite aggregated calcium carbonate obtained from steamed ammonia liquid waste for Cu2+ heavy metal ions removal by adsorption process. Applied Surface Science 2021;536:147958. https://doi.org/https://doi.org/10.1016/j.apsusc.2020.147958.
[292] Eshun J, Wang L, Ansah E, Shahbazi A, Schimmel K, Kabadi V, et al. Characterization of the physicochemical and structural evolution of biomass particles during combined pyrolysis and CO2 gasification. Journal of the Energy Institute 2019;92:82–93. https://doi.org/https://doi.org/10.1016/j.joei.2017.11.003.
[293] Trakal L, Šigut R, Šillerová H, Faturíková D, Komárek M. Copper removal from aqueous solution using biochar: Effect of chemical activation. Arabian Journal of Chemistry 2014;7:43–52. https://doi.org/https://doi.org/10.1016/j.arabjc.2013.08.001.
[294] Jian X, Zhuang X, Li B, Xu X, Wei Z, Song Y, et al. Comparison of characterization and adsorption of biochars produced from hydrothermal carbonization and pyrolysis. Environmental Technology & Innovation 2018;10:27–35. https://doi.org/https://doi.org/10.1016/j.eti.2018.01.004.
[295] Tizo MS, Blanco LA V, Cagas ACQ, Dela Cruz BRB, Encoy JC, Gunting J V, et al. Efficiency of calcium carbonate from eggshells as an adsorbent for cadmium removal in aqueous solution. Sustainable Environment Research 2018;28:326–32. https://doi.org/https://doi.org/10.1016/j.serj.2018.09.002.
[296] Tomczyk A, Boguta P, Sokołowska Z. Biochar efficiency in copper removal from Haplic soils. International Journal of Environmental Science and Technology 2019;16:4899–912. https://doi.org/10.1007/s13762-019-02227-4.
[297] Fisher. Methylene Blue hydrate, 96+%, high purity biological stain, ACROS Organics™ n.d. https://www.fishersci.fi/shop/products/methylene-blue-hydrate-96-high-purity-biological-stain-acros-organics-1/10741891 (accessed February 9, 2021).
[298] Ambaye TG, Vaccari M, van Hullebusch ED, Amrane A, Rtimi S. Mechanisms and adsorption capacities of biochar for the removal of organic and inorganic pollutants from industrial wastewater. International Journal of Environmental Science and Technology 2020. https://doi.org/10.1007/s13762-020-03060-w.
[299] Zubair M, Mu'azu ND, Jarrah N, Blaisi NI, Aziz HA, A. Al-Harthi M. Adsorption Behavior and Mechanism of Methylene Blue, Crystal Violet, Eriochrome Black T, and Methyl Orange Dyes onto Biochar-Derived Date Palm Fronds Waste Produced at Different Pyrolysis Conditions. Water, Air, Soil Pollut 2020;231:240. https://doi.org/10.1007/s11270-020-04595-x.
[300] Zhou Y, Sun L, Wang H, Liang W, Yang J, Wang L, et al. Investigation on the uptake and release ability of β-cyclodextrin functionalized Fe3O4 magnetic nanoparticles by methylene blue. Materials Chemistry and Physics 2015;170. https://doi.org/10.1016/j.matchemphys.2015.12.022.
[301] Pourret O, Houben D. Characterization of metal binding sites onto biochar using rare earth elements as a fingerprint. Heliyon 2018;4:e00543. https://doi.org/https://doi.org/10.1016/j.heliyon.2018.e00543.
[302] Sigma-Aldrich. Tetracycline hydrochloride n.d.
[303] Caminati G, Puggelli M. Europium in phospholipid nanoscaffolds for the photophysical detection of antibiotic traces in solution. Eur Compd Prod Appl 2011:203–28.
[304] Liu M, Hou L, Yu S, Xi B, Zhao Y, Xia X. MCM-41 impregnated with A zeolite precursor: Synthesis, characterization and tetracycline antibiotics removal from aqueous solution. Chemical Engineering Journal 2013;223:678–687. https://doi.org/10.1016/j.cej.2013.02.088.
[305] Zhou J, Chen H, Thring RW, Arocena JM. Chemical Pretreatment of Rice Straw Biochar: Effect on Biochar Properties and Hexavalent Chromium Adsorption. International Journal of Environmental Research 2019;13:91–105. https://doi.org/10.1007/s41742-018-0156-1.
[306] Li G, Yuan Q, Khan AA. Effect of solution pH on the kinetic adsorption of tetracycline by la-modified magnetic bagasse biochar. Nature Environment and Pollution Technology 2019.
[307] Ghazy S, Samra S, El-Morsy S. Removal of Copper(II) from Aqueous Solutions by Flotation Using Limestone Fines as the Sorbent and Oleic Acid as the Surfactant. Adsorption Science & Technology - ADSORPT SCI TECHNOL 2001;19:175–85. https://doi.org/10.1260/0263617011494060.
[308] Hu H, Li X, Huang P, Zhang Q, Yuan W. Efficient removal of copper from wastewater by using mechanically activated calcium carbonate. Journal of Environmental Management 2017;203:1–7. https://doi.org/https://doi.org/10.1016/j.jenvman.2017.07.066.
[309] Higdon J, Drake VJ, Delage B. Copper. Corvallis, Oregon: 2014.
[310] Shabbir Z, Sardar A, Shabbir A, Abbas G, Shamshad S, Khalid S, et al. Copper uptake, essentiality, toxicity,

detoxification and risk assessment in soil-plant environment. Chemosphere 2020;259:127436. https://doi.org/https://doi.org/10.1016/j.chemosphere.2020.127436.

[311] Zhou X, Pu X-Y, Xiao X, Chen D, Wu C, Li X, et al. Observation on the changes of clinical symptoms, blood and brain copper deposition in Wilson disease patients treated with dimercaptosuccinic acid for 2 years. Journal of Clinical Neuroscience 2020;81:448–54. https://doi.org/https://doi.org/10.1016/j.jocn.2020.09.017.

[312] Pino L, Beltran E, Schwarz A, Ruiz MC, Borquez R. Optimization of nanofiltration for treatment of acid mine drainage and copper recovery by solvent extraction. Hydrometallurgy 2020;195:105361. https://doi.org/https://doi.org/10.1016/j.hydromet.2020.105361.

[313] da Costa GA, Lira JB, Freitas-Lopes R do L, Lopes UP. Tank mix application of copper hydroxide either with cyproconazole or pyraclostrobin fungicides reduced the control of coffee leaf rust. Crop Protection 2019;124:104856. https://doi.org/https://doi.org/10.1016/j.cropro.2019.104856.

[314] Schutte GC, Kotze C, Gideon van Zyl J, Fourie PH. Assessment of retention and persistence of copper fungicides on orange fruit and leaves using fluorometry and copper residue analyses. Crop Protection 2012;42:1–9. https://doi.org/https://doi.org/10.1016/j.cropro.2012.04.015.

[315] Wang Q-Y, Sun J-Y, Xu X-J, Yu H-W. Integration of chemical and toxicological tools to assess the bioavailability of copper derived from different copper-based fungicides in soil. Ecotoxicology and Environmental Safety 2018;161:662–8. https://doi.org/https://doi.org/10.1016/j.ecoenv.2018.06.041.

[316] WHO. Guidelines for Drinking Water Quality. Fourth. Geneva: 2017.

[317] DWI. What are the drinking water standards? London: 2017.

[318] DEFRA. Water Framework Directive implementation in England and Wales: new and updated standards to protect the water environment. 2014.

[319] Exploring Liability and the Polluter Pays Principle. York, United Kingdom: 2010.

[320] Song J, Messele SA, Meng L, Huang Z, Gamal El-Din M. Adsorption of metals from oil sands process water (OSPW) under natural pH by sludge-based Biochar/Chitosan composite. Water Research 2021;194:116930. https://doi.org/https://doi.org/10.1016/j.watres.2021.116930.

[321] Sahoo TR, Prelot B. Chapter 7 - Adsorption processes for the removal of contaminants from wastewater: the perspective role of nanomaterials and nanotechnology. In: Bonelli B, Freyria FS, Rossetti I, Sethi RBT-N for the D and R of WP, editors. Micro Nano Technol., Elsevier; 2020, p. 161–222. https://doi.org/https://doi.org/10.1016/B978-0-12-818489-9.00007-4.

[322] Waiapu Timothy McMillan O. Characteristics and mechanisms of atrazine sorption to biochar for land remediation. University of Cambridge, 2018.

[323] Yang Y, Lin X, Wei B, Zhao Y, Wang J. Evaluation of adsorption potential of bamboo biochar for metal-complex dye: equilibrium, kinetics and artificial neural network modeling. International Journal of Environmental Science and Technology 2014;11:1093–100. https://doi.org/10.1007/s13762-013-0306-0.

[324] Abu Al-Rub F, El-Naas M, Ashour I, Al-Marzouqi M. Biosorption of copper on Chlorella vulgaris from single, binary and ternary metal aqueous solutions. Process Biochemistry 2006;41:457–64.

[325] Hu X, Song J, Wang H, Zhang W, Wang B, Lyu W, et al. Adsorption of Cr(VI) and Cu(II) from aqueous solutions by biochar derived from Chaenomeles sinensis seed. Water Science and Technology 2020;80:2260–72. https://doi.org/10.2166/wst.2020.036.

[326] Danková Z, Bekényiová A, Štyriaková I, Fedorová E. Study of Cu(II) Adsorption by Siderite and Kaolin. Procedia Earth and Planetary Science 2015;15:821–6. https://doi.org/https://doi.org/10.1016/j.proeps.2015.08.131.

[327] Zhu Y, Fan W, Zhang K, Xiang H, Wang X. Nano-manganese oxides-modified biochar for efficient chelated copper citrate removal from water by oxidation-assisted adsorption process. Science of the Total Environment 2020;709:136154. https://doi.org/https://doi.org/10.1016/j.scitotenv.2019.136154.

[328] Liu J, Cheng W, Yang X, Bao Y. Modification of biochar with silicon by one-step sintering and understanding of adsorption mechanism on copper ions. Science of the Total Environment 2020;704:135252. https://doi.org/https://doi.org/10.1016/j.scitotenv.2019.135252.

[329] Puchana-Rosero MJ, Lima E, Mella B, Costa D, Poll E, Gutterres M. A COAGULATION-FLOCCULATION PROCESS COMBINED WITH ADSORPTION USING ACTIVATED CARBON OBTAINED FROM SLUDGE FOR DYE REMOVAL FROM TANNERY WASTEWATER. J Chil Chem Soc 2018;63:3867–74.

[330] Bu F, Zhou W, Yue Q, Liu C, Wang W, Shen X. The Combination of Coagulation and Adsorption for Controlling Ultra-Filtration Membrane Fouling in Water Treatment. Water 2019;11:90. https://doi.org/10.3390/w11010090.

[331] Rosińska A, Dąbrowska L. Enhancement of coagulation process with powdered activated carbon in PCB

and heavy metal ions removal from drinking water. Desalination and Water Treatment 2016;57:26336–44. https://doi.org/10.1080/19443994.2016.1189851.

[332] Lamborn J. Characterisation of municipal solid waste composition into model inputs 2009.

[333] Valério Filho A, Xavaré Kulman R, Vaz Tholozan L, Felkl de Almeida AR, Silveira da Rosa G. Preparation and Characterization of Activated Carbon Obtained from Water Treatment Plant Sludge for Removal of Cationic Dye from Wastewater. Process 2020;8. https://doi.org/10.3390/pr8121549.

[334] Open University O. Preliminary treatment 2007. https://www.open.edu/openlearn/science-maths-technology/engineering-and-technology/technology/potable-water-treatment/content-section-4.2 (accessed February 19, 2021).

[335] Assmuth E (Aaltu U. Performance of roadside filtration systems in the treatment of stormwater. Aaltu University, 2017.

[336] Payne EGI, McCarthy DT, Deletic A, Zhang K. Biotreatment technologies for stormwater harvesting: critical perspectives. Current Opinion in Biotechnology 2019;57:191–6. https://doi.org/https://doi.org/10.1016/j.copbio.2019.04.005.

[337] Chen SS, Tsang DCW, He M, Sun Y, Lau LSY, Leung RWM, et al. Designing sustainable drainage systems in subtropical cities: Challenges and opportunities. Journal of Cleaner Production 2021;280:124418. https://doi.org/https://doi.org/10.1016/j.jclepro.2020.124418.

[338] Baruah N, Gogoi N, Farooq M. Influence of biochar and organic soil amendments on bioavailability and immobilization of copper and lead to common cocklebur in acidic sandy loam soil. Journal of Environmental Chemical Engineering 2020;8:104480. https://doi.org/https://doi.org/10.1016/j.jece.2020.104480.

[339] Tedoldi D, Chebbo G, Pierlot D, Kovacs Y, Gromaire M-C. Impact of runoff infiltration on contaminant accumulation and transport in the soil/filter media of Sustainable Urban Drainage Systems: A literature review. Science of the Total Environment 2016;569–570:904–26. https://doi.org/10.1016/j.scitotenv.2016.04.215.

[340] Rehrah D, Bansode RR, Hassan O, Ahmedna M. Physico-chemical characterization of biochars from solid municipal waste for use in soil amendment. Journal of Analytical and Applied Pyrolysis 2016;118:42–53. https://doi.org/https://doi.org/10.1016/j.jaap.2015.12.022.

[341] Bartocci P, Bidini G, Saputo P, Fantozzi F. Biochar Pellet Carbon Footprint. Chemical Engineering Transactions 2016;50:217–22. https://doi.org/10.3303/CET1650037.

[342] Abdallah M, Elfeky A. Impact of waste processing byproducts on the carbon footprint of integrated waste-to-energy strategies. Journal of Environmental Management 2021;280:111839. https://doi.org/https://doi.org/10.1016/j.jenvman.2020.111839.

[343] Rathnayake D, Ehidiamhen PO, Egene CE, Stevens C V, Meers E, Mašek O, et al. Investigation of biomass and agricultural plastic co-pyrolysis: Effect on biochar yield and properties. Journal of Analytical and Applied Pyrolysis 2021;155:105029. https://doi.org/https://doi.org/10.1016/j.jaap.2021.105029.

[344] Jouhara H, Ahmad D, van den Boogaert I, Katsou E, Simons S, Spencer N. Pyrolysis of domestic based feedstock at temperatures up to 300 °C. Thermal Science and Engineering Progress 2018;5:117–43. https://doi.org/https://doi.org/10.1016/j.tsep.2017.11.007.

[345] Katiyar R, Patel AK, Nguyen T-B, Singhania RR, Chen C-W, Dong C-D. Adsorption of copper (II) in aqueous solution using biochars derived from Ascophyllum nodosum seaweed. Bioresource Technology 2021;328:124829. https://doi.org/https://doi.org/10.1016/j.biortech.2021.124829.

[346] Lee M-E, Park JH, Chung JW. Comparison of the lead and copper adsorption capacities of plant source materials and their biochars. Journal of Environmental Management 2019;236:118–24. https://doi.org/https://doi.org/10.1016/j.jenvman.2019.01.100.

[347] Ma J, Huang W, Zhang X, Li Y, Wang N. The utilization of lobster shell to prepare low-cost biochar for high-efficient removal of copper and cadmium from aqueous: Sorption properties and mechanisms. Journal of Environmental Chemical Engineering 2021;9:104703. https://doi.org/https://doi.org/10.1016/j.jece.2020.104703.

[348] Kumar Sakhiya A, Aier I, Pathak S, Anand A, Jha S, Vijay VK, et al. Copper(II) removal from aqua solution using rice straw derived biochar. Materials Today Proceedings 2021. https://doi.org/https://doi.org/10.1016/j.matpr.2020.12.953.

[349] Wang J, Zhao M, Zhang J, Zhao B, Lu X, Wei H. Characterization and utilization of biochars derived from five invasive plant species Bidens pilosa L., Praxelis clematidea, Ipomoea cairica, Mikania micrantha and Lantana camara L. for Cd2+ and Cu2+ removal. Journal of Environmental Management 2021;280:111746. https://doi.org/https://doi.org/10.1016/j.jenvman.2020.111746.

[350] Ehrampoush M, Moussavi G, Ghaneian M, Bbbbbbbbb A, Ahmadian M. Removal of Methylene Blue (MB)

Dye from Textile Synthetic Wastewater Using TiO 2 /UV-C Photocatalytic Process. Australian Journal of Basic and Applied Sciences 4(9):4579-4285 2010;4:4285–579.

[351] Krishna Moorthy A, Govindarajan Rathi B, Shukla SP, Kumar K, Shree Bharti V. Acute toxicity of textile dye Methylene blue on growth and metabolism of selected freshwater microalgae. Environmental Toxicology and Pharmacology 2021;82:103552. https://doi.org/https://doi.org/10.1016/j.etap.2020.103552.

[352] Lin L, Jiang W, Chen L, Xu P, Wang H. Treatment of Produced Water with Photocatalysis: Recent Advances, Affecting Factors and Future Research Prospects. Catalysts 2020;10. https://doi.org/10.3390/catal10080924.

[353] Moradi G, Zinadini S, Rajabi L. Development of high flux nanofiltration membrane using para-amino benzoate ferroxane nanoparticle for enhanced antifouling behavior and dye removal. Process Safety and Environmental Protection 2020;144:65–78. https://doi.org/https://doi.org/10.1016/j.psep.2020.06.044.

[354] Sanmartino JA, Khayet M, García-Payo MC, El-Bakouri H, Riaza A. Treatment of reverse osmosis brine by direct contact membrane distillation: Chemical pretreatment approach. Desalination 2017;420:79–90. https://doi.org/https://doi.org/10.1016/j.desal.2017.06.030.

[355] Onstad GD, Strauch S, Meriluoto J, Codd GA, von Gunten U. Selective Oxidation of Key Functional Groups in Cyanotoxins during Drinking Water Ozonation. Environmental Science and Technology 2007;41:4397–404. https://doi.org/10.1021/es0625327.

[356] Ikehata K, Jodeiri Naghashkar N, Gamal El-Din M. Degradation of Aqueous Pharmaceuticals by Ozonation and Advanced Oxidation Processes: A Review. Ozone Science and Engineering 2006;28:353–414. https://doi.org/10.1080/01919510600985937.

[357] Reyes-Miranda J, Garcia-Murillo A, Garrido-Hernández A, Carrillo-Romo F de J. Fast and mild alkaline solvothermal synthesis of nanostructured flower-like Na2Ti3O7 and its methylene blue adsorption capacity. Materials Letters 2021:129589. https://doi.org/https://doi.org/10.1016/j.matlet.2021.129589.

[358] Olusegun SJ, de Sousa Lima LF, Mohallem NDS. Enhancement of adsorption capacity of clay through spray drying and surface modification process for wastewater treatment. Chemical Engineering Journal 2018;334:1719–28. https://doi.org/https://doi.org/10.1016/j.cej.2017.11.084.

[359] Gokce Y, Yaglikci S, Yagmur E, Banford A, Aktas Z. Adsorption behaviour of high performance activated carbon from demineralised low rank coal (Rawdon) for methylene blue and phenol. Journal of Environmental Chemical Engineering 2021;9:104819. https://doi.org/https://doi.org/10.1016/j.jece.2020.104819.

[360] Do TH, Nguyen VT, Dung NQ, Chu MN, Van Kiet D, Ngan TTK, et al. Study on methylene blue adsorption of activated carbon made from Moringa oleifera leaf. Materials Today Proceedings 2021. https://doi.org/https://doi.org/10.1016/j.matpr.2020.10.834.

[361] Albalasmeh A, Gharaibeh MA, Mohawesh O, Alajlouni M, Quzaih M, Masad M, et al. Characterization and Artificial Neural Networks Modelling of methylene blue adsorption of biochar derived from agricultural residues: Effect of biomass type, pyrolysis temperature, particle size. Journal of Saudi Chemical Society 2020;24:811–23. https://doi.org/https://doi.org/10.1016/j.jscs.2020.07.005.

[362] Yang G, Wu L, Xian Q, Shen F, Wu J, Zhang Y. Removal of Congo Red and Methylene Blue from Aqueous Solutions by Vermicompost-Derived Biochars. PLoS One 2016;11:e0154562.

[363] Ahmad MA, AswarEusoff M, Oladoye PO, Adegok KA, Bell OS. Optimization and batch studies on adsorption of Methylene blue dye using pomegranate fruit peel based adsorbent. Chemical Data Collections 2021:100676. https://doi.org/https://doi.org/10.1016/j.cdc.2021.100676.

[364] Yu KL, Lee XJ, Ong HC, Chen W-H, Chang J-S, Lin C-S, et al. Adsorptive removal of cationic methylene blue and anionic Congo red dyes using wet-torrefied microalgal biochar: Equilibrium, kinetic and mechanism modeling. Environmental Pollution 2021;272:115986. https://doi.org/https://doi.org/10.1016/j.envpol.2020.115986.

[365] Que W, Jiang L, Wang C, Liu Y, Zeng Z, Wang X, et al. Influence of sodium dodecyl sulfate coating on adsorption of methylene blue by biochar from aqueous solution. Journal of Environmental Sciences 2018;70:166–74. https://doi.org/https://doi.org/10.1016/j.jes.2017.11.027.

[366] Waiapu Timothy McMillan O. Characteristics and mechanisms of atrazine sorption to biochar for land remediation. University of Cambridge, 2018.

[367] Anah L, Astrini N. Isotherm adsorption studies of Ni(II) ion removal from aqueous solutions by modified carboxymethyl cellulose hydrogel. IOP Conference Series: Earth and Environmental Science 2018;160:12017. https://doi.org/10.1088/1755-1315/160/1/012017.

[368] Ayawei N, Ebelegi AN, Wankasi D. Modelling and Interpretation of Adsorption Isotherms. Journal of Chemistry 2017;2017:3039817. https://doi.org/10.1155/2017/3039817.

[369] Obaid SA. Langmuir, Freundlich and Tamkin Adsorption Isotherms and Kinetics For The Removal Aartichoke Tournefortii Straw From Agricultural Waste. Journal of Physics: Conference Series 2020;1664:12011. https://doi.org/10.1088/1742-6596/1664/1/012011.

[370] Stuart M, Lapworth D, Crane E, Hart A. Review of risk from potential emerging contaminants in UK groundwater. Science of the Total Environment 2012;416:1–21. https://doi.org/https://doi.org/10.1016/j.scitotenv.2011.11.072.

[371] Dupret J-M, Dairou J, Busi F, Silar P, Martins M, Mougin C, et al. Pesticide-Derived Aromatic Amines and Their Biotransformation, 2011, p. 601–14. https://doi.org/10.5772/18279.

[372] Sumalinog DAG, Capareda SC, de Luna MDG. Evaluation of the effectiveness and mechanisms of acetaminophen and methylene blue dye adsorption on activated biochar derived from municipal solid wastes. Journal of Environmental Management 2018;210:255–62. https://doi.org/https://doi.org/10.1016/j.jenvman.2018.01.010.

[373] Lyu H, Gao B, He F, Zimmerman AR, Ding C, Tang J, et al. Experimental and modeling investigations of ball-milled biochar for the removal of aqueous methylene blue. Chemical Engineering Journal 2018;335:110–9. https://doi.org/https://doi.org/10.1016/j.cej.2017.10.130.

[374] Zhuang Z, Wang L, Tang J. Efficient removal of volatile organic compound by ball-milled biochars from different preparing conditions. Journal of Hazardous Materials 2021;406:124676. https://doi.org/https://doi.org/10.1016/j.jhazmat.2020.124676.

[375] Singh A, Sharma R, Pant D, Malaviya P. Engineered algal biochar for contaminant remediation and electrochemical applications. Science of the Total Environment 2021;774:145676. https://doi.org/https://doi.org/10.1016/j.scitotenv.2021.145676.

[376] Liu S, Li J, Xu S, Wang M, Zhang Y, Xue X. A modified method for enhancing adsorption capability of banana pseudostem biochar towards methylene blue at low temperature. Bioresource Technology 2019;282:48–55. https://doi.org/https://doi.org/10.1016/j.biortech.2019.02.092.

[377] Sahu S, Pahi S, Tripathy S, Singh SK, Behera A, Sahu UK, et al. Adsorption of methylene blue on chemically modified lychee seed biochar: Dynamic, equilibrium, and thermodynamic study. Journal of Molecular Liquids 2020;315:113743. https://doi.org/https://doi.org/10.1016/j.molliq.2020.113743.

[378] Ahmad A, Khan N, Giri BS, Chowdhary P, Chaturvedi P. Removal of methylene blue dye using rice husk, cow dung and sludge biochar: Characterization, application, and kinetic studies. Bioresource Technology 2020;306:123202. https://doi.org/https://doi.org/10.1016/j.biortech.2020.123202.

[379] Fan S, Tang J, Wang Y, Li H, Zhang H, Tang J, et al. Biochar prepared from co-pyrolysis of municipal sewage sludge and tea waste for the adsorption of methylene blue from aqueous solutions: Kinetics, isotherm, thermodynamic and mechanism. Journal of Molecular Liquids 2016;220:432–41. https://doi.org/https://doi.org/10.1016/j.molliq.2016.04.107.

[380] Randolph P, Bansode RR, Hassan OA, Rehrah D, Ravella R, Reddy MR, et al. Effect of biochars produced from solid organic municipal waste on soil quality parameters. Journal of Environmental Management 2017;192:271–80. https://doi.org/https://doi.org/10.1016/j.jenvman.2017.01.061.

[381] Fernández D, Vermeirssen ELM, Bandow N, Muñoz K, Schäfer RB. Calibration and field application of passive sampling for episodic exposure to polar organic pesticides in streams. Environmental Pollution 2014;194:196–202. https://doi.org/https://doi.org/10.1016/j.envpol.2014.08.001.

[382] Liu Y, Lonappan L, Brar SK, Yang S. Impact of biochar amendment in agricultural soils on the sorption, desorption, and degradation of pesticides: A review. Science of the Total Environment 2018;645:60–70. https://doi.org/https://doi.org/10.1016/j.scitotenv.2018.07.099.

[383] Yoon J-Y, Kim JE, Song HJ, Oh K Bin, Jo JW, Yang Y-H, et al. Assessment of adsorptive behaviors and properties of grape pomace-derived biochar as adsorbent for removal of cymoxanil pesticide. Environmental Technology & Innovation 2021;21:101242. https://doi.org/https://doi.org/10.1016/j.eti.2020.101242.

[384] Yuan Y, Yang B, Wang H, Lai X, Li F, Salam MMA, et al. The simultaneous antibiotics and nitrogen removal in vertical flow constructed wetlands: Effects of substrates and responses of microbial functions. Bioresource Technology 2020;310:123419. https://doi.org/https://doi.org/10.1016/j.biortech.2020.123419.

[385] Xu X, Xu Z, Huang J, Gao B, Zhao L, Qiu H, et al. Sorption of reactive red by biochars ball milled in different atmospheres: Co-effect of surface morphology and functional groups. Chemical Engineering Journal 2020:127468. https://doi.org/https://doi.org/10.1016/j.cej.2020.127468.

[386] Nasrullah A, Khan AS, Bhat AH, Din IU, Inayat A, Muhammad N, et al. Effect of short time ball milling on

physicochemical and adsorption performance of activated carbon prepared from mangosteen peel waste. Renewable Energy 2021;168:723–33. https://doi.org/https://doi.org/10.1016/j.renene.2020.12.077.

[387] Takaesu H, Matsui Y, Nishimura Y, Matsushita T, Shirasaki N. Micro-milling super-fine powdered activated carbon decreases adsorption capacity by introducing oxygen/hydrogen-containing functional groups on carbon surface from water. Water Research 2019;155:66–75. https://doi.org/https://doi.org/10.1016/j.watres.2019.02.019.

[388] Lin Z, Zhen Z, Luo S, Ren L, Chen Y, Wu W, et al. Effects of two ecological earthworm species on tetracycline degradation performance, pathway and bacterial community structure in laterite soil. Journal of Hazardous Materials 2021;412:125212. https://doi.org/https://doi.org/10.1016/j.jhazmat.2021.125212.

[389] Lenart-Boroń A, Prajsnar J, Guzik M, Boroń P, Chmiel M. How much of antibiotics can enter surface water with treated wastewater and how it affects the resistance of waterborne bacteria: A case study of the Białka river sewage treatment plant. Environmental Research 2020;191:110037. https://doi.org/https://doi.org/10.1016/j.envres.2020.110037.

[390] Rogers K. Horizontal gene transfer. Encycl Br 2019. https://www.britannica.com/science/horizontal-gene-transfer (accessed March 10, 2021).

[391] Xu L, Sun Y, Du L, Zhang J. Removal of tetracycline hydrochloride from wastewater by nanofiltration enhanced by electro-catalytic oxidation. Desalination 2014;352:58–65. https://doi.org/https://doi.org/10.1016/j.desal.2014.08.013.

[392] Pan S-F, Zhu M-P, Chen JP, Yuan Z-H, Zhong L-B, Zheng Y-M. Separation of tetracycline from wastewater using forward osmosis process with thin film composite membrane – Implications for antibiotics recovery. Separation and Purification Technology 2015;153:76–83. https://doi.org/https://doi.org/10.1016/j.seppur.2015.08.034.

[393] Xia J, Gao Y, Yu G. Tetracycline removal from aqueous solution using zirconium-based metal-organic frameworks (Zr-MOFs) with different pore size and topology: Adsorption isotherm, kinetic and mechanism studies. Journal of Colloid and Interface Science 2021;590:495–505. https://doi.org/https://doi.org/10.1016/j.jcis.2021.01.046.

[394] Wang C, Lin C-Y, Liao G-Y. Degradation of antibiotic tetracycline by ultrafine-bubble ozonation process. Journal of Water Process Engineering 2020;37:101463. https://doi.org/https://doi.org/10.1016/j.jwpe.2020.101463.

[395] Chen X, Zhou J, Zhang T, Ding L. Enhanced degradation of tetracycline hydrochloride using photocatalysis and sulfate radical-based oxidation processes by Co/BiVO4 composites. Journal of Water Process Engineering 2019;32:100918. https://doi.org/https://doi.org/10.1016/j.jwpe.2019.100918.

[396] Liu H, Xu G, Li G. Preparation of porous biochar based on pharmaceutical sludge activated by NaOH and its application in the adsorption of tetracycline. Journal of Colloid and Interface Science 2021;587:271–8. https://doi.org/https://doi.org/10.1016/j.jcis.2020.12.014.

[397] Nguyen V-T, Nguyen T-B, Huang CP, Chen C-W, Bui X-T, Dong C-D. Alkaline modified biochar derived from spent coffee ground for removal of tetracycline from aqueous solutions. Journal of Water Process Engineering 2021;40:101908. https://doi.org/https://doi.org/10.1016/j.jwpe.2020.101908.

[398] Zhang D, He Q, Hu X, Zhang K, Chen C, Xue Y. Enhanced adsorption for the removal of tetracycline hydrochloride (TC) using ball-milled biochar derived from crayfish shell. Colloids and Surfaces A: Physicochemical and Engineering Aspects2021;615:126254. https://doi.org/https://doi.org/10.1016/j.colsurfa.2021.126254.

[399] Scaria J, Anupama K V, Nidheesh P V. Tetracyclines in the environment: An overview on the occurrence, fate, toxicity, detection, removal methods, and sludge management. Science of the Total Environment 2021;771:145291. https://doi.org/https://doi.org/10.1016/j.scitotenv.2021.145291.

[400] Hou J, Wang C, Mao D, Luo Y. The occurrence and fate of tetracyclines in two pharmaceutical wastewater treatment plants of Northern China. Environmental Science and Pollution Research 2016;23:1722–31. https://doi.org/10.1007/s11356-015-5431-5.

[401] Dai Y, Liu M, Li J, Yang S, Sun Y, Sun Q, et al. A review on pollution situation and treatment methods of tetracycline in groundwater. Separation Science and Technology 2020;55:1005–21. https://doi.org/10.1080/01496395.2019.1577445.

[402] Xiang W, Wan Y, Zhang X, Tan Z, Xia T, Zheng Y, et al. Adsorption of tetracycline hydrochloride onto ball-milled biochar: Governing factors and mechanisms. Chemosphere 2020;255:127057. https://doi.org/https://doi.org/10.1016/j.chemosphere.2020.127057.

[403] Cheng D, Ngo HH, Guo W, Chang SW, Nguyen DD, Zhang X, et al. Feasibility study on a new pomelo peel

derived biochar for tetracycline antibiotics removal in swine wastewater. Science of the Total Environment 2020;720:137662. https://doi.org/https://doi.org/10.1016/j.scitotenv.2020.137662.

[404] Yu H, Gu L, Chen L, Wen H, Zhang D, Tao H. Activation of grapefruit derived biochar by its peel extracts and its performance for tetracycline removal. Bioresource Technology 2020;316:123971. https://doi.org/https://doi.org/10.1016/j.biortech.2020.123971.

[405] Qureshi MS, Oasmaa A, Pihkola H, Deviatkin I, Tenhunen A, Mannila J, et al. Pyrolysis of plastic waste: Opportunities and challenges. Journal of Analytical and Applied Pyrolysis 2020;152:104804. https://doi.org/https://doi.org/10.1016/j.jaap.2020.104804.

[406] Yang X, Ng W, Wong BSE, Baeg GH, Wang C-H, Ok YS. Characterization and ecotoxicological investigation of biochar produced via slow pyrolysis: Effect of feedstock composition and pyrolysis conditions. Journal of Hazardous Materials 2019;365:178–85. https://doi.org/https://doi.org/10.1016/j.jhazmat.2018.10.047.

[407] Zhang Z, Li Y, Ding L, Yu J, Zhou Q, Kong Y, et al. Novel sodium bicarbonate activation of cassava ethanol sludge derived biochar for removing tetracycline from aqueous solution: Performance assessment and mechanism insight. Bioresource Technology 2021:124949. https://doi.org/https://doi.org/10.1016/j.biortech.2021.124949.

[408] Saremi F, Miroliaei MR, Shahabi Nejad M, Sheibani H. Adsorption of tetracycline antibiotic from aqueous solutions onto vitamin B6-upgraded biochar derived from date palm leaves. Journal of Molecular Liquids 2020;318:114126. https://doi.org/https://doi.org/10.1016/j.molliq.2020.114126.

[409] Yazdani MR, Duimovich N, Tiraferri A, Laurell P, Borghei M, Zimmerman JB, et al. Tailored mesoporous biochar sorbents from pinecone biomass for the adsorption of natural organic matter from lake water. Journal of Molecular Liquids 2019;291:111248. https://doi.org/https://doi.org/10.1016/j.molliq.2019.111248.

[410] Shan D, Deng S, Zhao T, Wang B, Wang Y, Huang J, et al. Preparation of ultrafine magnetic biochar and activated carbon for pharmaceutical adsorption and subsequent degradation by ball milling. Journal of Hazardous Materials 2016;305:156–63. https://doi.org/https://doi.org/10.1016/j.jhazmat.2015.11.047.

[411] Liu H, Xu G, Li G. The characteristics of pharmaceutical sludge-derived biochar and its application for the adsorption of tetracycline. Science of the Total Environment 2020;747:141492. https://doi.org/https://doi.org/10.1016/j.scitotenv.2020.141492.

[412] Chen Y, Du L, Li S, Song W, Jensen PA, Lin W. Pyrolysis of antibiotic mycelial dreg and characterization of obtained gas, liquid and biochar. Journal of Hazardous Materials 2021;402:123826. https://doi.org/https://doi.org/10.1016/j.jhazmat.2020.123826.

[413] Naderi Beni N, Snow DD, Berry ED, Mittelstet AR, Messer TL, Bartelt-Hunt S. Measuring the occurrence of antibiotics in surface water adjacent to cattle grazing areas using passive samplers. Science of the Total Environment 2020;726:138296. https://doi.org/https://doi.org/10.1016/j.scitotenv.2020.138296.

[414] Kaeseberg T, Schubert S, Oertel R, Zhang J, Berendonk TU, Krebs P. Hot spots of antibiotic tolerant and resistant bacterial subpopulations in natural freshwater biofilm communities due to inevitable urban drainage system overflows. Environmental Pollution 2018;242:164–70. https://doi.org/https://doi.org/10.1016/j.envpol.2018.06.081.

[415] Hossain N, Bhuiyan MA, Pramanik BK, Nizamuddin S, Griffin G. Waste materials for wastewater treatment and waste adsorbents for biofuel and cement supplement applications: A critical review. Journal of Cleaner Production 2020;255:120261. https://doi.org/https://doi.org/10.1016/j.jclepro.2020.120261.

[416] Chen Y, Wang R, Duan X, Wang S, Ren N, Ho S-H. Production, properties, and catalytic applications of sludge derived biochar for environmental remediation. Water Research 2020;187:116390. https://doi.org/https://doi.org/10.1016/j.watres.2020.116390.

[417] Lan L, Kong X, Sun H, Li C, Liu D. High removal efficiency of antibiotic resistance genes in swine wastewater via nanofiltration and reverse osmosis processes. Journal of Environmental Management 2019;231:439–45. https://doi.org/https://doi.org/10.1016/j.jenvman.2018.10.073.

[418] Gao M, Yang J, Liu C, Gu B, Han M, Li J, et al. Effects of long-term biochar and biochar-based fertilizer application on brown earth soil bacterial communities. Agriculture, Ecosystems & Environment 2021;309:107285. https://doi.org/https://doi.org/10.1016/j.agee.2020.107285.